Using waste foundry sands as reactive media in permeable reactive barriers. [DNR-147] 2002

Lee, Taeyoon; Benson, Craig H.
Madison, Wisconsin: Geo Engineering Program, Dept. of Civil and Environmental Engineering, University of Wisconsin-Madison, 2002

https://digital.library.wisc.edu/1711.dl/GPZ3HIF2ZEKTG8F

USING WASTE FOUNDRY SANDS AS REACTIVE MEDIA IN PERMEABLE REACTIVE BARRIERS

By Taeyoon Lee and Craig H. Benson

Geo Engineering Report No. 02-01

Geo Engineering Program
Dept. of Civil and Environmental Engineering
University of Wisconsin-Madison
Madison, Wisconsin 53706
USA

January 15, 2002

EXECUTIVE SUMMARY

The objective of this study was to evaluate the potential use of waste foundry sand as an inexpensive medium for permeable reactive barriers (PRBs). Batch and column tests were conducted to evaluate the reactivity and sorptive capacity of twelve foundry sands for four groundwater contaminants: TCE, the herbicides alachlor and metolachlor, and zinc. Parameters obtained from these tests were then used to size PRBs for typical field conditions. The sizing calculations showed that foundry-sand PRBs containing at least 1% iron appear are viable under typical conditions for remediating groundwater contaminated with solvents, herbicides, and metals to concentrations below the maximum contaminant level (MCL).

The batch and column tests showed that the relatively abundant organic carbon in foundry sands results in appreciable sorption of TCE, alachlor, and metolachlor. When typical concentrations in groundwater are considered, sorption of these compounds can be described with a partition coefficient from a linear isotherm model. Foundry sands were also found to be a good sorbent for zinc. However, the partition coefficient for zinc varies significantly with solution pH.

Rate constants for reduction of TCE, alachlor, and metolachlor with foundry sand were found to be comparable to those for conventional iron media used for PRBs. Additionally, the rate constant can be normalized by the surface area to solution ratio, as is done for conventional iron media. The rate constant for zinc was found to vary within a small range (typically 0.05 – 0.20 1/hr). Higher rate constants for zinc typically were obtained at higher pH.

Comparisons were made between partition coefficients and rate constants obtained from batch and column tests to determine if parameters obtained from batch tests can be used for design. The comparison for TCE showed that similar partition coefficients and rate constants are obtained using both methods. For the herbicides, the partition coefficients and rate constants obtained from the batch tests tended to be higher than those from the column tests. Conservative reduction factors of 2.0 and 1.6 have been recommended when using partition coefficients and rate constants obtained from batch tests for design of PRBs for alachlor and metolachlor. The comparison made for zinc indicated that the batch and column tests yield similar partition coefficients and rate constants provided that the solution pH is the same.

Empirical equations were developed using multivariate regression to predict partition coefficients and rate constants as a function of properties of the foundry sand such as iron content, total organic carbon content, and clay content. These equations can be used for feasibility assessments and preliminary design calculations. However, they are not meant as a substitute for batch and column testing.

Tests were also conducted to evaluate the leaching characteristics of foundry sands. Batch water leach tests, column leach tests, and total elemental analyses were conducted. The water leach tests and total elemental analyses were conducted to categorize the foundry sands in accordance with Section NR 538 of the Wisconsin Administration Code. The column leach tests were conducted to evaluate leaching that might occur under field conditions.

Results of the water leach tests and the total elemental analyses showed that all of the foundry sands are Category 2 materials as defined in NR 538. However, tests on Peerless iron, torpedo sand, and a typical fill material indicate that these materials, which are commonly placed below the groundwater table at remediation sites, also are Category 2 materials. Thus, using foundry sand as a PRB medium should pose no greater risk than that imposed using conventional construction materials.

Additional column leaching tests were conducted to determine characteristics of the leachate under flow conditions more representative of the field. Effluent from these tests was analyzed for three metals (Fe, Cr, and Pb). Chromium and lead in the effluent were always below MCLs. For iron, however, several pore volumes of flow were often required to meet the MCL.

The number of pore volumes required to meet the MCL (PVER) for iron was found to depend on the initial iron concentration in the effluent and the partition coefficient. A method was developed to predict the PVER using properties of the foundry sands and the results of water leach tests. Predictions of PVER made with this method were found to be comparable to PVER determined from the column tests.

ACKNOWLEDGEMENT

Financial support for this study was provided by the Wisconsin Department of Natural Resources (WDNR) and the University of Wisconsin System (UWS). Dr. Gerald Eykholt provided assistance regarding analytical methods and interpretation of the experimental data. Assistance in the environmental laboratory was provided by Ms. Jackie Bastyr Cooper. The findings in this report are solely those of the authors. Endorsement by WDNR or UWS is not implied and should not be inferred.

TABLE OF CONTENTS

LIST OF FIGURES

LIST OF TABLES

SECTION ONE

INTRODUCTION

Permeable reactive barriers (PRBs) are a relatively new groundwater treatment technology. As a contaminant plume flows through a PRB, contaminants react with the media contained in the PRB, and are converted into less toxic or innocuous by-products (Fig. 1). Effluent exiting a PRB is intended to meet groundwater quality requirements.

Groundwater treatment with PRBs is becoming popular because the PRB technology has several advantages. PRBs are an in situ treatment technology, and thus there is no need to transport contaminants removed from groundwater to a treatment plant or disposal site. Once PRBs are installed, operation and maintenance costs become significantly lower relative to those for other treatment methods. PRBs also operate under the natural hydraulic gradient, and require no input of energy after construction.

The type of reactive medium used in a PRB depends on the type of contaminants in the plume. Zero-valent iron (Fe^0) has been used to treat chlorinated ethene compounds (Blowes et al. 1995, Robert et al. 1996, and Arnold and Roberts 1998), toxic heavy metals (Benner et al. 1997, Francis and Dodge 1998, Shokes and Moller 1999, Su and Puls 2001), and chlorinated herbicides (alachlor and metolachlor) (Eykholt and Davenport 1998,

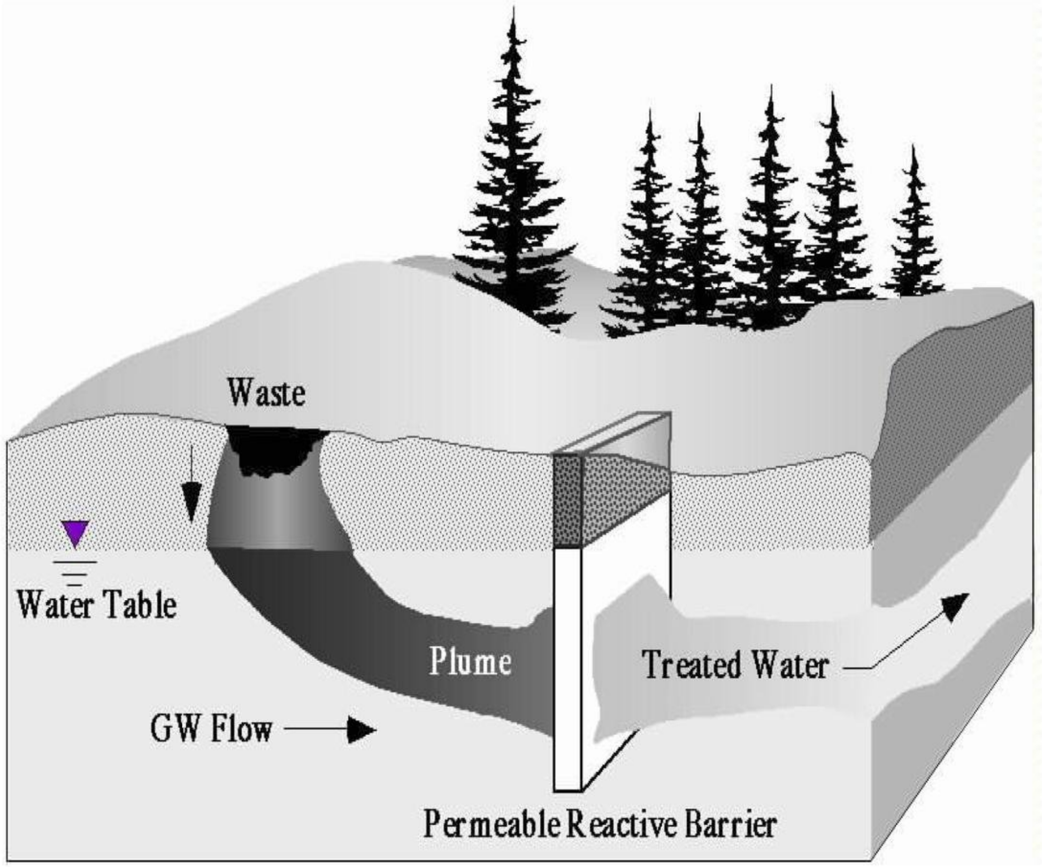

Fig. 1.1 Schematic of a PRB (http://www.powellassociates.com/sciserv).

Koppensteiner 1998). Media that provide sorption sites for organic compounds are also used (Rael et al. 1995, Kim 1997, Kershaw and Pamukcu 1997, Moo-Young and Zimmie 1996), such as straw, wood chips, peat, coal, and tire chips.

A drawback of PRBs is their high initial capital cost. The high cost often prevents their use at small-contaminated sites, which are common in United States. The objective of this study was to assess the feasibility of using waste foundry sands as a low-cost reactive medium for PRBs. Foundry sands are mixture of sand, clay binder, coal dust, and fine residual iron particles (Javed and Lovell 1994). The coal dust provides organic carbon as a sorbent and the iron particles act as a reducing agent. Besides cost savings, re-using foundry sand as a reactive medium saves valuable landfill space and allows the foundry industry to accrue savings through reduced disposal costs. Approximately 800,000 Mg of foundry sands are landfilled in Wisconsin alone, with an annual cost of $18 million to the foundry industry.

Twelve foundry sands from Wisconsin, Ohio, and Illinois were evaluated as reactive media in this study. Water leach tests and total elemental analyses were conducted to assess whether the foundry sands could be beneficially re-used in PRBs in accordance with Section NR 538 of the Wisconsin Administrative Code. Batch tests were conducted with common groundwater contaminants to assess reactivity and sorptive capacity, and column tests were conducted to determine if results of the batch tests were representative of more realistic conditions. Transport parameters were also obtained from the column tests for use in PRB design. A series of column leaching tests was also conducted to ascertain the temporal characteristics of leachate from foundry sands.

This report describes the findings of this study in nine sections. Section Two describes reaction mechanisms in PRBs. Section Three describes the methods that were used. Section Four describes results of the water leach tests and total elemental analyses. Results of the batch sorption tests, batch degradation tests, and column tests are described in Section Five (TCE), Section Six (Herbicides), and Section Seven (Zinc). Results of column leaching tests are described in Section Eight. A summary and conclusions are provided in Section Nine.

SECTION TWO

REACTION MECHANISMS IN PRBS

Contaminants passing through a PRB are treated by reacting with a medium in the barrier. Three treatment mechanisms are typically used in PRBs: sorption, precipitation, or reduction-oxidation (redox). These mechanisms are described in the following sections. A summary of current reactive media and compounds treated with these reactive media is shown in Table 2.1.

2.1 REDUCTION-OXIDATION

PRBs employing redox reactions are being used at 33 sites for treatment of chlorinated ethenes, heavy metals, and radionuclides (Jarre and Kociolek 1999). Most of these applications are to treat chlorinated organics and hexavalent chromium (Gillham and O'Hannesin 1994, Blowes et al. 1995, Lowry 1995, Mackenzie et al. 1995, Puls et al. 1995, Robert et al. 1996, Orth and Gillham 1996, Sivavec et al. 1997, Blowes et al. 1997, Tratnyek et al. 1997, Arnold and Roberts 1998, Powell et al. 1998). Redox reactions influence the solubility of metal ions, the chemical form of ions (McBride 1994), and cause degradation of chlorinated ethene compounds (Robert et al 1996, Gillham and O'Hannesin 1994, Lowry 1995, Arnold and Roberts 1998). Oxidation reactions occur when electrons are removed in the transfer process (Sparks 1995). Reduction reactions occur when electrons are accepted.

Table 2.1. Reactive Media and Treated Compounds.

Treated Compounds	Reactive Media	Reaction Mechanism
Chlorinated ethenes, ethanes, and herbicides	Metals (Fe, Zn)	Reductive dechlorination
Chlorinated organics, petroleum compounds (BTEX)	Peat, compost, tire chips, organic soils, activated carbon	Sorption
Metals (e.g. As, Cd, Cu, Fe, Ni, Pb, Zn)	Compost, wood chips, ferrous Iron (Fe^{2+}), and Fe	Reductive precipitation and/or sorption
Radioactive isotopes (e.g. uranium, vanadium)	Fe	Reductive precipitation

Various types of zero-valent metals (i.e., Ag, Al, Au, Cu, Fe, Ni, Pd, Zn, and Fe/Pd) have been investigated as reducing agents in PRBs. However, the lower cost and less toxic characteristics of iron make it the most common reactive medium used in PRBs, especially for reduction of chlorinated organic compounds (Shlimm and Heitz 1996, Roberts et al.1996, Gu et al. 1997, Lien and Zhang 1999).

Reductive dechlorination of organic compounds by zero-valent iron can be written as the sum of an oxidation reaction and a reduction reaction. In the oxidation reaction, Fe^0 is oxidized by releasing two equivalent electrons (e^-):

$$Fe^0 \rightarrow Fe^{2+} + 2e^- \qquad (2.1)$$

The reduction reaction is

$$RCl + 2e^- + H^+ \rightarrow RH + Cl^- \qquad (2.2)$$

where RCl represents a chlorinated alkene and RH represents a dechlorinated alkene. Combining the two reactions yields

$$Fe^0 + RCl + H^+ \rightarrow Fe^{2+} + RH + Cl^- \qquad (2.3)$$

Water is also reduced by iron metal forming hydrogen gas and releasing hydroxide ions into solution:

$$2H_2O + 2e^- \rightarrow H_2\,(g) + 2\,OH^- \qquad (2.4)$$

The reduction pathways for polychlorinated ethylene compounds by iron and zinc metals are shown in Fig. 2.1 (Roberts et al. 1996, Arnold and Roberts 1998). Three reaction mechanisms (i.e., reductive α and β elimination, dehydrohalogenation, and hydrogenolysis) are believed to be responsible for

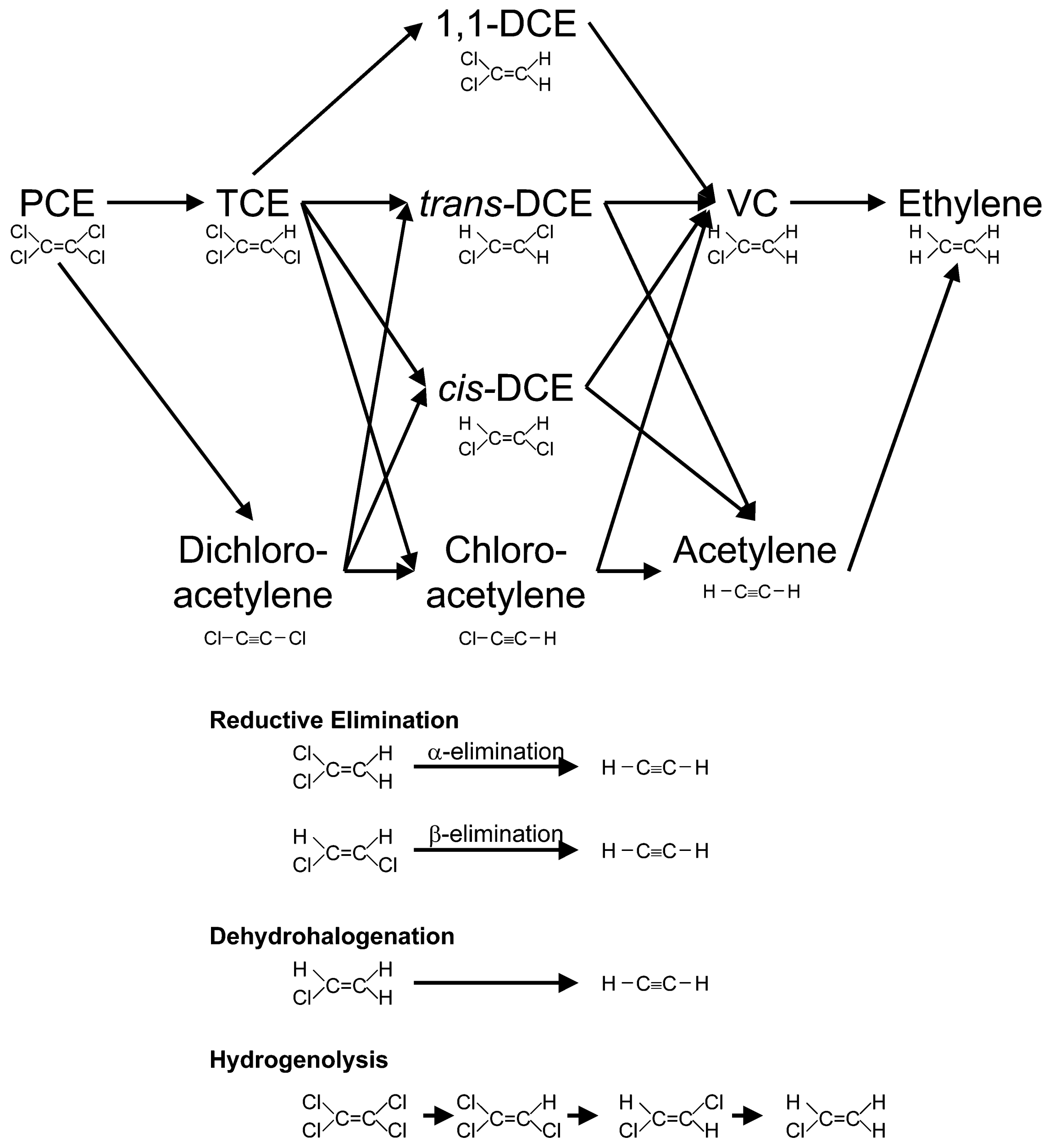

Fig. 2.1. Pathways of PCE Reduction by Zinc Metal to Ethylene (Roberts et al. 1996, Drawing from Elder 2000).

dechlorination. Reductive β elimination and hydrogenolysis play the most important role in reduction of chlorinated ethylene compounds, whereas reductive α elimination and dehydrohalogenation are not significant (Roberts et al. 1996). The percentage of the reaction occurring via reductive β elimination by zinc metal is 15% of PCE, 30% of TCE, 85% of cis-DCE, and 95% of trans-DCE reaction (Arnold and Roberts 1998). For iron metal, less than a 5% of TCE is degraded via hydrogenolysis (Orth and Gillham 1996, Sivavec et al. 1997).

Some dechlorinated byproducts from reduction reactions are more toxic and less reactive compared to their parent compounds (Tratnyek et al. 1997, Arnold and Roberts 1998). The hydrogenolysis pathway produces the most toxic chlorinated byproduct, vinyl chloride (the MCL of VC is 2 μg/L). The percentage of DCE isomers and VC generated by dechlorination is generally less than 5% of the TCE that is degraded by iron metal (Orth and Gillham 1996, Sivavec et al. 1997). These low concentrations of byproducts (i.e., DCE isomers and VC) are believed to be present because they are released from the iron surface before complete reduction of TCE is attained (Orth and Gillham 1996).

The predominant pathway, reductive β elimination, does not favorably produce DCE isomers and VC. The chlorinated acetylene compounds produced from reductive β elimination reaction are toxic, but their short half-life usually renders them unimportant in PRB design (Tratnyek et al. 1997, Arnold and Roberts 1998).

Four principle factors influence the rate of dechlorination of chlorinated ethylene compounds: surface area of the iron, pH of the solution, concentration of dissolved oxygen (DO), and presence of catalysts (Warren et al. 1995, Johnson et al. 1996, Tratnyek et al. 1997, Gu et al. 1997, Lien and Zhang 1999). Among these four factors, surface area of the iron is the most important because the reduction reaction is a surface mediated process (Johnson et al. 1996, Roberts et al. 1996, Weber 1996). High pH and DO in solution can affect the reaction rate because the oxide formed on the surface of the iron can prevent contact between organic molecules with the iron surfaces (Johnson et al. 1996, O’Hannesin and Gillham 1998, Phillips et al. 2000). The reaction rate for chlorinated organic compounds is significantly accelerated by metallic couples (Shoemaker et al. 1995, Sivavec et al. 1997, Lien and Zhang 1999, Gu et al 1997), but the long-term effectiveness of these couples has not been determined.

In most cases, the reaction is approximately first order. To compare rate constants obtained from the various testing conditions, a normalized reaction rate constant is employed that is obtained by dividing the first-order rate constant by the specific surface area of iron (Johnson et al. 1996). Normalized rate constants obtained from a variety of laboratory tests and field tests are summarized in Table 2.2.

Table 2.2. Reaction Rates for Dehalogenation by Iron Metal.

Chemical	Symbol	Specific Rate constant, $(K_{SA})^a$ (L/m^2-hr)	
		Laboratory Data[b]	Field Data[c]
tetrachloroethylene	PCE	2.1×10^{-3}	3.6×10^{-3}
trichloroethylene	TCE	5.7×10^{-5} - 1.1×10^{-3}	6.4×10^{-3}
1,1-dichloroethylene	1,1-DCE	6.4×10^{-5}	6.7×10^{-3}
trans-dichloroethylene	*trans*-DCE	1.2×10^{-4}	4.1×10^{-3}
cis-dichloroethylene	*cis*-DCE	4.1×10^{-5} – 3.0×10^{-4}	8.6×10^{-4}
Vinyl chloride	VC	5.0×10^{-5}	-
tetrachloromethane	PCM	1.2×10^{-1} - 1.0×10^{-4}	-
trichloromethane	TCM	9.2×10^{-4} – 8.4×10^{-5}	-
tribromomethane	TBM	1.7×10^{-2}	-
hexachloroethane	HCA	3.1×10^{-2}	-
1,1,2,2-tetrachloroethane	1122TeCA	1.3×10^{-2}	-
1,1,1,2-tetrachloroethane	1112TeCA	1.4×10^{-2}	-
1,1,2-trichloroethane	111TCA	1.1×10^{-2}	-
1,2,3-trichloropropane	123TCP	6.1×10^{-6}	-
Alachlor	-	2.4×10^{-3}	-
Metolachlor	-	2.0×10^{-3}	-

[a] Reaction rates (K_{SA}) are normalized by the surface area of iron per liter of solution

[b] Tratnyek et al (1997), Johnson et al (1996), Lien and Zhang (1999), Sivavec et al. (1997), Wűst et al. (1999), Eykholt and Davenport (1998)

[c] O'Hannesin and Gillham (1998)

2.2 SORPTION

2.2.1 Sorption of Organic Compounds on Organic Carbon and Mineral Surfaces

The existence of large nonpolar molecules in an aqueous solution causes disorder in the water molecules because the large nonpolar molecules have less affinity for water than water has for itself (McBride 1994). As a result, nonpolar molecules typically have low solubility, an energetically unfavorable condition, and tend to be forced out of solution or onto organic matter. Sorption on the organic matter is primarily via van der Walls interactions (McBride 1994). This mechanism is depicted in Fig. 2.2, and is referred to as hydrophobic attraction of nonionic organic molecules. When organic matter exists as particles or colloids, a nonpolar environment is provided allowing hydrophobic organic compounds to escape from water to the surface of organic matter without competition by the water molecules. Organic molecules are less likely to sorb onto mineral surfaces, because mineral surfaces typically are charged, which allows them to form hydrogen bonds with water molecules.

Sorption of nonpolar organic compounds on mineral surfaces requires replacing the water molecules sorbed on mineral surfaces, which is not favorable (Schwarzenbach et al. 1993). Some organic compounds having polar functional groups are sorbed on clay surfaces by hydrogen bonding to hydrated cations or by ion-dipole interaction with water on the clay surfaces (McBride 1994). However, most organic compounds are sorbed onto organic matter rather than mineral surfaces, because water molecules easily displace the organic

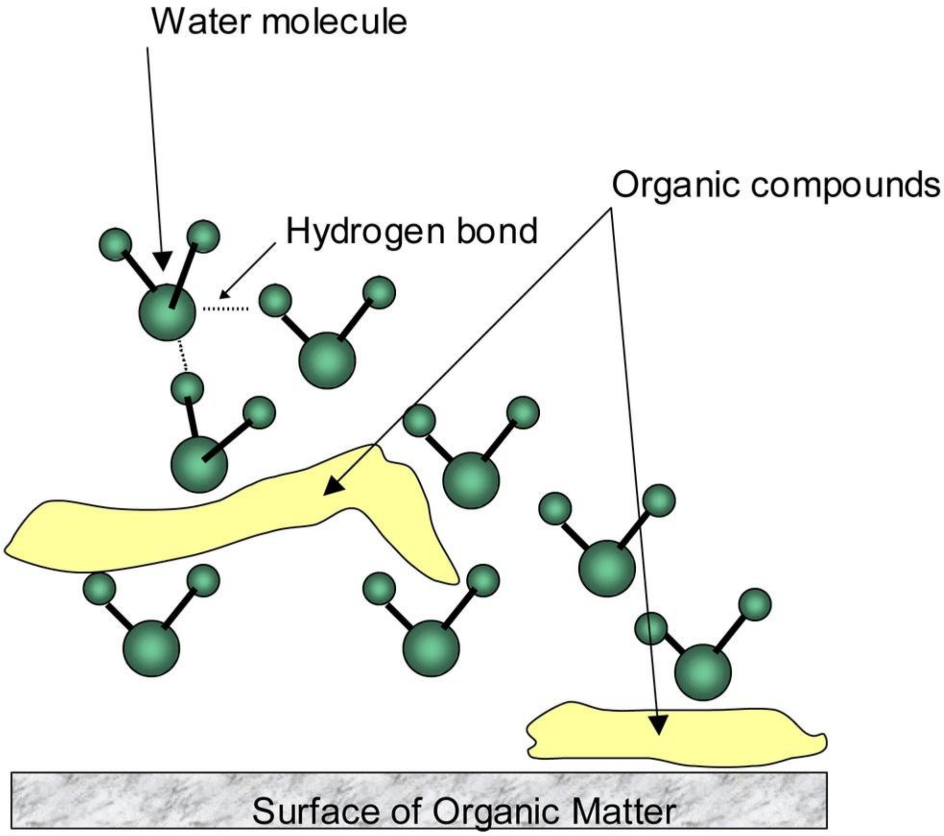

Fig. 2.2. Sorption of Non-Polar Organic Molecules onto the Surface of Organic Matter via Hydrophobic Attraction (Adapted from McBride 1994).

compounds sorbed on the clay surfaces (McBride 1994). Sorption of nonpolar organic compounds on organic matter, which is also hydrophobic, does not require the replacement of water molecules. However, organic matter does have limited polar characteristics due to the presence of carboxy, phenoxy, hydroxy, and carbonyl groups (McBride 1994). In general, the polar characteristics of organic matter are not as strong as mineral matter, but organic matter is not as nonpolar as hydrocarbons (Schwarzenbach et al. 1993).

Various laboratory tests have been performed to find effective sorbents for organic compounds. Materials such as activated carbon, straw, wood chips, peat, coal, shale, paper sludge, and tire chips have been found to be effective (Thain 1974, Knocke and Hemphill 1981, Rowley et al. 1984, Rael et al. 1995, Kershaw and Pamukcu 1997, Kim et al. 1997, Moo and Young 1998).

2.2.2 Sorption of Heavy Metals on Organic Carbon

Binding of metal cations on organic carbon can be described as an ion exchange process between H^+ and the metal acidic functional groups, L (McBride 1994):

$$M^{x+} + >LH_y => L - M^{(x-y)+} + yH^+ \tag{2.5}$$

where M^{x+} is a metal cation and L is a metal acidic functional group. The structure of the various metal acidic functional groups are carboxyl (R-COOH), phenol (C_6H_5OH), alcohol (R-CH_2OH), enol (R-CH=CH-OH), ketone (R-CO-R), quinone (O=C_6H_4=O), ether (R-CH_2-O-CH_2-R), and amino (R-NH_2) (Stevenson

1982), where R represents an alkyl group. Cationic attraction to organic matter is primarily through the carboxylate group (McBride 1994), which is reacted when a base is added:

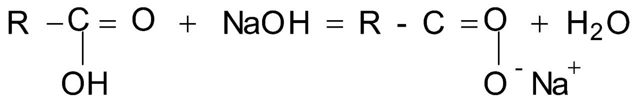

$$R-\underset{\displaystyle OH}{\underset{|}{C}}=O + NaOH = R-C=\underset{\displaystyle O^{-}\,Na^{+}}{\underset{|}{O}} + H_2O \qquad (2.6)$$

The organic surface creates a negative charge that is balanced by cations such as Na^+ in Eq. 2.6 (McBride 1994).

The order of affinity of metal cations is related to the electronegativity of the organic matter, which acts as a Lewis base (i.e., electron donor). The typical order of affinity of divalent metals for soil organic matter is described by McBride (1994). Metals of smaller radius tend to form a stronger complex with an amine or carboxylate group, according to the Irving-Williams series of complexing strength for divalent metals (McBride 1994).

2.2.3 Sorption of Heavy Metals on Metal Oxide Surfaces

Metal ions in solution can be sorbed on metal oxide surfaces via surface complexation. The metal oxide surface protonates at low pH:

$$>S-OH+H^{+} = >S-OH_2^{+} \qquad (2.7)$$

where S is a metal of the adsorbing surface and OH is a surface hydroxyl group. When the solution pH is high, the surface hydroxyl group deprotonates:

$$>S-OH => S-O^{-} + H^{+} \qquad (2.8)$$

Therefore, at high solution pH, the surface hydroxyl group can react with metal cations:

$$>S-O^{-}+M^{n+}=>S-O-M^{(n-1)+}+H^{+} \qquad (2.9)$$

Sorption of heavy metals on mineral surfaces is pH-dependent and also influenced by solute concentrations, surface coverage, and type of metal oxides (Sparks 1995). As the solution pH increases, more metal cations are sorbed on the metal oxides due to the negative charge of the metal oxides (Sparks 1995).

The literature on wastewater treatment shows that various types of heavy metals can be removed from aqueous solutions by sorption on oxide surfaces. The mechanisms used in wastewater treatment can also be used in groundwater treatment. Kuan et al. (1998) show that sand coated with aluminum oxide can remove Se(IV) and Se(VI) from aqueous solutions by adsorption. Joshi et al. (1996) show that arsenic (III) and arsenic (V) can be removed via adsorption-coprecipitation using sand coated with iron oxide. Basic yttrium carbonate (BYC) can remove arsenic (III) and arsenic (V) by sorption (Wasay et al. 1996) and Cu and Cd can be removed by cementation onto the surface of iron as zerovalent metals (Shokes and Moller 1999). Fe oxide and particulate organic carbon can also remove Pb, Cu, Zn, and Cd by sorption (Paulson 1999).

Namasivayam et al. (1995) report the effectiveness of Fe(III)/Cr(III) hydroxide for removing Cd(II) removal from solution. The influence of initial Cd(II) concentration, agitation time, temperature and pH on sorption were evaluated. Sorption of Cd(II) was found to increase as the agitation time, temperature, and pH increase. All of the Cd(II) in solution can be removed when the pH is above 8.3, which is the point of zero charge (pzc) of the adsorbent.

One of the most important factors for selecting sorbents is cost. To reduce material costs in treatment processes, naturally occurring and industrial by-products can replace high cost materials (i.e., activated carbon) that are used conventionally for adsorption. Natural materials or waste products such as bark, dead biomass, clay, fly ash, seaweed, and leaf mold have been used as sorbents for Cd, Cr, Pb, and Hg, as summarized by Bailey et al. (1999). Fly ash has been used as an adsorbent for Cu, Zn, and Pb, and its adsorption capacity can be increased by mixing it with lime (Ricou et al. 1999).

2.3 PRECIPITATION OF HEAVY METALS

PRBs have been used to treat inorganic contaminants by changing their valence state into more favorable forms for sorption and precipitation (Eykholt et al. 1995, Shoemaker et al. 1995, Ponder et al. 2000).

The solubility product of the crystalline solid (K_{so}) and the ion activity product (IAP) can be used to quantify the status of the solution phase with regard to precipitaiton. When the ratio of IAP/K_{so} is greater than unity, the solution is supersaturated with respect to a particular solid phase, and precipitation is favorable. The solution is saturated when the ratio is unity. Otherwise, the solution is undersaturated with respect to a particular solid phase and precipitation is unfavorable (Stumm and Morgan 1970, McBride 1994).

When K_{so} of the crystalline solid is high and the solution is homogeneous, IAP/K_{so} greater than 100 is often required to overcome an energy barrier to form crystal nuclei (McBride 1994). However, the extent of supersaturation required to start precipitation can be reduced or eliminated when mineral and organic surfaces are provided, which act to catalyze the precipitation of heavy metals from solutions (McBride 1994).

Shokes and Moller (1999) conducted a laboratory study evaluating removal of heavy metals derived from acid mine drainage (Shokes and Moller 1999). Zero-valent iron was used to remove heavy metals by increasing the pH of the solution. Reduction by iron metal promoted the removal of cadmium and copper by changing two metals into zero-valent metals. Aluminum, nickel, and zinc were removed slowly by forming hydroxide precipitate.

SECTION THREE

MATERIALS AND METHODS

3.1 MATERIALS

3.1.1 Foundry Sands

Twelve foundry sands were used in this study. The foundry sands were obtained from AFK Corporation (Ripon, WI), Baker Manufacturing (Evansville, WI), Brillion Iron Works (Brillion, WI), Honda of America (Anna, OH), Iroquois Foundry Corp. (Browntown, WI), Kohler Foundry (Kohler, WI), Sparta Manufacturing (Sparta, WI), Wagner Casting (Decatur, IL), and Waupaca Foundries (Waupaca, WI). Each sand is designated by a number (1 through 12).

Each of the foundry sands contains a large fraction of fine sand, as is evident in their particle size distribution curves (Fig. 3.1). Index properties of the foundry sands, which were obtained from Abichou et al. (2000), are summarized in Table 3.1. The liquid limit (LL) ranges from non-plastic to 29, and the plasticity index (PI) ranges from non-plastic to 7. The bentonite content ranges from 0 to 13%, and the specific gravity ranges from 2.51 to 2.73.

Total organic carbon (TOC) content of each foundry sand was measured using a Lab 2100 TOC analyzer (Zellweger Analytics). Inorganic carbon existing in the form of calcite or dolomite was removed beforehand by adding a few drops of 4 M HCl to a known amount of foundry sand as described in *Methods of Soil*

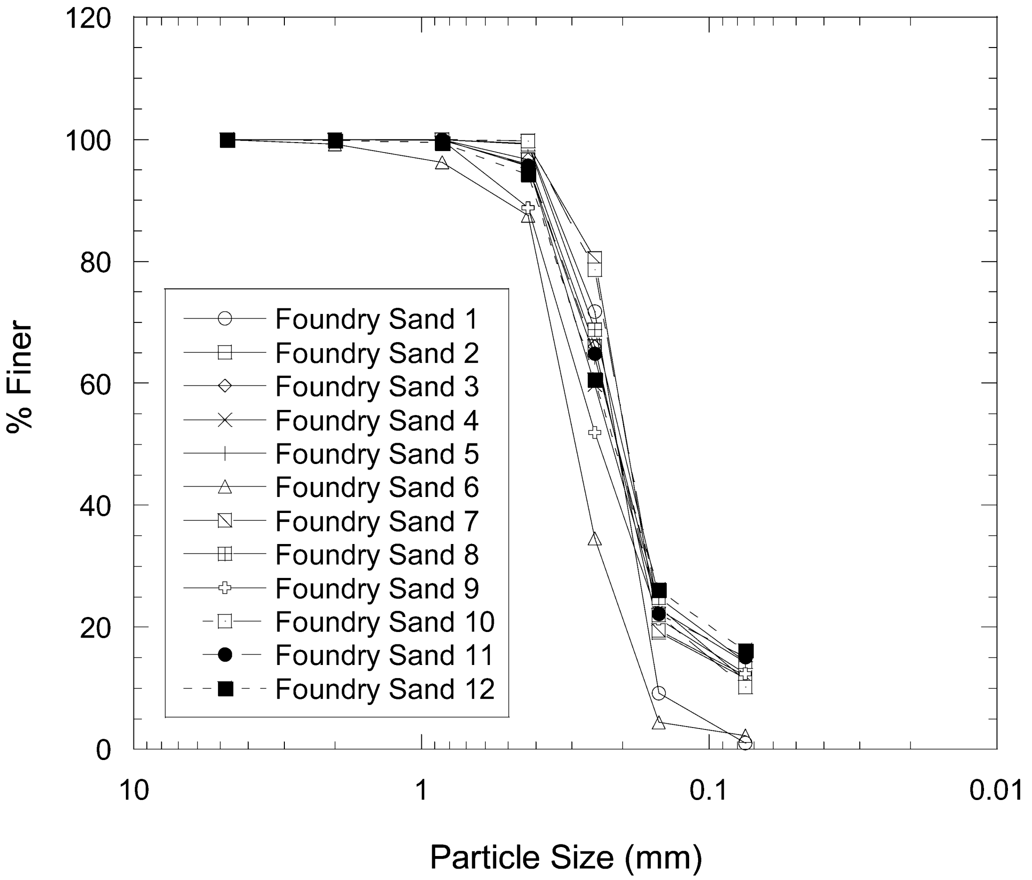

Fig. 3.1. Particle Size Distribution Curves for Foundry Sands.

Table 3.1. Index Properties of Foundry Sands (from Abichou et al. 2000)

Foundry Sand	Binder Type	Particle Size (%)			Atterberg Limits[b]			USCS Classification	Specific Gravity
		P_{200}	$P_{2\mu m}$	Active Clay[a]	LL	PL	PI	USCS	
Sand 1	Clay	10.7	6.7	5.1	N.P.[e]	N.P.	N.P.	SP-SM	2.62
Sand 2	Clay	14.3	9.2	7.0	18	17	1	SM	2.53
Sand 3	Clay	11.3	7.7	7.5	20	18	2	SW-SM	2.52
Sand 4	Clay	13.2	9.3	10.5	23	19	4	SC-SM	2.63
Sand 5	Clay	12.4	8.0	8.4	23	18	5	SC-SM	2.54
Sand 6	Clay	10.2	5.2	6.6	20	17	3	SP-SM	2.61
Sand 7	Clay	10.9	4.5	6.2	18	14	4	SC-SM	2.72
Sand 8	Clay	11.1	6.2	7.4	26	20	6	SP	2.68
Sand 9	Chemical	4.3	2.9	N.A.[d]	N.P.	N.P.	N.P.	SP	2.64
Sand 10	Clay	10.0	3.5	4.7	N.P.	N.P.	N.P.	SP-SM	2.73
Sand 11	Clay	16.0	13.2	13	27	20	7	SM-SC	2.51
Sand 12	Clay	10.0	3.5	4.7	N.P.	N.P.	N.P.	SP	2.73

[a] Active Clay determined by Methylene Blue Titration (ASTM C 837), [b] ASTM D 4318 with one week hydration period, [c] N.A. = Not applicable, [d] N.P. = Non-plastic, [e] N.T. = Not tested.

Analysis (Nelson and Sommers 1982). After application of HCl, the specimens were allowed to sit for 5 min. No visible effervescence was observed. The specimens were then loaded into the analyzer.

The calibration curve for the TOC analyzer was checked using a 0.0020 g specimen of sucrose. The measured TOC of the sucrose was 887 μg, which is within 5% of the theoretical value of 843 μg.

The total carbon (TC) contents range from 0.5% (Sand 4) to 4.7% (Sand 11), by weight (Table 3.2). TOC, which was measured after removal of inorganic carbon, ranges from 0.5% (Sand 4) to 4.0% (Sand 11).

3.1.2 Iron Particles

Zero-valent iron particles were obtained from Peerless Metal Powders and Abrasives Co. of Detroit, MI. The mean particle size was 0.7 mm and the specific surface area was 0.87 m^2/g (Fort 2000). The purity of the iron ranged from 92 to 95%, by weight. Composition of the iron particles is shown in Table 3.3.

3.1.3 Chemicals

3.1.3.1 Chlorinated Ethenes

Trichloroethylene (TCE) (99.5% purity) was obtained from Aldrich Chemical Co. Inc. The TCE by-products vinyl chloride (99% purity), 1,1-dichloroethylene (99% purity), trans-1,2-dichloroethylene (99% purity), and cis-1,2-dichloroethylene (99% purity) were purchased from Supelco Co. Physical

Table 3.2. Total Carbon and Total Organic Carbon of Foundry Sands.

Sands	Total Carbon (%)	Total Organic Carbon (%)
Sand 1	1.5	1.5
Sand 2	3.1	2.6
Sand 3	3.6	2.5
Sand 4	0.6	0.5
Sand 5	1.4	1.8
Sand 6	1.2	1.1
Sand 7	3.1	2.2
Sand 8	3.0	2.5
Sand 9	1.0	0.8
Sand 10	3.1	2.5
Sand 11	4.7	4.0
Sand 12	2.2	2.4

Table 3.3. Elemental Analysis of Iron Particles as Reported by Peerless Metal Powders and Abrasive Co. of Detroit, MI.

Elements	% by Weight
Iron	92.0
Carbon	3.5
Manganese	1.0
Silica	2.5
Copper	1.0

and chemical properties of these compounds are summarized with their maximum contaminant levels (MCLs) in Table 3.4.

3.1.3.2 Herbicides

Two herbicides, alachlor and metolachlor, and their dechlorination by-products (acetyl alachlor from alachlor and MBP from metolachlor) were used. Alachlor (94% purity) and acetyl alachlor (98% purity) were obtained from Monsanto Corporation (St. Louis, MO). Novartis Crop Protection donated the metolachlor (97.3% purity) and the MBP (99% purity). Physical and chemical properties of these compounds are summarized with their MCLs in Table 3.5.

3.1.3.3 Zinc

Granular zinc metal (97.8% purity) was obtained from Fisher Scientific.

3.2 CHEMICAL ANALYSIS OF FOUNDRY SANDS

3.2.1 Water Leach Tests

A water leach test was conducted on each foundry sand as required for characterization in Wisconsin Administrative Code Section NR 538. ASTM Method D 3987 was followed.

A 70-g sample of air-dried foundry sand and 1400 mL of DI water were placed in a Mason jar having a Teflon® closure. The jar was tumbled for 18

Table 3.4. Properties of Chlorinated Hydrocarbons Used in the Study and Corresponding Maximum Contaminant Levels (MCLs) (USEPA 1990).

Compound	Chemical Formula (Molecular Weight)	Melting/Boiling Point (^{0}C)	Density (g/mL)	Water Solubility (mg/L)	MCL (mg/L)
Vinyl Chloride	C_2H_3Cl (62.498)	-153.7/-13.9	0.9106	1100	0.002
1, 1-DCE	$C_2H_2Cl_2$ (96.944)	-122.1/31.7	1.213	2250	0.007
Trans-1,2-DCE	$C_2H_2Cl_2$ (96.944)	-50/47.5	1.257	6300	0.1
Cis-1,2-DCE	$C_2H_2Cl_2$ (96.944)	-80.5/60	1.284	800	0.07
TCE	C_2HCl_3 (131.389)	-86/86.7	1.462	1100	0.005

Table 3.5. Properties of Alachlor and Metolachlor and Corresponding Maximum Contaminant Levels (MCLs) (Chesters et al. 1989).

Compound	Chemical Formula (Molecular Weight)	Melting/Boiling Point (^{0}C)	Density (g/mL)	Water Solubility (mg/L)	MCL (mg/L)
Alachlor	$C_{14}H_{20}Cl\,NO_2$ (269.77)	(39.5-41.5)/100	1.133	240	0.0005
Metolachlor	$C_{15}H_{22}ClNO_2$ (283.79)	N.A.[a] /100	1.085	530	0.015

[a] N.A. = Not applicable.

hours at 22 ^{0}C at a speed of 29 rpm. After mixing, the jar was allowed to settle for 5 min. An aqueous sample was then extracted by vacuum filtering through a 0.45-μm glass fiber filter. The extract was acidified below pH 2 for preservation using nitric acid.

The aqueous samples were analyzed within 24 hrs using inductively coupled plasma mass spectrometry (ICP-MS) at the Soil and Plant Laboratory at the University of Wisconsin-Madison.

3.2.2 Total Elemental Analyses

3.2.2.1 Inorganic Analyses

An acid digestion was conducted on each foundry sand following USEPA Method 3051 to measure the total concentration of metals. A 0.5-g sample of foundry sand was digested in 10 mL of concentrated nitric acid for 10 min using a microwave oven. Fluorocarbon digestion vessels were used. Calibration of the microwave equipment is described in Appendix A.

Groups of six vessels were evenly located on the turntable in the microwave oven. When less than six vessels were used for digestion, the remaining vessels were filled with nitric acid to ensure that the energy delivered was similar to that applied when six specimens were digested. The vessels were irridated at 574 W for 10 min.

Concentrations of heavy metals in the digestions were measured by atomic adsorption using a Varian® SpectrAA 800 following USEPA Method SW

846 7000A. Solids and suspended materials were removed using a 0.45-μm glass fiber filter. The filtered samples were acidified with HNO_3 to pH less than 2. Calibration standards were prepared by diluting stock standard solutions purchased from Fisher Scientific, Inc. The calibration standards were acidified using HNO_3 to simulate conditions used for the samples. Calibration of the SpectraAA began with a blank and proceeded toward the highest concentration.

Concentration of a metal in a liquid sample (C in μg/L) was calculated by:

$$C = A\frac{(D+B)}{D} \tag{3.1}$$

where A is the concentration (μg/L) of metal in a diluted aliquot, B is the volume of the acid blank matrix used for dilution (mL), and D is the volume of the aliquot (mL).

For solid samples, the concentration (C_s in μg metal/kg soil) was computed as:

$$C_s = \frac{E\,V}{W} \tag{3.2}$$

where E is the concentration (μg/L) of metal in the digested sample from the calibration curve, V is the final volume of the diluted sample, and W is the weight of the sample (g).

Interference effects were compensated by using standard additions. Known amounts of standard were added to one or more aliquots of the sample solution. Standard solutions containing different known quantities of the analyte were prepared and then added to the sample solution. Additions were prepared so that the resulting concentrations were approximately 50, 100, and 150% of the expected absorbance from the endogenous analyte in the sample. The difference of the point zero absorbance and no addition absorbance of the abscissa is the endogenous concentration of the analyte in the sample. Graphs of the standard additions are in Appendix A.

Eh was measured using a Corning® Model Eh electrode. The electrode was calibrated using a ferrous-ferric reference solution with a response of 475±30 mV following ASTM Method D 1498. pH was measured with a Corning® pH electrode. The pH meter was calibrated with pH 4.0, 7.0, and 10.0 standards.

3.2.2.2 Polyaromatic Hydrocarbon Analyses

The amount of polynuclear aromatic hydrocarbons (PAHs) in each foundry sand was determined by the Wisconsin State Laboratory of Hygiene. A sample of each foundry sand was collected and stored in a 1-L sample jar provided by the State Laboratory of Hygiene. After sampling, the jars were placed in insulated sample boxes packed with ice. These boxes were delivered to the State Laboratory of Hygiene within 2 hours.

PAHs were extracted from the samples following USEPA Method 3540C with a Soxhlet extractor (40 mm ID, with 500-mL round bottom flask). The extract was analyzed by high performance liquid chromatograph (HPLC) using ultraviolet and fluorescence detectors following USEPA Method 8310C. A Hewlett-Packard 1090 Liquid Chromatograph equipped with an Envirosep-PP column was used for the analyses. The length of the column was 4.6 m and the inside diameter was 150 mm. A 40:60 mixture of acetonitrile and DI water was introduced into the column for 5 min followed by 100% acetonitrile for 25 min at a flow rate of 1.57 mL/min. A 25 μL sample was injected and the column temperature was 35^0 C.

3.3 BATCH SORPTION TESTS

Batch adsorption tests were conducted to determine the sorption capacity of foundry sands for TCE, alachlor, metolachlor, hexavalent chromium, and zinc. The method that was used depended on the contaminant being considered.

3.3.1 Sorption of TCE

3.3.1.1 Batch Procedure for TCE

A series of batch tests was initially conducted to determine the required duration of tumbling and sorption kinetic behavior of TCE (35 mg/L) on foundry sands. The sands were selected to provide a broad range of TOC (0.8% to 4.0%) and clay contents (0% to 13%). Vials with identical contents (5 g) were tumbled for various times and TCE concentration was measured at a designated sampling time.

TCE concentrations during the serial batch sorption tests are shown in Fig. 3.2. The rate of adsorption is highest at the beginning of the test, and diminishes as the test continues. After 16 hours, the concentrations cease decreasing when corrected using the control concentrations. The results are

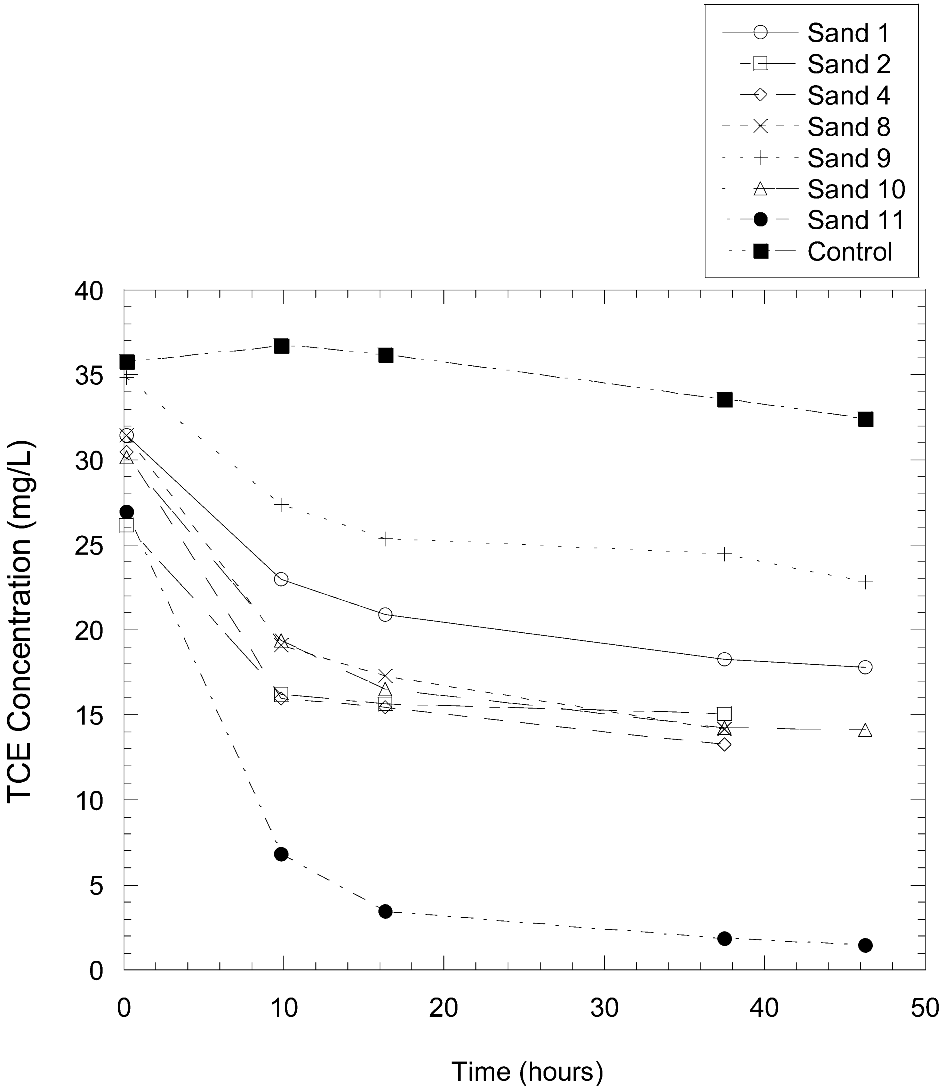

Fig. 3.2. TCE Concentrations During Serial Batch Kinetic Tests with Foundry Sands.

explained in Section 5. Nevertheless, a tumbling time of 24 hr was used for all subsequent tests to ensure equilibrium was attained.

For the batch sorption test with TCE, the amount of adsorbent (i.e., the foundry sand) was maintained constant (5 g) while the initial concentration of TCE was varied between 1 and 30 mg/L. Aqueous solutions containing TCE were placed along with the foundry sand into 40 mL Teflon® bottles, which were sealed with Teflon® caps. The bottles were tumbled at 30 rpm. Aqueous solutions with no adsorbent (i.e., foundry sand) were used as controls to estimate losses. Final concentrations of these controls were assumed to be the initial concentration of the mixtures to account for losses during the test (Zytner 1991). All samples and controls were tumbled at 30 rpm and centrifuged to maintain procedural similarities (Zytner 1991).

After tumbling, the liquid and solid phases were separated using a centrifuge. To determine the required time to complete phase separation, several different centrifuge times (i.e., 5, 10, 30, and 60 min) were tested with a fixed centrifuging speed of 8000 rpm and temperature of 0 ^{0}C. Results of these tests are shown in Fig. 3.3. The TCE concentration decreased from 7.9 to 7.5 mg/L as the centrifuge time increased to 10 min, but remained constant thereafter. As a result, all samples were centrifuged for at least 10 min.

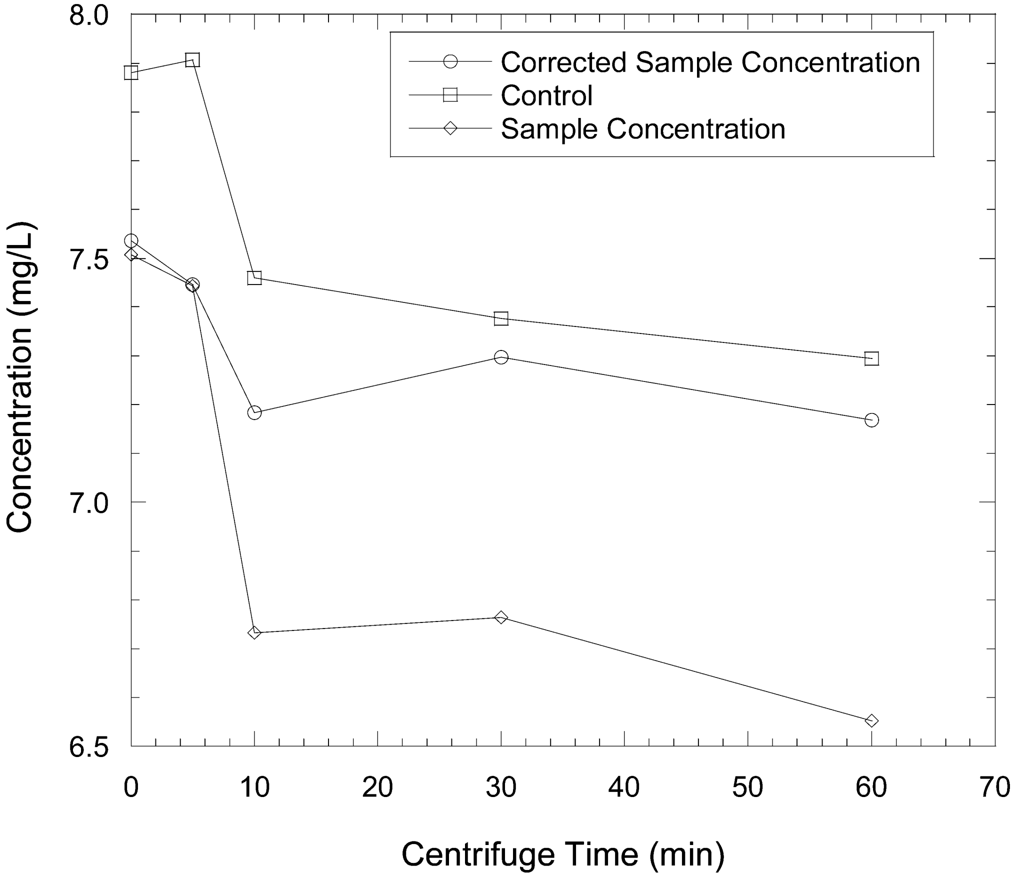

Fig. 3.3. TCE Concentrations as a Function of Centrifuge Time.

3.3.1.2 Analysis Procedure for TCE

Concentrations of TCE were measured using a Varian 3600 gas chromatograph (GC) equipped with an OI analytical discrete purging multisampler (DPM-16), an OI analytical multiple heater controller (MHC-16), and a Model 4560 purge-and-trap sample concentrator. A Supelcowax-10 megabore column (60 m × 0.25 mm inside diameter) and flame-ionization detector (FID) were installed on the GC.

Standards for calibration of the GC were prepared gravimetrically from TCE stock solution. Primary stock solutions were prepared by adding TCE in a 10 mL volumetric flask containing purge-trap grade methanol. Secondary stock solutions were prepared by diluting the primary stock solutions with purge-trap grade methanol. Type I DI water was added to the sampling tubes using a 5-mL glass syringe. A 100-μL aliquot of secondary stock solution containing an appropriate concentration of the calibration standard was then collected with a gas-tight syringe and directly injected into the sampling tubes. Similarly, a 10-μL internal standard was injected into the sampling tubes. For TCE analyses, toluene was used as an internal standard. All calibration curves were based on three standards prepared over the range of expected concentrations. Concentrations of 1, 5, 10, and 40 mg/L were used.

Supernatant liquid from the batch tests was sampled using a 100-μL gas-tight syringe and then directly injected into the multisampler tubes. To ensure complete purging, the multisampler tubes were heated to 75 ^{0}C for 2 min before purging and for 11 min during purging.

The column temperature was held at 40 ^{0}C for 2 min and then raised to 50 ^{0}C at a gradient of 1.0 ^{0}C/min. The temperature was then increased to 225 ^{0}C at a gradient of 40.0 ^{0}C/min and then held for 2.5 min to remove any residuals in the column. Other parameters used in the analysis followed USEPA Methods 502.2 and 524.2.

3.3.1.3 Data Analysis for TCE

Partition coefficients for TCE, alachlor, metolachlor, hexavalent chromium, and zinc were obtained by fitting the data to linear and Freundlich isotherm models. Each model was fitted to the data using a least-squares algorithm. The linear isotherm model is:

$$C_s = K_p\, C_e \tag{3.3}$$

where C_s is the concentration of adsorbate in the soil (mg/kg), C_e is the equilibrium concentration of the solution (mg/L), and K_p is the partition coefficient for the linear model (L/kg). The Freundlich model is:

$$C_s = K_f C_e^{1/n} \tag{3.4}$$

where K_f is the Freundlich partition coefficient and 1/n is a dimensionless constant. The Freundlich parameter, 1/n, describes the affinity of adsorbate for the foundry sand. If 1/n is greater than unity, the adsorbate has greater affinity for foundry sand as the equilibrium concentration increases.

3.3.2 Alachlor and Metolachlor

3.3.2.1 Serial Batch Kinetic Tests

Serial batch sorption tests for alachlor and metolachlor were conducted to determine an adequate mixing time to achieve equilibrium, and to obtain rate data regarding reduction of alachlor and metolachlor. The foundry sands were selected to provide a broad range of TOC (0.8% to 4.0%) and clay contents (0% to 13%). Bottles containing identical contents (5g) were tumbled for various times and concentration was measured at a designated sampling time.

Concentrations for alachlor and metolachlor during the serial batch kinetic tests are shown in Fig. 3.4. The data are analyzed in Section 3.4.2.2. The rate of sorption is highest at the beginning of the test, and decreases as the test continues. The alachlor concentrations became stable at about 5 hr, whereas approximately 24 hrs was required to reach equilibrium for metolachlor. Based on the results of these tests, a mixing time of 24 hrs was used to ensure equilibrium for alachlor and metolachlor.

3.3.2.2 Batch Sorption Tests

Batch sorption tests conducted with foundry sand and alachlor or metolachlor were performed using 2–7 g of sorbent (i.e., foundry sand). The concentration of sorbate (i.e., alachlor or metolachlor) was held constant. Other aspects of the tests were the same as those used for TCE (see Sec. 3.3.1.1).

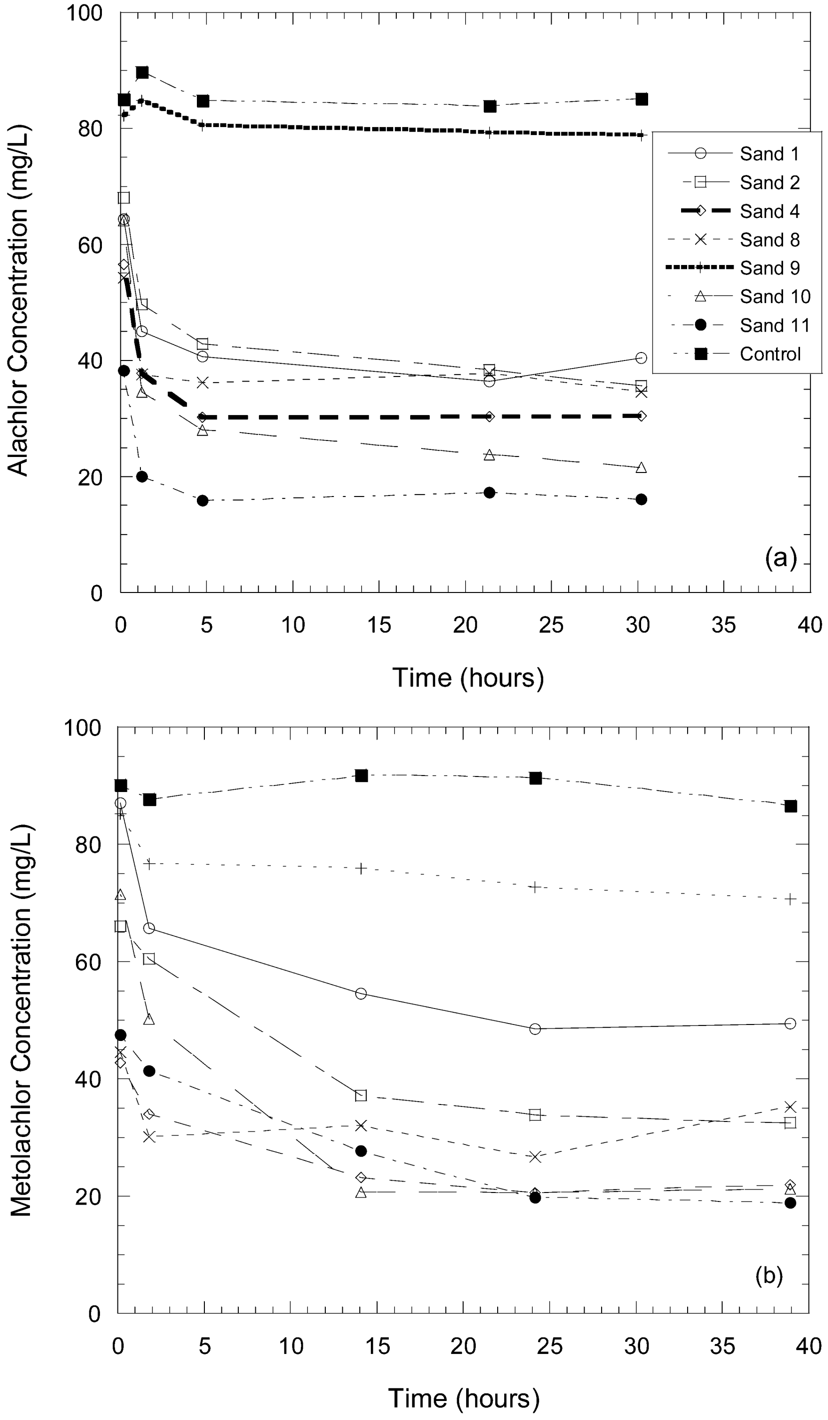

Fig. 3.4. Concentrations of (a) Alachlor and (b) Metolachlor During Serial Batch Kinetic Tests.

A Varian 3600 GC equipped with an electron capture detector (ECD) and a J&W Scientific DB-1 column (30 m × 0.25 mm) was used to measure the aqueous concentrations of alachlor and metolachlor. A typical chromatogram is shown in Fig. 3.5. A 1-μL of sample was extracted using a 10-μL gas-tight syringe and manually injected into the GC. The temperature of the injector was 225 ^{0}C, and for the detector it was 300 ^{0}C. The temperature of column was held at 70 ^{0}C for 2 min and increased to 240 ^{0}C at a rate of 25 ^{0}C/min. After 2 min of holding, the temperature was raised to 265 ^{0}C at a rate of 3 ^{0}C/min, and then was maintained for 6 min to remove any residuals in the column.

The samples were prepared for analysis using the method described in Koppensteiner (1998). A 2-mL sample of solution was extracted into 2 mL of methylene chloride and then mixed for 1 min with a vortex mixer. A gas-tight syringe was used to transfer 1 mL of solution (i.e., methylene chloride) into an autosampler vial with an open-top closure and a Teflon®-lined silicone septa. A 1-μL sample was extracted using a 10-μL gas-tight syringe, and then injected manually into the GC. Recovery factors for the methylene chloride extraction procedure determined by extracting alachlor and metolachlor stock solutions of known concentration (50 mg/L) were 104% and 102%, with a standard deviation of 6.3% and 8.1%, respectively. Method detection limits (MDL) for alachlor and metolachlor were 0.5 mg/L and 0.7 mg/L, respectively.

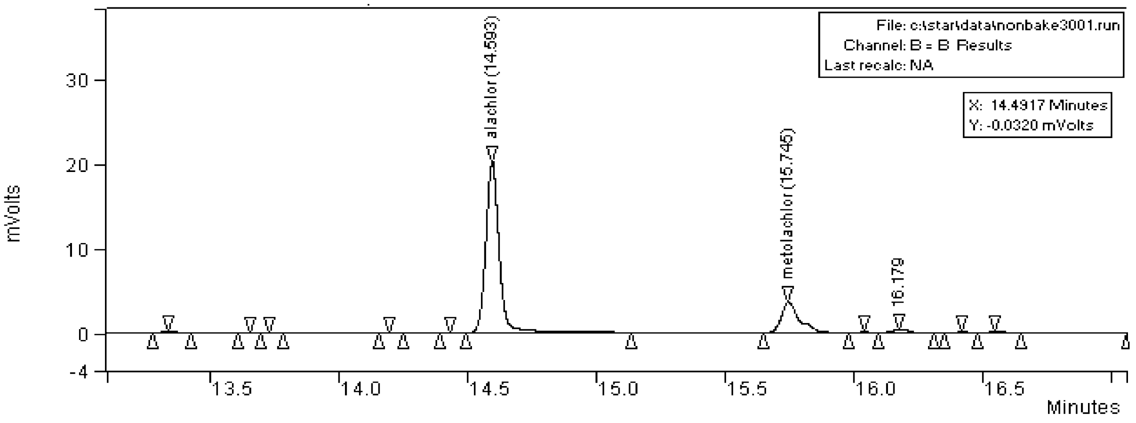

Fig. 3.5. Sample Chromatogram for Batch Sorption Test Using Varian 3600 Gas-Chromatograph Equipped with an Electron Capture Detector. Sand 11 was Used.

3.3.3 Zinc

Serial batch kinetic tests were performed to assess sorption kinetics (i.e., rate of sorption and amount of mass removed) for zinc when foundry sands are used as reactive media. Serial batch kinetic tests were conducted using Sands 1, 4, 10, 11, 12, and Peerless iron. The sands were selected to provide a broad range of TOC and clay content. Three different solution pHs were selected as initial pHs (i.e., 2.6, 3.0, and 4.8). The initial zinc concentration was 100 mg/L.

The procedure described in Sec. 3.3.1.1 was used for the sorption tests with zinc. Aqueous concentrations of zinc were measured using a Varian® SpectrAA 800 following USEPA Method 7950. A 1.000 g of analytical reagent grade zinc metal was dissolved in 10 mL of concentrated nitric acid, and diluted to 1 L with Type I DI water. Calibration standards were prepared by diluting stock solution with Type I DI water. Additional concentrated nitric acid was added in the calibration standards to balance the acid concentration (1% acid by volume). All samples were also balanced with nitric acid to contain 1% acid by volume. The MDL of zinc was 0.01 mg/L.

No pH buffer was used. The initial pH of the solution was adjusted with 1.0 M HNO_3 and 1.0 M NaOH. Zinc solution used for the batch tests was prepared by dissolving $ZnCl_2$ in DI water.

3.4 BATCH DEGRADATION TESTS

3.4.1 TCE

Batch tests were performed to evaluate the rate of degradation of TCE in aqueous solution in the presence of foundry iron and Peerless iron. Foundry iron or Peerless iron (1, 2, 4, 8 g) was placed in 40 or 50 mL glass VOC bottles, which were then filled with a solution. Glass bottles and controls (i.e., bottles with no iron particles) were loaded on a tumbler, which was rotated at 30 rpm. A sample was taken to analyze the aqueous TCE concentration at a specified time. A 100-μL sample was extracted using a gas-tight syringe, and injected into a multi-sampler of GC. Other elements of the test are same as those of Sec. 3.3.1.2.

A first-order decay model with instantaneous sorption from Koppensteiner (1998) was used to find a bulk reaction rate constant and the partition coefficient for TCE. The model is:

$$C_{aq}(t) = \frac{C_0}{R} \exp\left(\frac{-K_{obs}\, t}{R}\right) \tag{3.7}$$

where C_{aq} is the concentration of TCE in the batch reactor at time t (mg/L), C_0 is initial TCE stock concentration (mg/L), R is a retardation factor to account for sorption, and K_{obs} is a bulk first-order decay rate constant (hr^{-1}). Eq. 3.7 was fitted to the data using a least-squares algorithm.

Results for the dechlorination byproducts (i.e., vinyl chloride, 1,1-DCE, trans-DCE, and cis-DCE) are included in Appendix B.

3.4.2 Alachlor and Metolachlor

3.4.2.1 Sample Preparation and Iron Extraction

Batch degradation tests with alachlor and metolachlor were conducted using the same procedure developed for the TCE degradation tests (see Sec. 3.4.1.1). Samples were prepared using methylene chloride following the method described in Sec. 3.3.2.2.

After collecting an aqueous sample (2 mL) for concentration analysis, the remaining solution and iron were placed in a Buchner funnel and vacuum filtered through a Whatman No. 5 qualitative glass microfiber filter to conduct a mass balance analysis. After the filter and iron were dried by vacuum filtering for 5 min, the filter and iron were placed into the original VOC vial and 10 mL of a 50:50 (v/v) mixture of hexane and acetone was added to extract the sorbed analytes. The vial was shaken for 10 min, allowed to settle for 5 min, agitated again for 20 min, and again allowed to settle for 5 min. A gas-tight syringe was then used to collect a 2 mL aqueous sample from the vial. A Teflon® syringe filter was used to filter the sample. The filtrate was placed in an autosampler vial and stored in a refrigerator at 4 ^{0}C prior to analysis.

3.4.2.2 Chemical Analysis

A Varian 3400 GC with a flame ionization detector (FID) and DB-5 column was used to analyze for alachlor, metolachlor, and their chlorinated by-products. The temperature of the detector was set at 300 ^{0}C and that of the injector was set at 210 ^{0}C. Air was used as the carrier gas at a flow rate of 300 mL/min. Helium was used as the make-up gas using a flow rate of 30 mL/min.

The column temperature was maintained at 110 ^{0}C for 6 min and raised to 170 ^{0}C at 20 ^{0}C/min until 240 ^{0}C was reached, where it was held for 2 min to remove any residuals in the column. The total run time was 25 min.

The method detection limits (MDL) for alachlor, alachlor by-product, metolachlor, and metolachlor by-product (MBP) were 0.9, 1.1, 1.0, and 0.8 mg/L, respectively. A typical sample chromatogram is shown in Fig. 3.6.

3.4.2.3 Data Analysis

To determine partition coefficients for the parent compound and the daughter product, and the first-order decay rate constant, data obtained from batch degradation tests were fitted to analytical solutions provided by Eykholt (1999). The model for the parent compound is:

$$C_p = \frac{C_{p,0}}{R_p}\left[\exp\left(\frac{-K_{obs}\,t}{R_p}\right)\right] \tag{3.15}$$

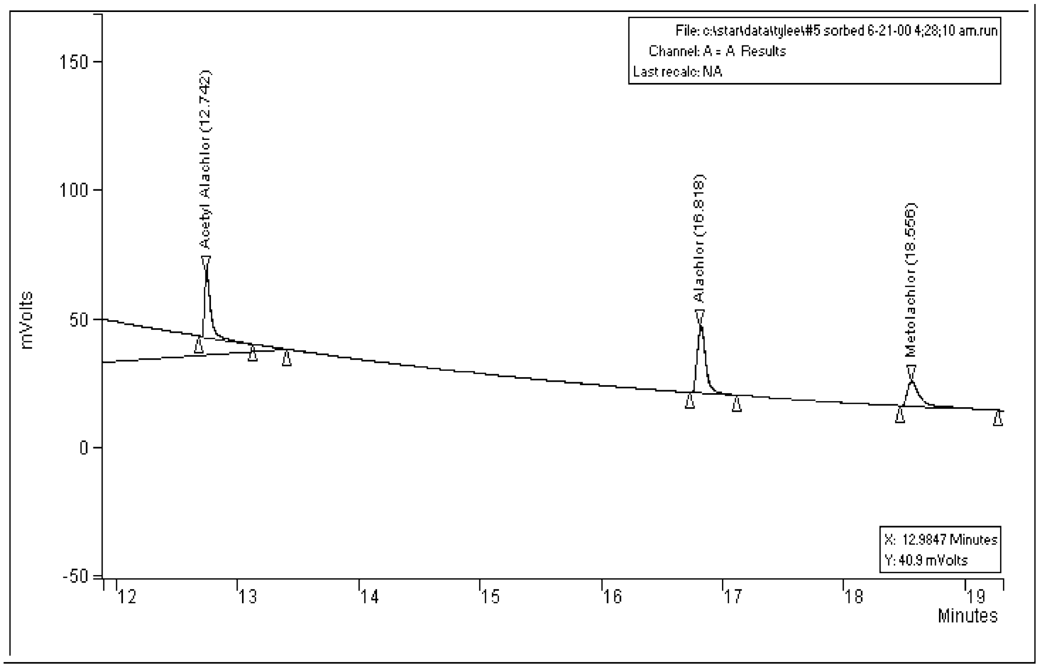

Fig. 3.6. Sample Chromatogram for Alachlor and Acetyl Alachlor using Varian 3400 Gas Chromatograph Equipped with a Flame Ionization Detector.

where $C_{P,0}$ = initial concentration of the parent compound, and R_p is the retardation factor for the parent compound. For the daughter compound, the model is:

$$C_d = \frac{C_{p,0}}{R_d}\left[1 - \exp\left(\frac{-K_{obs}\, t}{R_p}\right)\right] \qquad (3.16)$$

where R_d is the retardation factor for the daughter compound.

3.4.3 Heavy Metals

Degradation tests for Zn followed the procedure described in the Sec. 3.4.1.1. The chemical analyses and the data evaluation were also conducted following the methods in the Sec. 3.4.1.

3.5 COLUMN TESTS

Column tests were conducted to determine transport parameters (i.e., partition coefficients, rate constants, and dispersion coefficients) under more realistic conditions for foundry sands, iron, and mixtures of foundry sand and iron. Two types of tests were conducted with TCE solutions: constant hydraulic gradient tests and constant flow rate tests. Only constant flow rate tests were used for solutions containing alachlor, metolachlor, and zinc.

3.5.1 Experimental Set-up

Schematics of the column test set ups are shown in Fig. 3.7 (constant head test) and 3.8 (constant flow rate test). The reactive medium was tamped

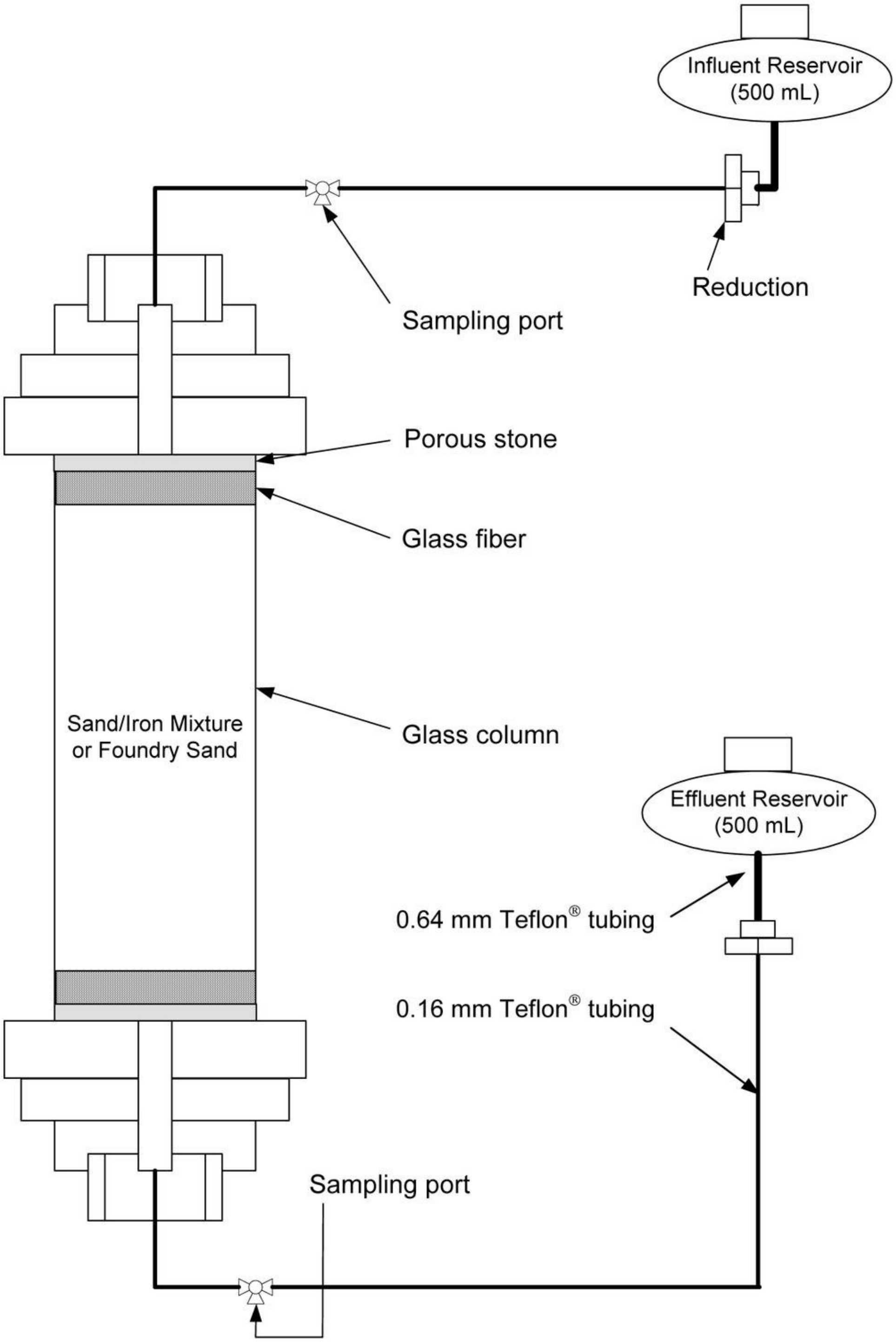

Fig. 3.7. Schematic of a Constant Head Test.

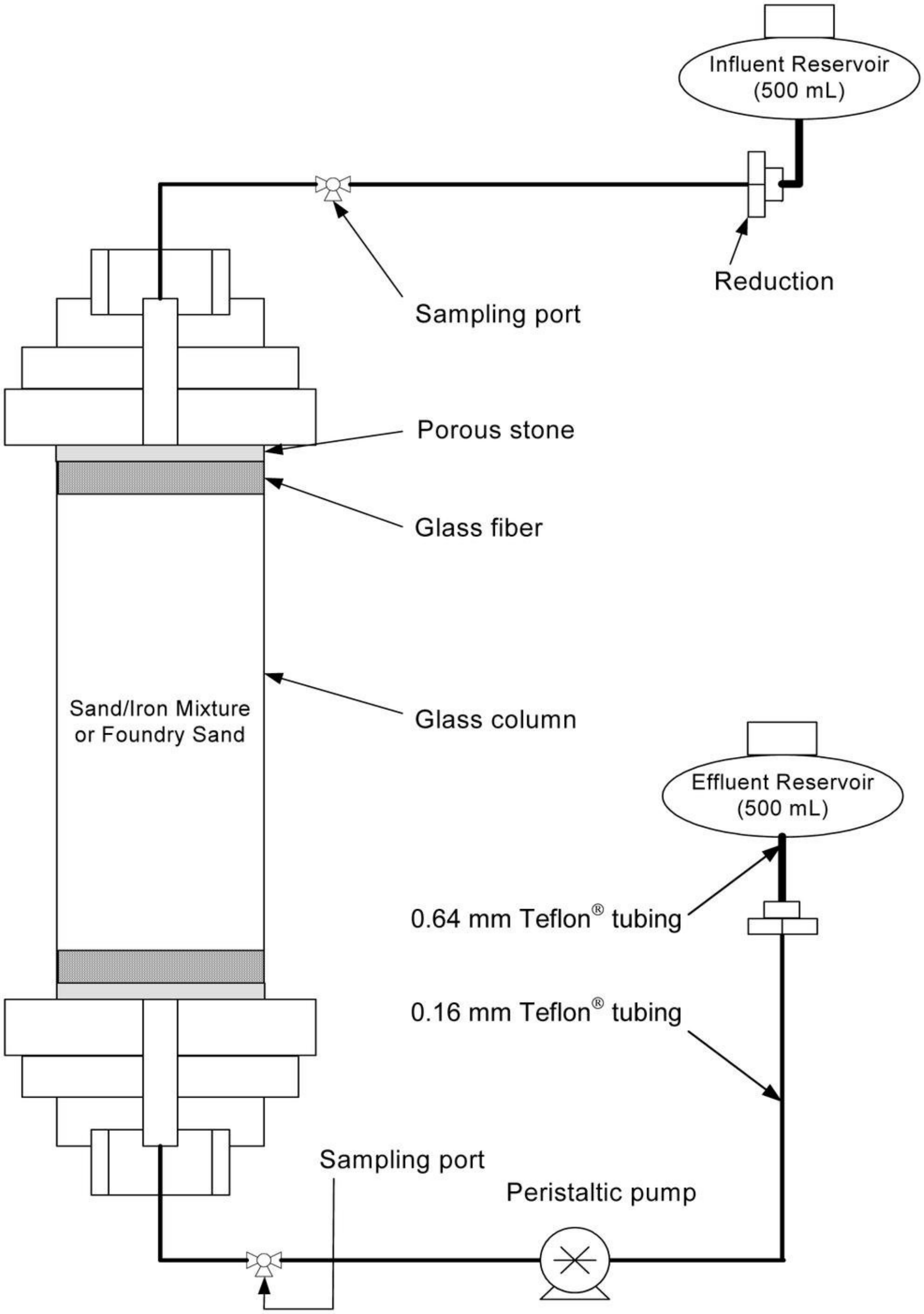

Fig. 3.8. Schematic of a Constant Flow Rate Test.

into a glass column in three layers to a dry density expected under field placement conditions. Teflon® adapters and porous stones were attached at the both ends of the column. A glass fiber filter was placed on the porous stone to prevent clogging.

The influent was prepared from stock solution diluted in a volumetric flask containing DI water and stirred for 24 hrs with a magnetic stirrer. The DI water was purged beforehand with N_2 to remove O_2, and then mixed with sodium azide (0.1% by weight) to prevent biological activity. To evaluate losses during preparation, aliquots of TCE (100-μL) and alachlor and metolachlor (1-μL) were injected into the GC and analyzed following the methods in Sec. 3.4.2.1. The variation was ±4% of expected value for TCE and ±5% for alachlor and metolachlor, which suggests that losses were minimal.

For the constant head tests, solution was introduced into the column from the influent Teflon® reservoir. The solution was introduced from the top to the bottom. A constant head drop was maintained by separating the influent and effluent bags a constant distance. The hydraulic gradient ranged from 4 to 28.

For the constant flow rate tests, solution was introduced into the columns at a constant flow rate using a peristaltic pump. All contact parts in the pump were made of Teflon®, except for the tubing, which was Viton®. Silicon tubing was not used because it exhibited unacceptable losses. A loss of approximately 10% occurred when TCE passed through the Viton® tubes, but a fairly constant influent concentration was maintained during testing. Loss in the tubing was less than 3% for the alachlor and metolachlor solutions.

A control column test was conducted to assess sorption on the tubes and glass column. Torpedo sand was used for control tests conducted with TCE. Silica sand was used for the herbicides. Torpedo sand is classified as poorly graded sand (SP) in the Unified Soil Classification System (USCS). The uniformity coefficient and coefficient of curvature are 2.6 and 0.84. Silica sand is a poorly graded sand (SP) with a uniformity coefficient of 2.0 and coefficient of curvature of 1.39. The sands were washed with DI water until any visible impurities were removed, and then were packed in the glass column. The test solution was then introduced using a peristaltic pump. The effluent concentrations of compounds were normalized to the concentrations at the influent reservoir. The breakthrough curve for TCE is shown in Fig. 3.9 and those for the herbicides are shown in Fig. 3.10. The porosity was 0.33 and seepage velocity was 1.02×10^{-2} cm/s for the column using TCE solution. For the column using the alachlor solution, the porosity was 0.40 and seepage velocity was 3.08×10^{-3} cm/s. The porosity was 0.36 and seepage velocity was 2.93×10^{-3} cm/s for the column with the metolachlor solution.

Partition coefficients for TCE, alachlor, and metolachlor were backcalculated from the retardation factors, which were obtained by fitting Eq. 3.18 to the data. Discussion of the fitting procedure is in Sec. 3.5.3. A higher partition coefficient was obtained for alachlor (1.56 L/kg) than for metolachlor

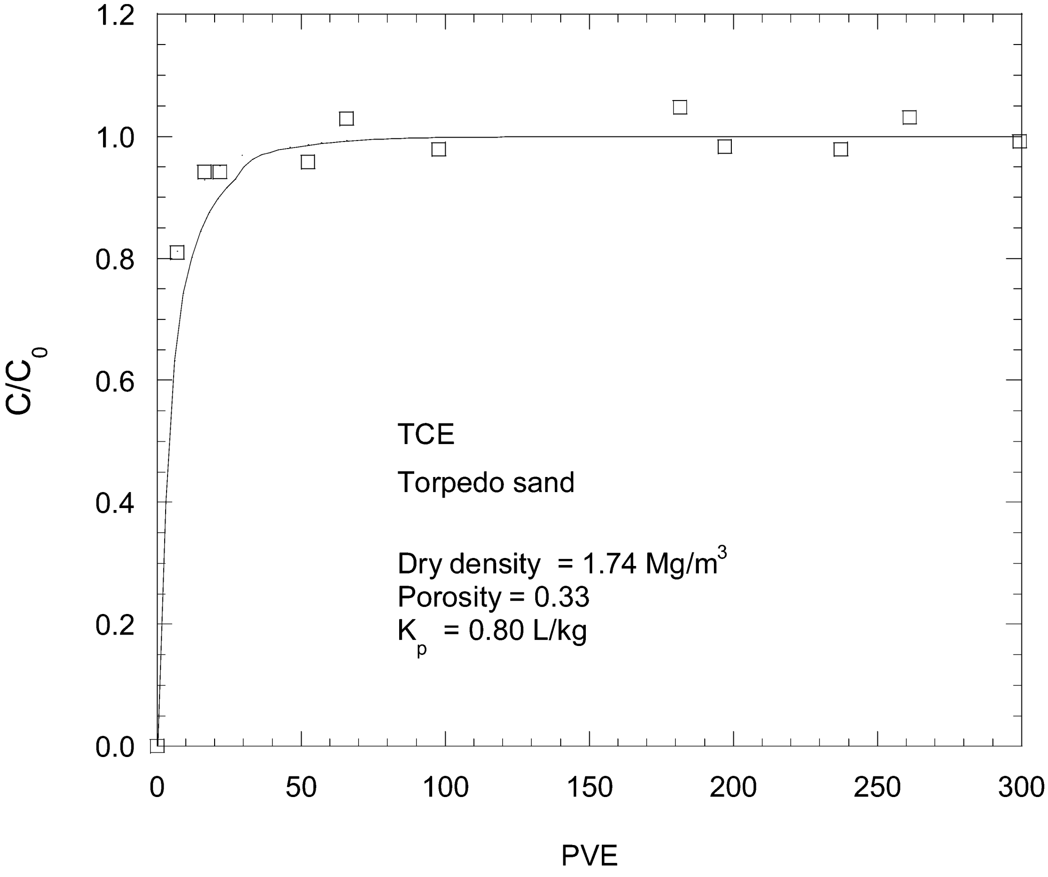

Fig. 3.9. TCE Concentrations for Control Column Test Containing Torpedo Sand.

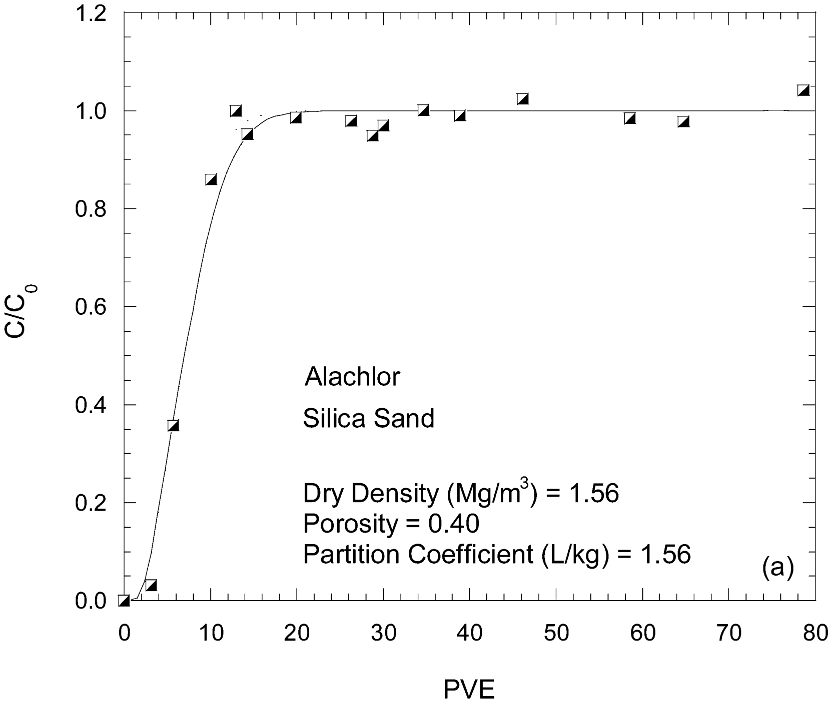

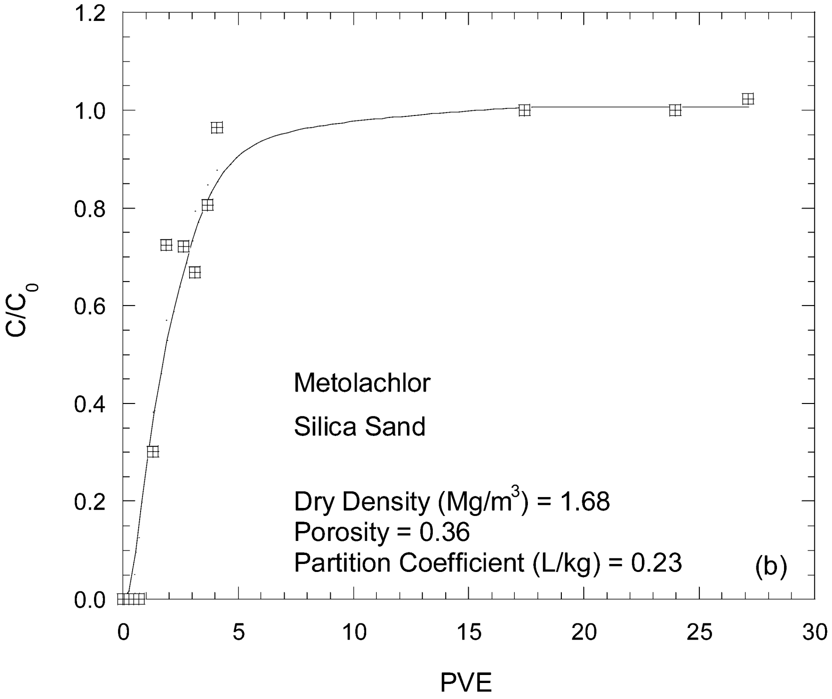

Fig. 3.10. Concentrations of (a) Alachlor and (b) Metolachlor for Control Column Tests Containing Silica Sand.

(0.23 L/kg). The partition coefficient for TCE was 0.79 L/kg. All of the breakthrough curves reached steady state at $C/C_0 = 1$, indicating that no loss was occurring.

The modest amount of partitioning that occurred is believed to be due to organic carbon in the media. To assess this possibility, partition coefficients (L/kg) for TCE, alachlor, and metoalchlor were estimated by:

$$K_p = f_{OC} 10^{A \log K_{ow} + B} \tag{3.17}$$

using measured values of TOC for the torpedo and silica sands. In Eq. 3.17, f_{OC} is weight fraction of organic carbon in the medium, K_{OW} is the octanol-water partition coefficient, and A and B are empirical constants. The empirical constants, A and B were set at 0.98 and –0.26, as reported by Shimizu et al. (1992). The TOC for silica sand and torpedo sand were found to be 0.2% and 0.4%, respectively.

The K_p estimated for alachlor and metolachlor were 0.4 L/kg and 2.6 L/kg, respectively, whereas K_p for TCE was 0.66 L/kg. The measured K_p for alachlor was almost four times greater than the estimated K_p. In contrast, the measured K_p for metolachlor was smaller than the K_p estimated with Eq. 3.17. For TCE, the estimated K_p was close to the measured K_p.

While this analysis doses not confirm that TOC in the sands was responsible for the retardation effect, the reasonable correspondence between the estimated and measured K_p suggests that TOC was likely responsible for sorption. Sorption onto the column may also have contributed to the retardation.

Nevertheless, the K_p from the control tests are small, and thus no correction was made to the results of the column tests with reactive media.

3.5.2 Chemical Analysis

TCE effluent concentrations were measured following the method described in Section 3.3.1.2. For alachlor and metolachlor, the methods described in Section 3.4.2.2 were followed. The methods described in Section 3.3.3 were used for zinc.

3.5.3 Data Analysis

Tracer tests were conducted with D_2O and bromide tracers to determine the porosity of the reactive media. Tracers were added to the influent after the TCE breakthrough curves were complete. The concentration of bromide was measured using an Orion® ion-selective probe. Concentration of D_2O was measured using a refractive index (RI) detector. Tracer tests were only performed on the media tested with TCE. No tests were conducted on media tested with alachlor and metolachlor given their similarity to the media used with TCE.

The column test data were fitted to an analytical solution of the advection-dispersion-reaction equation (ADRE) provided by van Genuchten (1981). The analytical solution, which is derived for the first-type initial (i.e., background concentration is assumed to be zero) and boundary conditions (i.e., the influent concentration is constant and the concentration gradient is zero at great distance from the influent boundary) is:

$$\frac{C(x,t)}{C_0} = \frac{1}{2}\exp\left[\frac{(v-u)x}{2D}\right]\mathrm{erfc}\left[\frac{Rx-ut}{2(DRt)^{1/2}}\right] + \frac{1}{2}\exp\left[\frac{(v+u)x}{2D}\right]\mathrm{erfc}\left[\frac{Rx+ut}{2(DRt)^{1/2}}\right] \tag{3.18}$$

where C(x,t) is the concentration at a given distance and time, C_0 is the influent concentration, v is the seepage velocity, D is the dispersion coefficient, R is the retardation factor, and the variable u is defined as:

$$u = v\left(1 + \frac{4\mu D}{v^2}\right)^{1/2} \tag{3.19}$$

In Eq. 3.19, μ is the bulk first-order degradation rate, which is defined as:

$$\mu = K_{obs} + \beta\frac{\rho_d K_d}{n} \tag{3.20}$$

where K_{obs} is the liquid phase first-order degradation rate constant, β is the solid phase first-order degradation rate constant, ρ_d is the dry density, K_d is the linear partition coefficient, and n is the porosity.

For the steady-state condition with dispersion, the effluent concentration (C_{SS}) for a column of length L is:

$$C_{SS} = C(L,\infty) = \exp\left[\frac{(v-u)L}{2D}\right] \tag{3.21}$$

When dispersion is ignored, the steady-state effluent concentration at L is:

$$C_{SS} = C(L,\infty) = C_0 \exp\left[\frac{-\mu L}{v}\right] \tag{3.22}$$

The hydrodynamic dispersion coefficient (D) obtained by fitting Eq. 3.18 to the column test data is the sum of the mechanical dispersion coefficient (D_m) and the molecular diffusion coefficient (D^*):

$$D = D_m + D^* \tag{3.23}$$

The mechanical dispersion coefficient D_m is related to the seepage velocity via:

$$D_m = \alpha_L v^m \tag{3.24}$$

where α_L is longitudinal dispersivity and m is an empirical constant between 1 and 2. In the column tests, D^* was assumed to be negligible because transport in the columns was dominated by the advection. Thus, α_L was calculated using Eqs. 3. 23 and 3.24 with D = D_m and m assumed to be unity.

3.6 COLUMN LEACH TESTS

3.6.1 Experimental Set-up

Column leach tests were conducted on the foundry sands, torpedo sand, and zero-valent iron. The set-up used for column leach tests on the foundry sands was identical to that shown in Fig. 3.8. Glass columns (200 mm length and 25 mm diameter, or 450 mm length and 25 mm diameter) fitted with Teflon® adapters were used. A constant flow rate was supplied to the bottom of the column by a peristaltic pump. The effluent was collected at the top of the column in Teflon® sampling bags. Two different influent solutions were used: DI water and Madison tap water. Three different flow rates were used for the tests conducted with Madison tap water.

For tests conducted earlier in the testing program, instantaneous concentrations were measured on 1 mL samples collected from the sampling ports. For all other tests, the effluent was allowed to accumulate in a Teflon® sampling bag until approximately 40 mL sample was obtained. A 10 mL sample was then removed from the bag and stored in a 20 mL glass bottle prior to analysis. The remaining effluent in the sampling bag was discarded, and the bag was washed with DI water. Samples collected from the bags represent the average concentration during the accumulation period. In contrast, samples collected from the sampling ports represent the instantaneous concentration at the sampling time.

Samples were acidified with HNO_3 and preserved in a refrigerator at 4^0C before analysis. Metal concentrations were measured using atomic absorption (AA) spectroscopy equipped with a graphite furnace following USEPA Method 7000A.

3.7.2 Data Analysis

Analysis of the column leach test data was conducted using an analytical mass leaching model described by Shackelford et al. (1997) that is based on the instantaneous concentration or the cumulative mass in the effluent. The model is based on the ADRE and assumes instantaneous equilibrium between the solid and liquid phases.

For the cumulative mass approach, the effluent is assumed to accumulate in a reservoir for a given volume of flow (ΔT), which is reported in pore volumes (T). The average concentration of the accumulated effluent is measured, and the mass (Δm) is calculated by multiplying the average concentration (c_e) by the accumulated volume (ΔV_e). The incremental mass that accumulated (Δm) is then normalized to the initial total mass (M_0) in the column, where M_0 is th summation of the mass in solution (m_0) and mass sorbed on the solid phase (m_s). After successive accumulations, the normalized mass accumulation is summed to obtain the normalized cumulative mass leach ratio (LMR).

$$\mathrm{LMR} = \sum \frac{(\Delta m)}{M_0} \tag{3.25}$$

The LMR can be written in the format of the advection-dispersion-reaction-equation (ADRE) as:

$$\mathrm{LMR} = \frac{T}{R} - \frac{1}{2}\left\{\left(\frac{T}{R} - 1\right)\mathrm{erfc}\left(\frac{R - T}{2(TR/P_L)^{1/2}}\right)\right\} + \left(\frac{T}{R} + 1\right)\exp(P_L)\,\mathrm{erfc}\left(\frac{R + T}{2(TR/P_L)^{1/2}}\right) \tag{3.26}$$

where T is non-dimensional time (total pore volumes of leachate), R is the retardation factor, and P_L is the column peclet number.

The concentration-basis solution was used when the instantaneous concentration of leachate was measured. This solution is written as:

$$\frac{C}{C_0}=1-\frac{1}{2}\left\{\operatorname{erfc}\left(\frac{R-T}{2(TR/P_L)^{1/2}}\right)+\exp(P_L)\operatorname{erfc}\left(\frac{R+T}{2(TR/P_L)^{1/2}}\right)\right\} \tag{3.27}$$

Nonlinear least-squares regression analyses were used to fit Eqs. 3.26 and 3.27 to the column leach test data.

3.8 HYDRAULIC CONDUCTIVITY TESTS

Glass columns with a diameter of 25 mm and a length of 200 mm were used to measure the hydraulic conductivity of the foundry sands. Testing was conducted using the constant head procedure using the apparatus shown in Fig. 3.8. Foundry sands were tamped into the glass column by rodding in three layers of equal thickness using 15 strokes or 20 strokes per layer. The number of strokes (15 or 20) was varied to produce different dry densities that bracket placement conditions occurring in the field.

The specimens were then permeated with Madison tap water using hydraulic gradients ranging between 4 and 28. Specimens were permeated until the hydraulic conductivity became steady and inflow equaled outflow.

Results of the hydraulic conductivity tests are summarized in Table 3.6. Hydraulic conductivity is shown as a function of clay content in Fig. 3.11. The hydraulic conductivities range from 2.7×10^{-2} cm/s (Sand 9) to 9.2×10^{-7} cm/s (Sand 11) for low dry density, and generally decrease as the clay content

Table 3.6. Summary of Hydraulic Conductivity Tests Including Dry Density and Clay Content.

Soil	Clay Content (%)	Dry Density (Mg/m^3)		Hydraulic Conductivity (cm/sec)	
		Low	Moderate	Low	Moderate
Sand 1	5.1	1.31	1.48	1.56×10^{-3}	1.00×10^{-4}
Sand 2	7.0	1.34	1.46	2.30×10^{-3}	1.20×10^{-4}
Sand 3	7.5	1.35	1.47	6.00×10^{-4}	6.50×10^{-5}
Sand 4	10.5	1.26	1.49	9.40×10^{-7}	1.40×10^{-7}
Sand 5	8.4	1.34	1.42	2.80×10^{-4}	1.20×10^{-4}
Sand 6	6.6	1.36	1.64	4.00×10^{-4}	7.00×10^{-5}
Sand 7	6.2	1.38	1.5	3.90×10^{-4}	1.40×10^{-5}
Sand 8	7.4	1.38	1.61	3.80×10^{-6}	1.20×10^{-7}
Sand 9	0	1.51	1.65	2.70×10^{-2}	8.60×10^{-3}
Sand 10	4.7	1.34	1.45	5.40×10^{-4}	1.00×10^{-4}
Sand 11	13	1.26	1.41	9.20×10^{-7}	4.40×10^{-7}
Sand 12	4.7	1.32	1.49	1.90×10^{-3}	6.50×10^{-5}

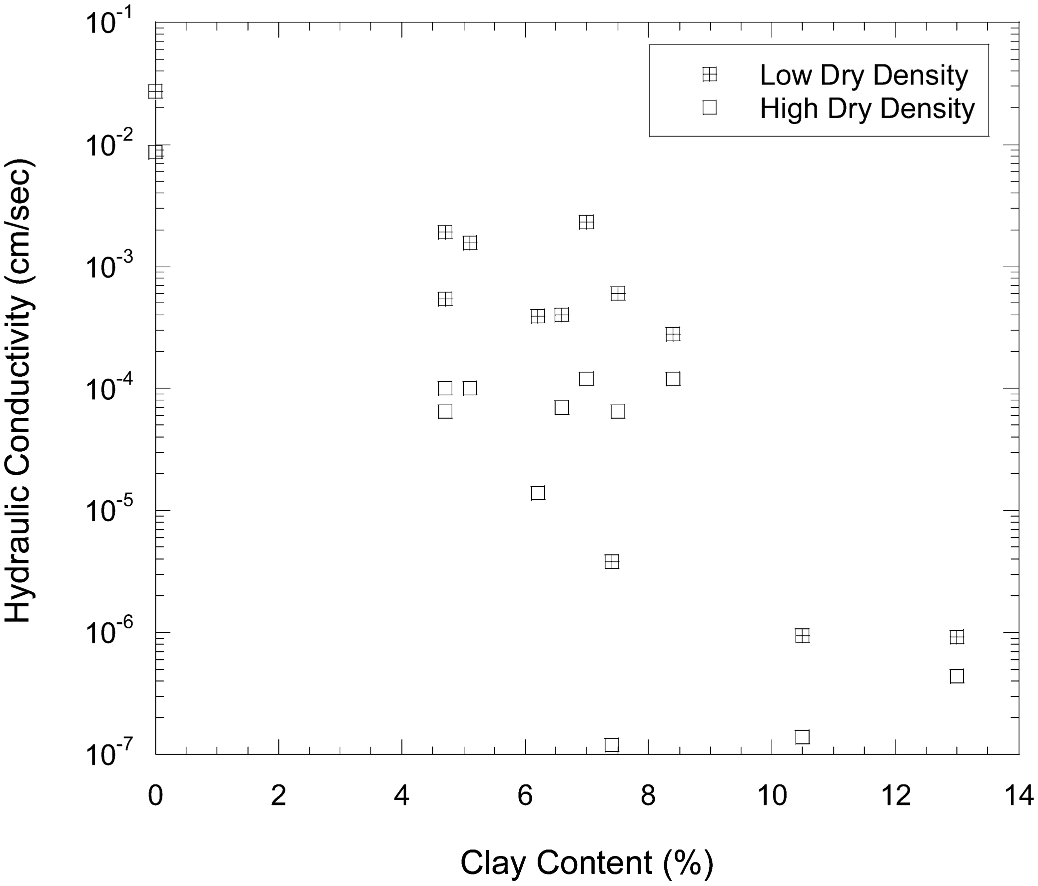

Fig. 3.11. Hydraulic Conductivities of Foundry Sands as a Function of Clay Content and Dry density.

increases. Also, at the same clay content, lower hydraulic conductivity was obtained at higher dry density, which was anticipated.

PRBs typically require that the hydraulic conductivity of the medium be at least that of the aquifer (Starr and Cherry 1994). Thus, foundry sands need to be selected that have hydraulic conductivity consistent with the hydrogeologic setting in which the PRB is to be installed. Most of the sands that were tested are suitable for aquifers with hydraulic conductivity of 10^{-4} cm/s. For more permeable aquifers, granular materials might be added to increase the hydraulic conductivity and reactivity of a foundry sand. This alternative was evaluated by conducting a series of tests with Sand 10. As shown in Fig. 3.12, the hydraulic conductivity increased linearly when Peerless iron was added to Sand 10. A less costly alternative would be to add gravel, crushed glass, or sand to the foundry sand provided additional reactivity was not necessary.

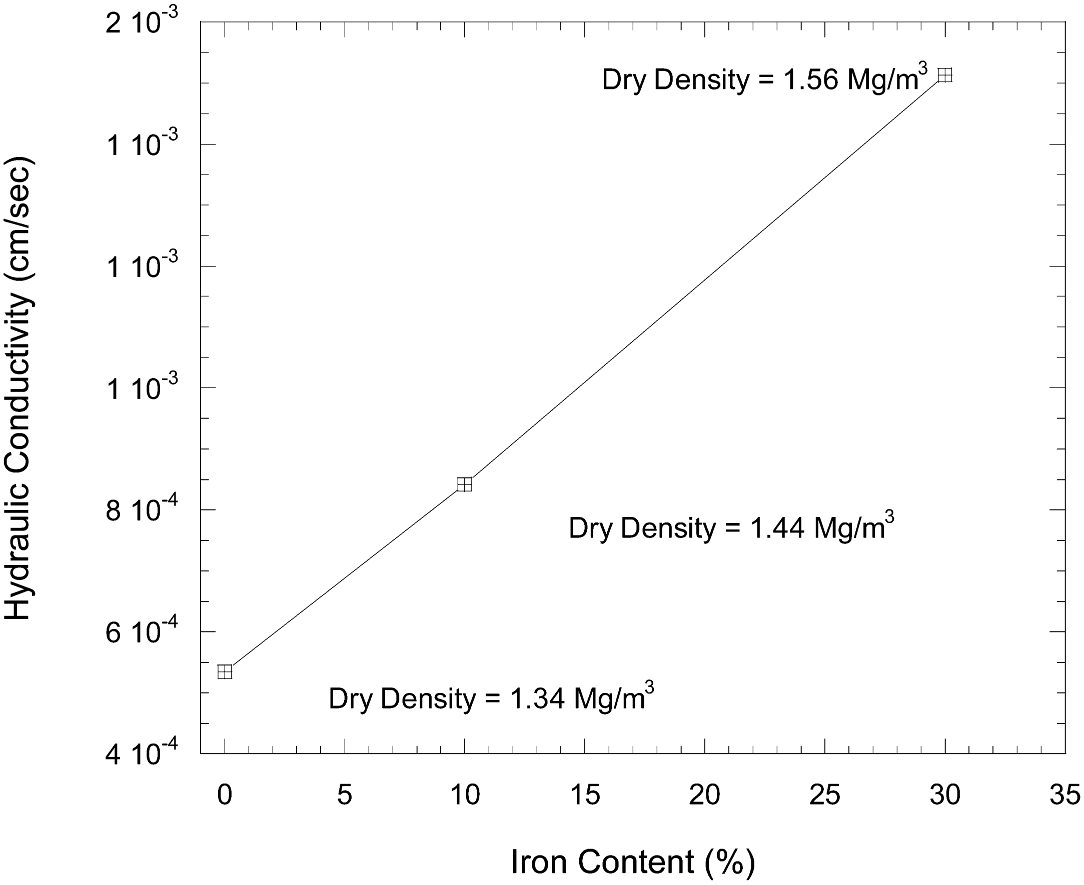

Fig. 3.12. Hydraulic Conductivity of Sand 10 when Peerless Iron was Mixed to Increase the Reactivity and Hydraulic Conductivity.

SECTION FOUR

RESULTS OF WATER LEACH TESTS AND TOTAL ELEMENTAL ANALYSES

4.1 WATER LEACH TESTS

Water leach tests were performed on the twelve foundry sands, Peerless iron, a local fill material, and torpedo sand. The latter three materials were tested to compare concentrations of heavy metals and anions found in other materials commonly placed below the groundwater table with those from the foundry sands. Results of the water leach tests are summarized in Table 4.1 along with the Category 1 standards from NR 538. The standards for Category 1 are shown because foundry sand used as a reactive medium will be placed below the groundwater table. Concentrations for 18 heavy metals and 4 anions were measured in accordance with Category 1 standards in NR 538. Exceedences of the Category 1 standards are shown in bold in Table 4.1.

4.1.1 Heavy Metals

NR 538 requires that the leachate from the foundry sands be analyzed for the following heavy metals if the foundry sand will be placed below the groundwater table: aluminum (Al), antimony (Sb), arsenic (As), barium (Ba), beryllium (Be), cadmium (Cd), total Chromium (Cr), copper (Cu), iron (Fe), lead (Pb), manganese (Mn), mercury (Hg), nickel (Ni), selenium (Se), thallium (Tl), and zinc (Zn).

Table 4.1. Metal Concentrations (μg/L) from Water Leach Tests (Metals) on Foundry Sands, Fill, Torpedo Sand, and Peerless Iron. Numbers in Parentheses Next to Atomic Symbol are NR 538 Cat. 1 Standards in μg/L. Numbers in Bold Indicate Exceedences of Cat. 1 Standard.

Sample	Be (0.4)	Al (1500)	Cr (10)	Mn (25)	Fe (150)	Ni (20)	Cu (130)	Zn (2500)	As (5)
Sand 1	0.1	250.4	1.1	4.4	91.6	1.8	12.4	2.3	3.5
Sand 1[a]	0.1	252.5	1.1	4.6	95.8	1.6	12.3	2.4	4.1
Sand 2	0.1	**1876.0**	1.6	8.1	**658.6**	2.0	13.5	5.7	4.2
Sand 3	0.1	376.0	2.2	2.1	**163.8**	0.9	8.4	2.3	2.6
Sand 4	0.2	**3131.0**	2.5	17.4	**1483.4**	3.1	17.1	8.8	**7.3**
Sand 5	0.1	1257.6	1.9	8.0	**376.2**	3.0	15.4	5.9	4.2
Sand 6	<0.1	859.5	1.0	5.7	**234.0**	2.2	17.9	2.4	1.1
Sand 7	<0.1	183.6	0.5	12.4	**515.0**	1.9	3.2	1.7	1.7
Sand 8	**0.5**	**2060.6**	1.7	7.1	**486.8**	2.4	15.0	2.9	2.1
Sand 9	0.1	240.5	1.7	**66.2**	**415.5**	7.0	11.2	57.0	0.6
Sand 10	<0.1	851.1	1.9	9.6	**256.0**	2.0	20.6	4.4	4.3
Sand 11	0.1	1217.0	2.3	5.7	**342.5**	1.6	12.2	5.0	**7.5**
Sand 12	<0.1	89.4	0.8	2.7	128.2	1.6	13.3	1.1	0.3
Fill	0.2	137.7	1.2	5.7	91.7	2.6	**208.4**	24.0	<0.2
Sand 4[b]	0.1	128.6	1.6	12.1	53.0	10.4	34.6	14.2	**5.4**
Peerless Iron	<0.1	22.0	**13.1**	**136.5**	**230.5**	14.8	9.0	7.1	**6.9**
Torpedo Sand	<0.1	141.84	1.41	3.2	7.72	1.29	3.58	<0.2	2.07

Sample	Se (10)	Mo (50)	Ag (10)	Cd (0.5)	Sb (1.2)	Ba (400)	Hg (0.2)	Tl (0.4)	Pb (1.5)
Sand 1	3.7	3.0	0.0	0.1	0.6	7.8	**1.0**	0.0	0.3
Sand 1[a]	3.6	3.4	<0.02	0.1	0.6	7.9	**1.1**	<0.02	0.4
Sand 2	5.5	3.0	0.2	<0.03	0.2	12.3	**0.8**	0.0	0.9
Sand 3	<2.0	2.2	0.1	0.0	0.4	2.7	**1.1**	0.1	0.2
Sand 4	5.5	5.0	0.1	0.0	**1.6**	18.6	**1.0**	0.0	**1.7**
Sand 5	<2.0	3.3	<0.02	0.1	0.6	14.4	**0.7**	0.0	0.5
Sand 6	5.9	9.9	0.3	0.3	**2.2**	9.1	**1.3**	0.2	**5.1**
Sand 7	<2.0	1.2	0.4	<0.03	0.3	7.0	**0.5**	<0.02	1.4
Sand 8	<4	7.9	3.1	**0.6**	**3.4**	10.3	**0.5**	0.3	**12.2**
Sand 9	<2.0	2.4	0.3	0.4	0.3	11.1	**0.5**	0.1	**5.3**
Sand 10	<2.0	2.9	0.1	<0.03	0.5	10.1	**0.5**	0.0	0.3
Sand 11	<2.0	6.6	0.1	0.1	0.7	6.4	**0.6**	0.0	0.4
Sand 12	<2.0	6.0	<0.02	<0.03	0.2	4.5	**0.4**	<0.02	0.2
Fill	<4	0.3	0.2	1.1	**1.6**	7.1	**1.0**	0.1	**32.1**
Sand 4[b]	<2.0	3.4	0.9	0.4	**1.6**	5.7	**1.1**	0.1	1.1
Peerless Iron	<2	6.8	0.1	**0.5**	**19.4**	24.8	**0.7**	0.3	**15.0**
Torpedo Sand	<2	0.33	<0.02	<0.03	0.18	7.11	**1.1**	0.04	0.08

[a] Duplicate, [b] Admixture with 10% Calcite

For all of the materials that were tested (i.e., foundry sands, fill soil, iron, and torpedo sand), the concentrations of barium (Ba), molybdenum (Mo), nickel (Ni), selenium (Se), silver (Ag), thallium (Tl), and zinc (Zn) are below the NR 538 Category 1 standards. In many cases, the concentrations were below detection limits. In addition, there is no distinct difference between concentrations obtained from the fill soil, the torpedo sand, and the foundry sands.

Concentrations of arsenic (As) and antimony (Sb) occasionally are slightly higher than the Category 1 standards for a few of the foundry sands (Sands 4, 6, 8, and 11) as shown in Table 4.1 and Figs. 4.1 - 4.2. Exceedences for these metals were also obtained for Peerless iron. In fact, the concentrations for Peerless iron are comparable to, or exceed concentrations for the foundry sands.

Exceedances of the Category 1 standards for mercury (0.2 μg/L) were obtained for all of the materials tested, including Peerless iron and torpedo sand, which is a typical aquifer material (Fig. 4.3). In fact, only one foundry sand yielded a mercury concentration exceeding the concentration obtained for torpedo sand. In general, however, all of the mercury concentrations were very low (<1.3 μg/L).

Three of the foundry sands have concentrations exceeding the Category 1 standards for lead (Sands 4, 6, 8, and 9) as shown in Table 4.1 and Fig. 4.4. However, much higher concentrations of lead were obtained for the fill soil (32.1 μg/L) and for Peerless iron (15.0 μg/L).

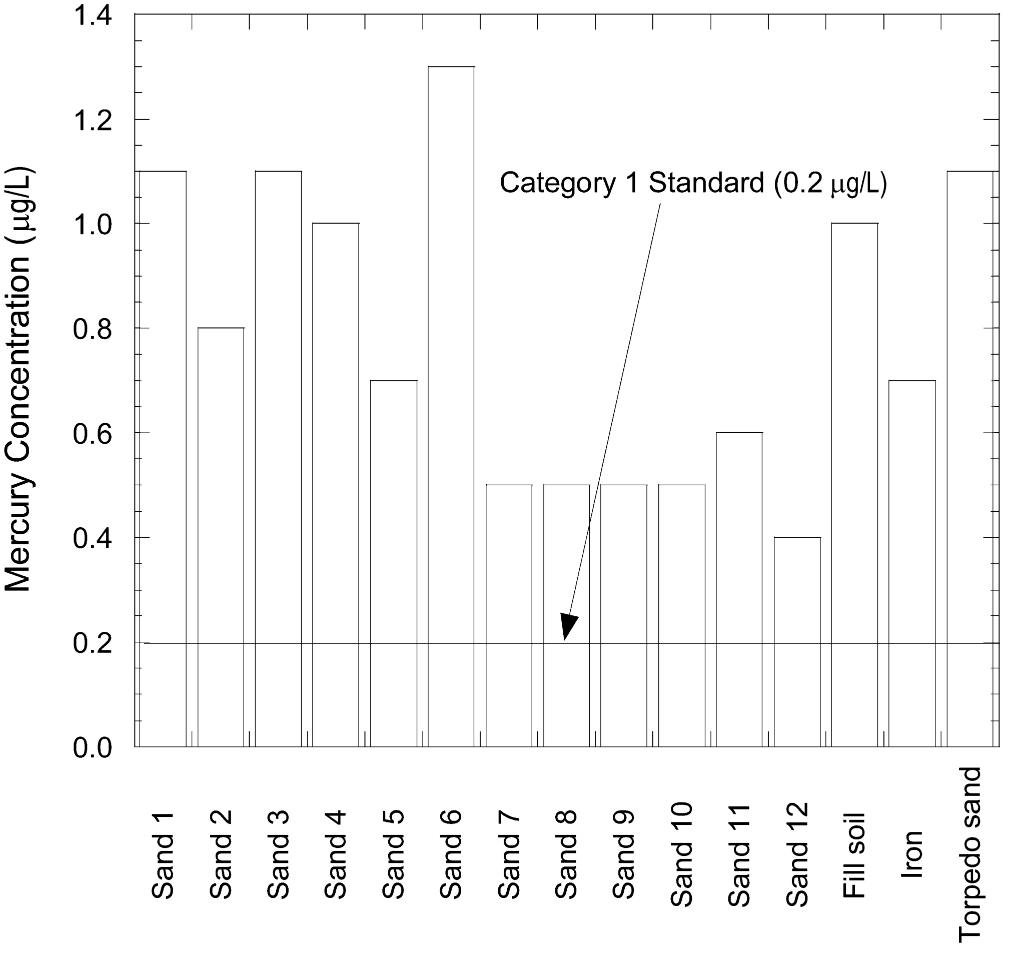

Fig. 4.1. Arsenic Concentrations from the Water Leach Tests.

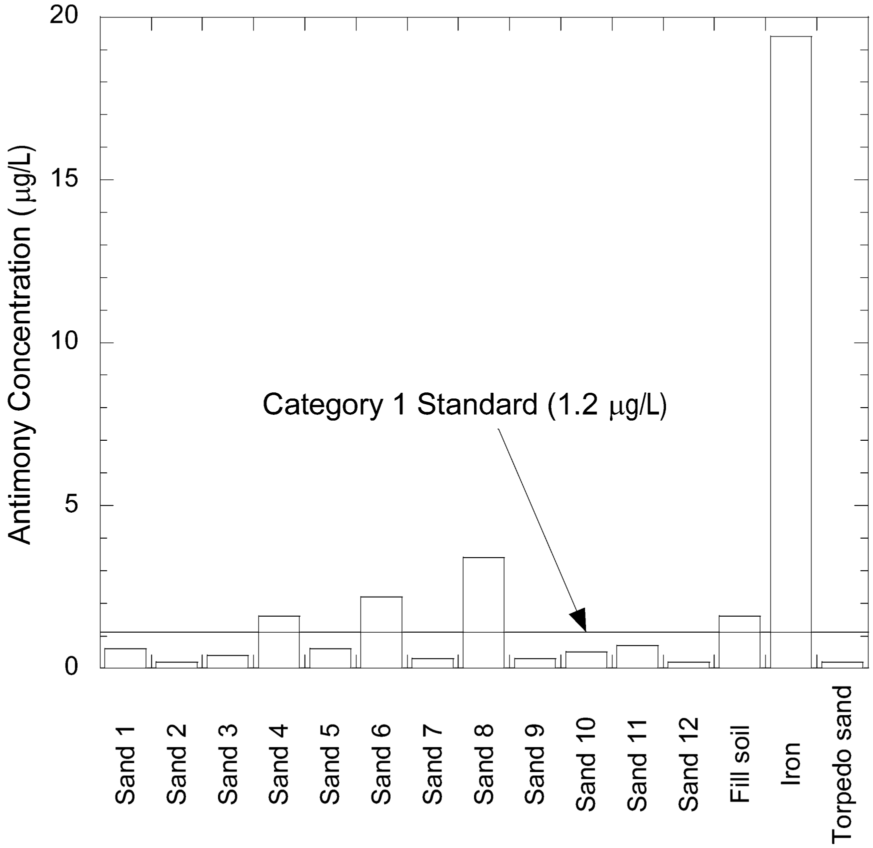

Fig. 4.2. Antimony Concentrations from the Water Leach Tests.

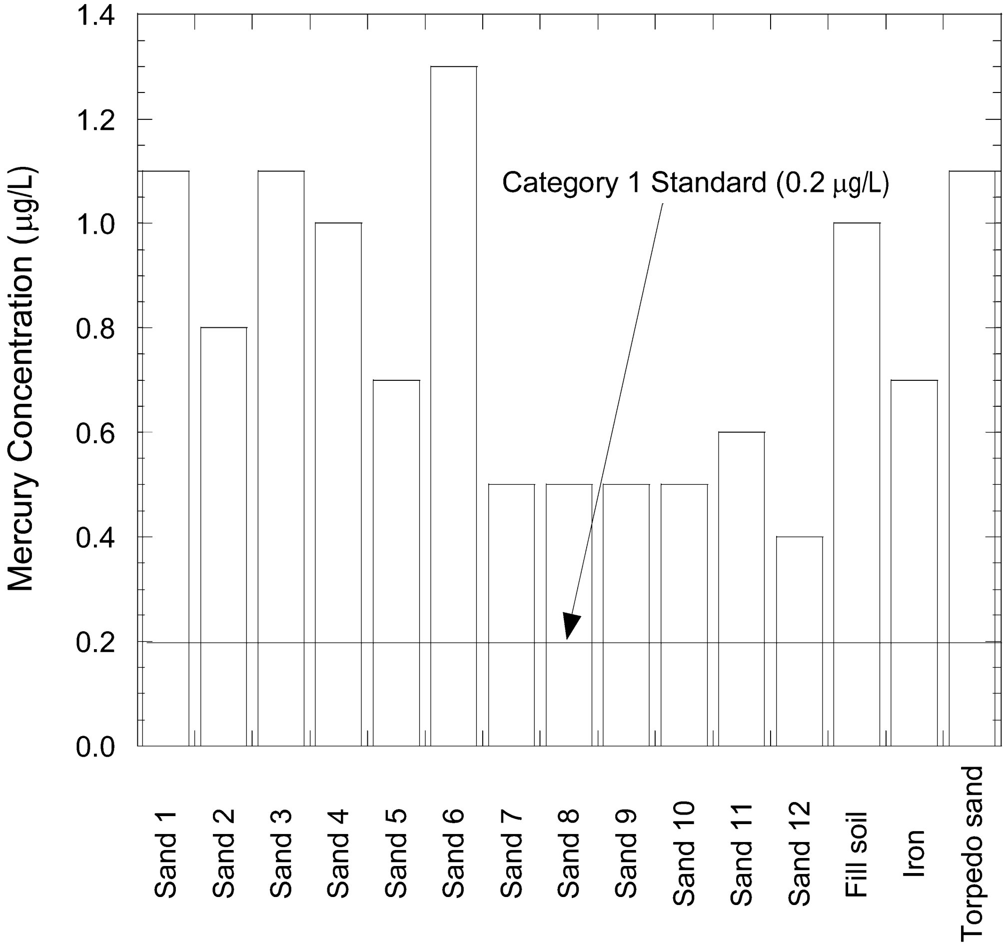

Fig. 4.3. Mercury Concentrations from the Water Leach Tests.

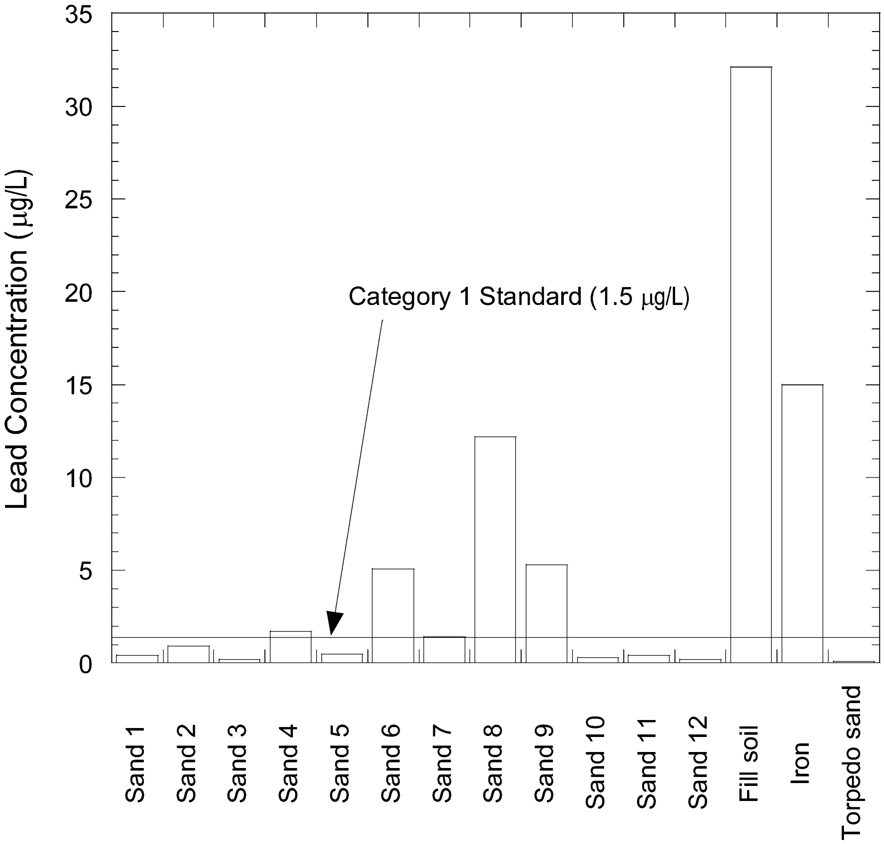

Fig. 4.4. Lead Concentrations from the Water Leach Tests.

Significant exceedances of the Category 1 standard for aluminum were obtained for three foundry sands (Sands 2, 4, and 8), as shown in Table 4.1 and Fig. 4.5. No exeedances of the standard for aluminum were obtained for the other materials.

An experiment was conducted to determine if leaching of metals could be reduced by adding calcite to the foundry sand. A 10% admixture of calcite ($CaCO_3$) was mixed with Sand 4, which exhibited elevated concentrations of Al, As, Fe, Pb, and Sb. The mixture was then subjected to a water leach test. Results of the test are shown in Fig. 4.6 along with the Category 1 standards. Concentrations of Al and Fe were significantly reduced, and fell below the Category 1 standards. A slight decrease in concentration of Pb occurred, and no significant changes in the concentrations of As, Hg, and Sb were observed.

4.1.2 Anions

NR 538 requires that the leachate from water leach tests on foundry sands be tested for the following anions if the foundry sand is to be placed below the groundwater table: chloride (Cl^-), fluoride (F^-), nitrite & nitrate (NO_2^- & NO_3^-), and sulfate (SO_4^{2-}). Concentrations of these anions from the water leach tests are summarized in Table 4.2. The Category 1 standards are shown in parenthesis in the column headings. Exceedances of the Category 1 standards are shown in bold.

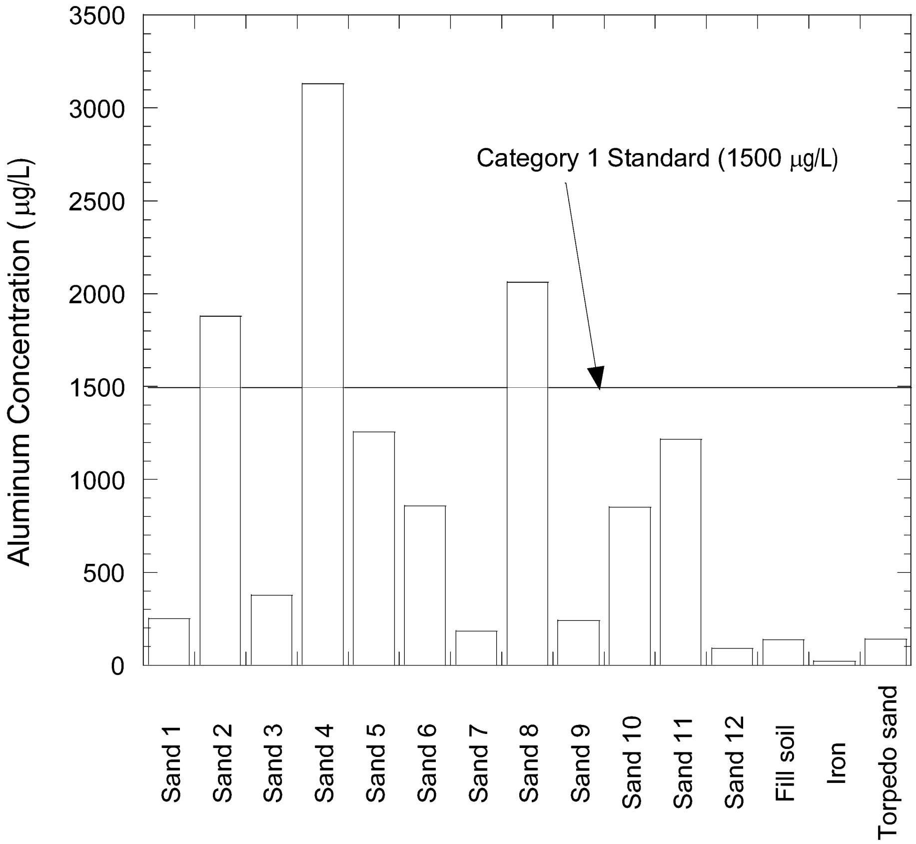

Fig. 4.5. Aluminum Concentrations from the Water Leach Tests.

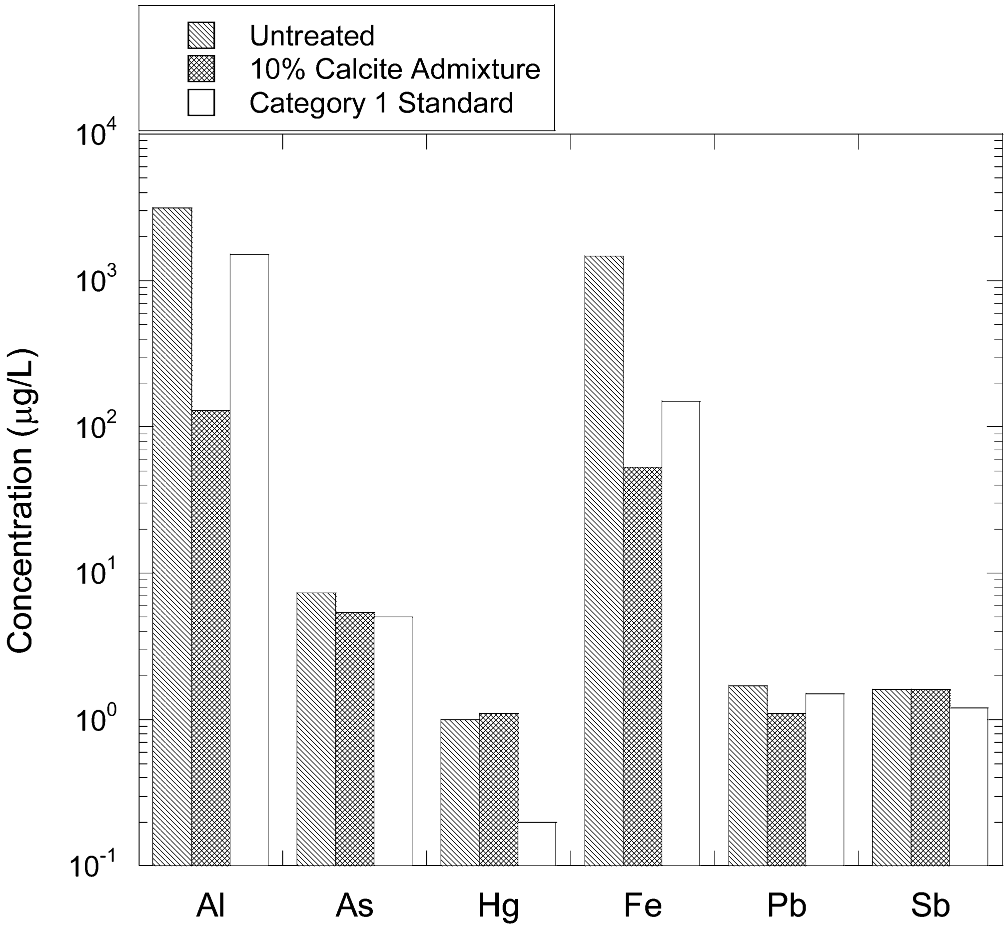

Fig. 4.6. Concentrations of Al, As, Hg, Fe, Pb, and Sb from Water Leach Tests on Sand 4 with and without 10% Admixture of Calcite.

Table 4.2. Anion Concentrations (mg/L) from Water Leach Tests on Foundry Sands, Fill, Torpedo Sand, and Peerless Iron. Numbers in Parentheses Next to Atomic Symbol are NR 538 Cat. 1 Standards in mg/L. Numbers in Bold Indicate Exceedances of Cat. 1 Standard.

Material	Anion Concentration (mg/L)				
	Cl (125)	F (0.8)	NO_2	NO_3 (2.0)	SO_4 (125)
Sand 1	3.2	0.2	< 0.05	0.7	9.5
Sand 2	6.0	0.4	< 0.05	0.8	11.7
Sand 3	5.6	0.4	< 0.05	0.7	4.0
Sand 4	6.6	0.5	< 0.05	0.7	10.4
Sand 5	5.7	0.4	< 0.05	0.9	12.3
Sand 6	8.4	**0.9**	< 0.05	< 0.1	18.1
Sand 7	3.0	0.4	< 0.05	0.03	2.0
Sand 8	7.8	**0.9**	< 0.05	< 0.1	12.8
Sand 9	2.5	0.6	< 0.05	0.03	2.7
Sand 10	4.5	0.3	< 0.05	0.7	9.6
Sand 11	4.9	0.5	< 0.05	0.7	6.3
Sand 12	6.4	0.7	< 0.05	0.7	7.5
Fill soil	4.0	0.4	< 0.05	< 0.1	1.9
Iron	0.7	**1.9**	<0.05	<0.1	N.A.
Torpedo sand	3.4	**2.6**	<0.05	<0.1	0.24

Exceedances exist for only two sands and for a single anion (fluoride), and these concentrations are only slightly higher than the Category 1 standard. Exceedances of the fluoride standard were also obtained for the torpedo sand and for Peerless iron. Additionally, the fluoride concentration for torpedo sand, a typical aquifer material, is the highest of all fluoride concentrations that were measured.

4.1.3 Total Elemental Analyses - Metals

NR 538 requires that total elemental analyses be conducted for the following metals if foundry sands are to be placed below the groundwater table: arsenic (As), beryllium (Be), hexavalent chromium (Cr^{6+}), antimony (Sb), and thallium (Tl). Results of these analyses are summarized in Table 4.3. Exceedances of the Category 1 standards are shown in bold.

Exceedances of the Category 1 standard for arsenic were obtained for all sands except for Sand 9. In general, the concentrations were typically 10 to 100 times the standard (42 μg/L), as shown in Fig. 4.7. Exceedances were also obtained for Peerless iron, fill soil, and torpedo sand. In fact, the highest arsenic concentration was obtained for Peerless iron, and the arsenic concentration for torpedo sand was higher than those for all other materials besides Peerless iron and Sand 7.

Table 4.3. Metal Concentrations (μg/kg) from Total Elemental Analyses on Twelve Foundry Sands, Fill, Torpedo, and Peerless Iron. Numbers in Parentheses Next to Atomic Symbol is NR 538 Cat. 1 Standard in μg/kg. Numbers in Bold Indicate Exceedances of Cat. 1 Standard.

Material	As (42)	Be (14)	Cr (14500)	Sb (6300)	Tl (1300)
Sand 1	**239**	**253**	2,915	6	29
Sand 2	**160**	**373**	6,389	4	38
Sand 3	**962**	**179**	2,527	5	41
Sand 4	**729**	**320**	6,729	16	82
Sand 5	**459**	**310**	5,444	4	36
Sand 6	**564**	**310**	4,805	11	53
Sand 7	**2,883**	**149**	**51,497**	41	23
Sand 8	**1,050**	**459**	8,997	7	60
Sand 9	2	14	3,219	928	4
Sand 10	**512**	**292**	4,420	4	46
Sand 11	**555**	**285**	1,501	4	47
Sand 12	**585**	**298**	**66,374**	19	35
Fill soil	**794**	**96**	2,832	4	17
Iron	**6,490**	**20**	**198,770**	70	**24,290**
Torpedo sand	**1,560**	**140**	7,600	10	**27,700**

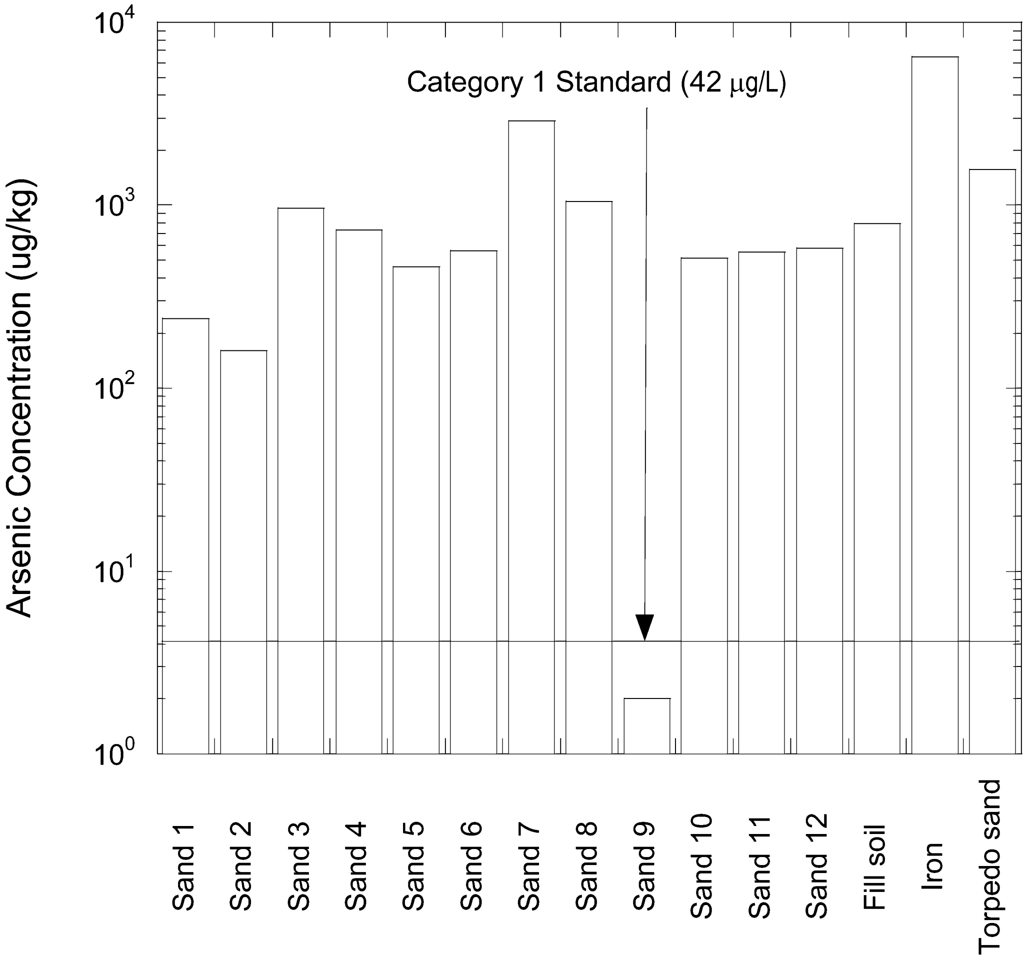

Fig. 4.7. Concentrations of Arsenic from Total Elemental Analyses.

Exceedances for hexavalent chromium were obtained for two sands and for Peerless iron. The highest concentration of hexavalent chromium was obtained for Peerless iron (Fig. 4.8).

No exceedances for Sb were obtained for any of the materials. Two exccedances for Tl were obtained for Peerless iron and torpedo sand. Both materials exceeded the standard for thallium by at least one order of magnitude.

Additional analyses were conducted for three redox active metals that are not regulated in NR 538: copper, iron, and zinc. The concentrations are tabulated in Table 4.4. The copper concentration ranges from 2 mg/kg to 182 mg/kg. No zinc was detected in Sand 9 sand. Zinc concentrations for the other sands ranged from 1 mg/kg to 35.8 mg/kg. High iron concentrations were measured for all sands. The iron concentrations were converted to iron contents (%) by weight (Table 4.4). The iron contents for the foundry sands ranged from 0.12% to 11.3%.

4.1.4 Total Elemental Analyses - Polyaromatic Hydrocarbons

Results of the PAH analyses are summarized in Table 4.5. The concentrations are reported on a dry weight and a wet weight basis. The first line for a compound corresponds to the wet weight and the second to the dry weight. Exceedances of the concentration limits for Category 1 in NR 538 are shown in bold. A designation of E means that the dry weight concentration for this compound could not be determined because the compound was not detected or

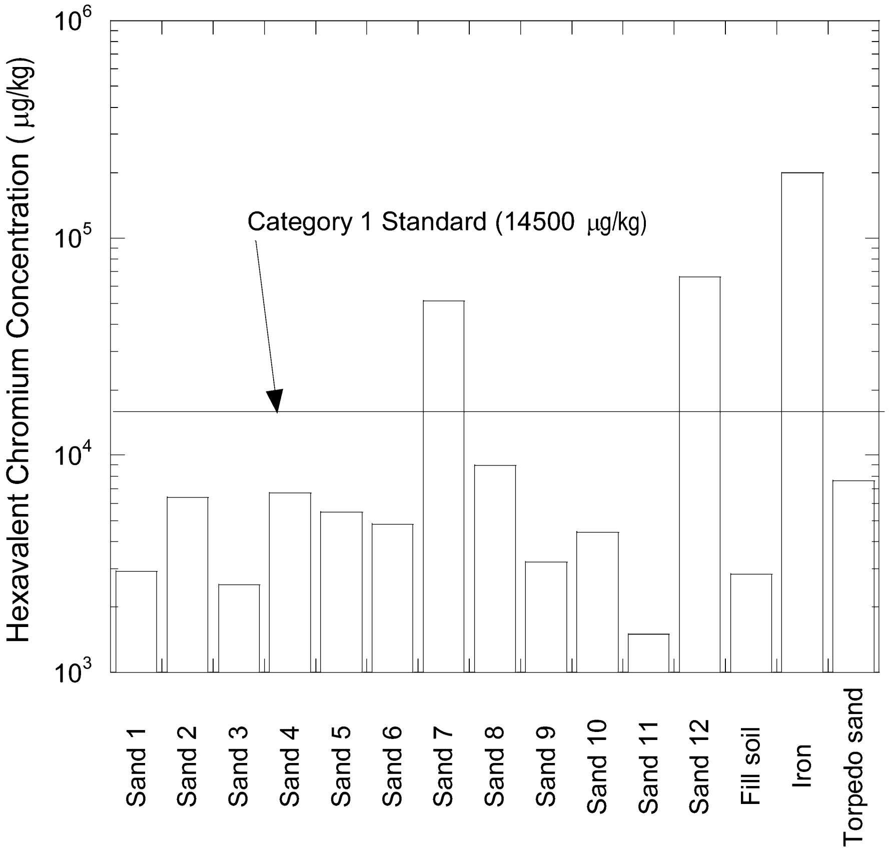

Fig. 4.8. Concentrations of Hexavalent Chromium from Total Elemental Analyses.

Table 4.4. Concentrations of Cu, Fe, and Zn from Total Elemental Analyses on Foundry Sands.

Foundry Sand	Copper (mg/kg)	Iron Fraction		Zinc (mg/kg)
		mg/kg	% Iron by Weight	
Sand 1	41.2	28,253	2.83	34.6
Sand 2	11.4	1546	0.15	9.4
Sand 3	4.4	11,928	1.19	35.8
Sand 4	2.0	2851	0.29	0.2
Sand 5	5.8	1370	0.14	20.6
Sand 6	11.6	1627	0.16	15.4
Sand 7	2.6	6491	0.65	10.6
Sand 8	5.4	7820	0.78	1.0
Sand 9	15.0	1167	0.12	0.0
Sand 10	13.2	1378	0.14	18.4
Sand 11	3.6	1849	0.18	29.6
Sand 12	182	112,563	11.26	26.6

Table 4.5. Summary of PAH Concentrations (μg/kg) from Total Elemental Analyses.

Compound	Cat.1 standard	Foundry Sand											
		1	2	3	4	5	6	7	8	9	10	11	12
Acenaphthene (wet)	900,000	ND	ND	ND	*D<61	ND	ND	*D<30	*D<61	*D<150	*D<150	*I<140	ND
Acenaphthene (dry)		*E	*E	*E	*E	*E	*E	*E	*E	*E	*E	*E	*E
Acenaphthylene	8800	*LML ND	*LML ND	*LML ND	*LML*D<84	*LML ND	*LML ND	*LML*D<130	*LML*D<84	*LML*D<210	*LML*D<210	*LML*D<210	*LML ND
Acenaphthylene		*E	*E	*E	*E	*E	*E	*E	*E	*E	*E	*E	*E
Anthracene	5,000,000	17	36	ND	*I<70	*I<16	13	120	*I<70	*I<130	87	110	15
Anthracene		17	37	*E	*E	*E	13	120	*E	*E	88	110	15
Benz(a)anthracene	88	39	62	ND	*I<120	*I<35	*I<40	*I<250	*I<230	*I<230	*I<300	*I<300	*I<60
Benz(a)anthracene		39	63	*E	*E	*E	*E	*E	*E	*E	*E	*E	*E
Benzo(a)pyrene	8.8	30	*I<60	ND	*I<80	*I<15	ND	*I<120	*I<78	*I<140	*D<200	*D<200	*I<24
Benzo(a)pyrene		30	*E	*E	*E	*E	*E	*E	*E	*E	*E	*E	*E
Benzo(b) fluoranthene	88	65	*I<120	ND	*I<230	*I<50	*I<70	*I<250	*I<180	*I<300	*I<300	*I<260	*I<60
Benzo(b) fluoranthene		66	*E	*E	*E	*E	*E	*E	*E	*E	*E	*E	*E
Benzo(ghi)perylene	880	58	110	ND	160	39	*I<50	*I<220	*I<180	280	*D<230	*I<310	*I<70
Benzo(ghi)perylene		58	110	*E	170	39	*E	*E	*E	290	*E	*E	*E
Benzo(k)fluoranthene	880	27	26	ND	*D<80	ND	*I<15	*I<60	*I<80	*D<200	*D<200	*D<200	*I<18
Benzo(k)fluoranthene		27	27	*E	*E	*E	*E	*E	*E	*E	*E	*E	*E
Chrysene	8,800	44	*I<80	ND	*I<150	*I<25	*I<15	*I<160	*I<120	*I<150	*I<160	*I<180	*I<40
Chrysene		44	*E	*E	*E	*E	*E	*E	*E	*E	*E	*E	*E
Dibenzo(ah)anthracene	8.8	*I<20	*I<20	ND	*I<60	ND	*I<30	*I<48	*I<32	*D<100	*D<80	*D<80	*I<14
Dibenzo(ah)anthracene		*E	*E	*E	*E	*E	*E	*E	*E	*E	*E	*E	*E
Fluoranthene	600,000	*I<140	*I<160	ND	*I<330	*I<60	*I<40	*I<300	*I<230	*I<300	*I<300	*I<400	*I<70
Fluoranthene		*E	*E	*E	*E	*E	*E	*E	*E	*E	*E	*E	*E
Fluorene	600,000	ND	*I<40	ND	*I<160	ND	ND	*I<190	*I<260	*D<650	*D<650	*I<180	*I<60
Fluorene		*E	*E	*E	*E	*E	*E	*E	*E	*E	*E	*E	*E

Compound	Cat. 1 Standard	Foundry Sand											
		1	2	3	4	5	6	7	8	9	10	11	12
Indeno(123-cd)pyrene	88	56	69	ND	*D<170	*I<40	*I<100	*I<220	*I<130	*D<350	*D<320	*D<320	*I<50
Indeno(123-cd)pyrene		57	70	*E	*E	*E	*E	*E	*E	*E	*E	*E	*E
2-methyl naphthalene	8,800	220	820	4.1	1400	490	550	8700	2300	3500	5800	**9800**	610
2-methyl naphthalene		220	830	4.1	1400	490	560	8800	2300	3600	5900	**9900**	610
Naphthalene	600,000	530	1200	20	1200	510	900	4100	1900	2300	4000	4600	710
Naphthalene		540	1200	20	1200	510	910	4100	1900	2400	4100	4600	720
Phenanthrene	880	160	450	78	**920**	160	110	**900**	740	**900**	720	**880**	170
Phenanthrene		160	460	78	**920**	160	110	**910**	740	**930**	730	**890**	170
Pyrene	500,000	51	50	ND	*I<270	*I<50	*I<30	*I<240	*I<180	*I<200	*I<180	*I<230	*I<60
Pyrene		51	51	*E	*E	*E	*E	*E	*E	*E	*E	*E	*E

Note: ND = Not detected, E = the dry weight concentration for the compound could not be determined, I = due to the interferences, the report limit of the compound interest is elevated to the level that is identified, LML MD = the laboratory matrix spike exceeds the lower quality control limit for the compound (LML) and the compound is not detected (ND), LML D = the laboratory matrix spike exceeds the lower quality control limit for the compound (LML), but the compound is detected.

there was interference in determining the concentration of the compound in the wet sample. The designation I means that there is an interference with the compound of interest and the reporting limit is elevated to the level that is identified (e.g., I<60 μg/kg). LML ND means that the laboratory matrix spike exceeds the lower quality control limit for this compound (LML) and the compound was not detected (ND) in the sample. I<20 means that there is an interference with this compound and because of this interference, if the compound is present, its concentration is less than 20 μg/kg.

For most compounds, the dry-weight and wet-weight concentrations are similar or the same. This occurs because most foundry sands are nearly dry when they are discarded. Exceedances were only obtained for phenanthrene (Sands 4, 7, 9, and 11) and 2-methyl naphthalene only (Sand 11). For phenanthrene, the exceedance was by no more than 40 μg/kg at most (maximum concentration measured – Category 1 Standard). For Sand 11, the concentration of 2-methyl naphthalene is 9800 μg/kg, whereas the Category 1 standard is 8800 μg/kg. No other exceedances were measured.

4.2 CHARACTERIZATION ACCORDING TO NR 538

Results of the water leach tests and the total elemental analyses were used to categorize the foundry sands, fill soil, torpedo sand, and Peerless iron in accordance with NR 538. The results are summarized in Table 4.6. All of the materials are Category 2 materials, including the torpedo sand, fill soil, and

Table 4.6. Categorization in Accordance with NR 538.

Materials	Metals		Anions	PAHs	Summary
	Water Leach Test	Total Elemental Analysis			
Sand 1	2	2	1	1	2
Sand 2	2	2	1	1	2
Sand 3	2	2	1	2	2
Sand 4	2	2	1	1	2
Sand 5	2	2	1	1	2
Sand 6	2	2	2	1	2
Sand 7	2	2	1	2	2
Sand 8	2	2	2	2	2
Sand 9	2	1	1	1	2
Sand 10	2	2	1	2	2
Sand 11	2	2	1	1	2
Sand 12	2	2	1	1	2
Fill soil	2	2	1	1	2
Iron	2	2	2	1	2
Torpedo sand	2	2	2	1	2

Peerless iron. Except for those sands exhibiting high concentrations of aluminum in the water leach tests (i.e., Sands 4 and 8), there appears to be no significant difference between any of the materials. Also, the foundry sands leach many constituents at lower concentrations than Peerless iron, a common material placed below the groundwater table in PRBs.

SECTION FIVE

RESULTS OF BATCH AND COLUMN TESTS USING TCE

5.1 BATCH DEGRADATION TESTS

Six sets of batch tests (Tests A through F) were performed to evaluate degradation rates for TCE in the presence of iron particles extracted from Sand 12. The tests were conducted under a variety of conditions, as summarized in Table 5.1. Four other tests (Test G through Test J) were conducted using Peerless iron particles. These additional tests were conducted to compare rate constants with other studies using similar iron to ensure that the laboratory protocols were reliable, and to determine if reaction rates for foundry iron are comparable to those for conventional iron used in PRBs. All tests were performed using the procedures and analyses described in Sec. 3.4.1.1 at room temperature (23 ± 2 ^{0}C).

Iron particles for the batch tests were separated from Sand 12 using a magnet. The extracted iron particles were washed with methanol to remove any impurities (i.e., organic carbon and metal oxides) that might affect the sorption and degradation processes, and then dried with an external heater. No oxides were visible on the washed particles. Afterwards, a known mass of iron was placed in a bottle and a batch test was conducted following the methods in Sec. 3.4.1.

Table 5.1. Experimental Conditions for Batch Degradation Tests Using Iron Particles Extracted from Sand 12 and Peerless Iron Particles.

Test	Initial Conc. (mg/L)	Iron surface area/volume (m^2/L)	Dissolved Oxygen (mg/L)	NaCl (M)
A	5.2	54	5.4	0
B	31.9	57	< 0.6	0
C	31.9	58	5.4	0.02
D	8.8	58	< 0.6	0
E	15.2	86	6.0	0
F	40.3	125	5.8	0
G	40.3	22	5.6	0
H	40.3	44	5.6	0
I	40.3	89	5.6	0
J	40.4	180	5.6	0

Three factors were varied to determine their effects on the rate constant and partition coefficient: initial TCE concentration, dissolved oxygen (DO) concentration, and presence of chloride. Lineralized and non-linear forms of Eq. 3.7 were used to determine partition coefficients and rate constants.

The rate constants and partition coefficients obtained from the tests are summarized in Table 5.2. Examples of non-linear fits of Eq. 3.7 to the batch data are shown in Fig. 5.1 for iron from Sand 12 and in Fig. 5.2 for Peerless iron. In general, no distinct difference exists for the rate constants and partition coefficients obtained using the linear and non-linear fits, except for Test J (Table 5.2). For Test J, similar rate constants were obtained, but the partition coefficient obtained from the linear model fit was four times lower than that obtained from the non-linear model fit. The difference in the partition coefficients for Test J is due to scatter in the experimental data.

5.1.1 Initial TCE Concentration

The rate constants and partition coefficients are shown as a function of initial TCE concentration in Fig. 5.3. Neither the rate constant nor the partition coefficient appears to depend on the initial TCE concentration. The scatter in the partition coefficients is largely due to variability in the foundry sand iron. Partition coefficients for the foundry sand iron ranged between 0.77 L/kg and 2.41 L/kg, whereas partition coefficients for the Peerless iron ranged between 1.52 L/kg and 2.12 L/kg.

Table 5.2. Rate Constants and Partition Coefficients for TCE Obtained from Batch Degradation Tests Using Iron Extracted from Sand 12 and Peerless Iron.

Test	Non-Linear Fitting		Linear Fitting	
	Rate Constant (L/m^2-hr)	Partition Coefficient (L/kg)	Rate Constant (L/m^2-hr)	Partition Coefficient (L/kg)
A	2.37×10^{-4}	2.13	2.32×10^{-4}	2.36
B	1.02×10^{-4}	1.22	1.06×10^{-4}	1.08
C	1.03×10^{-4}	0.77	1.02×10^{-4}	0.79
D	1.14×10^{-4}	1.76	1.13×10^{-4}	1.82
E	2.06×10^{-4}	1.72	1.02×10^{-4}	2.03
F	1.17×10^{-4}	2.41	1.16×10^{-4}	2.45
G	1.76×10^{-4}	2.12	1.77×10^{-4}	2.11
H	1.65×10^{-4}	1.79	1.68×10^{-4}	1.59
I	1.71×10^{-4}	1.52	1.77×10^{-4}	1.04
J	1.72×10^{-4}	1.61	1.77×10^{-4}	0.37

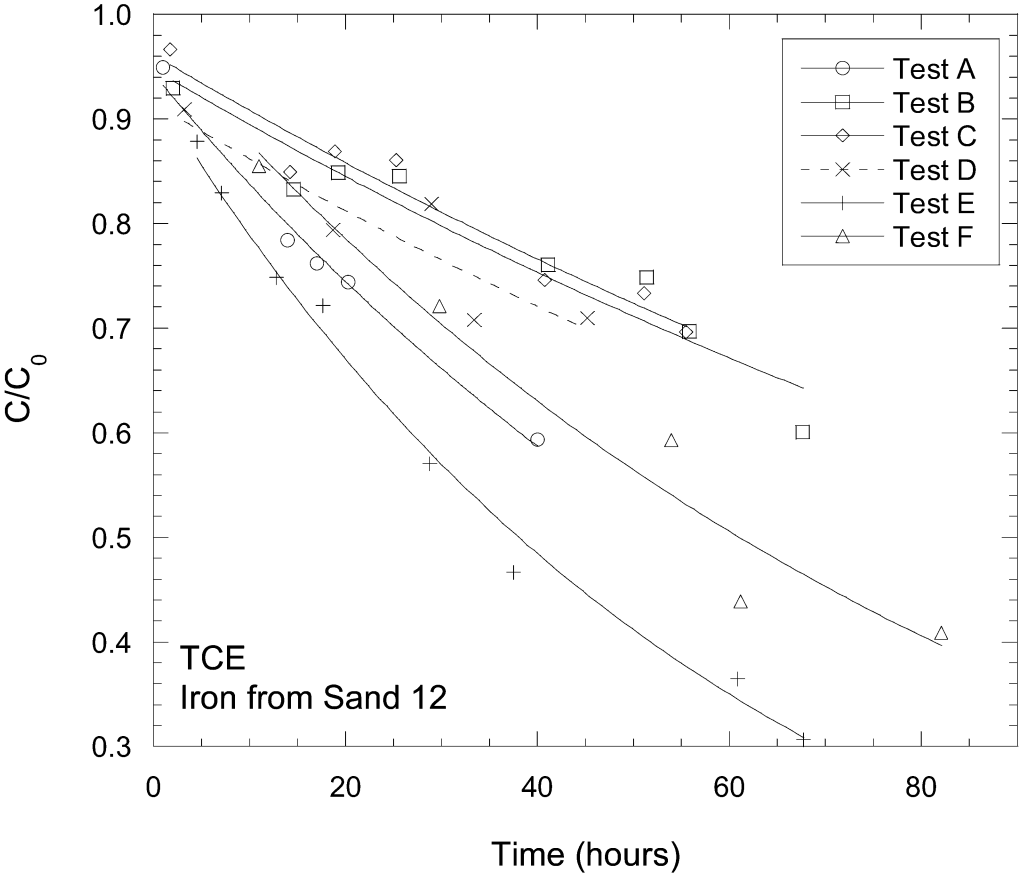

Fig. 5.1. Degradation of TCE Under Various Experimental Conditions. Batch Degradation Tests Using Iron Extracted from Sand 12.

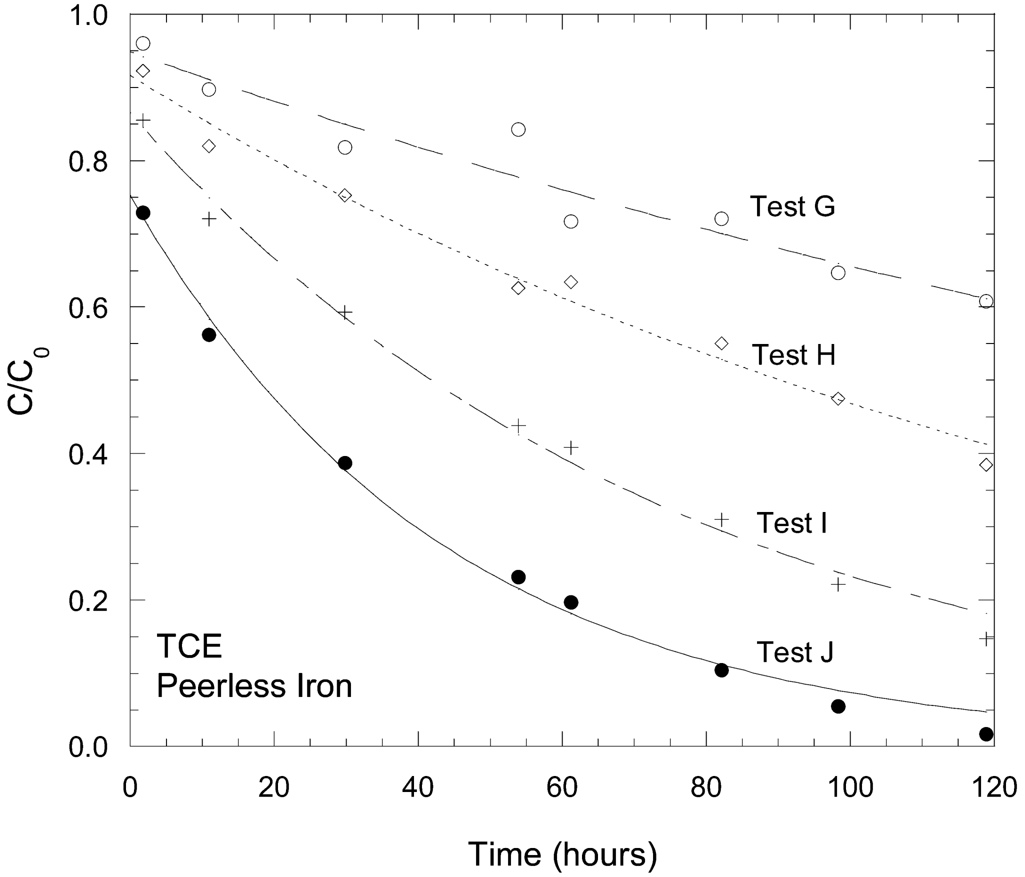

Fig. 5.2. Degradation of TCE in Batch Tests Using Various Amounts of Peerless Iron.

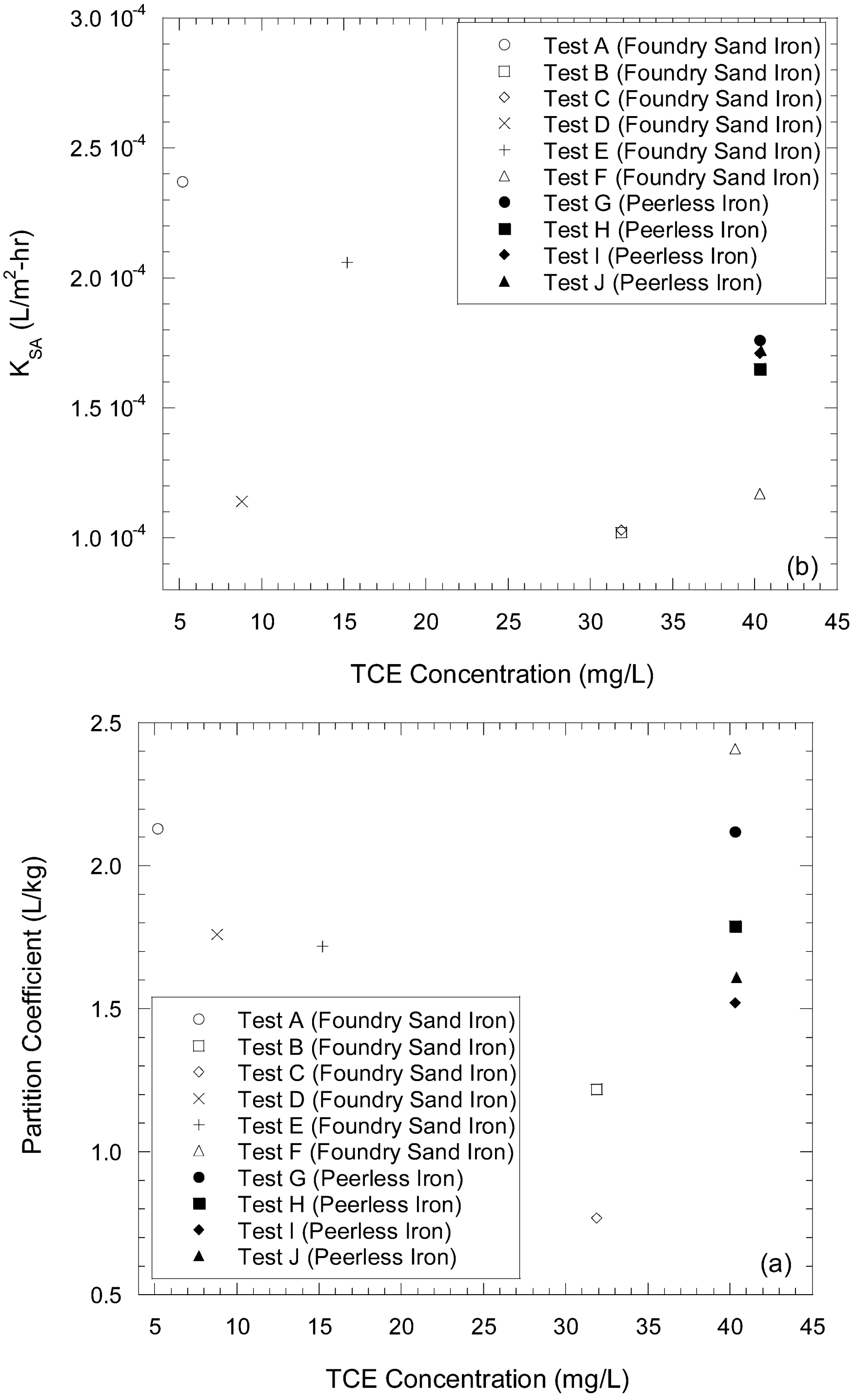

Fig. 5.3. Effect of Initial TCE concentration on (a) K_{SA} and (b) Partition Coefficient.

5.1.2 Surface Area of Iron to Solution Volume Ratio

The iron surface area (SA) to solution volume ratio was varied between 22 m^2/L and 180 m^2/L to evaluate if the rate constant for foundry sand iron could be normalized by the surface area of the iron. As shown in Fig. 5.4, the bulk first-order rate constant, K_{obs}, is linearly proportional to the specific surface area of iron (SSA), where SSA was calculated by normalizing the SA to the volume of solution. The slope of the graph (Fig. 5.4) is equal to the average normalized rate constant (K_{SA}), which is 1.64×10^{-4} L/m^2-hr.

5.1.3 Dissolved Oxygen (DO) Concentration

In many cases where VOCs contaminate groundwater, the DO concentration in groundwater is near zero (the groundwater is anoxic). However, moderate DO (2.8 mg/L) has been reported when the groundwater table is near the ground surface (McMahon et al. 1999). Therefore, two different DO concentrations were used to evaluate if dissolved oxygen concentration affects the rate constant for foundry iron and TCE. Tests with high DO were conducted using unprocessed DI water, which has DO ranging from 5.4 to 6.0 mg/L. Tests with low DO were conducted using DI water purged with N_2 gas for 20 min. The tests with low DO had DO concentrations less than 0.6 mg/L.

Box plots for the rate constants and partition coefficients are shown in Fig. 5.5. The rate constants for the tests with high DO are slightly (approximately 1.6 times) higher than those from the tests with low DO. The partition coefficients were also slightly lower in water with low DO.

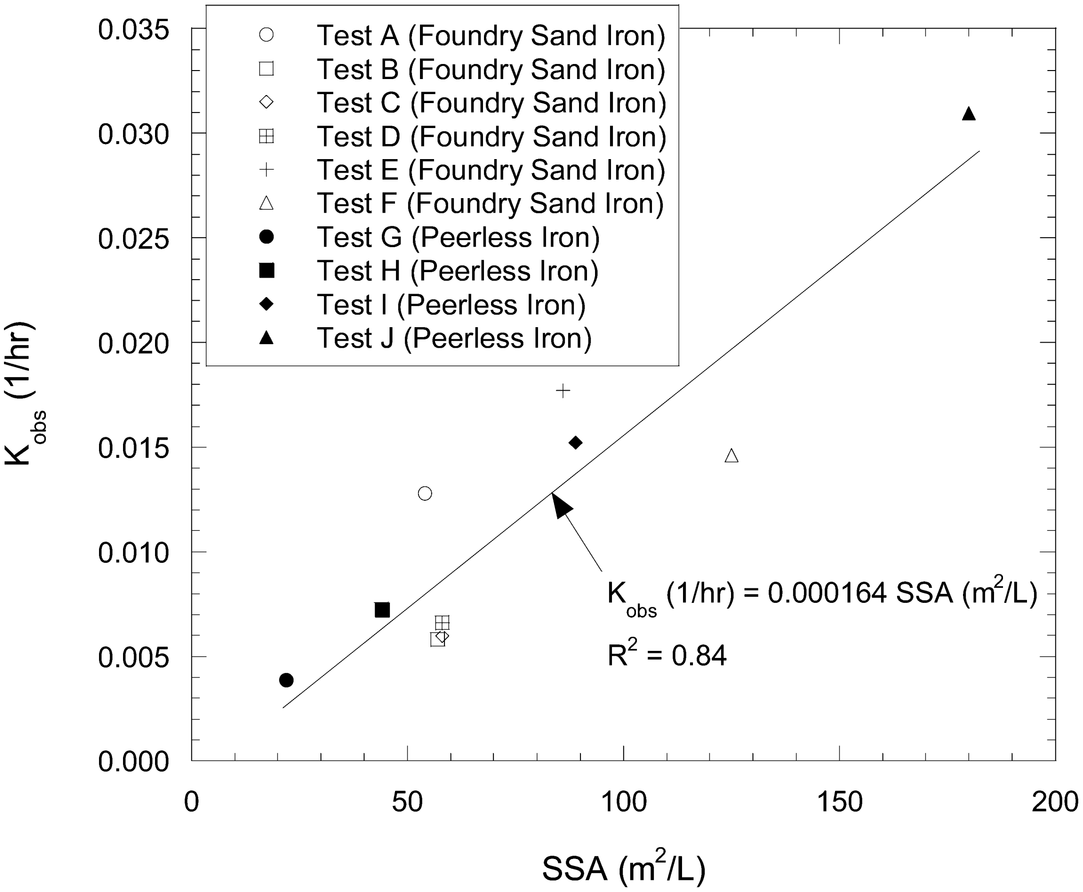

Fig. 5.4. Apparent Rate Constant (K_{obs}) as a Function of Specific Surface Area (SSA) of Iron.

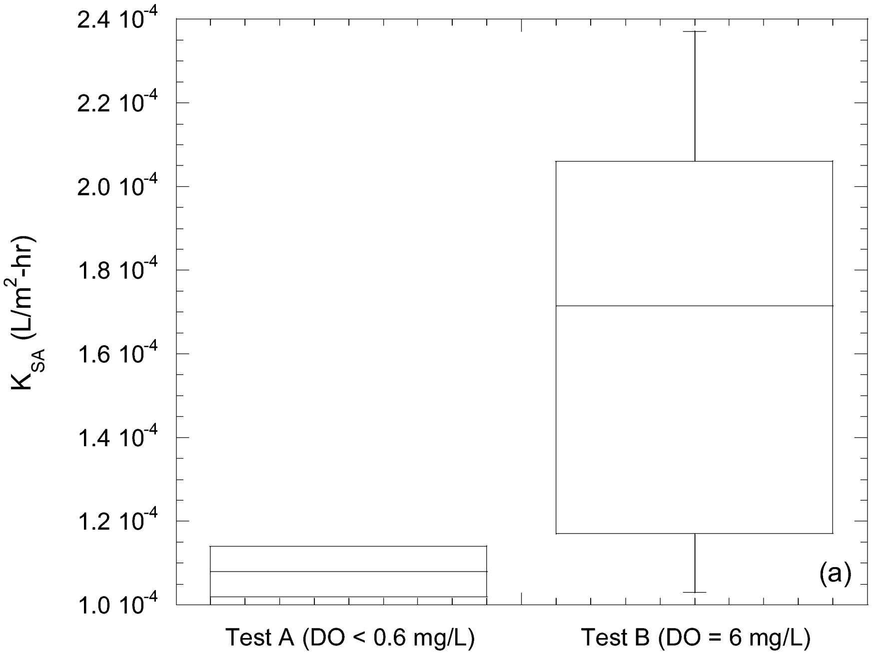

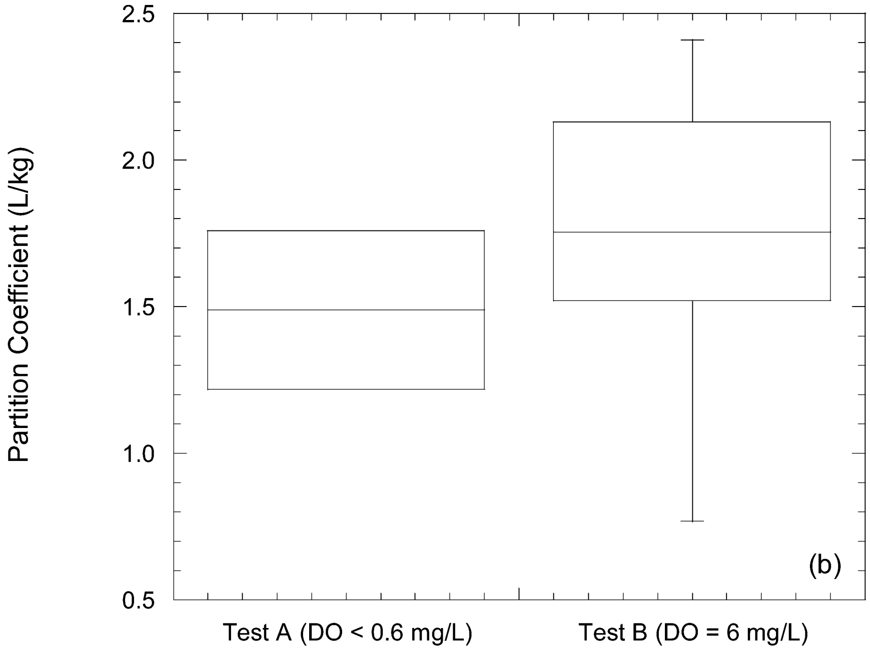

Fig. 5.5. Effect of DO Concentrations on (a) Rate Constants and (b) Partition Coefficients.

Additional batch tests were performed to find the rate constant for uptake of DO by corrosion of the iron. However, the DO concentration decreased so quickly that the kinetics of DO degradation could not be obtained.

5.1.4 Chloride Effect

The chloride iron accelerates the oxidation of iron (Montgomery 1985) or depassivates iron oxyhydroxide (Reardon 1995). A low concentration of sodium chloride (0.01 M or higher) can also inhibit sorption of TCE on clay or organic matter (Estes et al. 1988).

To assess the effect of Cl^-, Test C was conducted with TCE in a 0.02 M solution of NaCl. The rate constant from this test (1.03×10^{-4} L/m^2-hr, Table 5.2) is one of the lowest values obtained, but is not appreciably different from the rate constants obtained from the other tests. Because the effect of Cl^- was small, no further attempts were initiated to determine the effect of chloride on the rate constant.

5.1.5 TCE By-Products

TCE by-products (1,1-DCE and cis-1,2-DCE) were measured in Tests F – J to confirm that the dechlorination reaction was occurring and to quantify the amount of by-products that were generated. Concentrations of 1,1-DCE and cis-1,2-DCE are shown in Fig. 5.6.

The concentrations of 1,1-DCE were mostly lower than 0.06 mg/L,

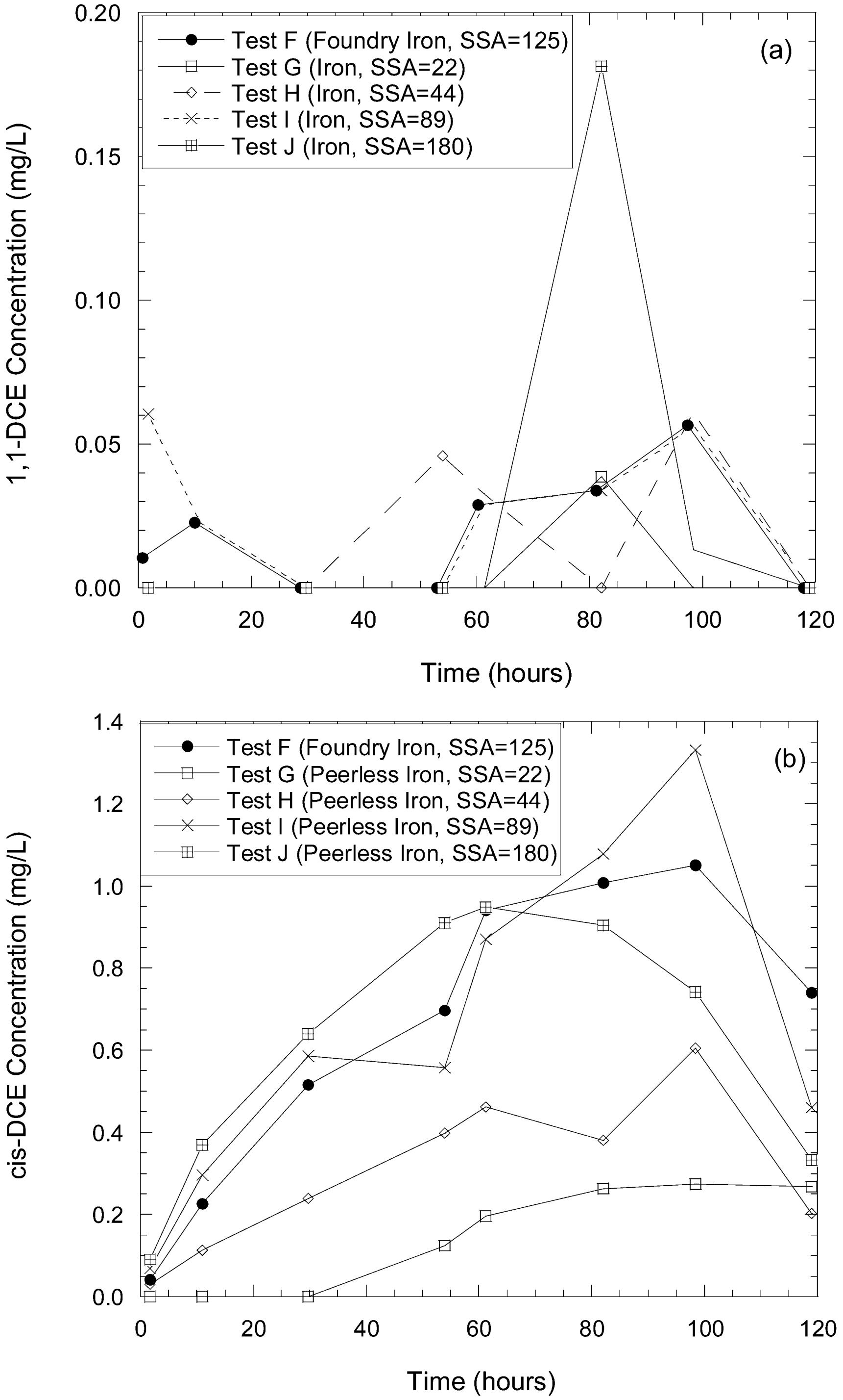

Fig. 5.6. Concentrations of 1,1-DCE and cis-DCE Produced from Reduction of TCE During Batch Degradation Tests.

except for one data point from Test J, which was 0.18 mg/L. Concentrations of 1,1-DCE obtained from the foundry iron were no different from those obtained with Peerless iron. Because the concentrations of 1,1-DCE were low, no attempt was made to find the rate constants for 1,1-DCE.

Higher concentrations were obtained for cis-1,2-DCE, with the highest concentrations obtained for tests conducted with the highest SSA. For all tests except Test I, the concentration peaked at about 60 hours, and then leveled off or decreased as the cis-1,2-DCE degraded. The formation of cis-1,2-DCE for the test with foundry iron (Test F) was comparable to that for the tests with Peerless iron having comparable SSA (Tests I and J).

The network model described in Sec. 3.4.1 was fit to the data shown in Fig. 5.6 to obtain rate constants and branching ratios for the reduction processes, as summarized in Table 5.3. Similar rate constants and branching ratios were obtained for the foundry sand iron and Peerless iron. The branching ratio for β-elimination ranges from 0.94 to 0.98, indicating that at most a 6% of TCE reduction follows the hydrogenolysis pathway that produces the DCE isomers (i.e., 1,1-DCE, trans-DCE, and cis-DCE) and the most toxic TCE by-product, VC. These branching ratios are consistent with those reported by Orth and Gillham (1996) and Sivavec et al. (1997). The rate constants for TCE obtained from the network model fits are also comparable to those obtained using the linear and non-linear model fits (Table 5.2). The rate constants for cis-DCE range from 7.0×10^{-5} L/m^2-hr to 2.8×10^{-5} L/m^2-hr, which are approximately two times higher than those reported by Johnson et al. (1996).

Table 5.3. Branching Ratio and Rate Constants for TCE and cis-DCE Obtained from Network Model Fits.

Test	Source of Iron	f_β	K_{SA} (L/m^2-hr)	
			$K_{cis\text{-}DCE}$	K_{TCE}
F	Sand 12	0.94	7.5×10^{-5}	1.2×10^{-4}
G	Peerless Iron	0.98	7.0×10^{-5}	2.0×10^{-4}
H	Peerless Iron	0.95	2.8×10^{-4}	1.8×10^{-4}
I	Peerless Iron	0.94	7.9×10^{-5}	1.8×10^{-4}
J	Peerless Iron	0.95	8.4×10^{-5}	1.8×10^{-4}

5.2 BATCH SORPTION TESTS

5.2.1 Serial Batch Kinetic Tests

Seven sands were selected to assess sorption of TCE on foundry sands and to determine the reduction capacity of foundry sands for TCE. Sands were selected that provided a broad range of TOC (0.8% to 4%) and clay contents (0% to 13%) (Table 5.4). TCE concentrations during the serial batch kinetic tests are shown in Fig. 3.2 in Sec. 3.3.1. The concentration decreases rapidly at the beginning of the test, and more slowly as the test continues. After 16 hours, the concentrations cease decreasing when corrected using the control concentrations.

The mass of TCE sorbed on the foundry sands at equilibrium, C_s (mg/kg), is summarized in Table 5.4. Multivariate regression was used to identify the parameters influencing sorption of TCE. The following regression equation was obtained by regression at the 0.05 significance level ($R^2 = 0.83$).

$$C_S = 51.8 + 31.7\ TOC + 6.45\ C \qquad (5.1)$$

where C_S is the concentration of TCE sorbed on the foundry sand (mg/kg) and C is clay content (%). Eq. 5.1 indicates that both clay content (%) and TOC (%) affect sorption, which is expected since both TOC and clay provide sorption sites. However, Eq. 5.1 indicates that foundry sands still have the affinity to sorb TCE (approximately 51.8 mg/kg) when TOC and clay content are zero. Other sorbents may exist that provide for TCE sorption, such as metal oxides.

Table 5.4. Sorptive Capacity for TCE for Foundry Sands with Different Clay and TOC Contents.

Sands	Clay (%)	TOC (%)	Mass Sorbed (mg/kg)
Sand 1	5.1	1.5	123
Sand 2	7.0	2.6	156
Sand 4	10.5	0.5	162
Sand 7	4.7	2.5	146
Sand 9	4.4	0.8	85
Sand 10	N.A.	2.5	166
Sand 11	13	4.0	270

N.A. = Not Applicable.

Alternatively, the sorption may be non-linearly related to TOC and clay content when either is near zero.

TCE by-products were found from the tests with Sands 1, 4, 8, and 11 (Table 5.5). For Sand 1, the by-products were formed at about 46 hours and a cis-DCE was found for Sand 4 at about 37.5 hours. A consistent by-product formation was observed for Sand 11 showing all three by-products (1,1-DCE, trans-DCE, and cis-DCE). Thus, some degradation was occurring during the sorption tests, which probably resulted in a small over-estimate in the partition coefficients.

5.2.2 Sorption Isotherms

Sorption isotherms from the batch sorption tests are shown in Fig. 5.7. All tests had approximately linear isotherms in the range of the equilibrium concentrations that were considered. However, significant non-linearity may occur at lower concentrations since many of the linear isotherms appear to have a y-intercept greater than zero. Parameters obtained by fitting the linear and Freundlich model fits to the data are summarized in Table 5.6. The first column (Method 1) contains the parameters of linear model fit using a non-zero intercept. The parameters for Method 2 were obtained from the linear model with a zero-intercept enforced. The third column contains parameters of Freundlich model.

For the entire concentration range, essentially all tests were well explained by the Freundlich model. Most sands have a convex non-linearity (i.e., $1/n<1$),

Table 5.5. TCE By-products in the Batch Kinetic Tests.

Sand	TCE By-product Concentration (mg/L) at Various Times				
	0.2 hr	9.8 hr	16.3 hr	37.5 hr	46.3 hr
1	N.D.[d]	N.D.	N.D.	N.D.	0.024 (trans)[a], 0.084 (cis)[c]
2	N.D.	N.D.	N.D.	N.D.	N.T.[e]
4	N.D.	N.D.	N.D.	0.006 (cis)	N.T.
8	N.D.	N.D.	N.D.	0.02 (cis)	0.02 (trans), 0.03 (cis)
9	N.D.	N.D.	N.D.	N.D.	N.T.
10	N.D.	N.D.	N.D.	N.D.	N.D.
11	N.D.	N.D.	0.01 (cis)	0.02 (1,1)[b], 0.01 (cis)	0.02 (trans)

Note: [a]trans = trans-DCE, [b]1,1 = 1,1-DCE, [c]cis = cis-DCE, [d]N.D. = Not Detectable, [e]N.T. = Not Tested.

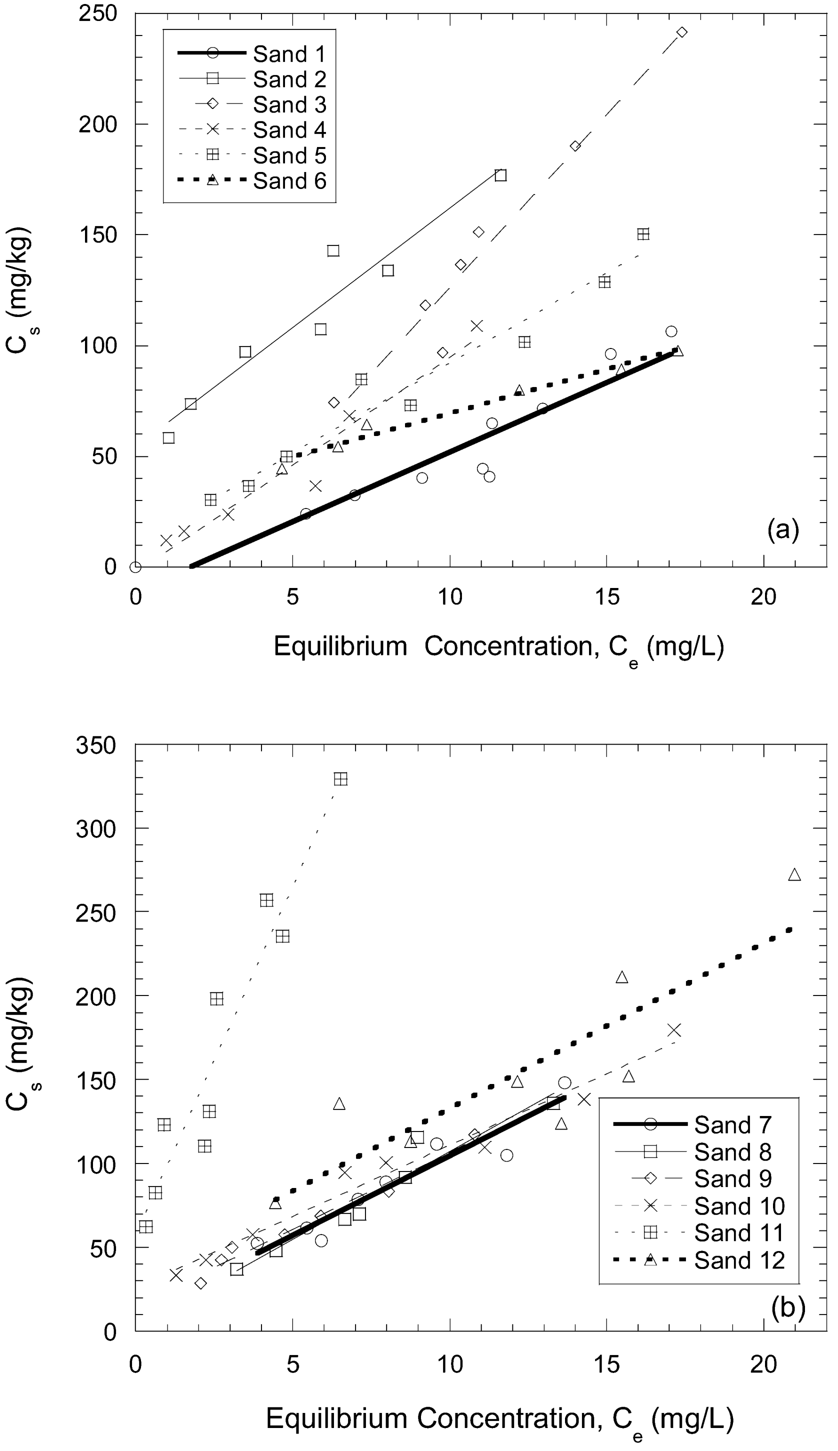

Fig. 5.7. Sorption Isotherms for TCE on Foundry Sands.

Table 5.6. Partition Coefficients Obtained from Fitting Linear and Freundlich Models to Data from Batch Sorption Tests.

Foundry Sands	Linear Model				Freundlich Model		
	Method 1		Method 2				
	K_p (L/kg)	R^{2a}	K_p (L/kg)	R^2	K_f	1/n	R^2
1	5.4	0.82	5.4	0.82	3.64	1.09	0.93
2	10.8	0.94	17.9	0.36	56.4	0.44	0.96
3	15.6	0.96	13.1	0.93	9.1	1.13	0.92
4	9.7	0.95	9.4	0.94	10.9	0.88	0.94
5	8.1	0.96	9.1	0.94	13.9	0.83	0.97
6	4.0	0.98	6.3	0.57	18.9	0.58	0.98
7	9.5	0.91	10.5	0.90	14.8	0.85	0.90
8	10.5	0.94	10.7	0.94	11.4	0.97	0.96
9	9.2	0.98	11.3	0.90	18.6	0.75	0.96
10	8.5	0.97	10.7	0.88	23.9	0.67	0.99
11	41.6	0.92	55.5	0.77	106.5	0.52	0.88
12	9.8	0.76	12.2	0.70	31.3	0.64	0.73

[a] Coefficient of Determination.

but Sand 1 and 3 showed a concave non-linearity (i.e., 1/n>1). An example of model fits using Method 1 and Freundlich model for Sand 10 is shown in Fig. 5.8. The non-linearity is expected at low concentrations, but the isotherm is linear at the equilibrium concentrations ranging from 1 mg/L to 17 mg/L. This type of isotherm corresponds to sand with a high affinity for TCE at low concentrations, and lower affinity at higher concentrations.

Moderate affinity for TCE at higher concentrations is characteristic of a high surface-area carbonaceous material (HSACM), such as charcoal-like substances. Chiou et al. (2000) found that HSACM was responsible for non-linearity in TCE adsorption on a peat. The isotherms of the tests on foundry sands are similar to those of Chiou et al. (2000), with high sorption affinity at low concentrations and a moderate affinity at higher concentrations. The similarity of the foundry sand isotherms and those reported by Chiou et al. is probably due to the presence of "sea coal," a powdered coal additive in foundry sands, which can be considered to be a HSACM.

The partition coefficients obtained from the batch sorption tests are plotted against TOC in Fig. 5.9. A linear relationship is observed for TOC ranging from 1% to 3.5%, which is characteristic of most foundry sands (Table 3.2). An empirical equation can be expressed to describe the relationship between K_p and TOC in the moderate TOC ranges (Fig. 5.9b):

$$K_p = 4.76\ \mathrm{TOC} \tag{5.2}$$

where K_p is in L/kg and TOC is in percent. The R^2 for Eq. 5.2 is 0.93.

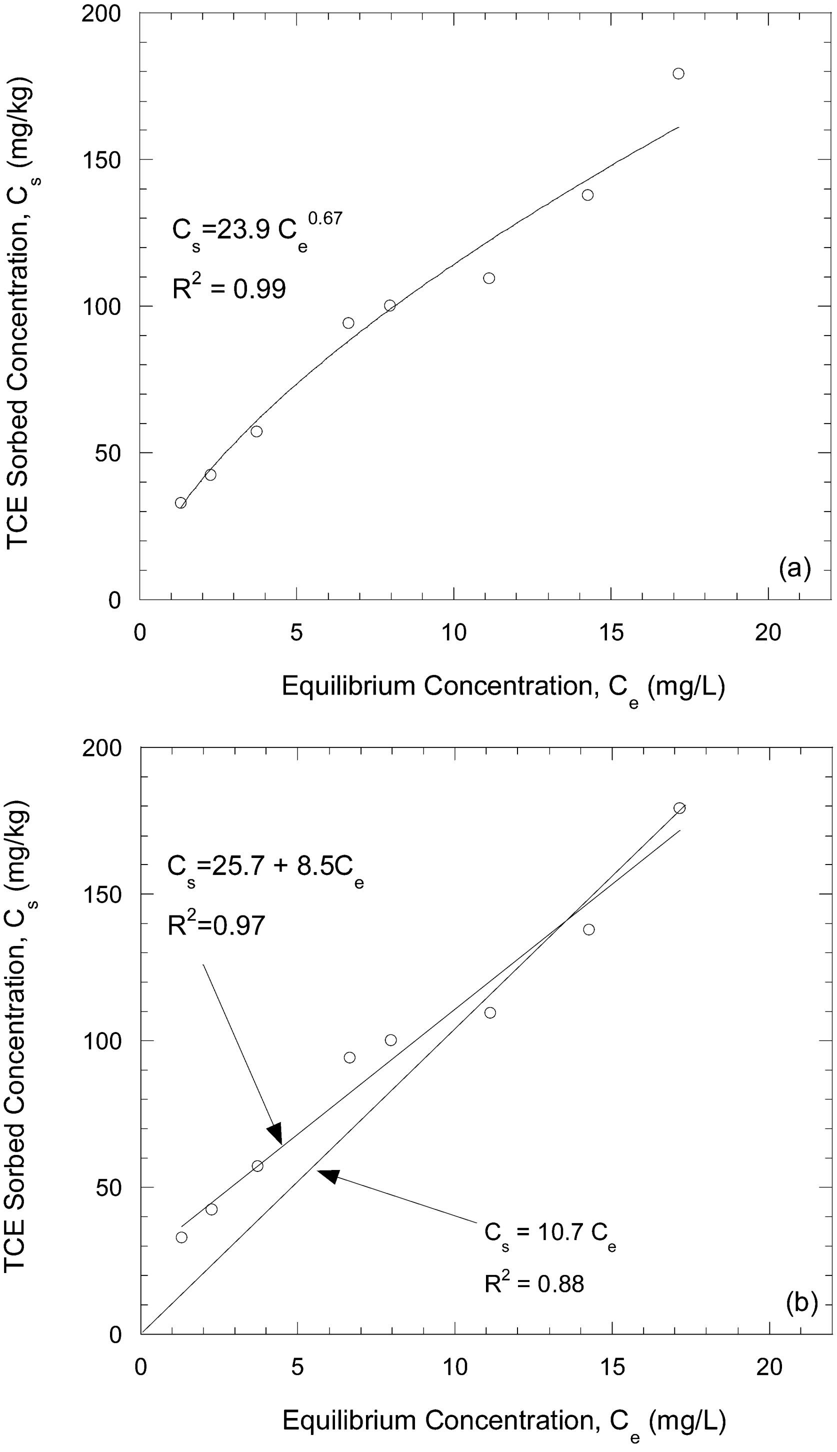

Fig. 5.8. Fits to TCE Sorption Data for Sand 10 Using (a) Freundlich Model and (b) Linear Model.

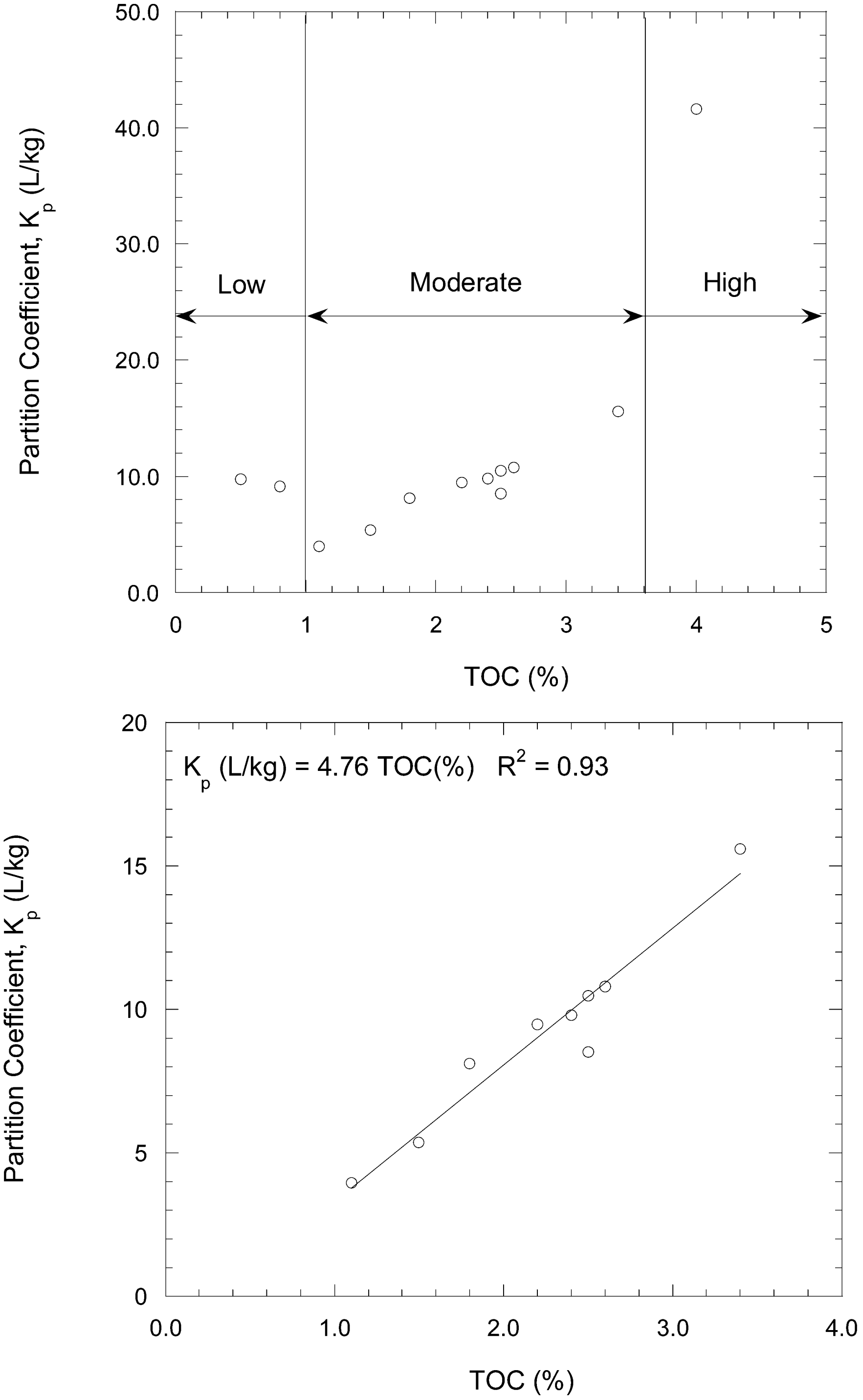

Fig. 5.9. Relationship Between K_p and TOC at (a) Full Range and (b) Moderate Range.

For both the low and high TOC ranges, higher K_p were obtained than those predicted by Eq. 5.2. Sands 4 and 11 have high clay content (10.5% and13%), which may provide additional sorption sites for TCE sorption than is characteristic of most sands. Sand 9 includes an additive for binding, which is not present in the other sands. This additive may be responsible for the additional sorptive capacity of Sand 9.

5.3 COLUMN TESTS

Column tests were conducted to determine transport parameters (i.e., partition coefficients, rate constants, and dispersion coefficients) under more realistic conditions. Two types of tests were conducted: constant head tests and constant flow rate tests. The methods are described in Sec. 3.5. The experimental conditions are summarized in Table 5.7.

5.3.1 Tracer Tests

Tracer tests were conducted to find the effective porosity of the media in the column tests. Two tracers (i.e., D_2O and Br^-) were used. Typical breakthrough curves for D_2O tracer tests conducted on Sand 12 are shown in Fig. 5.10. Eq. 3.18 was used to obtain the seepage velocity and the dispersion coefficient. The effective porosity was calculated by dividing the specific discharge by the seepage velocity. As shown in Fig. 5.10, the effective porosities are comparable

Table 5.7. Experimental Conditions Used for Column Tests Containing Foundry Sands and Peerless Iron.

Reactive Media	L^c (cm)	q^d (cm/s)	C_0^e (mg/L)	ρ_d^f (Mg/m^3)	n_t^g
Sand 1[a]	12.8	3.1×10^{-4}	20.4	1.65	0.39
Sand 3[a]	6.2	3.9×10^{-4}	18.9	1.64	0.34
Sand 12[a]	12	1.9×10^{-3}	20.0	1.70	0.46
Sand 1[b]	26	2.8×10^{-3}	20.4	1.59	0.42
50% Iron[b]	42	3.3×10^{-3}	21.9	2.79	0.46
Iron (100 %)[b]	28	1.2×10^{-3}	21.8	2.34	0.70
Iron (100 %)[b]	26	1.2×10^{-3}	22.0	2.61	0.66
Sand 11[b]	30	8.4×10^{-3}	21.9	1.49	0.41
Sand 12[b]	29	1.1×10^{-3}	20.5	1.60	0.42

[a] Constant head test, [b] Constant flow rate test, [c] Length of column, [d] Specific discharge, [e] Influent concentration, [f] Dry density, [g] Total porosity.

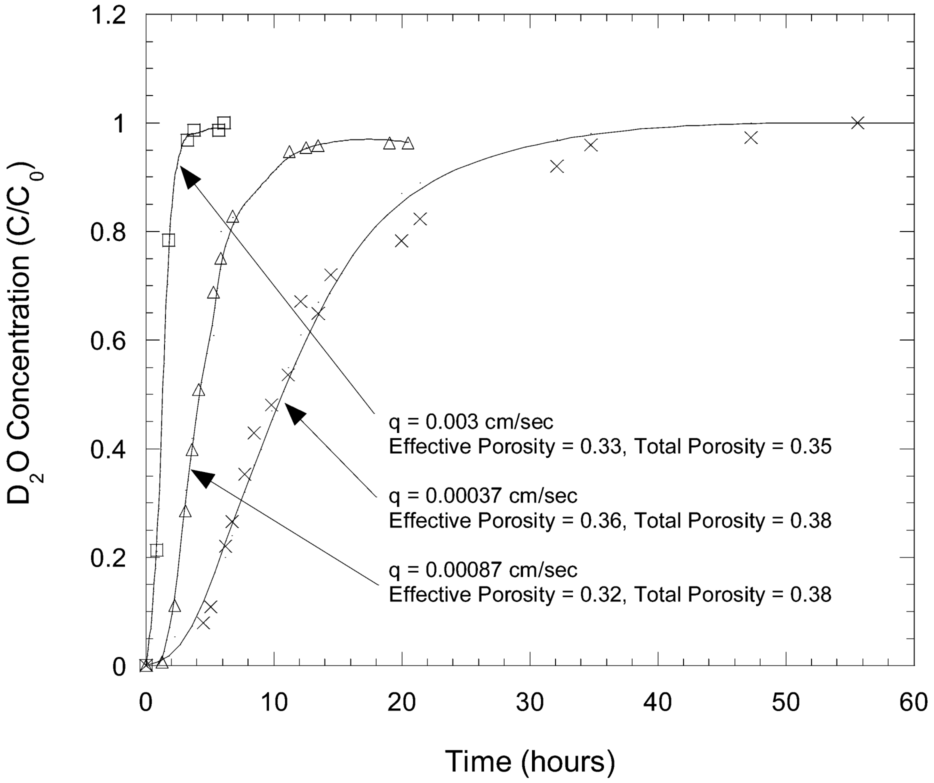

Fig. 5.10. D_2O Breakthrough Curves and Model Fits for Sand 12.

to, but slightly smaller (4.5 – 15.9%) than the total porosities determined by weight-volume calculations.

Effective and total porosities for the other media that were tested are summarized in Table 5.8. As with the foundry sands shown in Fig. 5.10, the effective porosities are generally, but not always, smaller than the total porosities. This effect is shown as the effective porosity ratio, which is the effective porosity divided by the total porosity. The effective porosity ratio varies between 0.63 (Peerless iron) and 1.12 (Sand 11). When only the foundry sands are considered, the effective porosity ratio varies between 0.84 (Sand 12) and 1.12 (Sand 11), and is 0.97 on average.

Higher total porosities were obtained for Peerless iron because the angularity of the iron particles prevents packing into a dense state. The effective porosities for the columns with Peerless iron were significantly lower than the total porosities. The low effective porosities for Peerless iron may have been lower due to formation of precipitates or by gas generation (i.e., H_2). Sosnowski (1996) reports losses of porosity for iron columns ranging between 3% and 37%, by mineral precipitates and occlusion of pores by H_2 gas.

5.3.2 Partition Coefficient

Column tests were conducted with TCE using three foundry sands (i.e., Sands 1, 3, 11, and 12) and a Peerless iron-sand mixture (50:50 by weight). Typical TCE breakthrough curves are shown in Fig. 5.11 and 5.12. Sand 11 was

Table 5.8. Total Porosity and Effective Porosity Obtained from Tracer Tests.

Reactive Media	Dry Density (Mg/m^3)	Tracer	Effective Porosity (n_e)	Total Porosity (n)	Effective Porosity Ratio (n_e/n)
Sand 1[a]	1.65	N.A.[e]	N.A.	0.39	N.A.
Sand 1[b]	1.59	D_2O	0.44	0.42	1.05
Sand 3[b]	1.64	N.A.	N.A.	0.34	N.A.
Sand 11[b]	1.49	Br^-	0.46	0.41	1.12
Sand 12[a]	1.70	D_2O	0.32	0.38	0.84
Sand 12[b]	1.60	Br^-	0.44	0.42	1.05
Sand 12[b]	1.78	D_2O	0.33	0.35	0.94
Sand 12[b]	1.70	D_2O	0.36	0.38	0.95
Sand 12[b]	1.70	D_2O	0.32	0.38	0.84
10% Iron[b]	1.97	D_2O	0.33	0.39	0.85
20% Iron[b]	2.06	D_2O	0.30	0.44	0.68
50% Iron[b]	2.79	D_2O	0.37[c]	0.46	0.80
100% Iron[b]	2.34	N.A.	0.44[d]	0.70	0.63
100% Iron[b]	2.61	N.A.	0.42[d]	0.66	0.64

[a] Constant head test, [b] Constant flow rate test, [c] Effective porosity calculated assuming loss of porosity is proportional to the amount of iron, based on the results from Sosnowski (1996), [d] Effective porosity obtained from Sosnowski (1996), [e] N.A. = Not applicable.

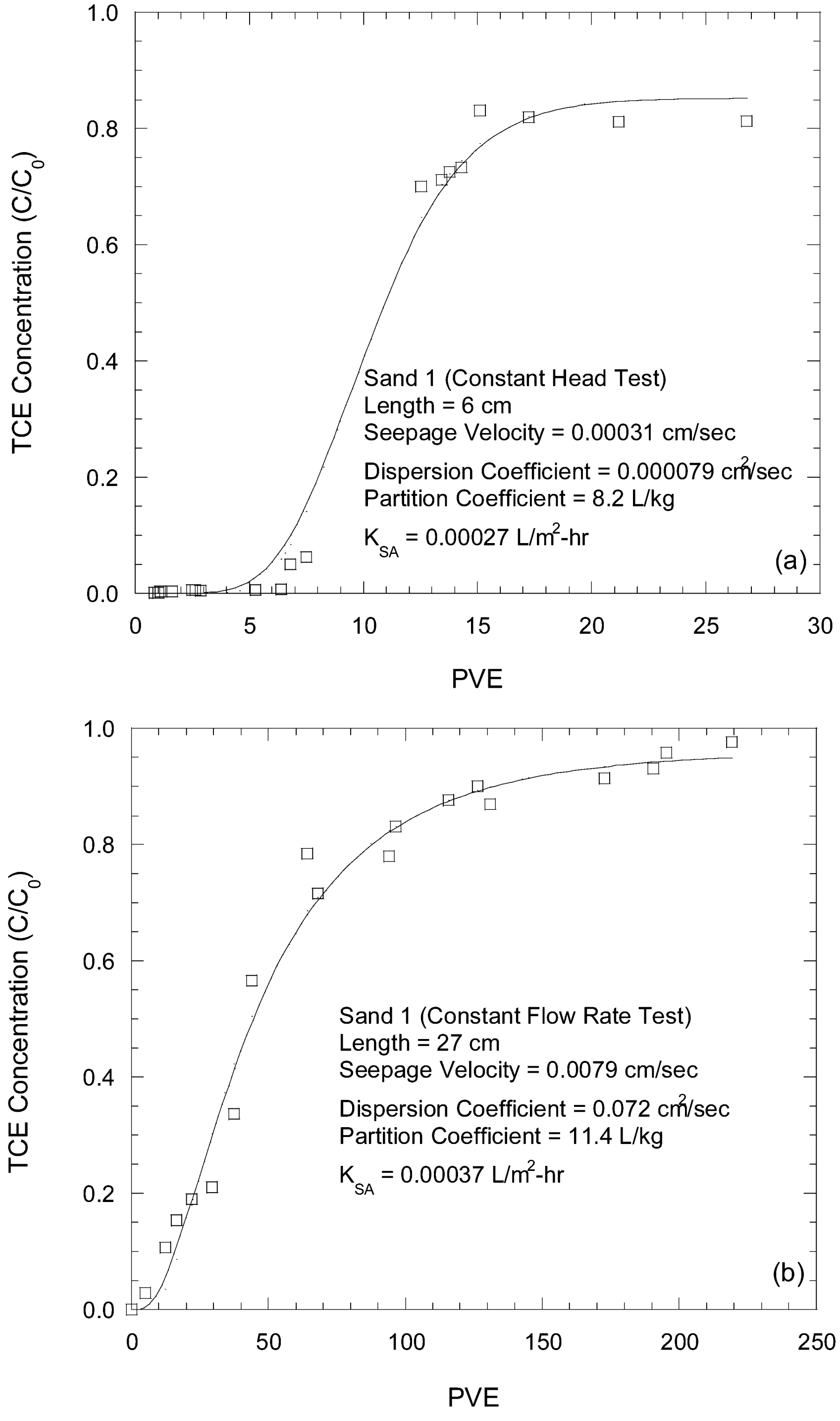

Fig. 5.11. TCE Breakthrough Curves for Sand 1: (a) Constant Head Test and (b) Constant Flow Rate Test.

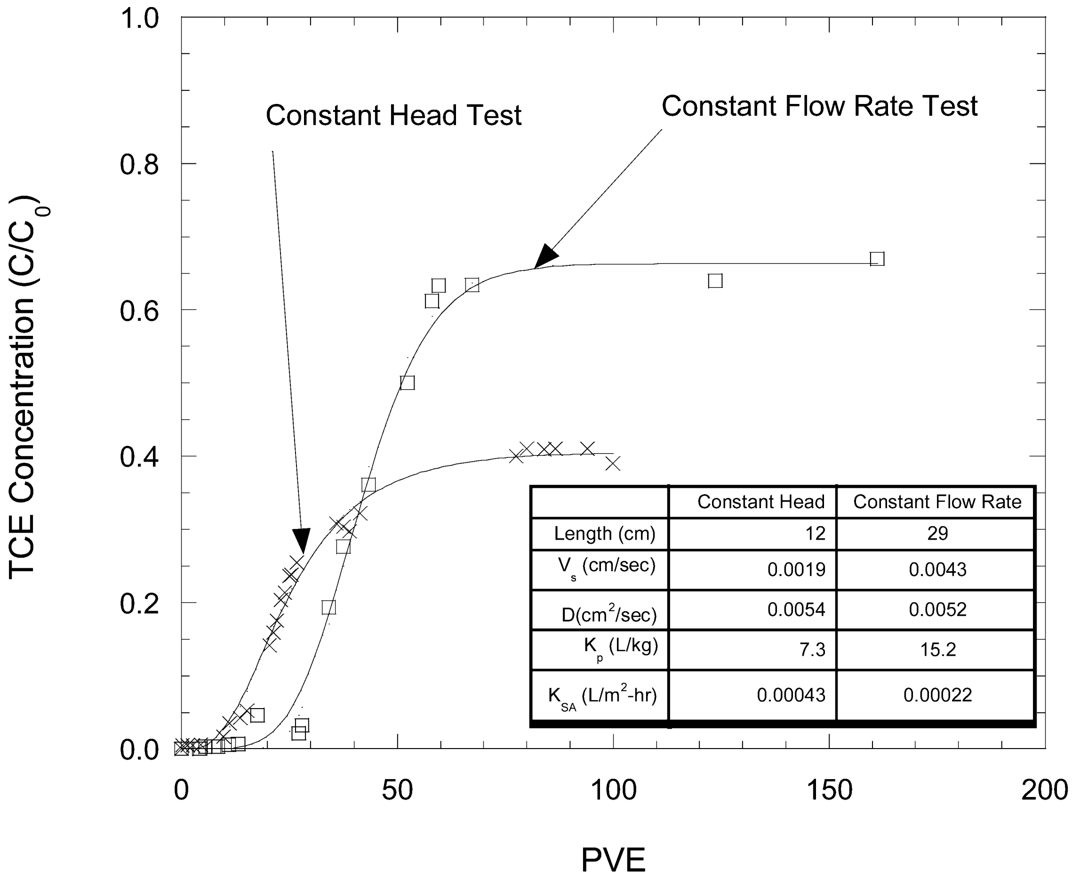

	Constant Head	Constant Flow Rate
Length (cm)	12	29
V_s (cm/sec)	0.0019	0.0043
D(cm^2/sec)	0.0054	0.0052
K_p (L/kg)	7.3	15.2
K_{SA} (L/m^2-hr)	0.00043	0.00022

Fig. 5.12. TCE Breakthrough Curves for Sand 12 Obtained Using Constant Flow Rate and Constant Head Methods.

mixed in equal proportions with silica sand (50% - 50% by weight) to increase the hydraulic conductivity. The partition coefficient obtained from the column test for Sand 11 was doubled under the assumption that sorption of TCE on the silica sand would be negligible.

A summary of the partition coefficients is in Table 5.9. For Sands 1 and 12, the partition coefficients obtained from constant head and constant flow rate tests are significantly different (Fig. 5.11 and 5.12). Greater partition coefficients were obtained from the constant flow rate tests. The reason for the discrepancy between these two tests is unclear.

Partition coefficients from the column tests are graphed against those from the batch sorption tests in Fig. 5.13. The partition coefficients from both tests are comparable, but in general the partition coefficients obtained from column tests are slightly higher than those from the batch tests. Thus, designs based on results of batch tests should be conservative.

5.3.3 First-Order Rate Constant

Transport parameters obtained from the column tests are summarized in Table 5.10. The K_{SA} for foundry sands and Peerless iron were calculated using Eq. 3.18. For Peerless iron, K_{SA} was computed using the steady-state solutions (Eqs. 3.22 – 3.23). Similar K_{SA} for Peerless iron were obtained using Eqs. 3.22 – 3.23 with and without dispersion, where the dispersion coefficient was estimated

Table 5.9. Summary of Partition Coefficients Obtained from Batch and Column Tests.

Reactive Media	Partition Coefficient (L/kg)		Batch/Column Ratio
	Batch Test	Column Test	
Sand 1	5.4	8.2[a]/11.0[b]	0.66[a]/0.49[b]
Sand 3	4.0	6.5[a]	0.62[a]
Sand 11	41.6	54.2[b]	0.77[b]
Sand 12	9.8	7.0[a]/13.1[b]	1.4[a]/0.75[b]
Iron/Sand Admixture	1.8	1.60[b]	1.13[b]

[a] Constant Head Test, [b] Constant Flow Rate Test

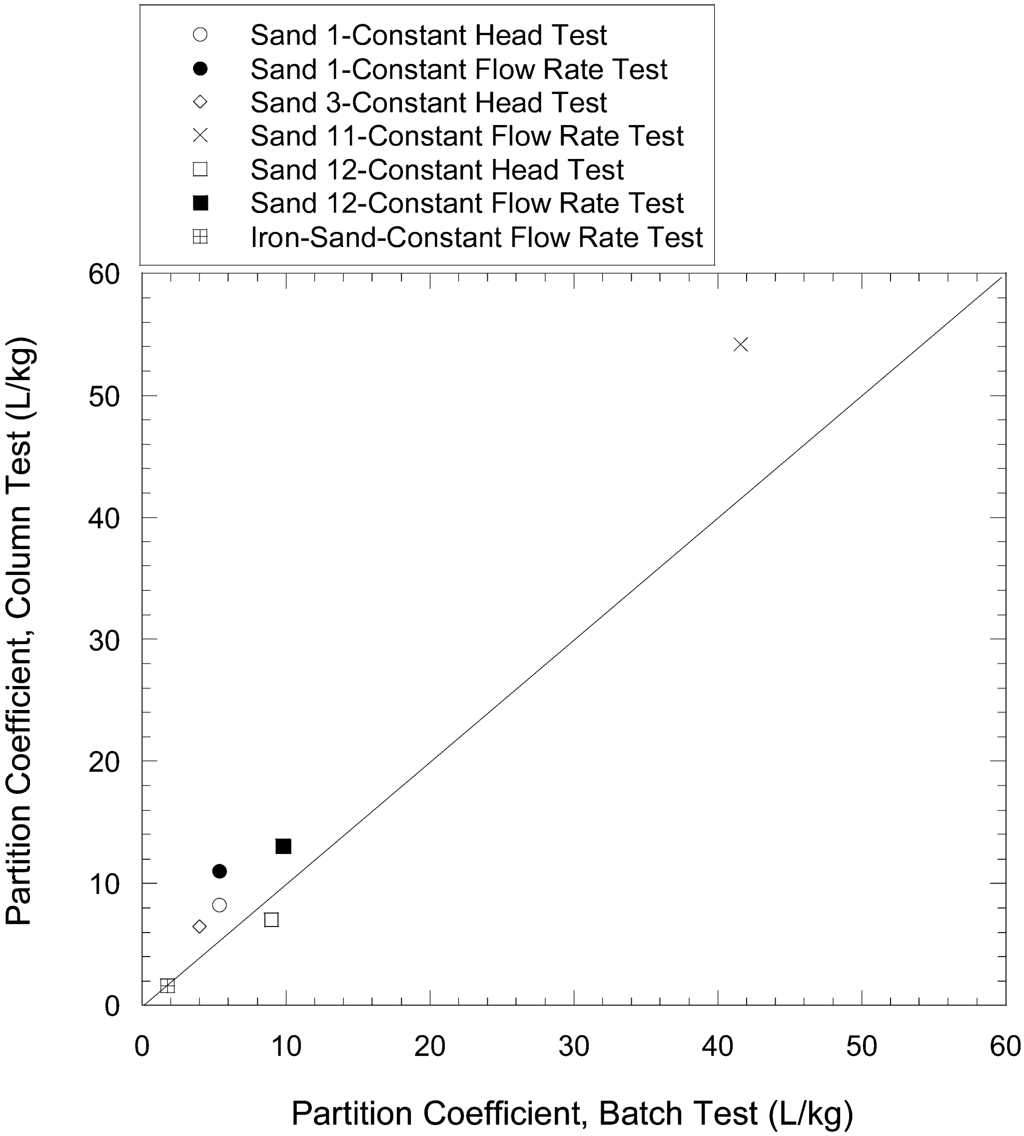

Fig. 5.13. Partition Coefficients Obtained From Batch Sorption Tests and ColumnTests.

Table 5.10. Transport Parameters from Column Tests: Dispersion Coefficient (D), Longitudinal Dispersivity (α_L), and Normalized Rate Constant (K_{SA}).

Reactive Media	V_s[c] (cm/sec)	D[d] (cm^2/sec)	α_L[e] (cm)	α_L[e] (estimated) (cm)	K_{obs}[f] (1/hr)	SA[g] (m^2/L)	K_{SA}[h] (L/m^2-hr)
Sand 1[a]	3.11×10^{-4}	7.87×10^{-5}	0.3	0.6	0.029	108.8	2.70×10^{-4}
Sand 1[b]	7.93×10^{-3}	7.23×10^{-2}	9.1	2.7	0.043	115	3.74×10^{-4}
Sand 3[a]	4.01×10^{-4}	1.05×10^{-3}	2.6	0.6	0.211	138	1.57×10^{-3}
Sand 11[b]	1.92×10^{-2}	3.26×10^{-1}	16.9	3.0	N.A.	N.A.	N.A.
Sand 12[a]	1.89×10^{-3}	5.37×10^{-3}	2.8	1.2	0.62	1312	4.70×10^{-4}
Sand 12[b]	4.29×10^{-3}	5.13×10^{-3}	1.2	2.9	0.23	1034	2.18×10^{-4}
Iron/Sand[b]	9.35×10^{-3}	5.28×10^{-2}	5.6	4.2	0.15	3491	4.32×10^{-5}
Iron[b]	2.62×10^{-3}	N.A.	N.A.	N.A.	0.21	4421	4.89×10^{-5}
Iron (replicate)[b]	2.67×10^{-3}	N.A.	N.A.	N.A.	0.27	5407	5.21×10^{-5}

[a] Constant head test, [b] Constant flow rate test, [c] Seepage velocity, [d] Dispersion coefficient, [e] Longitudinal dispersivity, [f] First-order rate Constant, [g] Surface area of iron per volume of solution, [h] Normalized first-order rate constant.

using Eq. 3.24. Thus, only those computed with dispersion are shown in Table 5.10.

The bulk first-order rate constants (K_{obs}) obtained from the column tests under equilibrium conditions are shown in Fig. 5.14 as a function of SSA. As was observed for the batch tests, K_{obs} increases linearly with increasing SSA. In contrast to the batch tests, however, K_{obs} for the foundry sands is appreciably higher than that for Peerless iron.

The slopes of the lines in Fig. 5.14 represent the normalized rate constant (K_{SA}). The average K_{SA} is 3.5×10^{-4} L/m^2-hr for the foundry sands and 6.0×10^{-5} L/m^2-hr for Peerless iron; that is, K_{SA} for foundry sands is approximately six times higher than that for Peerless iron. The average K_{SA} for the foundry sands (3.5×10^{-4} L/m^2-hr) is comparable to values reported by Johnson et al. (1996) and Sivavec et al. (1997). Johnson et al. (1996) report a K_{SA} of $3.9 \pm 3.6\times10^{-4}$ L/m^2-hr for a variety of irons based on data obtained from batch and column tests. Sivavec et al. (1997) report K_{SA} between 5.7×10^{-5} and 1.2×10^{-4} L/m^2-hr for Peerless iron from column tests. The higher K_{SA} for the foundry sands may be due to different characteristics of iron surfaces in the foundry sands compared to those for Peerless iron.

The average K_{SA} for the batch tests (1.64×10^{-4} L/m^2-hr) falls between that of foundry sands and Peerless iron. The K_{SA} from the column tests on the foundry sands are approximately two times higher than the K_{SA} from the batch

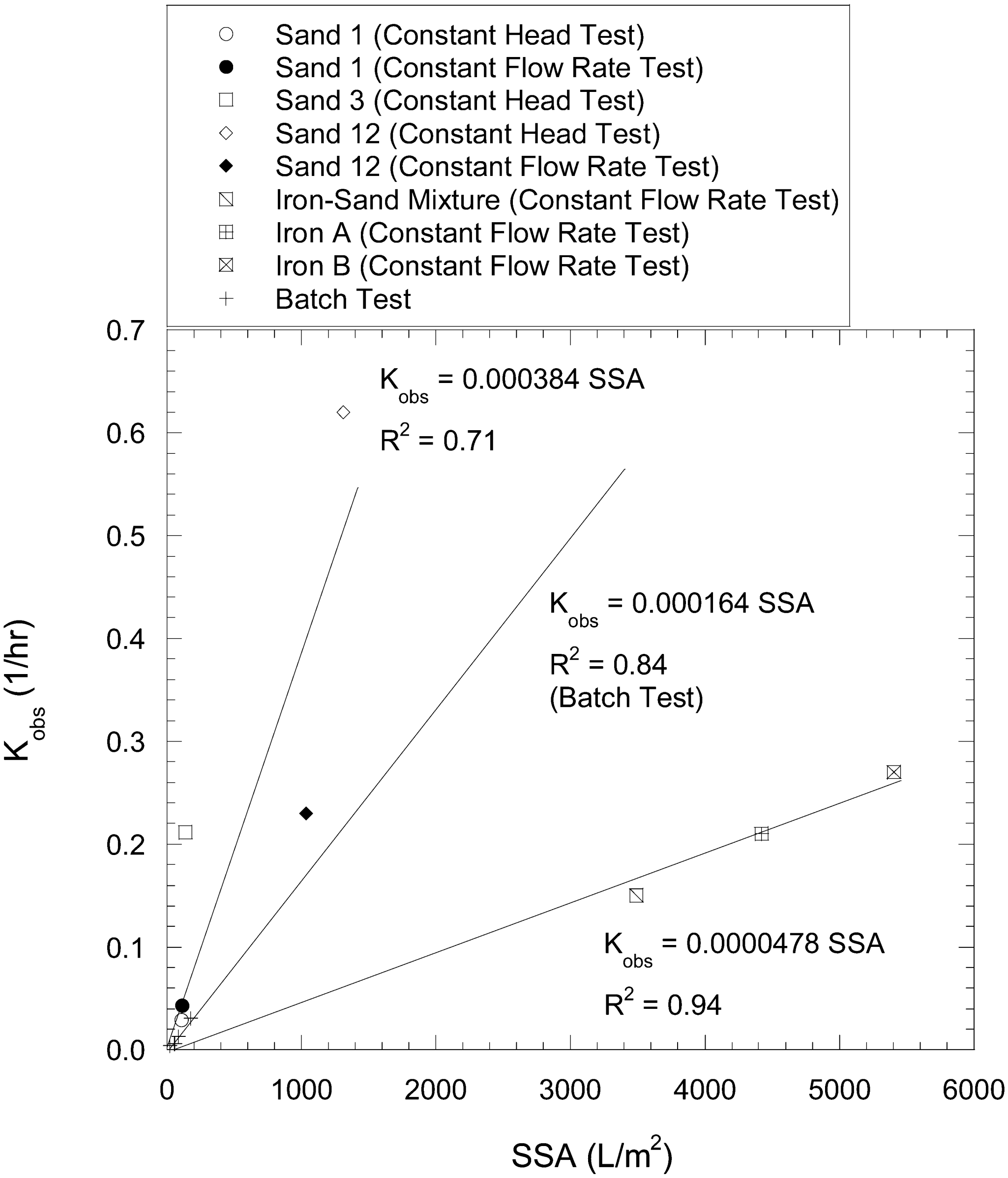

Fig. 5.14. K_{obs} for Foundry Sands and Peerless Iron as a Function of SSA. Central Line is for Data from Batch Tests.

tests. In contrast, the K_{SA} from the column tests on Peerless iron is almost three times lower than that from the batch tests. Even though similar K_{SA} for foundry sands and Peerless iron were obtained for the batch tests, significantly different K_{SA} were obtained for foundry sands and Peerless iron. The reason for the discrepancy between the K_{SA} for the foundry sands and Peerless iron is unknown.

The effect of seepage velocity on K_{SA} for foundry sands and Peerless iron is shown in Fig. 5.15. There is no apparent effect of seepage velocity on K_{SA}.

5.3.4 Dispersion Coefficient and Longitudinal Dispersivity

Dispersivities were computed from the dispersion coefficients obtained from the column tests using the method described in Sec. 3.5.3. The dispersivities are shown in Table 5.10, along with dispersivities computed as one-tenth of the column length. The estimated dispersivities are comparable, but slightly less than those obtained from the column tests. The effect of seepage velocity on the dispersion coefficient is shown in Fig. 5.16. For the range of seepage velocities used in the column tests, the dispersion coefficient can be expressed as:

$$D_h = 336.8\ V_S^{1.88} \tag{5.3}$$

Eq. 5.3 has a coefficient of determination of 0.99. Dispersion coefficients computed with Eq. 5.3 are valid only for seepage velocities exceeding 0.25 m/d (3.0×10^{-4} cm/s).

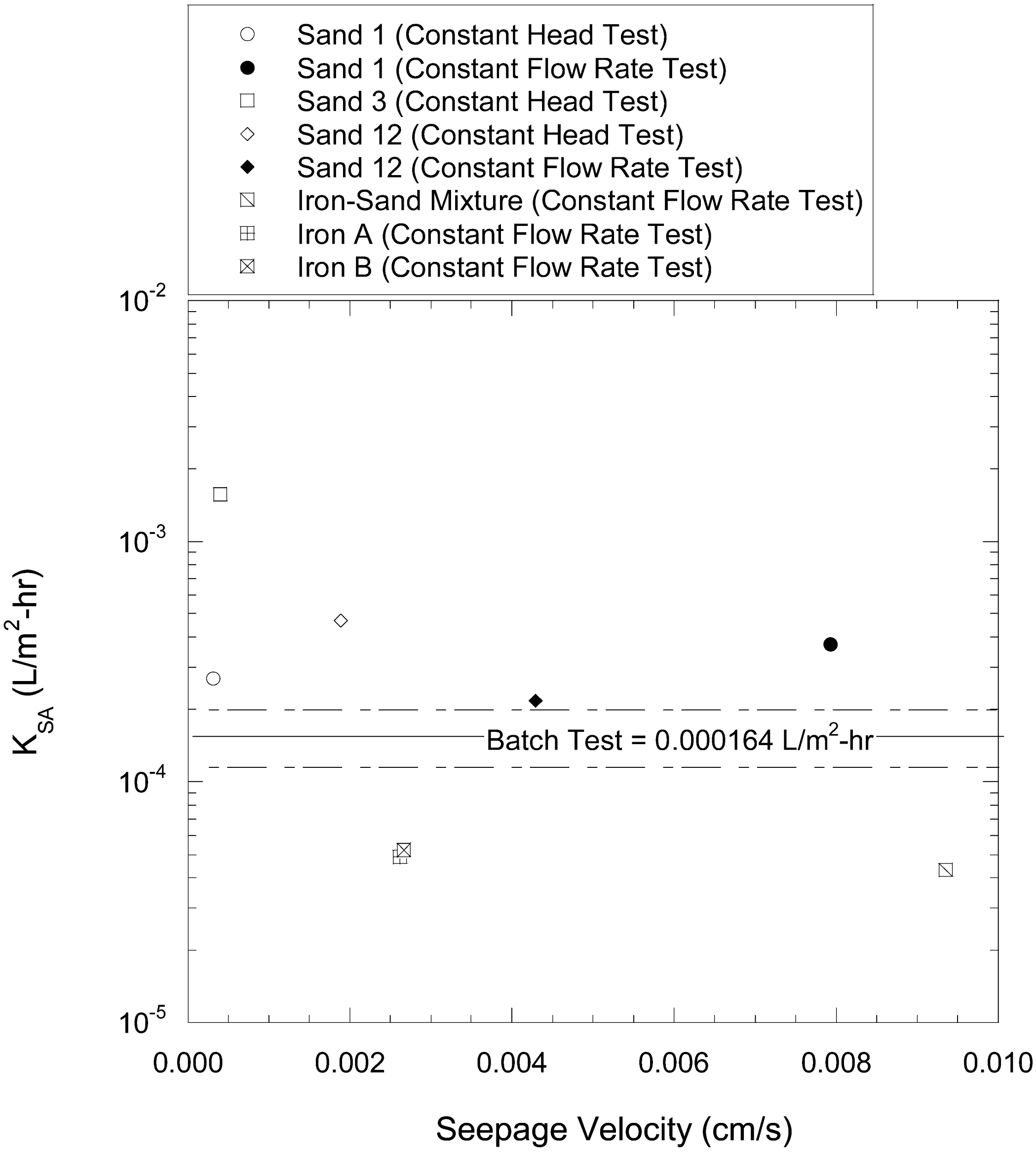

Fig. 5.15. Effect of Seepage Velocity on K_{SA} for Foundry Sands and Peerless Iron. Dashed Lines Depict Range of K_{SA} from Batch Tests.

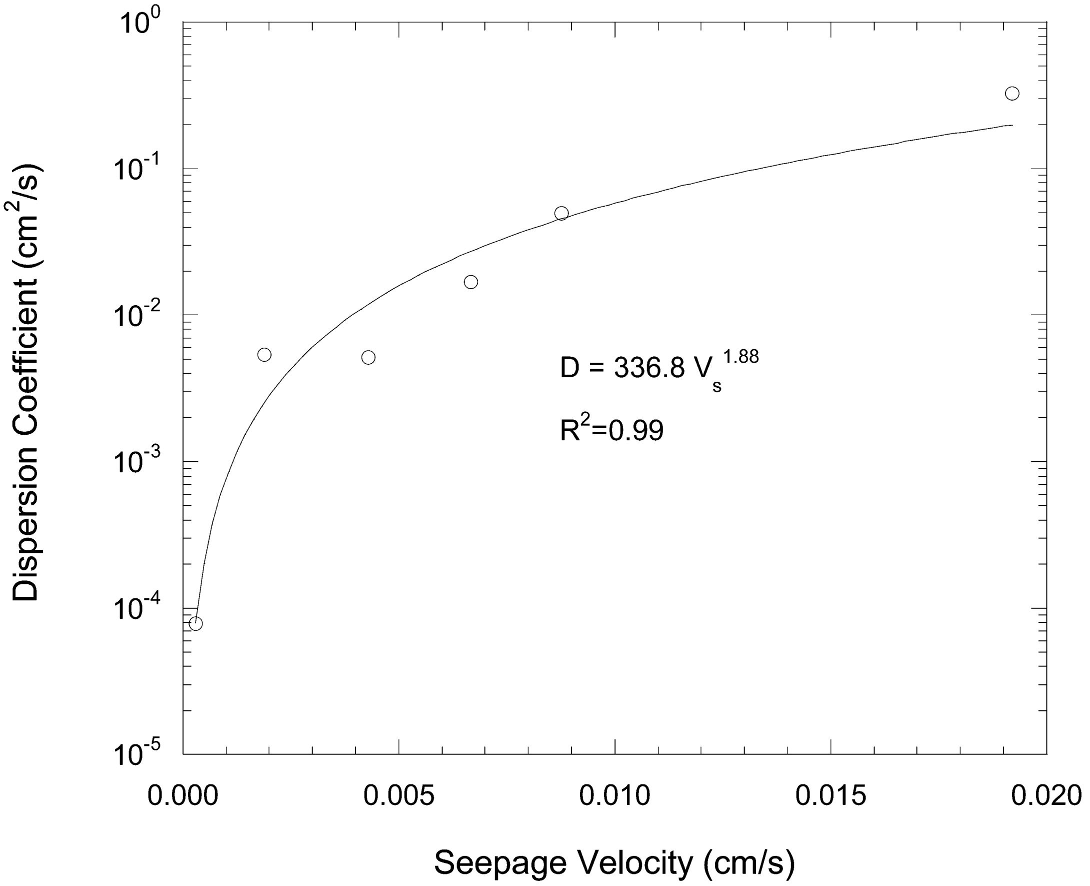

Fig. 5.16. Effect of Seepage Velocity on Dispersion Coefficient.

5.4 PRB DESIGN

The required barrier thickness of PRBs with foundry sands having different iron contents and TOC was estimated using Eq. 3.21. Eq. 3.22 was not used because the effluent concentration was underestimated when dispersion was not considered. The dispersion coefficient used in Eq. 3.21 was computed using Eqs. 3.23 and 3.24. The mechanical dispersion coefficient was calculated by multiplying one-tenth of barrier thickness by seepage velocity. The molecular diffusion coefficient (4.4×10^{-6} cm^2/s) was obtained from Kim (1996).

The seepage velocity used in the calculations ranged between 0.01 m/day and 0.1 m/day, which is characteristic of field conditions (Rust Environement & Infrastructure 1995, Benner et al. 1997, Mueller et al. 1997). TCE concentrations in groundwater typically range between 0.4 to 300 mg/L (USEPA 1997, McMahon et al. 1999). Thus, the source TCE concentration (C_0) was assumed to vary between 0.4 to 400 mg/L. Accordingly, the normalized concentration of TCE (C/C_0) required to meet the MCL for TCE (C = 0.005 mg/L) ranged between 0.0125 and 0.0000125.

The zero-valent iron content was varied from 0.1% to 10% to bracket iron contents typically in foundry sands. Values typical of foundry sands were assumed for dry density (1.5 Mg/m^3) and specific gravity of solids (2.62) when calculating SSA. The bulk first-order rate constant was calculated by multiplying SSA by the average K_{SA} for the foundry sands (3.84×10^{-4} L/m^2-hr).

The TOC was varied from 0.1 to 4.0% to represent the range of TOC normally found in foundry sands. Eq. 5.2 was used to calculate the partition coefficients from TOC. The partition coefficients were used to calculate retardation factors using a conventional linear sorption model.

The normalized TCE concentrations are shown in Fig. 5.17 for various zero-valent iron contents and barrier thicknesses. PRBs less than 1 m wide can be constructed with foundry sands provided the seepage velocity is less than 0.01 m/day, the zero-valent iron content is at least 0.6%, and the source concentration is less than 400 mg/L. For more severe conditions, a thicker barrier may be required or the reactivity of the barriers may need to be enhanced by adding a modest amount of iron particles to the foundry sands.

The retardation of TCE afforded by the foundry sands is evident in Fig. 5.18, which shows that the equilibrium time increases as the TOC of the foundry sand increases. For example, when the seepage velocity is 0.01 m/d, the time to equilibrium increases from 20 yr to 39 yr when the TOC is increased from 1 to 2%. In comparison, if no retardation occurred, the time to equilibrium would be 1 yr. The additional residence time afforded by the TOC of the foundry sand may permit biodegradation of compounds by naturally occurring microorganisms, resulting in lower effluent concentrations.

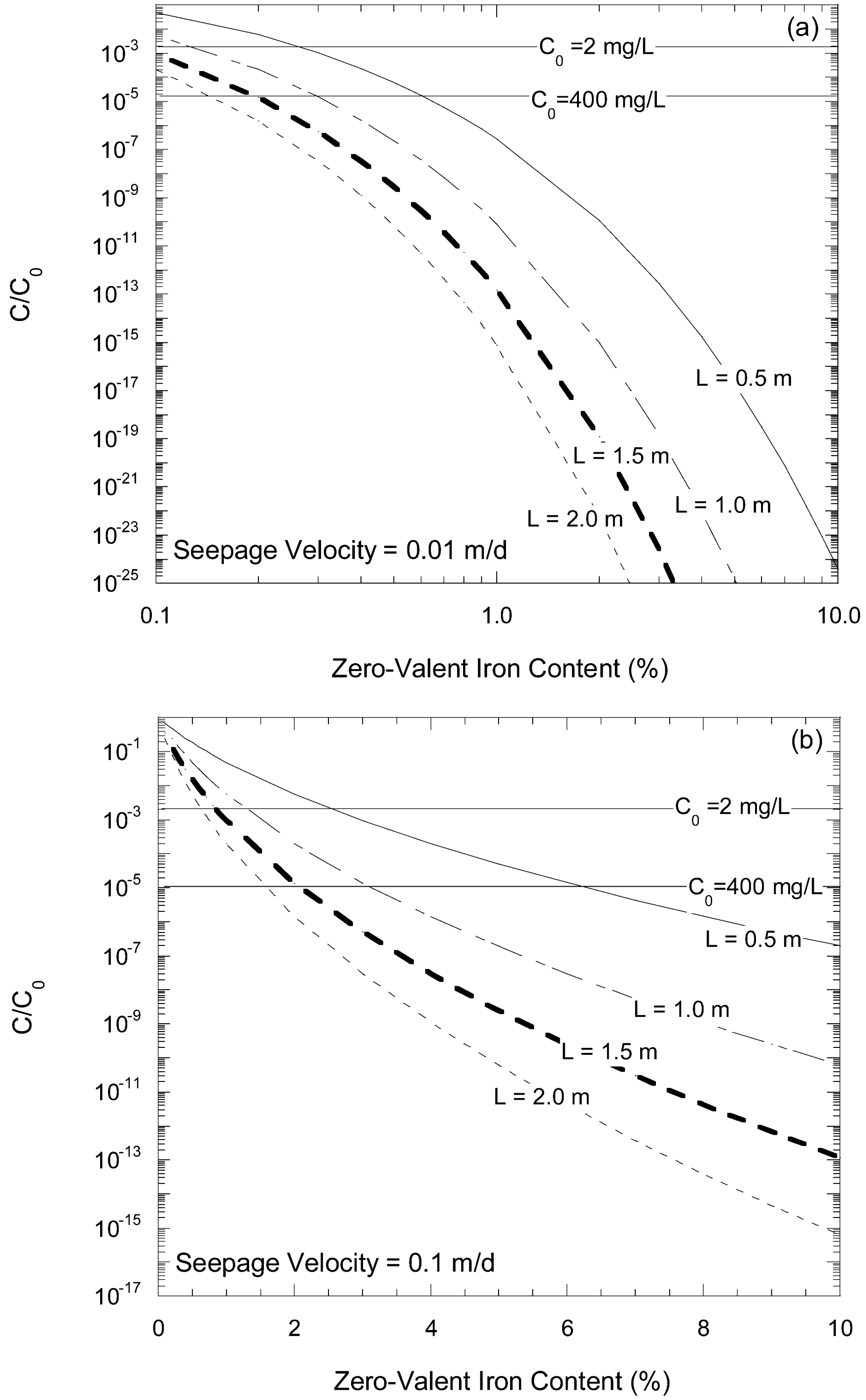

Fig. 5.17. Required Barrier Thickness as a Function of Zero-Valent Iron Content and Barrier Thickness: (a) V_S = 0.01 m/d and (b) V_s = 0.1 m/d.

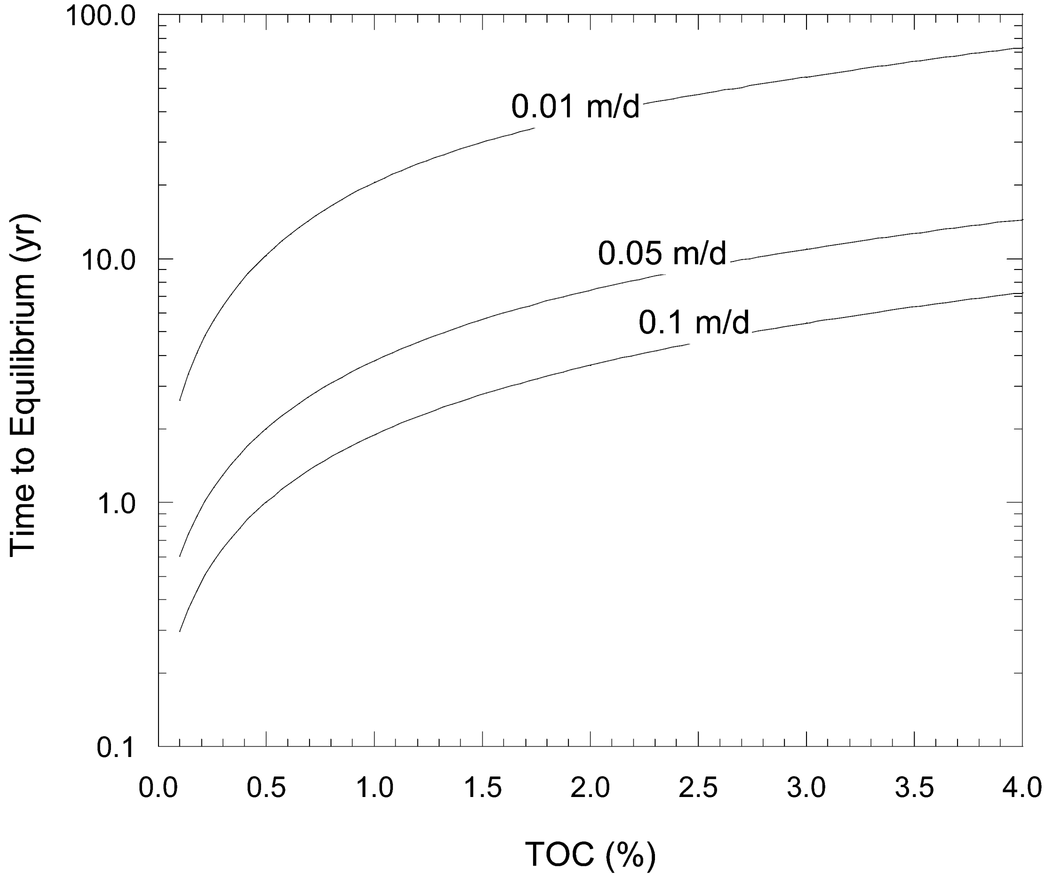

Fig. 5.18. Time to Reach Equilibrium as a Function of TOC and Seepage Velocity.

SECTION SIX

RESULTS OF BATCH AND COLUMN TESTS USING HERBICIDES

6.1 BATCH DEGRADATION TESTS

Batch degradation tests were conducted with alachlor and metolachlor following the methods described in Sec. 3.4.2. As in Sec. 5, tests were conducted with iron from the foundry sands as well as Peerless iron. Concentrations of the herbicides and their byproducts (acetyl alachlor and MBP) are shown in Fig. 6.1. Model fits using Eqs. 3.15 and 3.16 are also shown in Fig. 6.1. Results of all of the batch degradation tests are summarized in Table 6.1.

When the first order rate constants are normalized by the specific surface area, K_{SA} for the foundry sand iron and Peerless iron are similar (Table 6.1). The retardation factors for the foundry iron and Peerless iron are similar as well. Koppensteiner and Eykholt (2000) report K_{SA} for alachlor and metolachlor based on batch tests conducted with Peerless iron. Their K_{SA} (1.5×10^{-3} L/m^2-hr for alachlor and 1.0×10^{-3} L/m^2-hr for metolachlor) are approximately two times higher than those reported in Table 6.1. However, the retardation factors for parent and daughter compounds reported in Table 6.1 are comparable to those from Koppensteiner (1998).

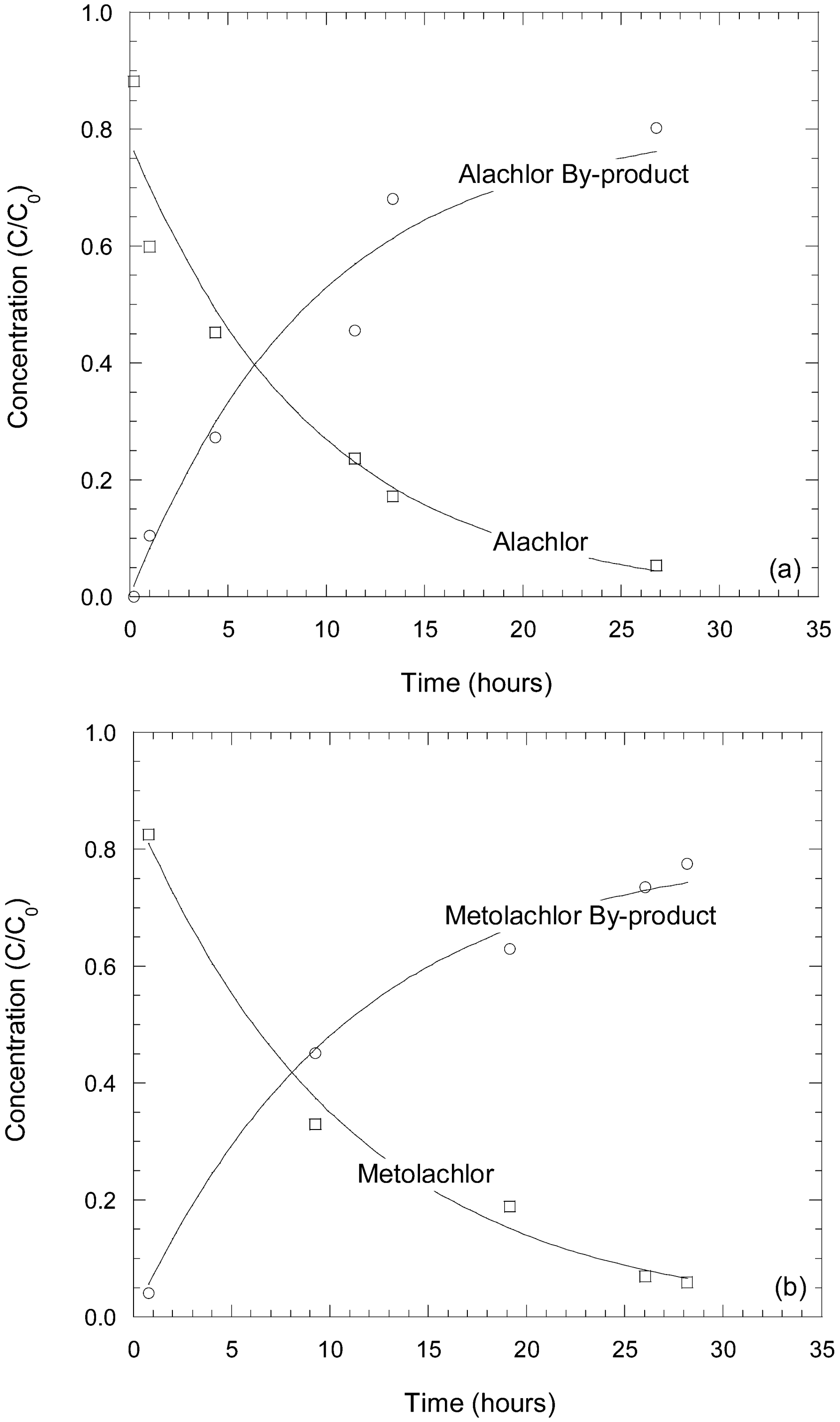

Fig. 6.1. Concentrations of (a) Alachlor and Alachlor By-product and (b) Metolachlor and Metolachlor By-product from a Batch Degradation Test Conducted with Iron from Sand 12.

Table. 6.1. Results of Batch Degradation Tests for Alachlor and Metolachlor Using Foundry Iron and Peerless Iron.

Compound	Iron Source	Initial Concentration (mg/L)	ρ_a[a] (m^2/L)	K_{obs}[b] (1/hr)	K_{SA}[c] (L/m^2-hr)	R_P[d]	R_d[e]
Alachlor	Sand 12	49	171	0.14	8.0×10^{-4}	1.28	1.24
Alachlor	Peerless Iron	49	40	0.03	7.1×10^{-4}	1.17	1.20
Metolachlor	Sand 12	84	186	0.11	5.7×10^{-4}	1.15	1.24
Metolachlor	Peerless Iron	38	22	0.012	5.3×10^{-4}	1.12	1.53

[a] Specific Surface Area of Iron per Unit Volume of Solution, [b] First-Order Rate Constant, [c] Normalized First-Order Rate Constant, [d] Retardation Factor for Parent Compound, [e] Retardation Factor for Daughter Compound.

6.2 SERIAL BATCH KINETIC TEST

Concentrations of alachlor and metolachlor for the serial batch kinetic tests using alachlor and metolachlor are shown in Fig. 3.4 in Sec. 3.3.2.1. Chlorinated by-products (i.e., acetyl alachlor and MBP) were observed in the serial batch tests containing Sands 1, 2, 4, and 11. However, concentrations of both by-products were close to or below the MDL. In general, more metolachlor was sorbed on foundry sands than alachlor, which is consistent with the higher octanol-water partition coefficient for metolachlor than for alachlor (K_{OW} = 430 for alachlor, and 2800 for metolachlor). Longer contact times were required to reach equilibrium for metolachlor than alachlor (24 vs. 5 hrs). Longer times may have been required for metolachlor due to the higher solubility of metolachlor (530 mg/L) relative to that of alachlor (240 mg/L), and the greater amount of metolachlor that was sorbed.

6.3 BATCH SORPTION TESTS

6.3.1 Alachlor

Batch sorption tests were conducted on Sands 1 – 5 and 7 – 12. Before conducting the tests, the zero-valent iron was removed with a magnet so that reactivity and sorptivity could be evaluated separately. Based on the results of the serial batch kinetic test, 24 hrs of tumbling was deemed sufficient to reach equilibrium in the batch sorption tests. Sorption isotherms for alachlor are shown in Fig. 6.2. All of the isotherms were approximately linear within the range of

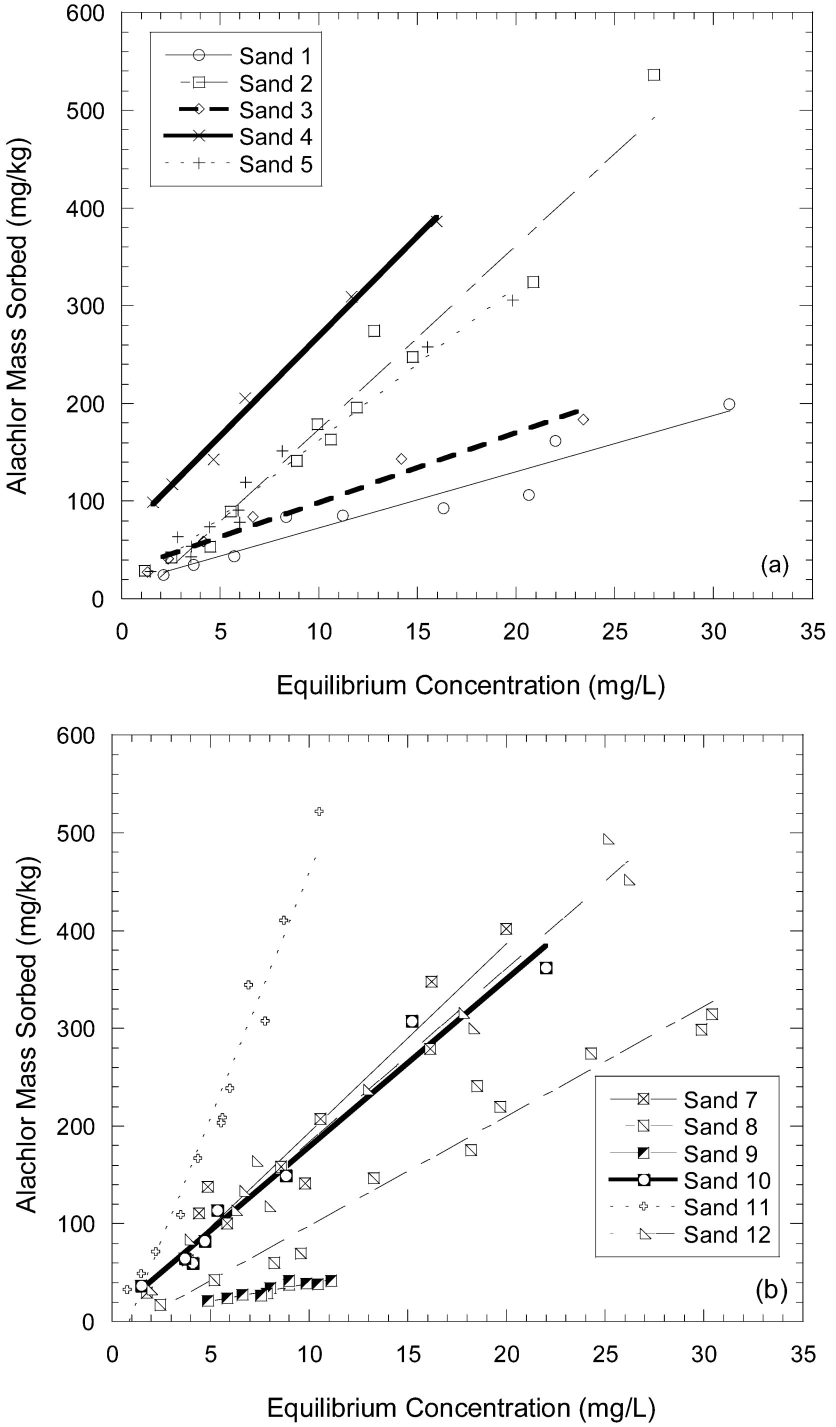

Fig. 6.2. Alachlor Sorption Isotherms for Foundry Sands: (a) Sands 1 - 5 and (b) Sands 7 - 12.

concentrations that was tested.

Parameters of the linear and Freundlich models fitted to the isotherm data are summarized in Table 6.2. For the linear model, Method 1 consisted of fitting a linear equation to the data. Method 2 required that the intercept of the linear model be zero. Partition coefficients obtained from the linear model (first column in Table 6.2) for alachlor ranged from 3.6 L/kg (Sand 9) to 50.2 L/kg (Sand 11). Slightly different partition coefficients were obtained when the linear model was forced to have a zero intercept due to the non-linearity of the isotherms near the origin. The fits with the Freundlich model also confirm that the isotherms are essentially linear. Except for Sands 1, 3, and 4, the Freundlich parameter n is approximately 1.

6.3.2 Metolachlor

Sorption isotherms for metolachlor are shown in Fig. 6.3. As with alachlor, the metolachlor isotherms are approximately linear over the range of concentrations that was used. Partition coefficients obtained from the linear model ranged from 1.0 to 54.8 L/kg, as summarized in Table 6.3. The linearity is also evident in Freundlich model fits. The Freundlich coefficients 1/n is approximately 1 for all sands, but Sands 5 – 9. Additionally, the deviations of n from 1 are due to scatter in the data than true non-linearity.

Table 6.2. Results of Partition Coefficients for Alachlor Obtained from Batch Sorption Tests.

Foundry Sands	Linear Model				Freundlich Model		
	Method 1		Method 2				
	K_p (L/kg)	R^{2a}	K_p (L/kg)	R^{2a}	K_f	1/n	R^{2a}
1	5.8	0.93	6.5	0.90	13.5	0.75	0.95
2	18.8	0.96	17.9	0.96	18.3	0.97	0.96
3	7.1	0.97	8.9	0.86	23.1	0.67	0.99
4	20.5	0.99	26.4	0.87	67.1	0.61	0.97
5	15.6	0.98	16.1	0.98	17.8	0.95	0.94
7	19.3	0.94	19.4	0.94	19.0	1.0	0.93
8	11.2	0.96	10.6	0.96	5.6	1.20	0.98
9	3.6	0.86	4.0	0.85	5.0	0.90	0.89
10	17.2	0.97	17.7	0.97	21.5	0.92	0.96
11	50.2	0.96	43.9	0.94	33.8	1.10	0.97
12	17.8	0.98	18.1	0.98	19.4	0.98	0.98

[a] Coefficient of Determination.

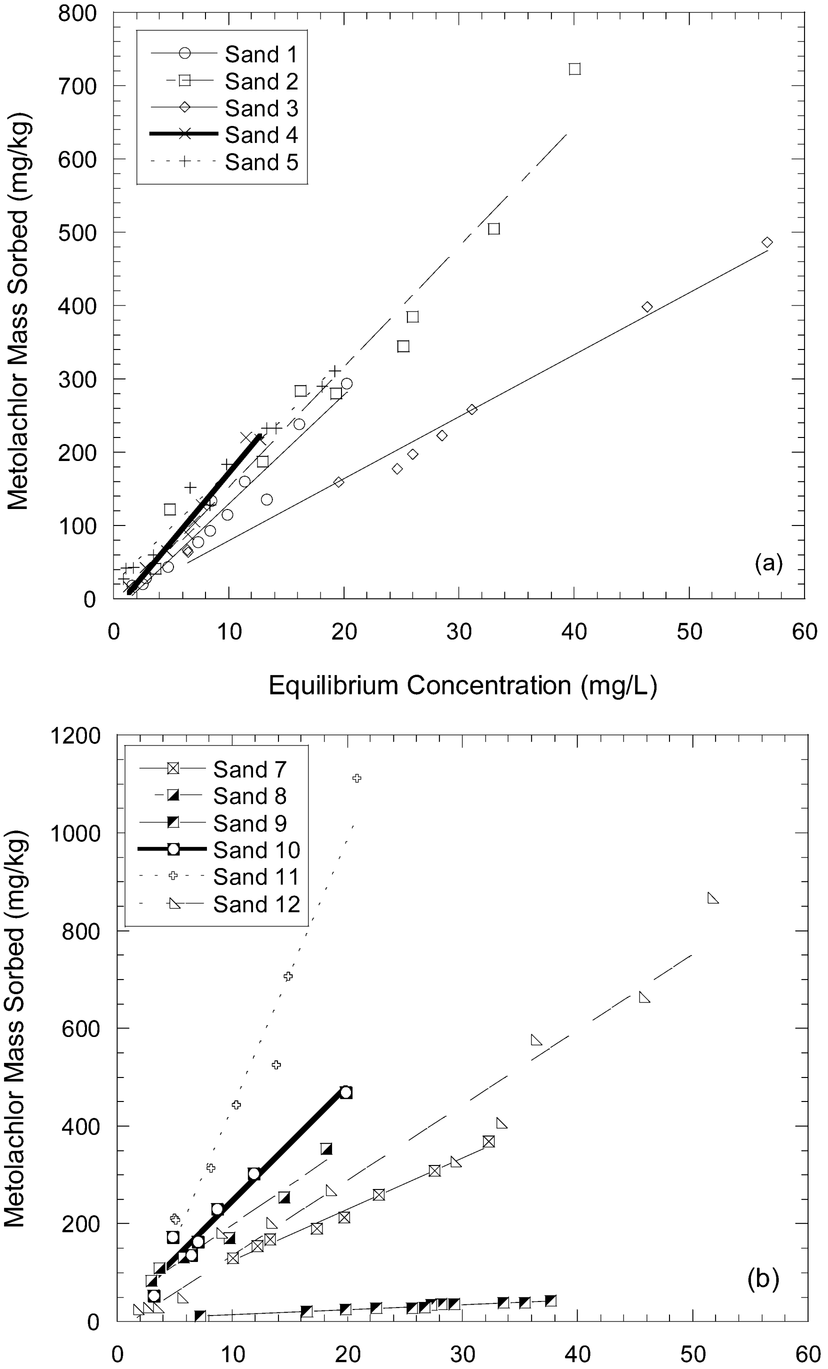

Fig. 6.3. Metolachlor Sorption Isotherms for Foundry Sands: (a) Sands 1 – 5 and (b) Sands 7 – 12.

Table 6.3. Results of Partition Coefficients for Metolachlor Obtained From Batch Sorption Tests.

Foundry Sands	Linear Model				Freundlich Model		
	Method 1		Method 2		K_f	1/n	R^{2a}
	K_p (L/kg)	R^{2a}	K_p (L/kg)	R^{2a}			
1	14.9	0.95	13.3	0.94	8.2	1.17	0.97
2	16.5	0.95	16.0	0.95	15.8	0.99	0.93
3	8.5	0.99	8.30	0.99	11.5	0.90	0.98
4	18.9	0.98	16.9	0.96	11.7	1.15	0.99
5	15.3	0.98	16.8	0.97	30.4	0.77	0.97
7	10.5	0.99	11.4	0.98	17.1	0.87	0.98
8	16.3	0.97	19.0	0.93	38.5	0.72	0.96
9	1.0	0.96	1.2	0.94	2.1	0.83	0.98
10	23.6	0.96	24.4	0.95	20.3	1.1	0.89
11	54.8	0.96	46.9	0.93	32.4	1.1	0.97
12	15.4	0.96	14.9	0.96	10.5	1.1	0.97

[a] Coefficient of Determination.

6.3.3 Effect of TOC and Clay Content on Partition Coefficient

Partition coefficients for alachlor and metolachlor are graphed vs. TOC and clay content in Fig. 6.4. For both alachlor and metolachlor, K_p increases as the TOC and clay content increase due to greater availability of sorption sites. Significant scatter exists, some of which is due to multivariate interactions. For example, Sand 4 has relatively high K_p (18.9 L/kg), even though its TOC is low (0.5%), because it has a high clay content (10.5%).

Multivariate linear regression analysis was conducted at the 0.05 significance level to determine a relationship between K_p, clay content, and TOC. The equation for alachlor and metolachlor is ($R^2 = 0.62$).

$$\log K_{p,\,ala} = 0.666 + 0.0723\ C \tag{6.3}$$

where $K_{p,\,ala}$ is the partition coefficient for alachlor (L/kg), C is clay content (%).

The equation for metolachlor is ($R^2 = 0.62$):

$$\log K_{p,meto} = 0.460 + 0.101\ C \tag{6.4}$$

where $K_{p,\ meto}$ is the partition coefficient for metolachlor (L/kg) and the other variables are as defined previously. Equations 6.3 and 6.4 indicate that metolachlor is sorbed more than alachlor, when all other factors are equal.

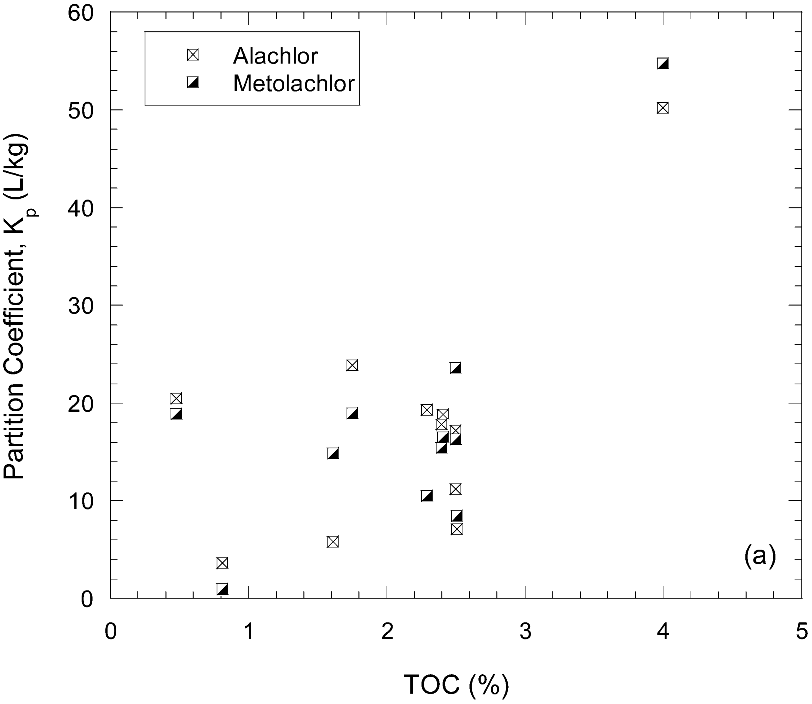

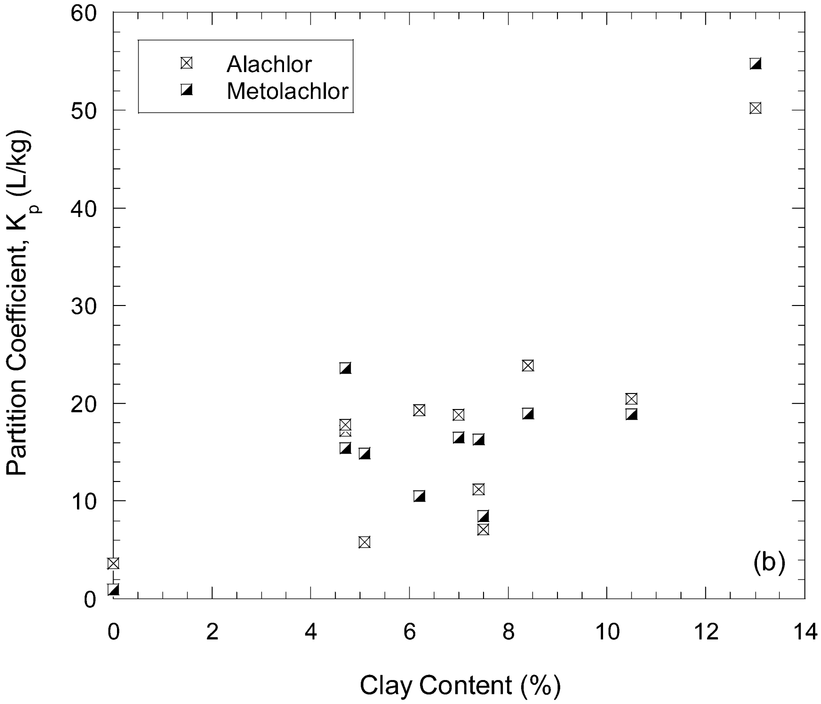

Fig. 6.4. Effect of (a) TOC and (b) Clay Content on Partition Coefficients for Alachlor and Metolachlor.

6.4 COLUMN TESTS

6.4.1 Alachlor

Experimental conditions for the column tests conducted with alachlor are summarized in Table 6.4. Five foundry sands were used (1, 2, 4, 5, and 12) that had a broad range of TOC, clay content, and iron content. Tests were also conducted with Sands 1 and 5 with admixtures of Peerless iron to evaluate how elevated iron content affects reactivity of the foundry sand. An additional five comparative tests were conducted using a mixture of Peerless iron and silica sand. Influent concentrations ranging from 34 mg/L to 53 mg/L were used.

The total iron contents for Sand 1 and Sand 12 were 2.8% and 11.3%, respectively. However, the zero-valent iron contents for these two sands, as measured by magnetic separation, are 1.0% and 10%. The zero-valent iron contents were used to analyze the data for column tests for Sands 1 and 12. For Sands 2, 4, and 5, the zero-valent iron contents were similar to the total iron contents. Thus, the total iron contents were used for these sands when analyzing the data from the column tests.

Dispersion coefficients, dispersivities, partition coefficients, and rate constants from the column tests are summarized in Table 6.5. The degradation of alachlor was confirmed by the presence of acetyl alachlor in the effluent. The mass balances ranged between 97 (Sand 4) and 101% (Sand 2).

Table 6.4. Experimental Conditions for Column Tests with Alachlor.

Reactive Media	C^c (mg/L)	L (cm)[d]	$\rho_d{}^e$ (Mg/m^3)	n^f	$n_e{}^g$	Iron Content (%)	SSA[h] (m^2/L)	$V_s{}^i$ (cm/sec)
Sand 1	34	42	1.67	0.36	0.36	1	113	3.23×10^{-3}
Sand 1[a]	35	42	1.66	0.47	0.40	11	364	3.23×10^{-3}
Sand 2	35	28	1.69	0.33	0.33	0.2	19	3.49×10^{-3}
Sand 4	35	28	1.69	0.36	0.36	0.3	34	3.47×10^{-3}
Sand 5[b]	48	30	1.83	0.49	0.40	20	791	2.48×10^{-3}
Sand 12	42	15	1.56	0.43	0.36	10	1053	3.74×10^{-3}
Iron	20	43	2.07	0.34	0.29	10	624	4.43×10^{-3}
Iron	53	42	2.06	0.34	0.29	10	620	4.86×10^{-3}
Iron	49	44	1.88	0.40	0.34	10	486	3.30×10^{-3}
Iron	50	45	2.14	0.42	0.35	20	1073	2.88×10^{-3}
Iron	50	45	1.97	0.38	0.32	10	532	2.43×10^{-3}

[a] Admixture with a 10% Peerless Iron, [b] Admixture with a 20% Peerless Iron, [c] Influent Alachlor Concentration, [d] Length of Sample, [e] Dry Density, [f] Total Porosity, [g] Effective Porosity, [h] Surface Area of Iron per Volume of Solution, [i] Seepage Velocity.

Table 6.5. Results of Column Tests: Dispersion Coefficient, Partition Coefficient, First-Order Rate Constant, and K_{SA} from Column Tests Using Alachlor.

Reactive Media	Dispersion Coefficient (cm^2/sec)	Dispersivity (cm)		Partition Coefficient (L/kg)		K_{obs} [c] (hr^{-1})	K_{SA} [d](L/m^2-hr)	
		Model Fit	Estimated	Batch	Column		Model Fit[e]	Steady-State[f]
Sand 1	5.5×10^{-3}	1.71	4.2	5.8	6.52	0.036	3.21×10^{-4}	2.56×10^{-4}
Sand 1[a]	2.44×10^{-2}	7.54	4.2	5.8	8.46	0.082	2.95×10^{-4}	3.07×10^{-4}
Sand 2	1.37×10^{-2}	3.92	2.8	18.8	11.72	0.009	4.69×10^{-4}	4.51×10^{-4}
Sand 4	1.06×10^{-2}	3.07	2.8	20.5	16.36	0.032	9.36×10^{-4}	1.11×10^{-3}
Sand 5[b]	2.86×10^{-3}	1.15	3.0	15.6	9.02	0.453	5.67×10^{-4}	5.89×10^{-4}
Sand 12	N.A.	N.A.	N.A.	N.A.	N.A.	0.570	N.A.	4.78×10^{-4}
Iron	8.77×10^{-3}	1.98	4.3	2.24	0.49	0.267	5.03×10^{-4}	5.00×10^{-4}
Iron	N.A.	N.A.	N.A.	N.A.	N.A.	0.345	6.55×10^{-4}	5.56×10^{-4}
Iron	N.A.	N.A.	N.A.	N.A.	N.A.	0.150	N.A.	3.34×10^{-4}
Iron	4.87×10^{-3}	1.69	4.5	2.24	1.89	0.617	6.94×10^{-4}	6.02×10^{-4}
Iron	4.91×10^{-3}	2.02	4.5	2.24	1.03	0.166	3.67×10^{-4}	1.26×10^{-4}

[a] Admixture with a 10% Peerless Iron, [b] Admixture with a 20% Peerless Iron, [c] Bulk first-order rate constant, [d] Normalized first-order rate constant, [e] Normalized first-order rate constant calculated by Eq. 3.18, [f] Normalized first-order rate constant calculated by Eq. 3.21.

6.4.1.1 First-Order Rate Constant

The first-order rate constants were obtained by fitting the data with Eq. 3.18, 3.21, or 3.22. Typical fits obtained using Eq. 3.18 are shown in Fig. 6.5. A summary of the rate constants is in Table 6.5. All of the normalized rate constants are similar, even though the influent concentration and seepage velocity were varied. Thus, concentration and seepage velocity appear to have no significant effect on K_{SA} for herbicides. The lack of an influence of seepage velocity is also shown in Fig. 6.6, which shows K_{SA} vs. seepage velocity for all tests that were conducted with the herbicides.

The K_{SA} obtained from the steady-state condition are tabulated in Table 6.5. Similar K_{SA} were obtained using the steady-state model with and without dispersion. Thus, only the K_{SA} determined with dispersion are included in Table 6.5.

As with the tests using TCE (Sec. 5), the bulk first-order rate constant (K_{obs}) is directly proportional to the surface area of iron per volume of solution (SSA) (Fig. 6.7). The slope of the linear regression equation in Fig. 6.7 is equal to the average K_{SA}, which is 5.85×10^{-4} L/m^2-hr. This average K_{SA} is slightly lower (1.3 times) than the K_{SA} obtained from the batch degradation tests (8.0×10^{-4} and 7.1×10^{-4} L/m^2-hr for the foundry sand iron and Peerless iron, respectively).

6.4.1.2 Partition Coefficient

Partition coefficients, K_p, obtained from the column tests are summarized

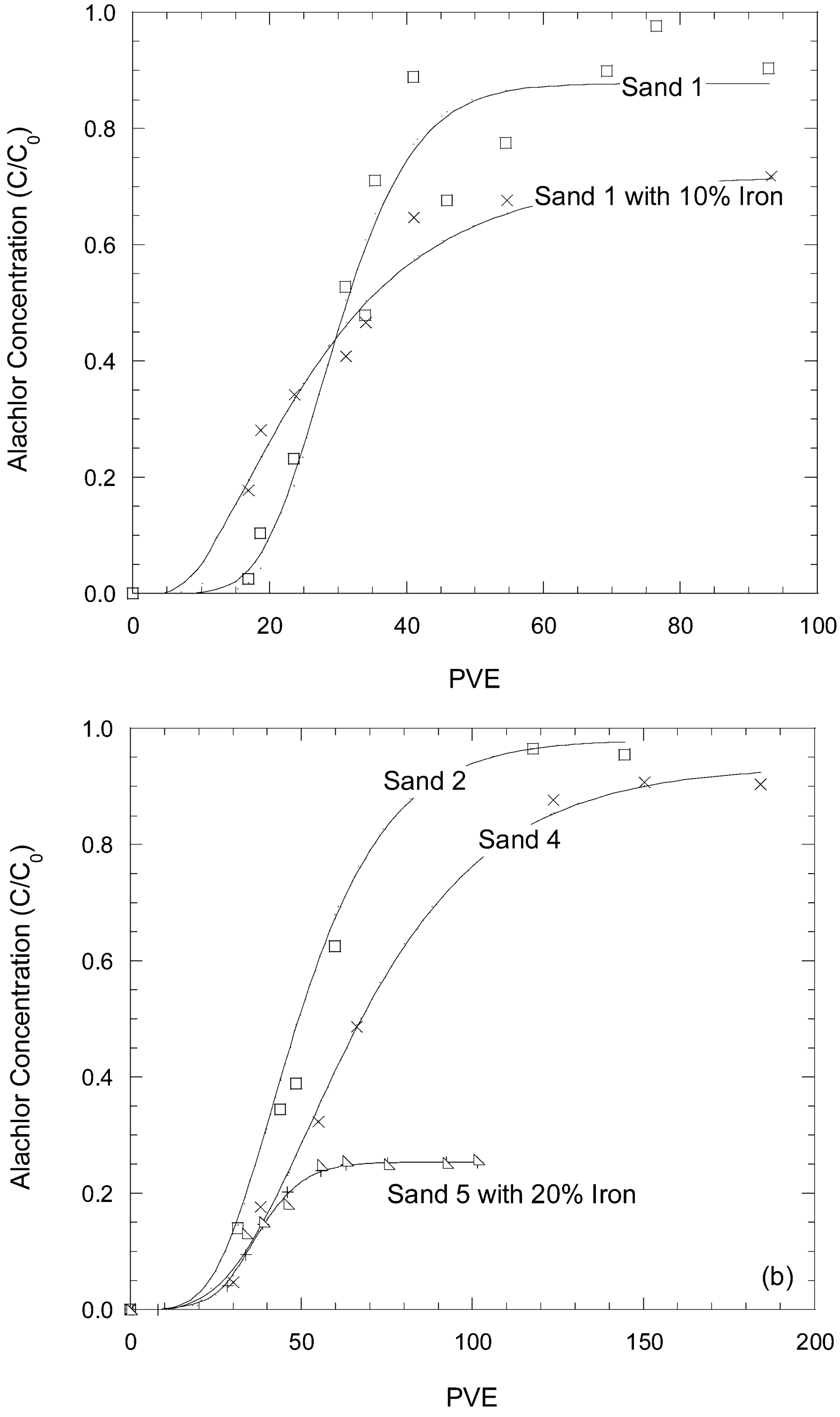

Fig. 6.5. Concentrations of Alachlor and Fits of Eq. 3.18 for (a) Sand 1 and Sand 1 with 10% Iron, and (b) Sands 2 and 4, and Sand 5 with 20% Iron.

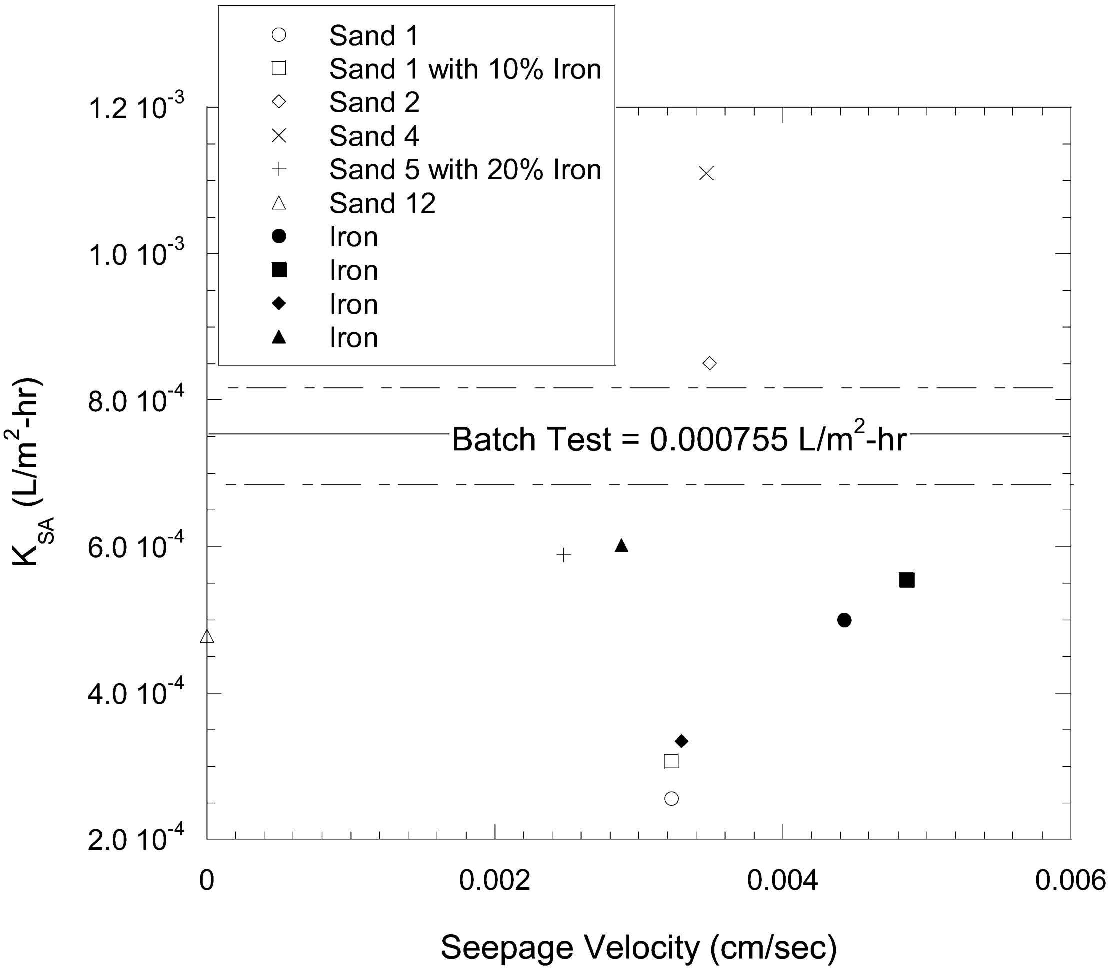

Fig. 6.6. Effect of Seepage Velocity on K_{SA} for Foundry Sands and Peerless Iron. Alachlor was Used. Dashed Lines Depict Range of K_{SA} from Batch Tests.

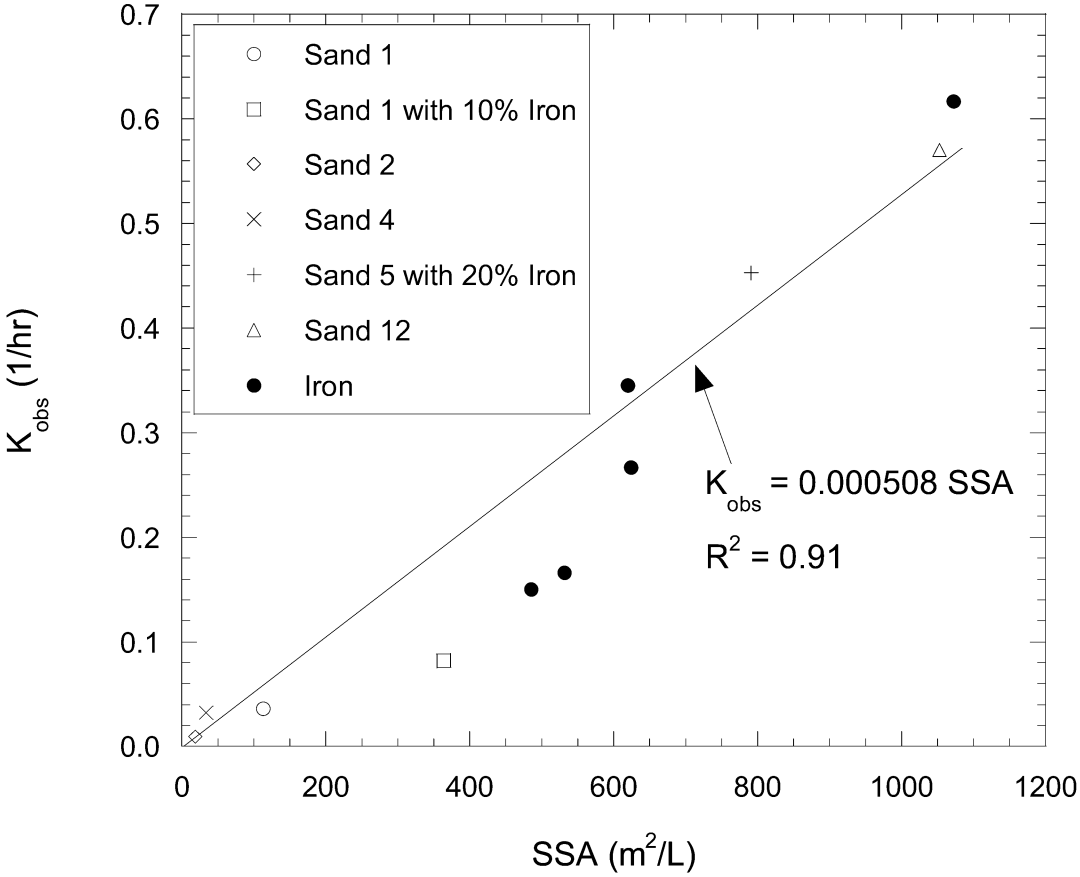

Fig. 6.7. Bulk First-Order Rate Constant (K_{obs}) for Alachlor as a Function of Specific Surface Area (SSA) of Iron.

in Table 6.5. In general, K_p from the column tests are smaller than those obtained from batch sorption tests (Fig. 6.8). The exception is for Sand 1, where K_p from the column test is slightly higher than that from the batch tests. The greatest difference (42%) in K_p was observed for Sand 5 with an admixture of 20% iron. Adding the iron reduced the sorption capacity because the iron has less sorptive capacity than that of foundry sand.

One possible reason for the higher K_p from the batch tests is reduction of the alachlor during the batch sorption tests by residual iron remaining after magnetic separation. Another possible reason is the solid-solution ratio was different in the batch and column tests. Solid concentrations in solution ranged from 125 mg/L (batch) to 4250 mg/L (column); i.e., the soil solid concentration for the batch tests typically was 34 times that of the column tests. O'Connor and Connolly (1980) report that partition coefficients for organic compounds can be reduced as much as a factor of 1.6 when the solid concentration is increased by an order of magnitude. The partition coefficient is lower because closer contact between the soil solids prevents organic compounds from accessing the solid surface. Doust and Huang (1992) also report that K_p decreases as the solids concentration increases. Because of these factors, the K_p from the column tests are believed to be more reliable than those from the batch sorption tests.

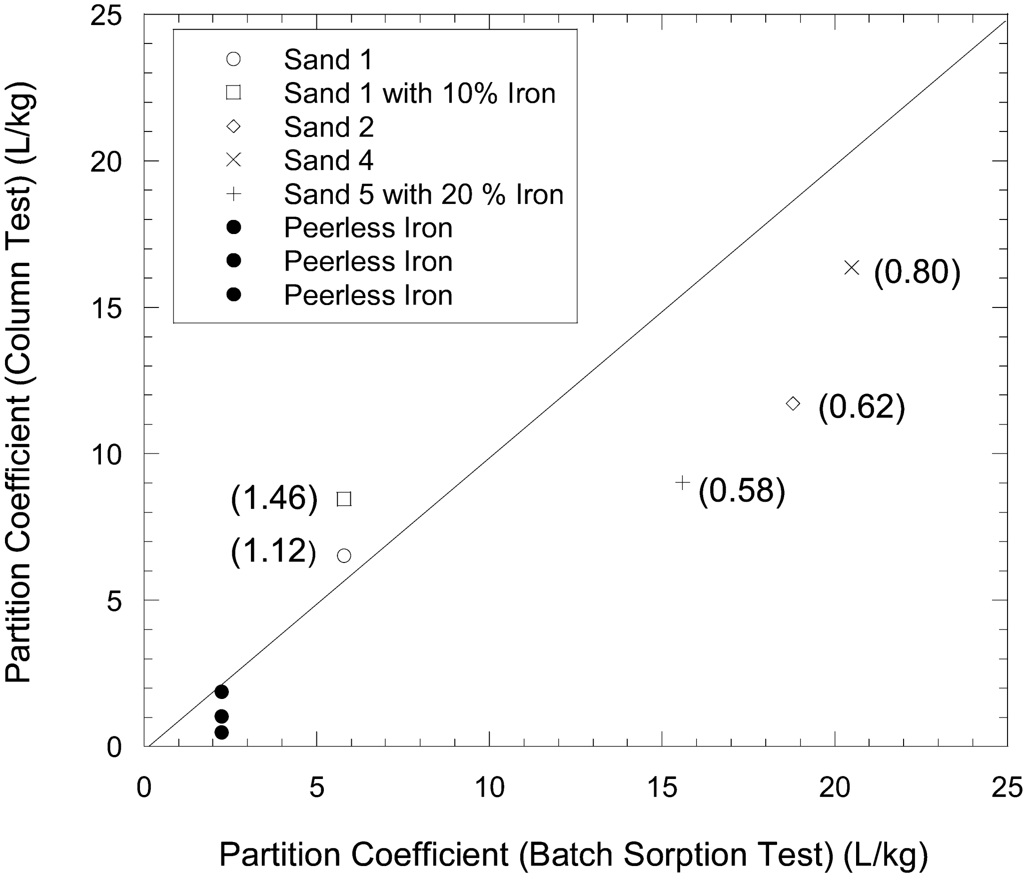

Fig. 6.8. Comparison of Partition Coefficients Obtained from Column Tests and Batch Sorption Tests. Number Adjacent to Data Point is Ratio of Partition Coefficient from Column Test to that from Batch Sorption Test.

6.4.1.3 Dispersion Coefficient and Longitudinal Dispersivity

Dispersion coefficients obtained from the column tests using Eq. 3.18 are summarized in Table 6.5. To check the model fit, the dispersion coefficients were estimated using Eq. 3.24 and a dispersivity equal to one-tenth of the length of the column. The measured and estimated dispersion coefficients are typically within a factor of 2, as shown in Fig. 6.9. Accordingly, the dispersion coefficients are believed to be reliable.

6.4.2 Metolachlor

Experimental conditions for column tests conducted with metolachlor are summarized in Table 6.6. Sands 1, 5, and 12 were used. Two of the tests with Sands 1 and 5 contained an admixture of 20% Peerless iron. Three additional tests were conducted with mixtures of Peerless iron and silica sand for comparison. The influent concentration ranged from 38 mg/L to 55 mg/L.

Seepage velocities were calculated using the effective porosity. For Sand 1, the effective porosity was assumed to be 100% of the total porosity based on the data in Sec. 5.3.1. For the silica sand-iron mixtures, foundry sand-iron mixtures, and Sand 12, the effective porosity was assumed to be 85% of the total porosity.

Results of the column tests are summarized in Table 6.7. Typical metolachlor breakthrough curves are shown in Fig. 6.10.

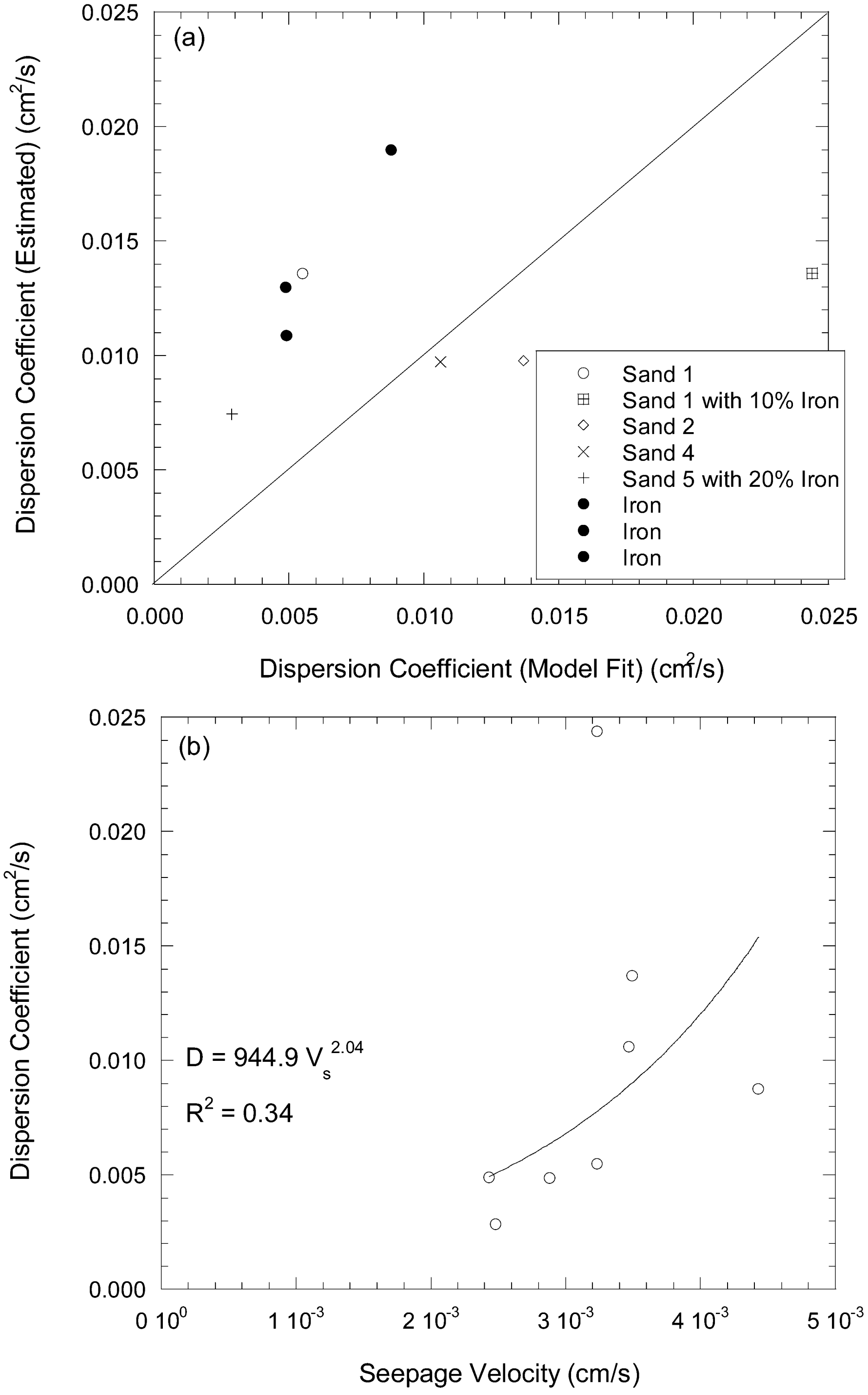

Fig. 6.9. Comparison of Dispersion Coefficient Obtained from Model Fit and Estimation (a) and Effect of Seepage Velocity on Dispersion Coefficient (b).

Table 6.6. Experimental Conditions for Column Tests Using Metolachlor.

Reactive Media	C^b (mg/L)	L $(cm)^2$	$\rho_d{}^c$ (Mg/m^3)	n^d	$n_e{}^e$	Iron Content (%)	SSA^f (m^2/L)	$V_s{}^g$ (cm/s)
Sand 1	50	30	1.68	0.36	0.36	1	114	3.20×10^{-3}
Sand 1[a]	49	30	1.89	0.48	0.40	21	945	1.74×10^{-3}
Sand 5[a]	49	30	1.89	0.48	0.40	20	828	2.29×10^{-3}
Sand 12	49	14.5	1.64	0.47	0.40	10	1002	4.12×10^{-3}
Iron	55	45	1.98	0.38	0.32	10	539	3.90×10^{-3}
Iron	38	45	2.04	0.44	0.37	20	960	2.38×10^{-3}
Iron	52	43	2.10	0.43	0.35	20	1034	2.68×10^{-3}

[a] Admixture with a 20% Peerless Iron, [b] Influent Alachlor Concentration, [c] Dry Density, [d] Total Porosity, [e] Effective Porosity, [f] Surface Area of Iron per Volume of Solution, [g] Seepage Velocity.

Table 6.7. Experimental Conditions for Column Tests and Normalized First-Order Rate Constants.

Reactive Media	Dispersion Coefficient (cm^2/s)	Dispersivity (cm)		Partition Coefficient (L/kg)		K_{obs} [b] (hr^{-1})	K_{SA} [c] (L/m^2-hr)	
		Model Fit	Estimated	Batch	Column		Model Fit[d]	Steady-State[e]
Sand 1	3.80×10^{-3}	1.19	3.0	14.9	9.64	0.023	2.02×10^{-4}	2.85×10^{-4}
Sand 1[a]	2.55×10^{-3}	1.47	3.0	14.9	8.45	0.448	4.74×10^{-4}	4.90×10^{-4}
Sand 5[a]	2.28×10^{-3}	1.08	3.0	15.3	12.38	0.433	5.23×10^{-4}	5.58×10^{-4}
Sand 12	N.A.	N.A.	N.A.	N.A.	N.A.	0.301	N.A.	2.97×10^{-4}
Iron A	N.A.	N.A.	N.A.	N.A.	N.A.	N.A.	N.A.	2.02×10^{-4}
Iron B	1.11×10^{-2}	4.65	4.25	1.87	1.57	0.209	2.18×10^{-4}	2.16×10^{-4}
Iron C	2.22×10^{-2}	8.28	4.3	1.87	1.38	0.273	2.64×10^{-4}	2.20×10^{-4}

[a] Admixture with a 20% Peerless Iron, [b] Bulk first-order rate constant, [c] Normalized rate constant, [d] Obtained from the model fit (Eq. 3.18), [e] Obtained from steady-state solution (Eq. 3.21).

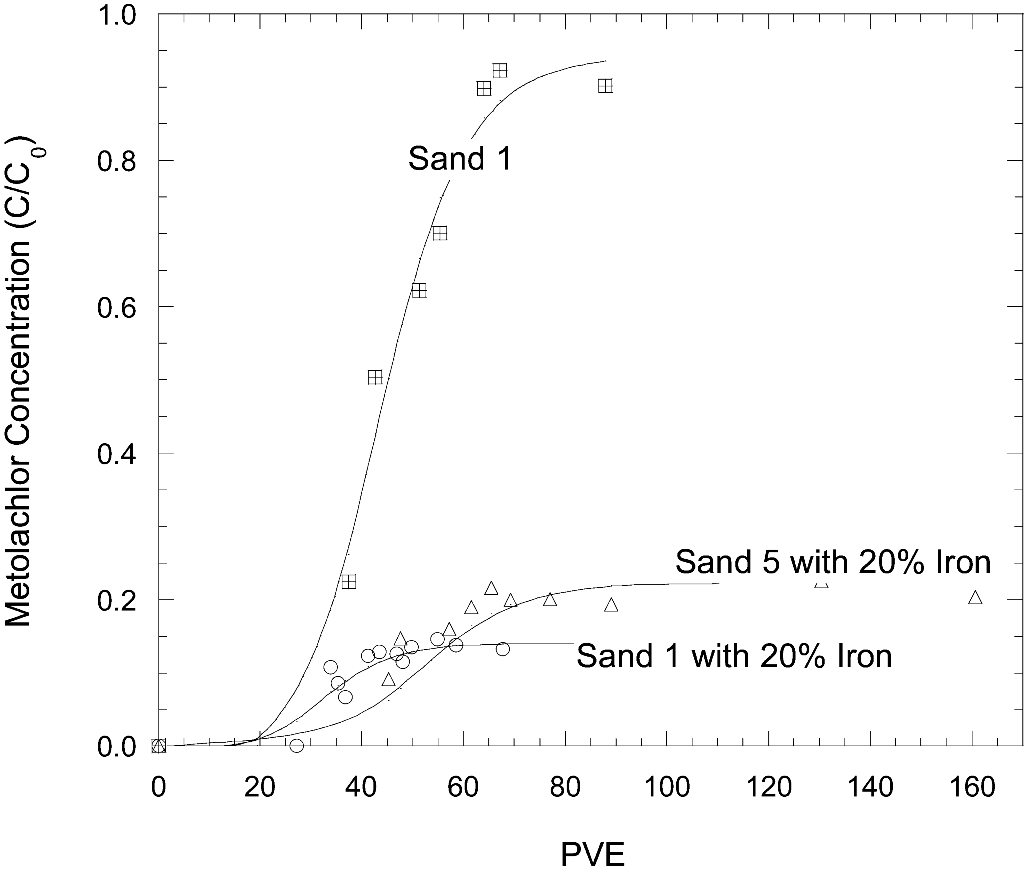

Fig. 6.10. Metolachlor Concentrations and Model Fits for Sand 1, Sand 1 with 20% Iron, and Sand 5 with 20% Iron.

6.4.2.1 First-Order Rate Constant

The K_{SA} for the foundry sands and Peerless iron for metolachlor are summarized in Table 6.7. Similar K_{SA} were obtained from all of the tests, indicating that the foundry iron has comparable reactivity to Peerless iron. Additionally, variations in initial concentration and seepage velocity apparently had no effect on K_{SA}, as shown in Fig. 6.11.

As with the tests using TCE (Sec. 5) and alachlor (Sec. 6.4.1.1), the bulk first-order rate constant (K_{obs}) is directly proportional to the surface area of iron per volume of solution (SSA) (Fig. 6.12). The slope of the linear regression equation in Fig. 6.12 is equal to the average K_{SA}, which is 3.44×10^{-4} L/m^2-hr. This average K_{SA} is slightly lower (1.6 times) than the K_{SA} obtained from the batch degradation tests (5.7×10^{-4} L/m^2-hr for the foundry sand iron and 5.3×10^{-4} L/m^2-hr for Peerless iron).

A long-term test was conducted with Sand 12 to assess the persistence of the reactivity of foundry iron. The test was conducted until 1500 pore volumes had passed through the column. The K_{SA} are shown in Fig. 6.13. A reduction in K_{SA} occurred between 300 and 400 pore volumes of flow. The final K_{SA} was 1.73×10^{-4} L/m^2-hr, which is approximately 2 times lower than the initial K_{SA}. A similar reduction in K_{SA} was observed during a long-term test with Peerless iron. The initial K_{SA} for the Peerless iron was 2.64×10^{-4} L/m^2-hr, and final K_{SA} was 1.11×10^{-4} L/m^2-hr.

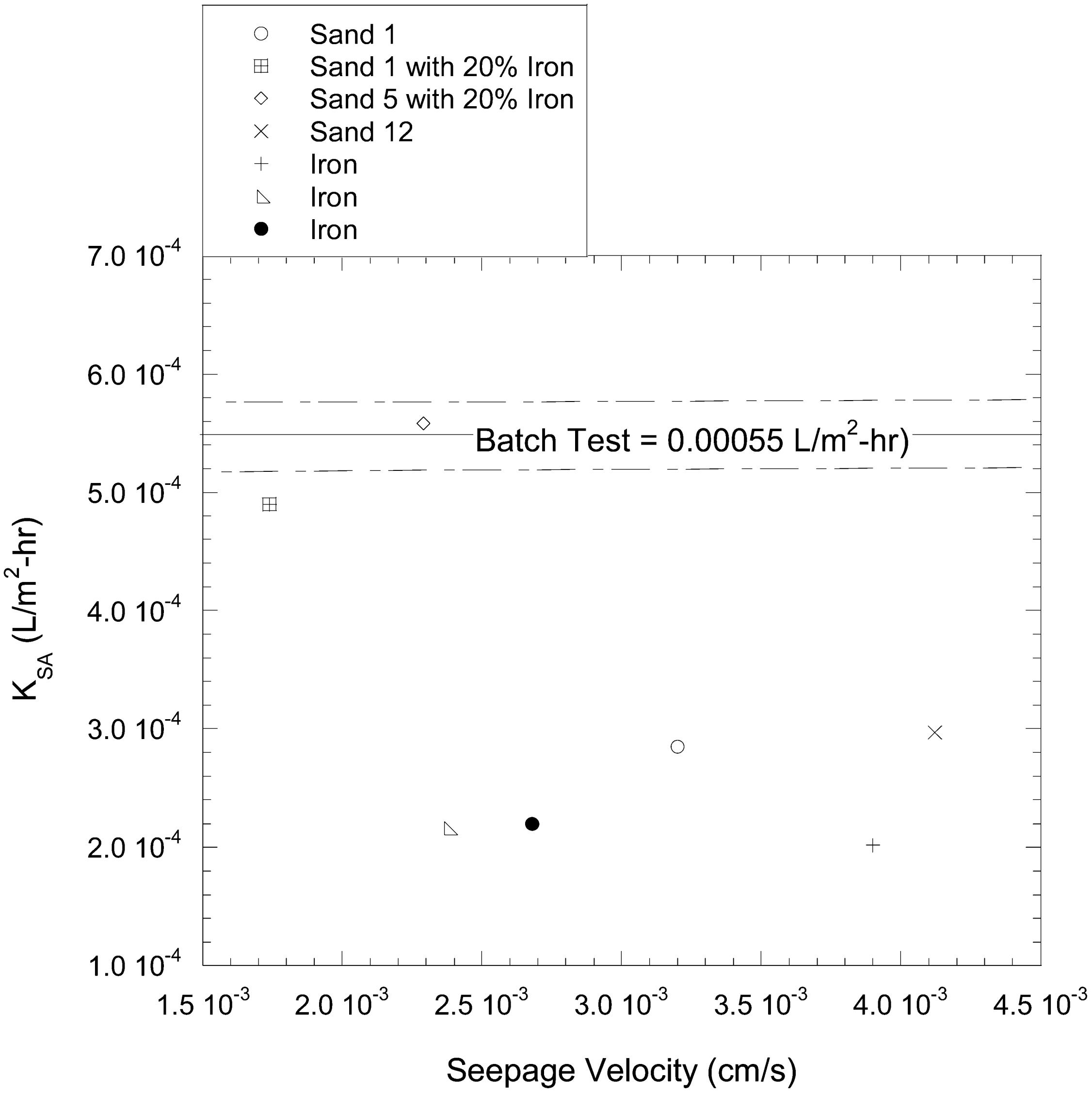

Fig. 6.11. Effect of Seepage Velocity on K_{SA} for Metolachlor for Foundry Sands and Peerless Iron. Dashed Lines Depict Range of K_{SA} from Batch Tests.

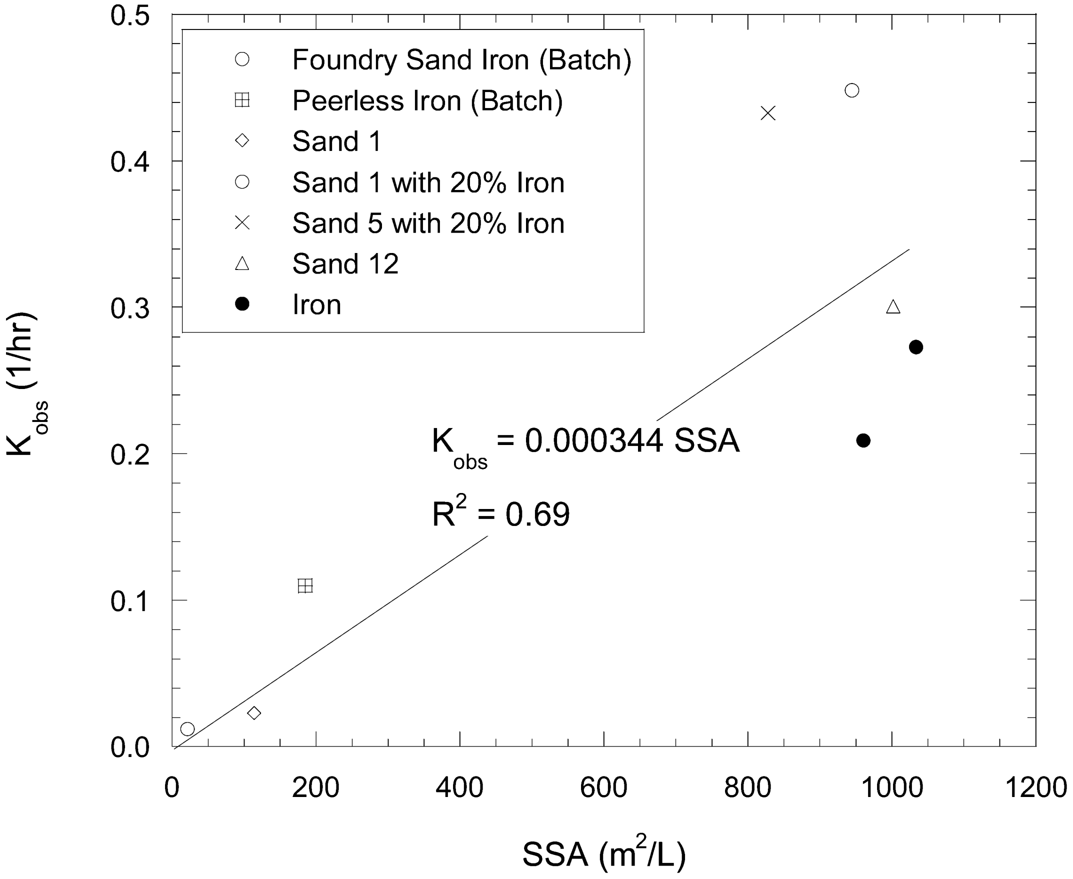

Fig. 6.12. Bulk First-Order Rate Constant (K_{obs}) for Metolachlor as a Function of Specific Surface Area (SSA) of Iron.

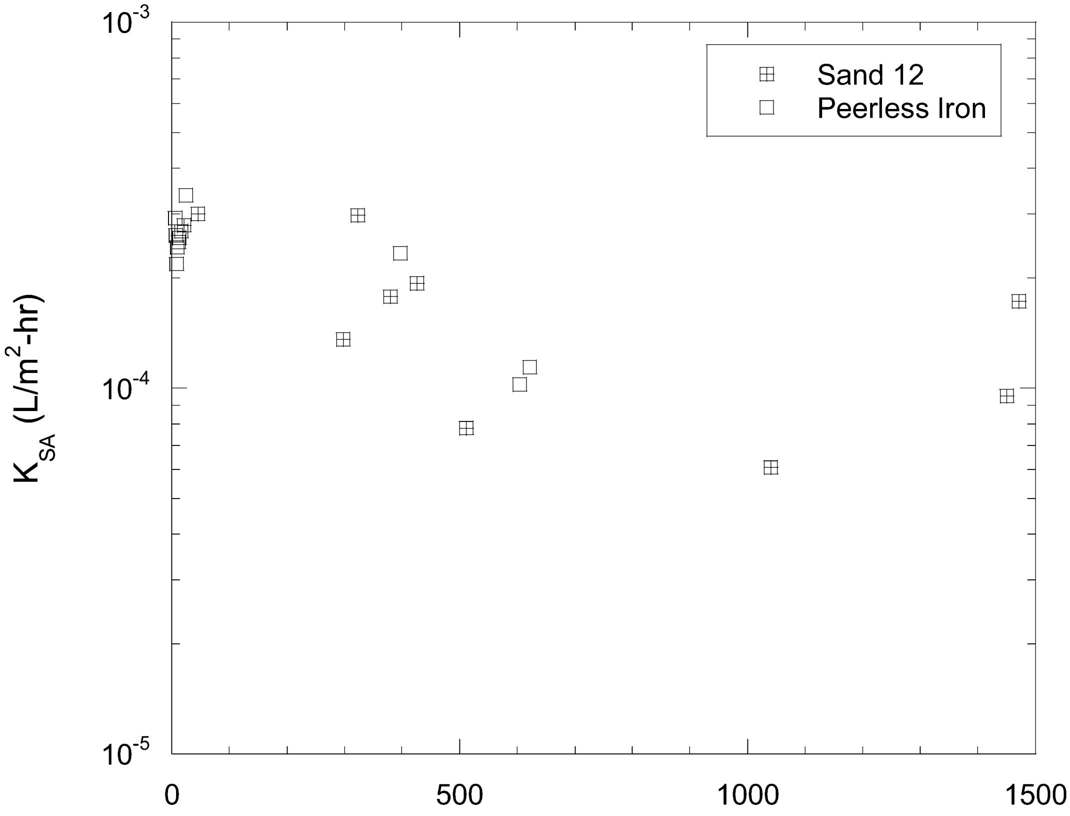

Fig. 6.13. Normalized Rate Constant (K_{SA}) for Sand 12 and Peerless Iron During the Long-Term Test.

The slight reduction in K_{SA} that was observed may have been due to oxide formation on the surface of iron.

6.4.2.2 Partition Coefficient

Partition coefficients obtained from the column tests and batch sorption tests with metolachlor are shown in Fig. 6.14. The partition coefficients from the column tests with foundry sands are lower than those from the batch sorption tests. The numbers adjacent to the data in Fig. 6.14 indicate the ratio of the partition coefficient from the column test to that from the batch sorption test. For example, for Sand 1, the ratio of the partition coefficient from the column test to that from the batch sorption test is 0.65. As with alachlor, the difference in partition coefficients is likely due to reaction with residual iron and differences in the solid-solution ratio, as discussed in Sec. 6.4.1.2.

6.4.2.3 Dispersion Coefficient

Dispersion coefficients obtained from Eq. 3.18 and by estimation using a dispersivity equal to one-tenth of the column are shown in Fig. 6.15. They were not identical to the estimated dispersion coefficient. But the dispersion coefficients are comparable, indicating that model fits are reliable.

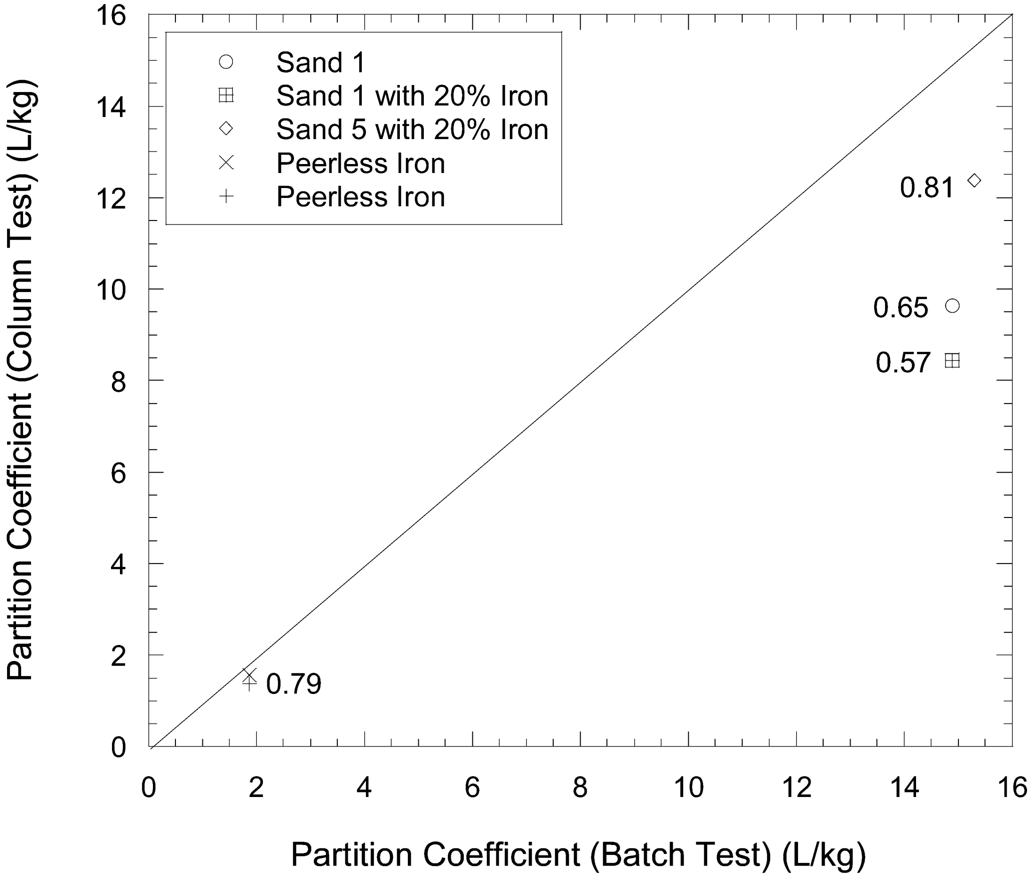

Fig. 6.14. Comparison of Partition Coefficients for Metolachlor Obtained from Column Tests and Batch Sorption Tests. Number Adjacent to Data Point is Ratio of Partition Coefficient from Column Test to that from Batch Sorption Test.

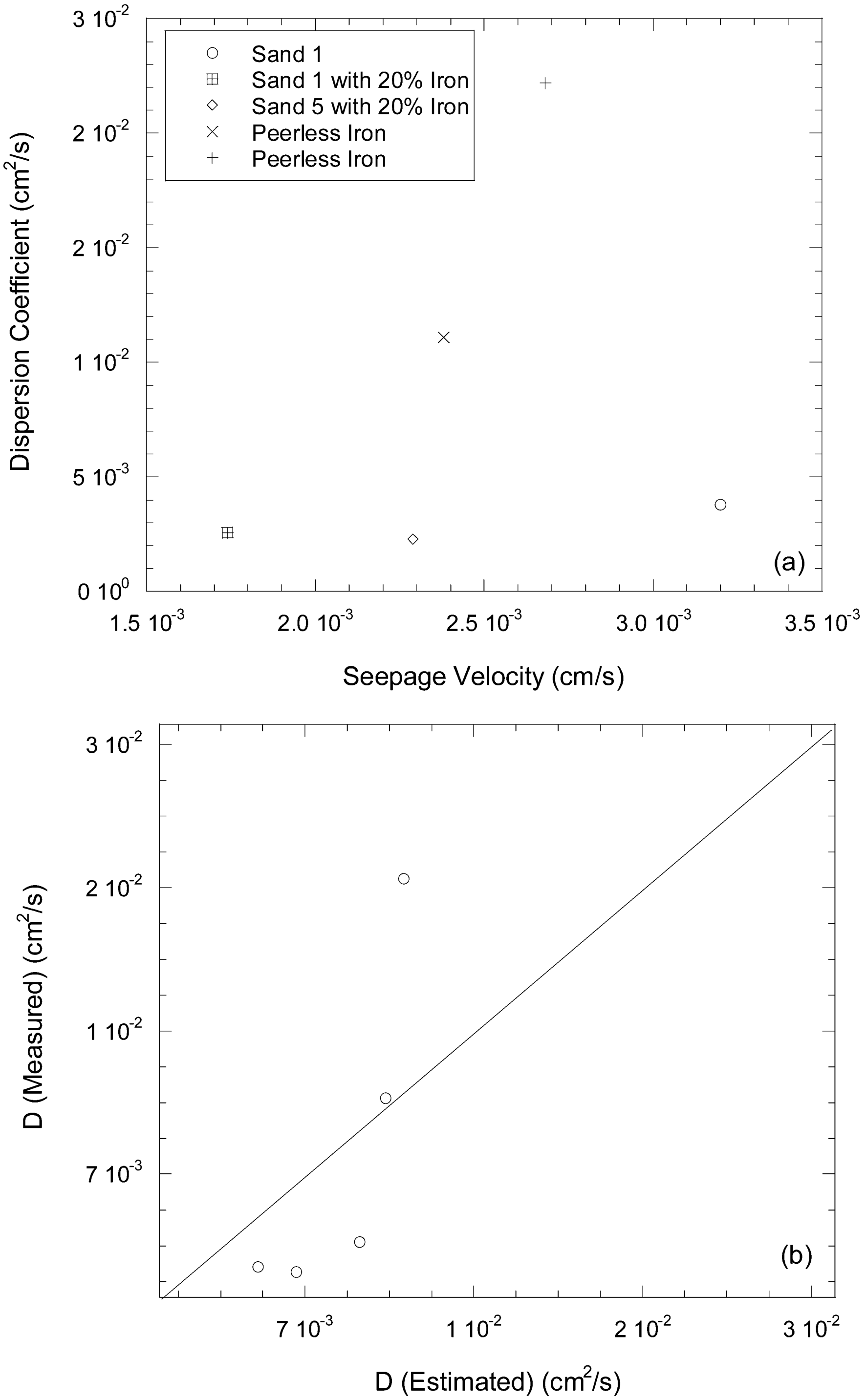

Fig. 6.15. Effect of Seepage Velocity on Dispersion Coefficient (a) and Comparison of Dispersion Coefficients Obtained from the Model Fit and Estimation (b).

6.5 PRB DESIGN

The required barrier thickness of PRBs with foundry sands having different iron contents and TOC was estimated using Eq. 3.21. The procedure described in Sec. 5.4 was used.

Concentrations of alachlor and metolachlor in groundwater are generally less than 0.05 μg/L (Kalkhoff et al. 1998, Phillips et al. 1999), although higher concentrations (0.55 μg/L for alachlor and 5.40 μg/L for metolachlor) have been reported (Kolpin et al. 1998). Thus, the source concentration (C_0) was assumed to vary between 5 μg/L to 50 μg/L for alachlor and 150 μg/L to 1500 μg/L for metolachlor. The MCLs for alachlor and for metolachlor are 0.5 and 15 μg/L, respectively. Accordingly, the normalized concentration required to meet the MCLs ranged between 0.1 and 0.01.

Partition coefficients for alachlor and metolachlor were calculated using Eqs. 6.3 and 6.4. Because the partition coefficients are a function of clay content, the clay content was varied between 5% and 9%.

Normalized concentrations for alachlor and metolachlor are shown in Figs. 6.16 and 6.17 for various zero-valent iron contents and barrier thicknesses. For alachlor and metolachlor, barriers less than 1 m thick can be constructed provided the iron content is higher than 1% and the seepage velocity is less than 0.1 m/d.

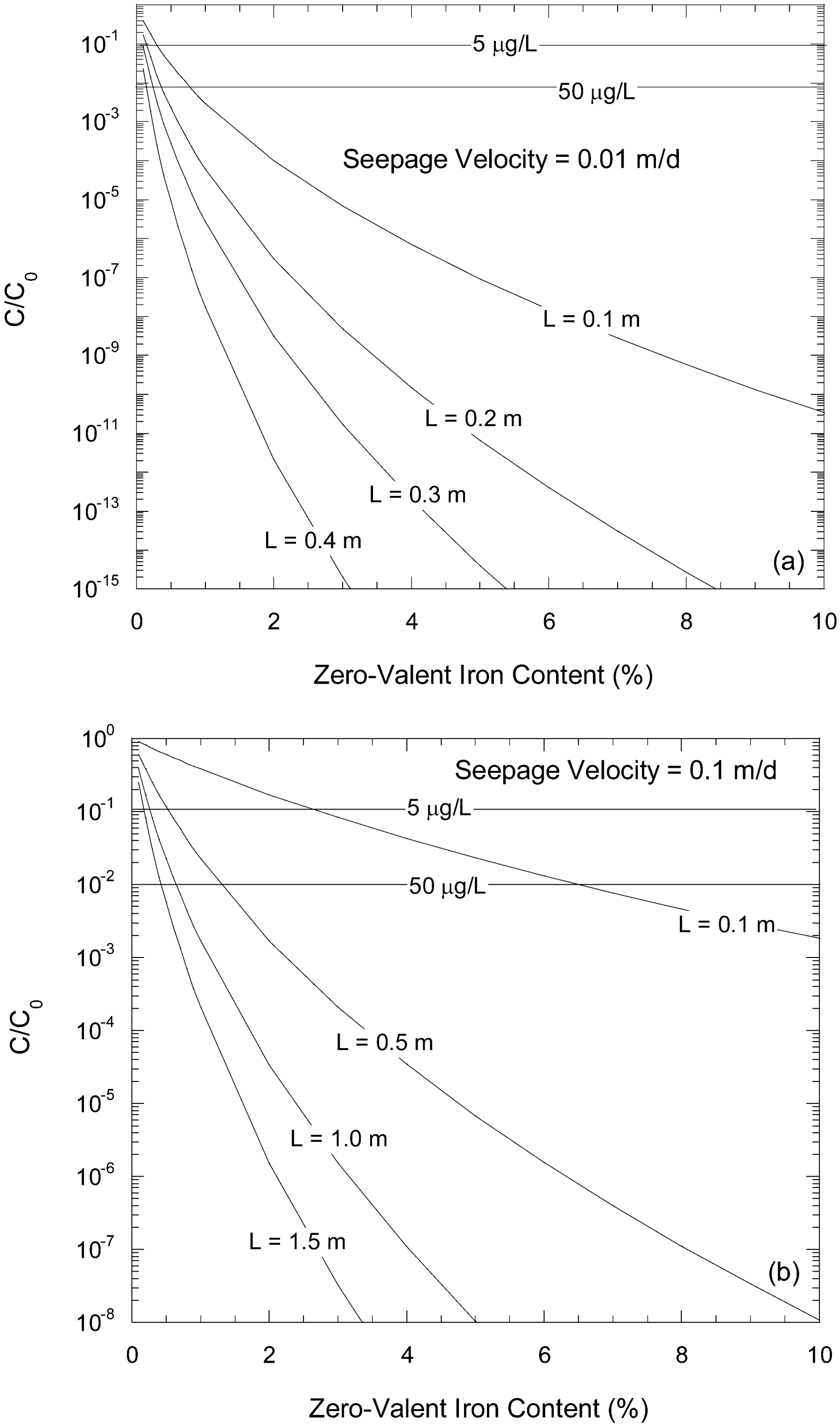

Fig. 6.16. Normalized Alachlor Concentrations as a Function of Zero-Valent Iron Content and Barrier Thickness: (a) V_s = 0.01 m/d (b) V_s = 0.1 m/d.

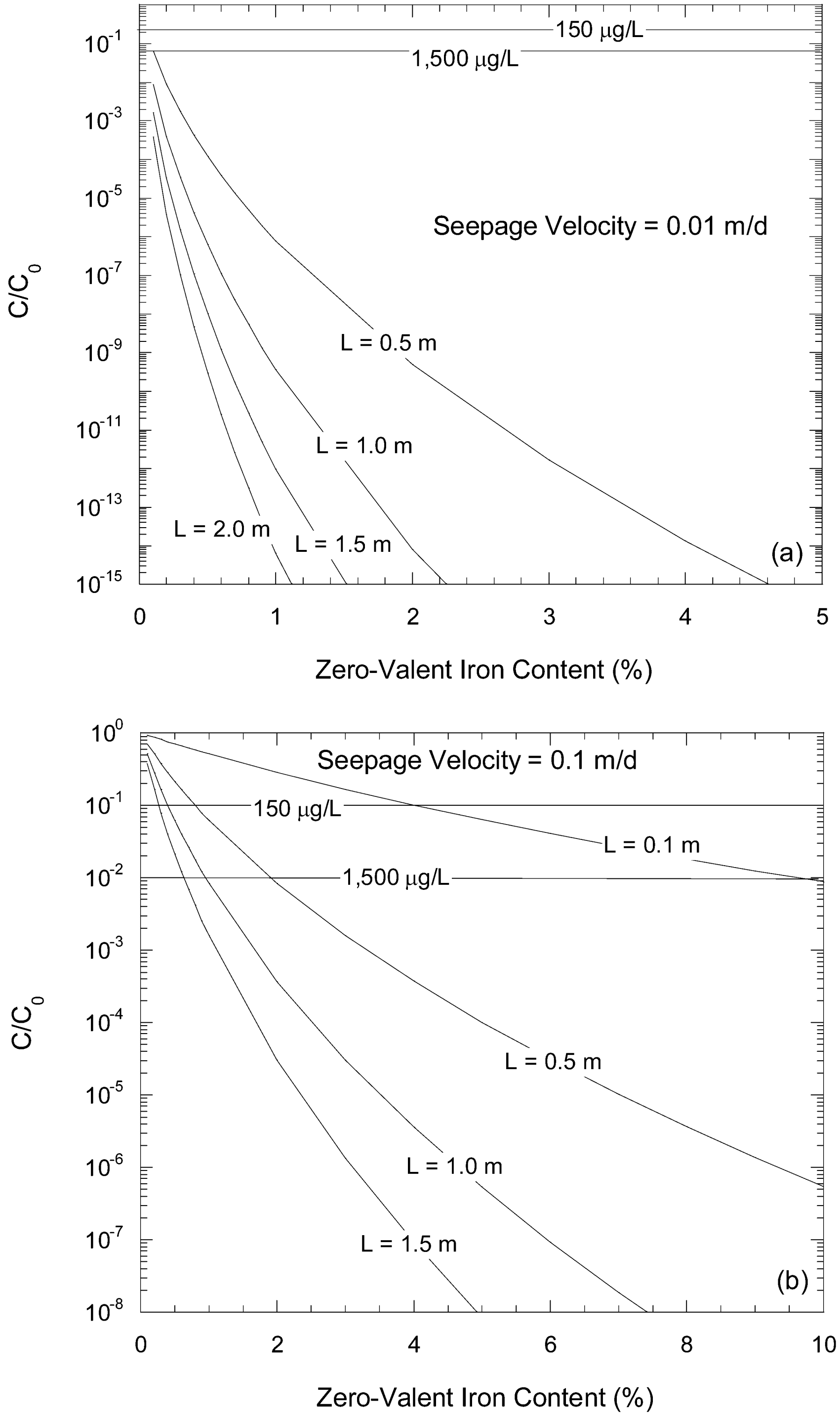

Fig. 6.17. Normalized Metolachlor Concentrations as a Function of Zero-Valent Iron Content and Barrier Thickness: (a) V_s = 0.01 m/d (b) V_s = 0.1 m/d.

The effect of retardation of alachlor and metolachlor on the time to equilibrium is shown in Figs. 6.18 and 6.19, respectively. The equilibrium time increases as the clay content of the foundry sands increases. The equilibrium time varies between 2 and 166 yrs, with larger times corresponding to high clay content and low seepage velocity. When no sorbent is provided (i.e., retardation factor is 1), the time to equilibrium is approximately 42 (V_s = 0.1 m/d) and 467 days (V_s = 0.01 m/d). The long residence time provided by foundry sands will be favorable for biodegradation of compounds by naturally occurring microorganisms. The resulting effluent will have lower concentration than would be anticipated for a conventional PRB having similar iron content.

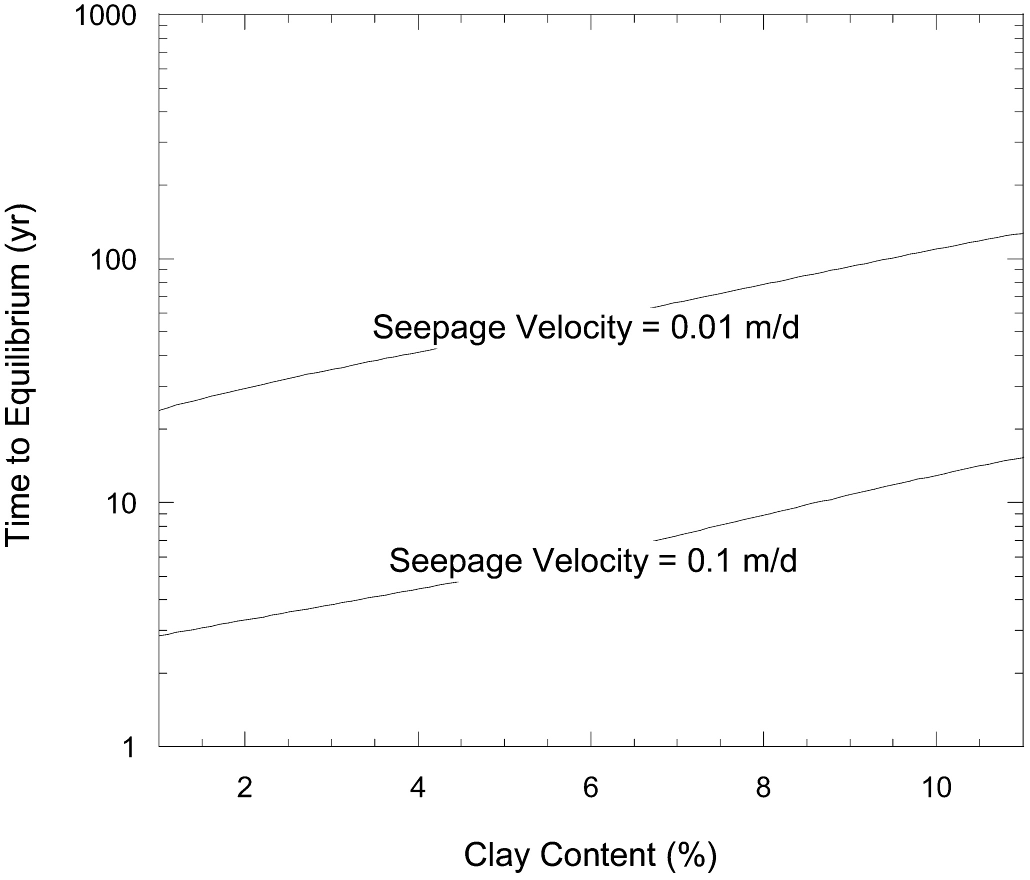

Fig. 6.18. Time to Reach Equilibrium for Alachlor as a Function of Clay Content and Seepage Velocity.

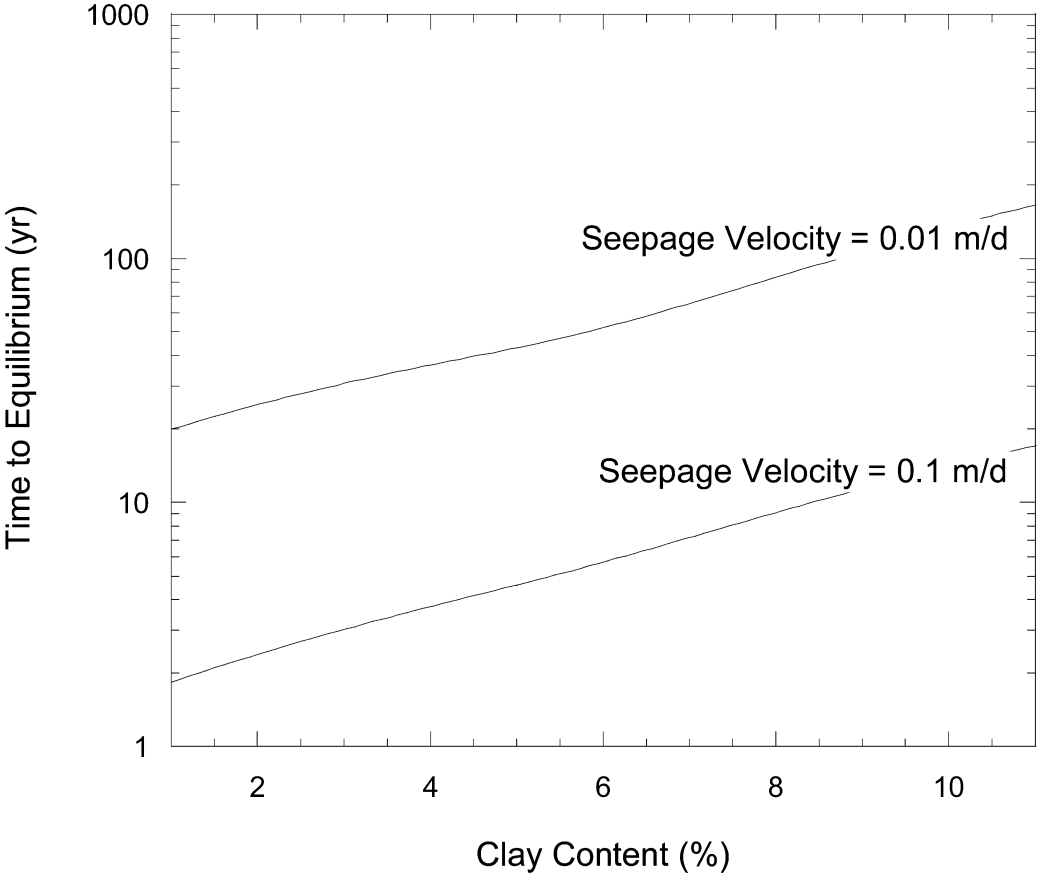

Fig. 6.19. Time to Reach Equilibrium for Metolachlor as a Function of Clay Content, and Seepage Velocity.

SECTION SEVEN

RESULTS OF BATCH AND COLUMN TESTS USING ZINC

7.1 SERIAL BATCH KINETIC TESTS

Batch kinetic tests were conducted to determine the sorption kinetics (i.e., rate of sorption and amount of mass removed) for zinc in the presence of foundry sands as reactive media. Serial batch kinetic tests were conducted using Sands 1, 4, 10, 11, 12, and Peerless iron (Table 7.1). The sands were selected to bracket the anticipated range of TOC and clay content (%). The clay content ranged from 3.5% to 13.2%, and the TOC ranged from 0.5% to 4.0%. Iron contents for the foundry sands are presented in Table 7.1 in terms of zero-valent iron content. No data were available for clay, TOC, and total inorganic carbon (TIC) for Peerless iron.

The experimental conditions are summarized in Table 7.1. Three different solution pHs were selected as initial pHs (i.e., 2.6, 3.0, and 4.8). No pH buffer was used. The initial pH of solution was adjusted with 1.0 M HNO_3 and 1.0 M NaOH. Zinc solutions were prepared by dissolving $ZnCl_2$ in DI water to yield an initial zinc concentration of 100 mg/L.

7.1.1 Effect of Contact Time on Concentration

The zinc concentrations decreased as the contact time increased for the foundry sands and Peerless iron for all pHs (Figs. 7.1 - 7.3). The greatest

Table 7.1. Experimental Conditions for the Batch Kinetic Test for Zinc Removal.

Reactive Media	Mass of Media (g)	Clay Content (%)	TOC Content (%)	TIC[b]Content (%)	Iron Content (%)
Sand 1	2	5.1	1.5	0.0	1.00
Sand 4	2	10.5	0.5	0.1	0.29
Sand 10	2	4.7	2.5	0.6	0.14
Sand 11	2	13.2	4.0	0.7	0.18
Sand 12	2	3.5	2.4	0.0	10
Iron	2	N.A.[a]	N.A.	N.A.	100

[a] N.A. = Not applicable, [b] TIC = Total inorganic carbon.

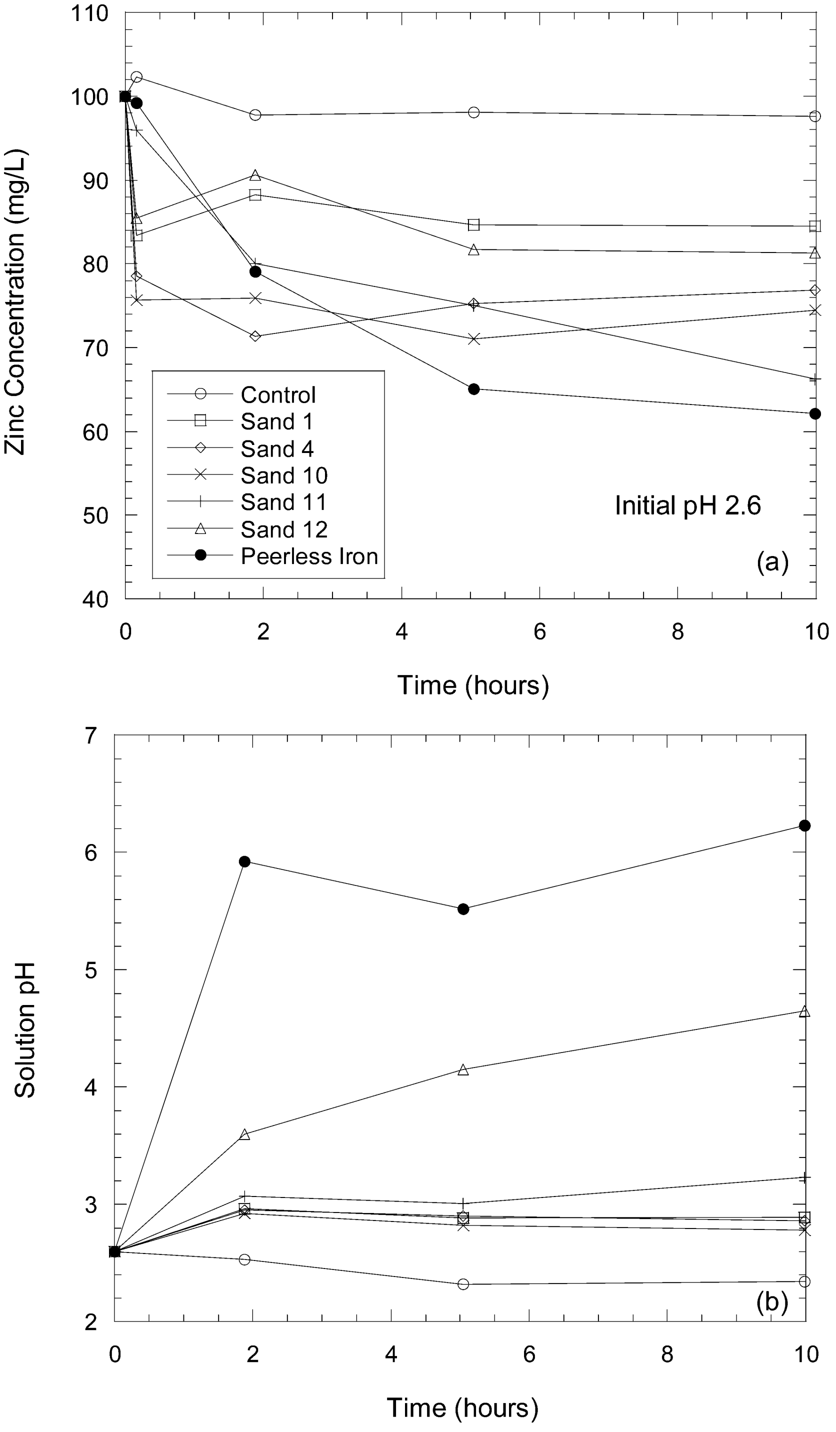

Fig. 7.1. Results of Batch Kinetic Tests at Initial pH 2.6: (a) Zinc Concentration and (b) Solution pH.

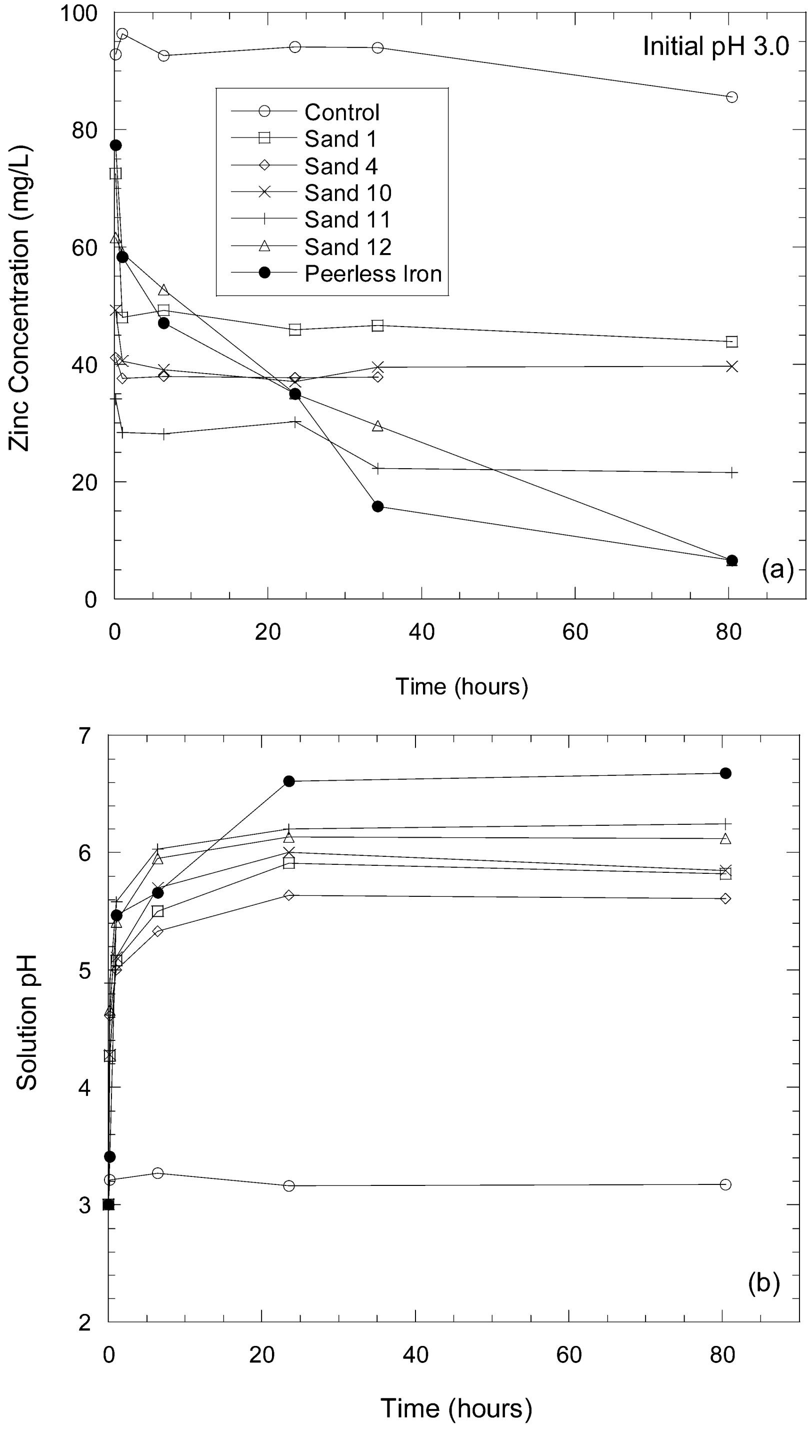

Fig. 7.2. Results of Batch Kinetic Tests at Initial pH 3.0: (a) Zinc Concentration and (b) Solution pH.

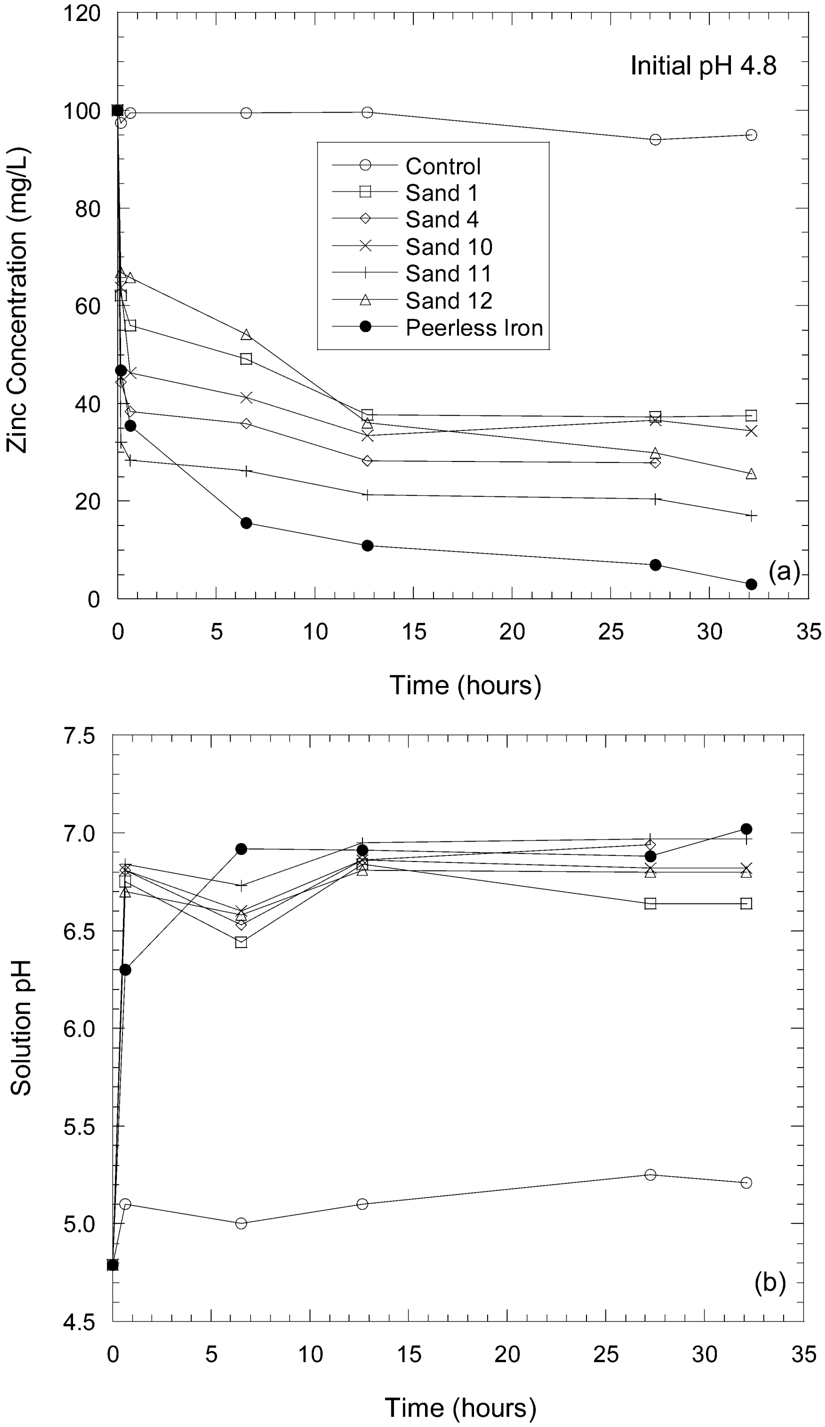

Fig. 7.3. Results of Batch Kinetic Tests at Initial pH 4.8: (a) Zinc Concentration and (b) Solution pH.

decreases in concentration typically occurred within 10 min for the foundry sands, regardless of the initial pH. The decreases in concentration were also higher when the pH was higher.

The initial decreases in concentration for Peerless iron were smaller relative to those for Sands 1, 4, 10, 11, and 12. However, at later times, zinc concentrations for the tests with foundry sands leveled out, whereas the zinc concentrations continuously decreased for Peerless iron, regardless of initial pH. The exception is for Sand 11 with pH 2.6 solution. For this test, the concentration continued to decrease for approximately 35 hrs.

7.1.2 Solution pH

The solution pH of the tests with the foundry sands generally increased and then stabilized. An equilibrium pH was generally established within 21 hrs. An exception was the test with Sand 12 in pH 2.6. The pH continued to increase throughout the duration of this test, as it did with the tests conducted with Peerless iron. The increases in equilibrium or final solution pH were proportional to the initial pH (Figs. 7.1 – 7.3). At pH 2.6, solution pHs slightly increased for Sands 1, 4, 10, and 11. As initial pH increased to 3.0 and 4.8, the solution pH increased above 5.5 and 6.5, respectively. Relatively higher solution pHs were observed for Sands 11, 12, and Peerless iron.

The changes in pH that occurred can be attributed to buffering reactions. For the foundry sands, buffering was probably caused by the carbonate minerals, exchangeable base cations, and decomposition of aluminosilicate minerals (McBride 1994). For the Peerless iron, the pH change can be attributed primarily to corrosion of the iron, which is explained by the following reaction:

$$Fe^0 + 2H_2O \rightarrow Fe^{2+} + H_2(g) + 2OH^- \qquad (7.1)$$

where Fe^0 is zero-valent iron, Fe^{2+} is ferrous iron, H_2 (g) is hydrogen gas, and OH^- is a hydroxide ion.

7.1.3 Zinc Mass Removal by Sorption and Precipitation

Serial control tests were conducted at several different initial pHs to separate the contributions of sorption and precipitation to removal of Zn. No solids (i.e., foundry sand or Peerless iron) were used in the control tests so that zinc would be removed only by precipitation. A wide range of pH (3.0 through 10.0) was considered. The initial pH was adjusted with 1.0 M of HCl or 1.0 M of NaOH.

Zinc removed via precipitation in the control tests is shown in Fig. 7.4 as a function of the initial solution pH. Precipitation of zinc begins between pH 5.0 and 6.0. Also shown in Fig. 7.4 is the zinc removal from the batch kinetic tests, which was computed from the last concentration that was measured. The removal data are also summarized in Table 7.2. Comparison of the zinc removal in the control tests and the batch kinetic tests indicates zinc removal by foundry sands is primarily by sorption for pH less than 5, and by a combination of sorption and precipitation for pH greater than 6.0.

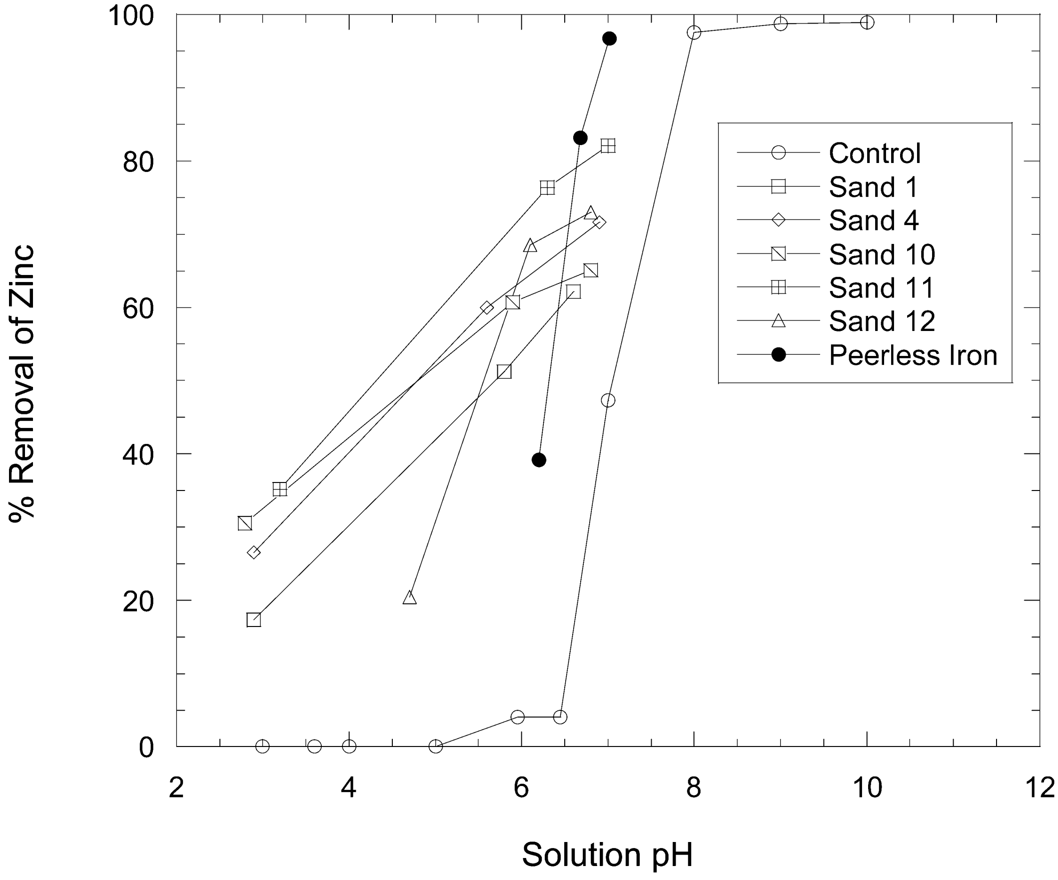

Fig. 7.4. Zinc Removal During Batch Kinetic Tests for Foundry Sands and Peerless Iron as a Function of Solution pH. Also Shown is Mass Removed During Serial Control Tests.

Table 7.2. Zinc Removed by Foundry Sands and Peerless Iron for Different Initial pHs.

Media	Clay (%)	TOC (%)	TIC (%)	Iron Content (%)	Mass Removed per Mass Solid (mg/kg) for Various Initial pH		
					pH=2.6	pH=3.0	pH=4.8
Sand 1	5.1	1.5	0	2.83	287 (2.9)[a]	1,031 (5.8)[a]	1,227 (6.6)[a]
Sand 4	10.5	0.5	0.1	0.29	488 (2.9)[a]	1,255 (5.6)[a]	1,415 (6.9)[a]
Sand 10	4.7	2.5	0.6	0.14	466 (2.8)[a]	1,192 (5.9)[a]	1,296 (6.8)[a]
Sand 11	13.2	4.0	0.7	0.18	669 (3.2)[a]	1,366 (6.3)[a]	1,666 (7.0)[a]
Sand 12	3.5	2.4	0	11.3	348 (4.7)[a]	1,687 (6.1)[a]	1,583 (6.8)[a]
Iron	N.A.	N.A.	N.A.	100	758 (6.2)[a]	1,688 (6.7)[a]	1,844 (7.0)[a]

[a] Final pH of solution shown in parentheses. N.A. = Not applicable.

7.1.4 Reaction Rate for Zinc Removal

Zinc concentrations in solution for the foundry sands and Peerless iron are shown in Figs. 7.5 – 7.6 along with fits of Eq. 3.7 that were made to obtain rate constants and instantaneous partition coefficients. Partition coefficients and rate constants obtained from fitting are summarized in Table 7.3. The good correspondence between the data and the fits of Eq. 3.7 indicates that zinc removal follows a first-order reaction.

The partition coefficient is shown in Fig. 7.7 as a function of clay content. The partition coefficient increases with clay content, indicating that sorption is primarily on the mineral surfaces of the clay in the foundry sands. Partition coefficients for the Peerless iron are comparable to partition coefficients for sands with lower clay content (<4%). The partition coefficient for Peerless iron also is a function of initial pH, which probably reflects a change in surface charge.

A multivariate regression analysis was conducted at the 0.05 level using the data from the batch kinetic tests with foundry sands. The equation is (R^2 = 0.97):

$$\log K_p = -2.30 + 0.48\ \text{pH} + 0.048\ C \tag{7.2}$$

where K_p is the partition coefficient (L/kg) for zinc, pH is the final solution pH, and C is clay content (%). TOC is not included in regression equation because it was not statistically significant.

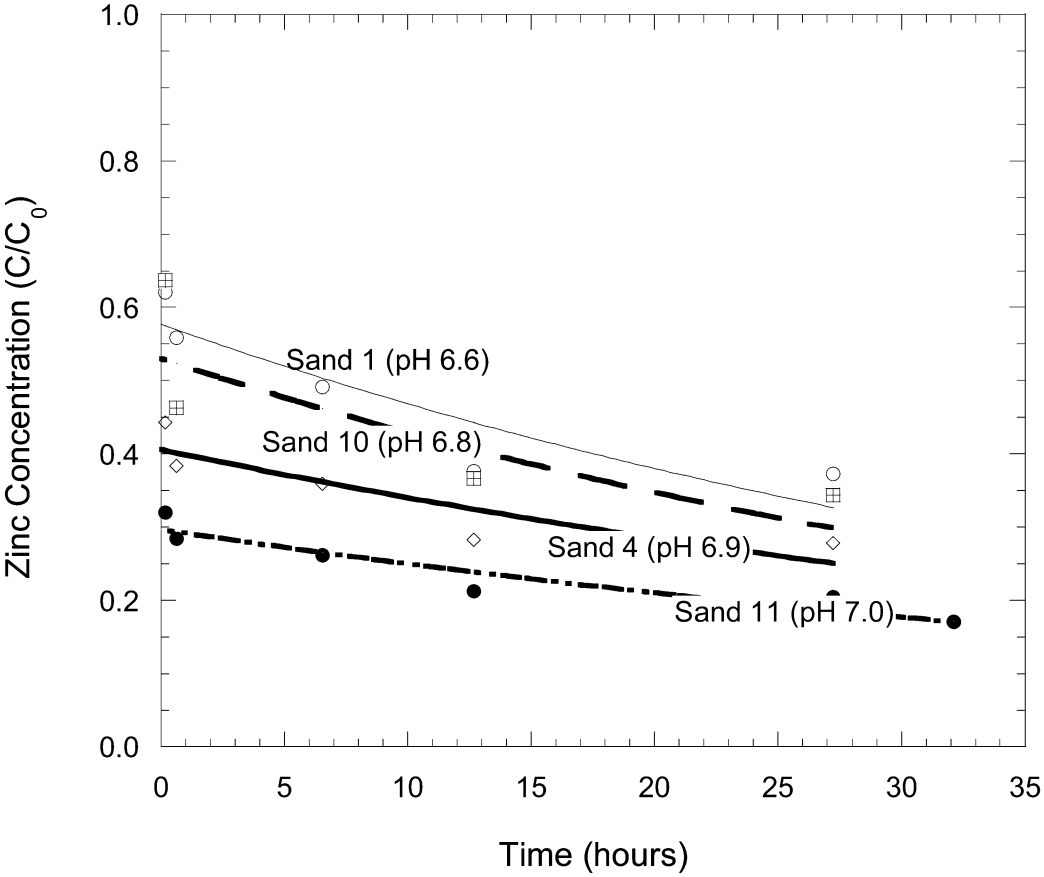

Fig. 7.5. Zinc Concentrations and Fits of Eq. 3.7 for Sands 1, 4, 10, and 11. The initial pH was 4.8.

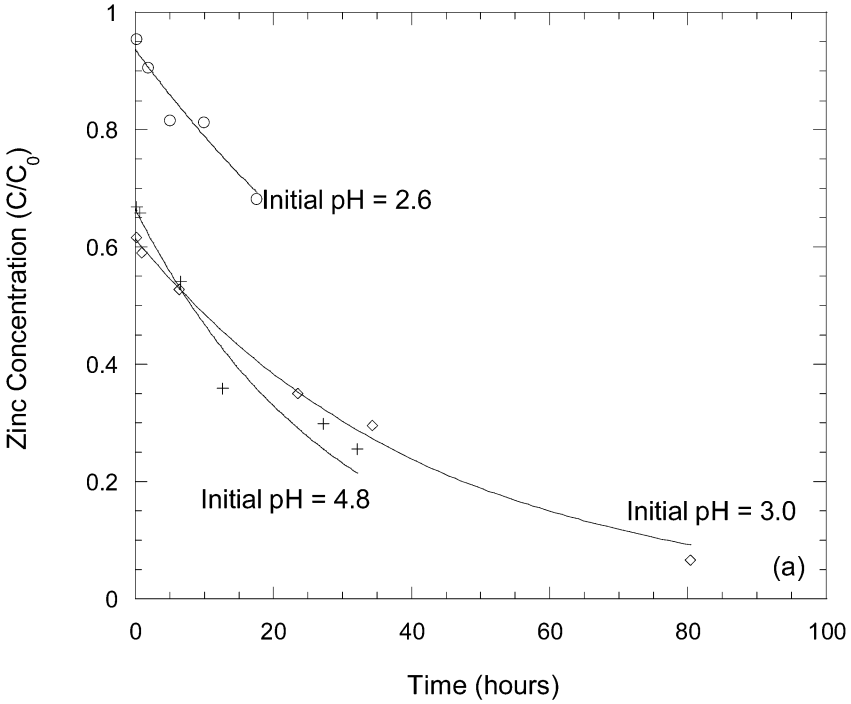

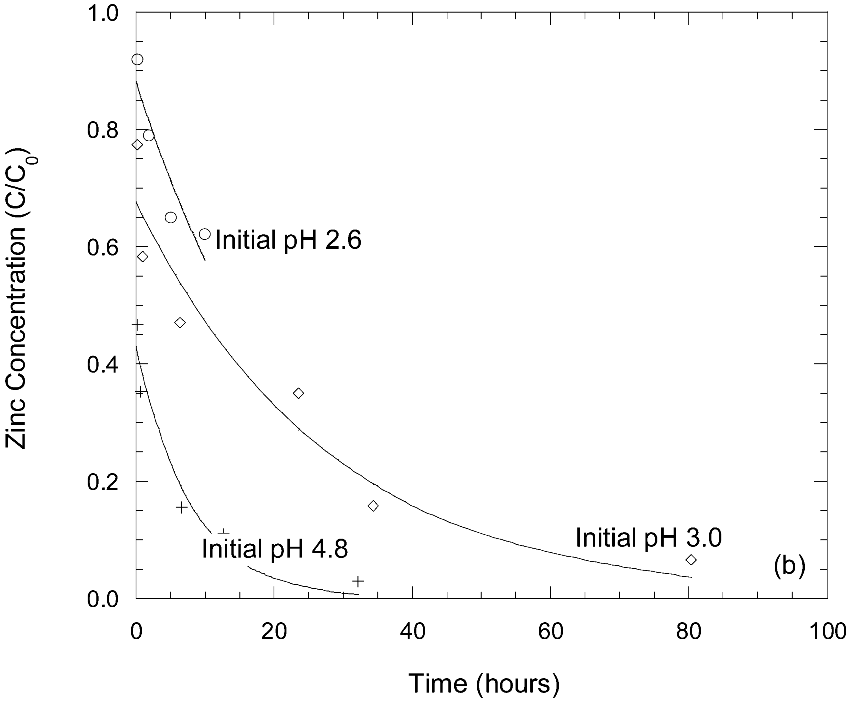

Fig. 7.6. Zinc Concentrations and Fits of Eq. 3.7 for (a) Sand 12 and (b) Peerless Iron.

Table 7.3. Partition Coefficients and Rate Constants for Zinc Removal Using Foundry Sands and Peerless Iron.

Medium	Clay (%)	TOC (%)	TIC (%)	Iron (%)	SSA (m^2/L)	K_p (L/kg)	Rate Constant (1/hr)	K_{SA} (L/m^2-hr)	Initial pH	Final pH
Sand 1	5.1	1.5	0	2.83	TS [b]	15.7	0.036	UH[c]	4.8	6.6
Sand 4	10.5	0.5	0.1	0.29	TS	31.2	0.044	UH	4.8	6.9
Sand 10	4.7	2.5	0.6	0.14	TS	18.9	0.040	UH	4.8	6.8
Sand 11	13.0	4.0	0.7	0.18	TS	50.5	0.058	UH	4.8	7.0
Sand 12	4.7	2.4	0	11.3	12.6	1.4	0.018	1.45×10^{-3}	2.6	4.7
Sand 12	4.7	2.4	0	11.3	12.6	7.5	0.042	3.32×10^{-3}	3.0	6.1
Sand 12	4.7	2.4	0	11.3	12.6	10.8	0.053	4.19×10^{-3}	4.8	6.8
Iron	N.A.[a]	N.A.	N.A.	100	40.7	2.9	0.048	1.18×10^{-3}	2.6	6.2
Iron	N.A.	N.A.	N.A.	100	40.7	10.2	0.054	1.32×10^{-3}	3.0	6.2
Iron	N.A.	N.A.	N.A.	100	40.7	28.4	0.295	7.24×10^{-3}	4.8	6.8

[a] N.A. = Not applicable, [b] TS = Values are too small, [c] UH = Values are unrealistically high.

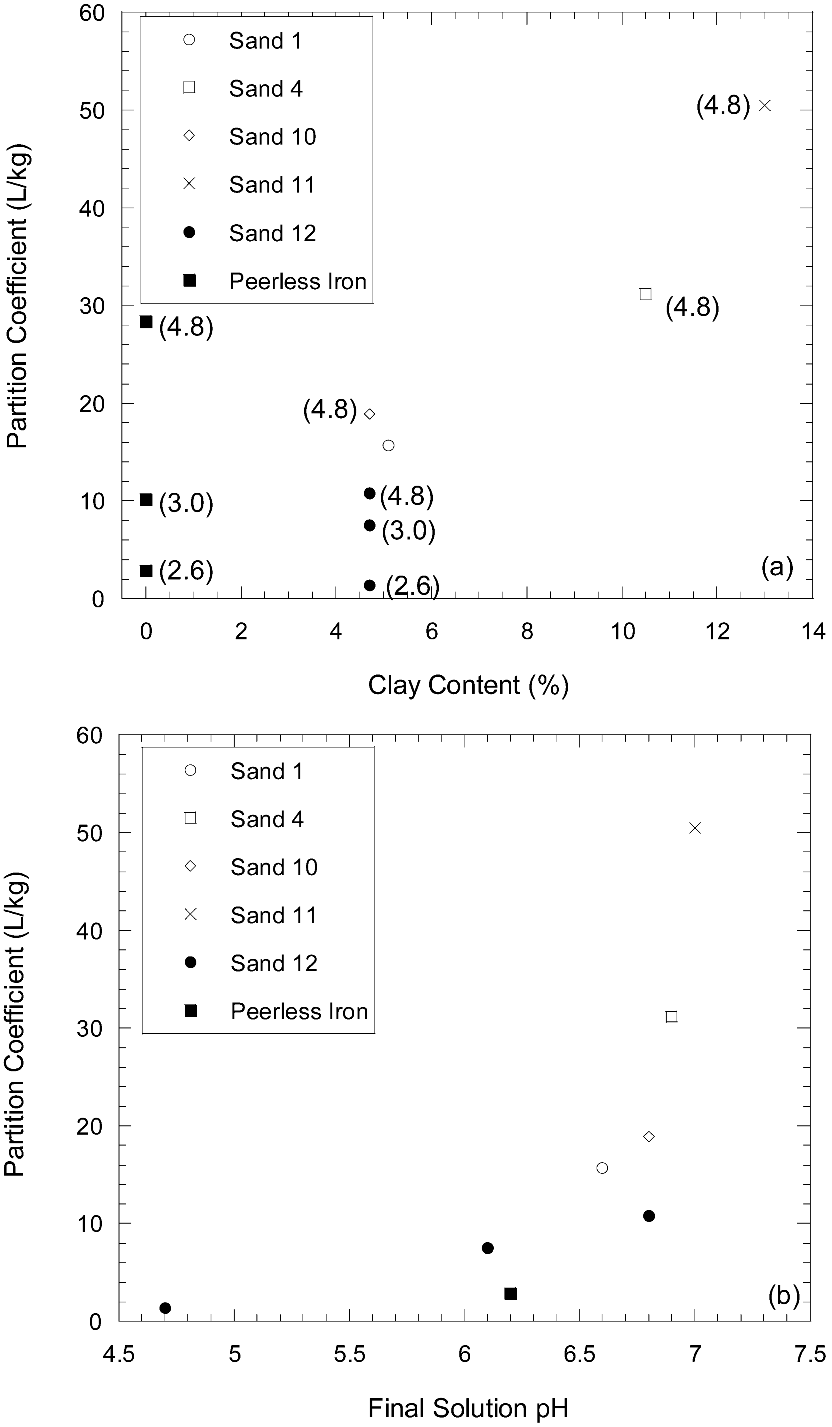

Fig. 7.7. Effect of (a) Clay Content and (b) Final Solution pH on the Instantaneous Partition Coefficient for Zinc. Numbers in Parentheses in (a) Represent Initial Solution pH.

First-order rate constants obtained from fitting Eq. 3.7 are shown in Fig. 7.8 as a function of clay content, final pH, TOC, and total iron content. TOC and total iron content have a slight effect on the rate constant. The rate constant increases modestly as the solution pH increases, which may be due to the favorable formation of zinc hydroxide or zinc oxide in higher pH solutions. The rate constants for Peerless iron and the foundry sands are similar when the solution pH is approximately 6.2. At higher pH, however, the rate constant for Peerless iron is approximately 6 times higher than those for the foundry sands at similar pH (Table 7.3).

A multivariate regression analysis was conducted to determine the effect of solution pH and clay content on the rate constants for the foundry sands. A significance level of 0.05 was used. The regression equation for foundry sands is ($R^2 = 0.99$):

$$K_{obs} = -0.0852 + 0.00138\ C + 0.00277\ TOC + 0.00126\ I + 0.0163\ pH \qquad (7.3)$$

where K_{obs} is a bulk first-order rate constant (1/hr), C is clay content (%), I is total iron content, and pH is the final solution pH.

7.2 BATCH SORPTION TESTS

The batch kinetic tests were conducted using a single zinc concentration. To evaluate whether the partition coefficients obtained from the batch kinetic tests were valid for other concentrations (i.e., whether the isotherm was approximately linear), a series of conventional batch sorption tests was

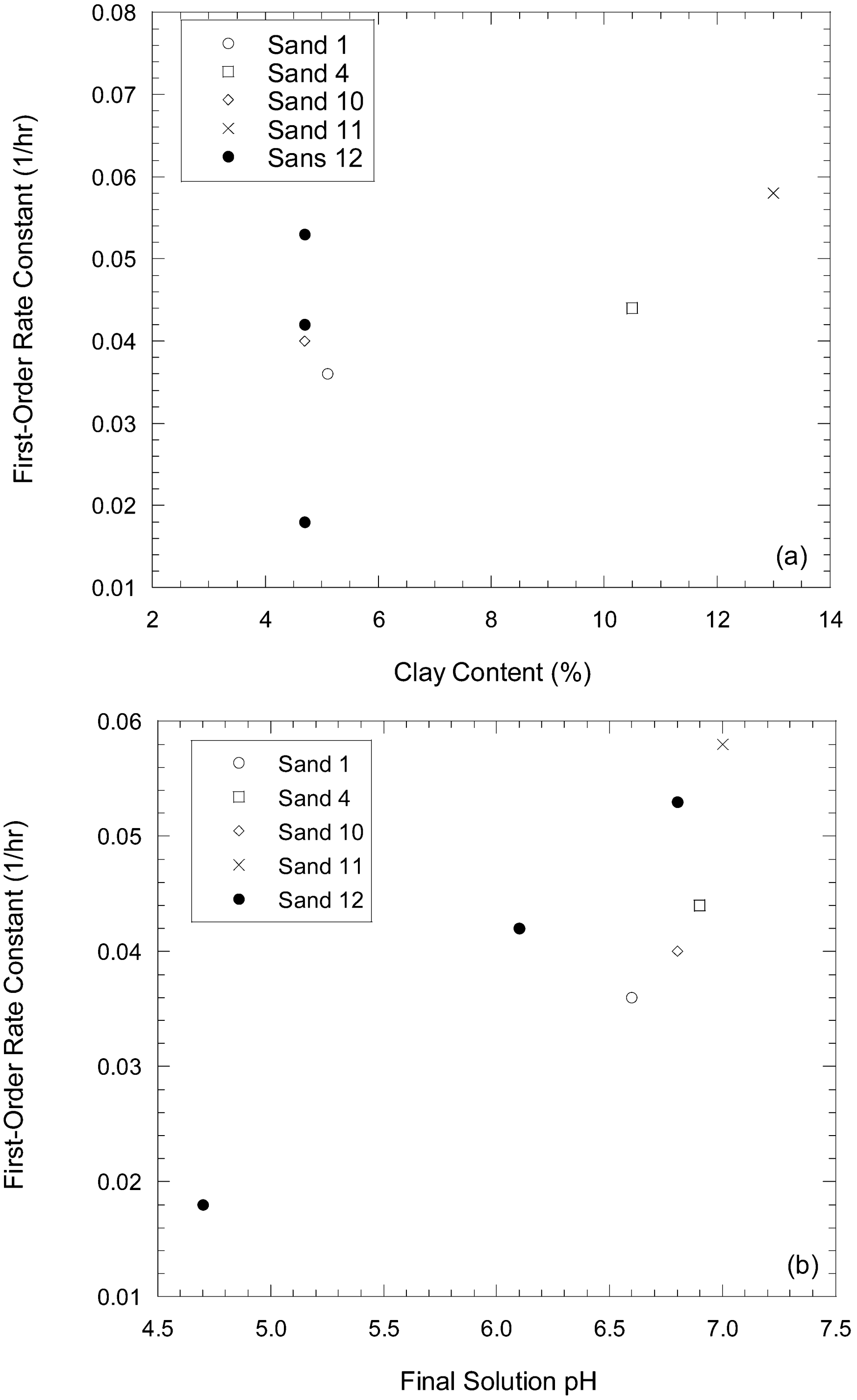

Fig. 7.8. First-Order Rate Constant as a Function of (a) Clay Content and (b) Final Solution pH, (c) TOC, and (d) Total Iron Content.

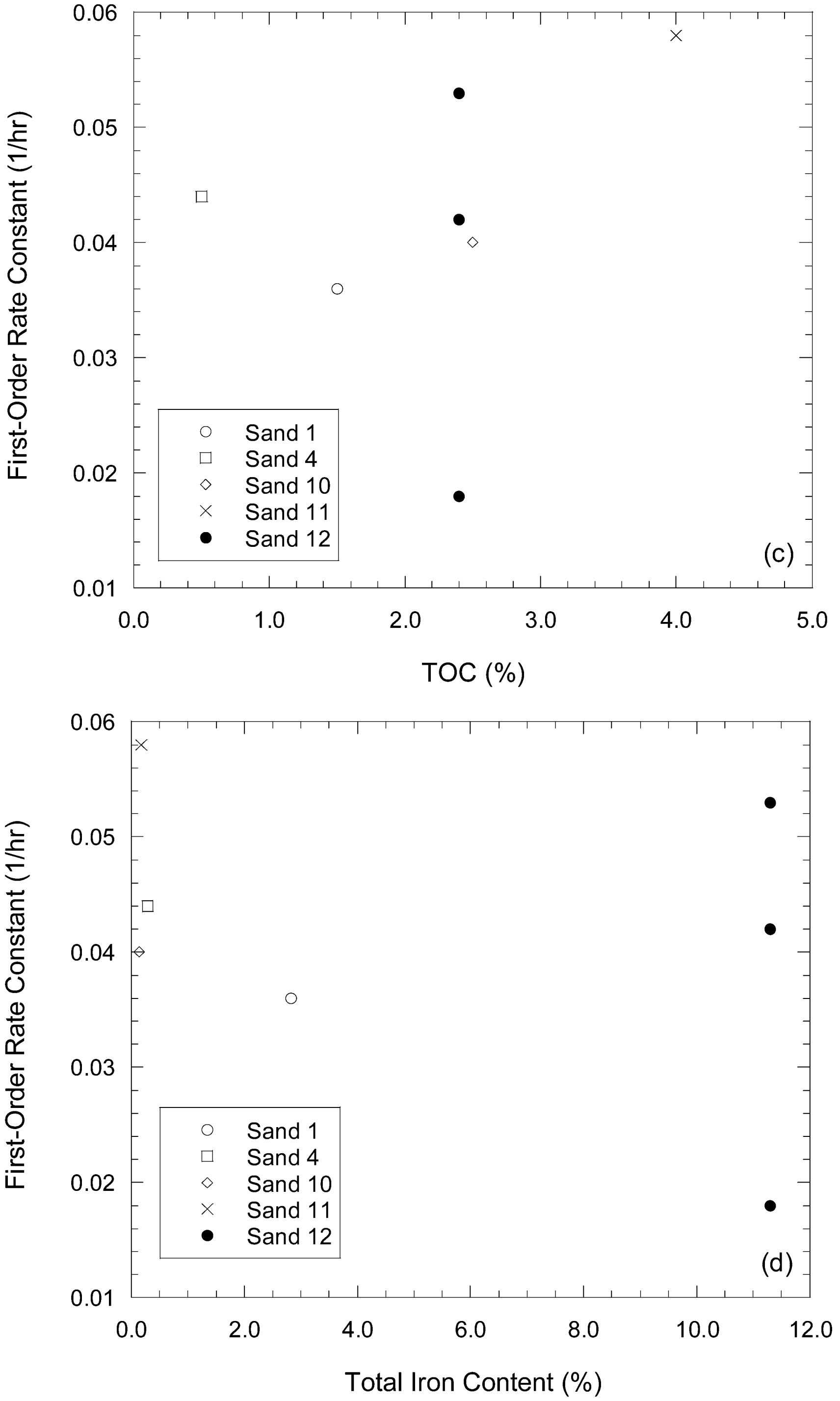

Fig. 7.8. First-Order Rate Constant as a Function of (a) Clay Content, (b) Final Solution pH, (c) TOC and (d) Total Iron Content (%) (Continued).

conducted. Sands 1, 2, 5, 10, and 12 were used to provide a broad range of TOC and clay content in the batch sorption tests. The mass of the foundry sand was maintained constant (2 g), and the zinc concentration was varied between 10 and 75 mg/L. The initial pH was adjusted to 2.6. The tumbling time was set at 10 hrs, which was found to be sufficient to ensure equilibrium (Fig. 7.1).

Sorption isotherms from the batch sorption tests are shown in Fig. 7.9. The isotherms exhibit some non-linearity, particularly at lower concentrations. Fits of the linear and Freundlich isotherm models are summarized in Table 7.4. Method 1 corresponds to fits of the linear model with a non-zero intercept. A zero-intercept was forced for Method 2. Comparable fits were obtained with the Freundlich model and the linear model with a non-zero intercept.

Partition coefficients obtained from the batch sorption tests were compared to those obtained from the batch kinetic tests for Sands 1, 10, and 12. For Sands 2 and 5, the partition coefficients were estimated using Eqs. 7.2, which was developed using data from the batch kinetic tests. In general, the partition coefficients from the batch kinetic tests and those predicted by Eq. 7.2 are comparable to the partition coefficients obtained from the batch sorption tests (Fig. 7.10). Therefore, partition coefficients estimated using Eq. 7.2 should be reliable for a relatively broad range of concentrations.

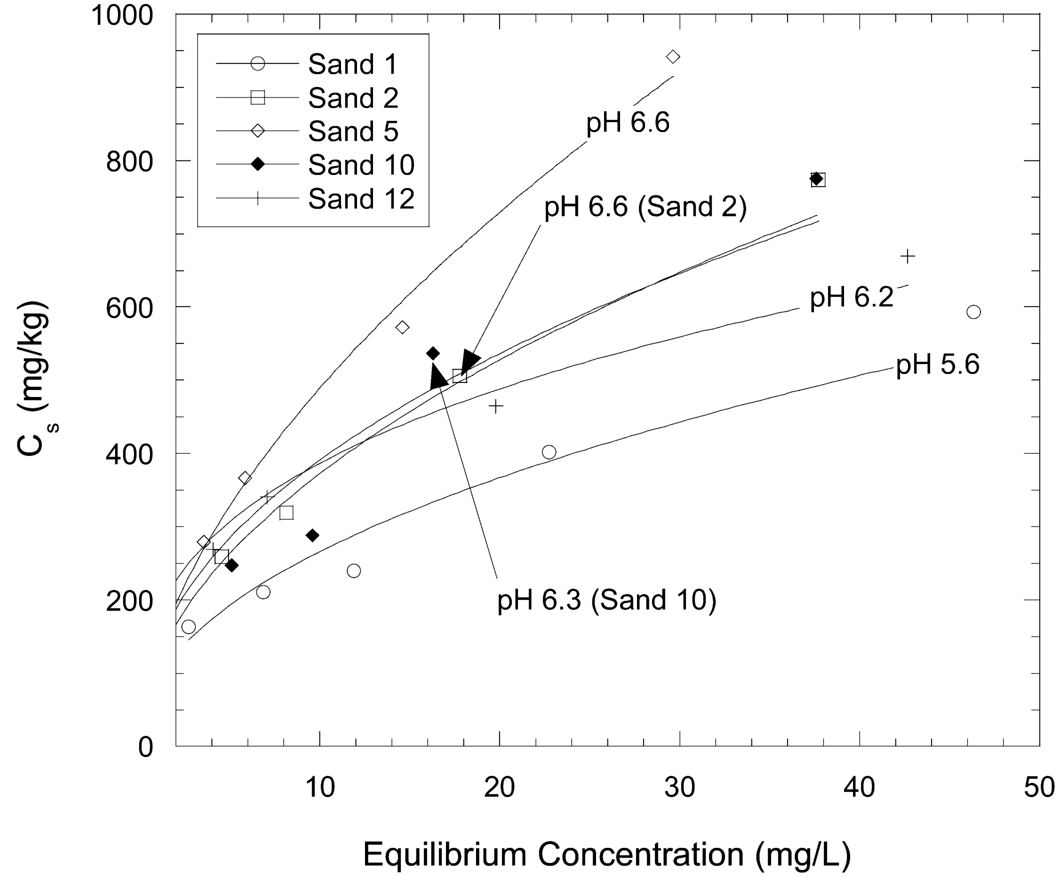

Fig. 7.9. Zinc Sorption Isotherms at Initial Solution pH 2.6. Numbers Adjacent to Data Correspond to Final pHs.

Table 7.4. Sorption Parameters of Freundlich Model for Zinc Sorption Using Sands 1, 2, 5, 10, and 12.

Foundry Sand	Linear Model				Freundlich Model		
	Method 1[a]		Method 2[b]		K_f (L/kg)	1/n	R^2
	K_p(L/kg)[a]	R^2	K_p (L/kg)	R^2			
Sand 1	10.0	0.99	14.5	0.65	91.1	0.46	0.94
Sand 2	16.1	0.99	23.1	0.64	136.3	0.46	0.98
Sand 5	26.2	0.99	34.8	0.79	129.5	0.58	0.99
Sand 10	16.9	0.95	23.5	0.70	116.9	0.50	0.93
Sand 12	10.7	0.97	18.2	0.01	178.6	0.34	0.99

[a] Method 1 is fit of linear isotherm with non-zero intercept, [b] Method 2 is fit of linear isotherm with intercept forced to zero.

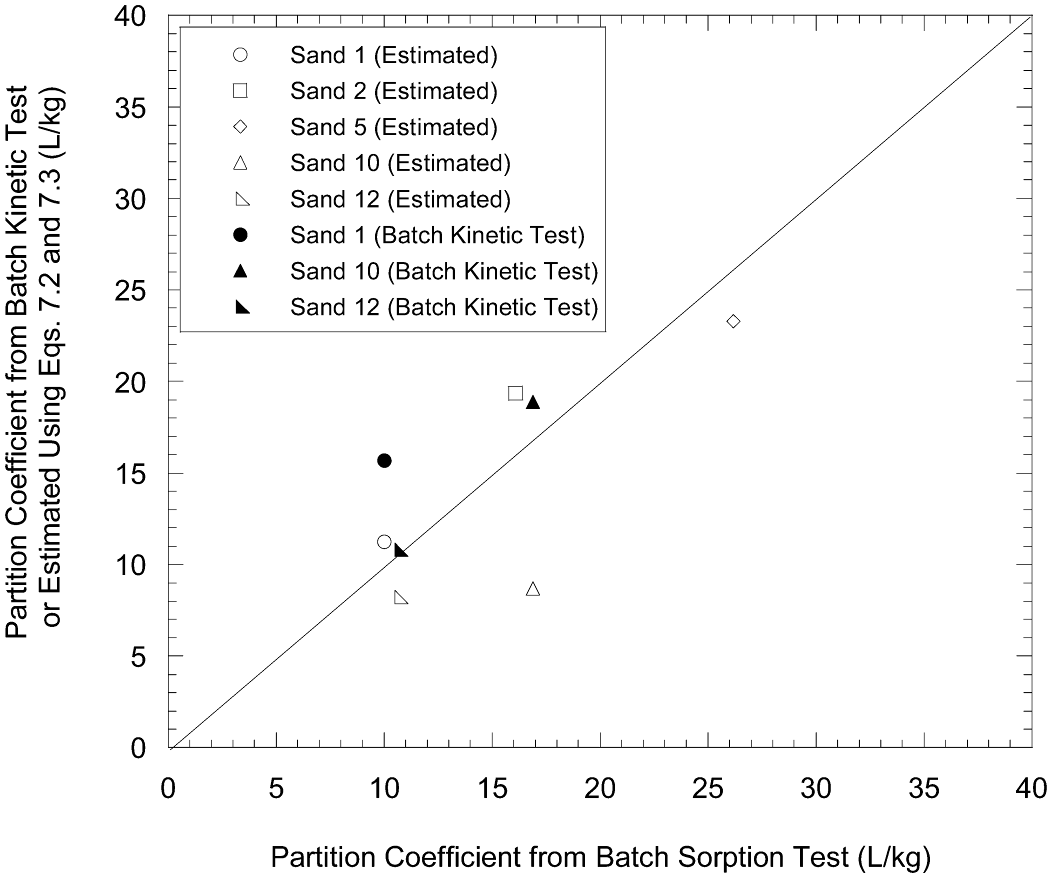

Fig. 7.10. Comparison of Partition Coefficients Obtained from Batch Sorption Tests and Batch Kinetic Tests.

7.3 COLUMN TESTS

Column tests were conducted using Sands 1, 2, 5, 10, and 12. Properties of the sands and the experimental conditions are summarized in Table 7.5. Two different sets of column tests were conducted. One set had initial pH 3.0 and the other pH 4.0. Sands 1 and 10 were used for the pH 3.0 tests. Sands 1, 2, 5, and 12 were used with pH 4.0. Zinc concentrations in the influent were maintained at 50 mg/L. The pH was adjusted by using 1.0 M HNO_3 or 1.0 M NaOH.

Typical data from the column tests are shown in Figs. 7.11 – 7.12. Data from the column tests were fit with Eq. 3.18 following the methods described in Sec. 3.5.3. The seepage velocity used in Eq. 3.18 was calculated by dividing the discharge velocity by the total porosity. Because all of the column tests were conducted with foundry sands having a dry density less than 1.60 Mg/m^3, the total porosity was assumed to be equal to the effective porosity. As shown in Table 5.8, the effective porosity is comparable to the total porosity when the dry density is less than 1.60 Mg/m^3. Transport parameters obtained from fitting Eq. 3.18 to the data are summarized in Table 7.6.

7.3.1 Partition Coefficient

Partition coefficients obtained from the column tests ranged from 7.4 (Sand 1) to 77.7 L/kg (Sand 5). Relationships between the partition coefficients and TOC, clay content, total iron content, and pH are shown in Fig. 7.13. TOC

Table 7.5. Soil Properties and Experimental Conditions Used in Column Tests with Zinc Solution.

Foundry Sand	TOC (%)	TIC (%)	Clay (%)	Iron (%)	pH	V_S[a] (cm/sec)	Dry Density (Mg/m^3)	Length (cm)	Porosity	Influent Concentration (mg/L)
Sand 1	1.5	0	5.1	2.83	3.0±0.3	8.7×10^{-3}	1.60	29	0.39	50±2.0
Sand 1	1.5	0	5.1	2.83	4.0±0.3	1.8×10^{-3}	1.49	28	0.43	50±2.0
Sand 2	2.6	0.5	7.0	0.15	4.0±0.3	2.6×10^{-3}	1.47	18	0.43	50±2.0
Sand 5	1.8	0	8.4	0.14	4.0±0.3	2.7×10^{-3}	1.51	18	0.41	50±2.0
Sand 10	2.5	0.6	4.7	0.14	3.0±0.3	8.2×10^{-3}	1.53	42	0.43	50±2.0
Sand 12	2.4	0	4.7	11.26	4.0±0.3	2.5×10^{-3}	1.51	18	0.42	50±2.0

[a] Seepage Velocity

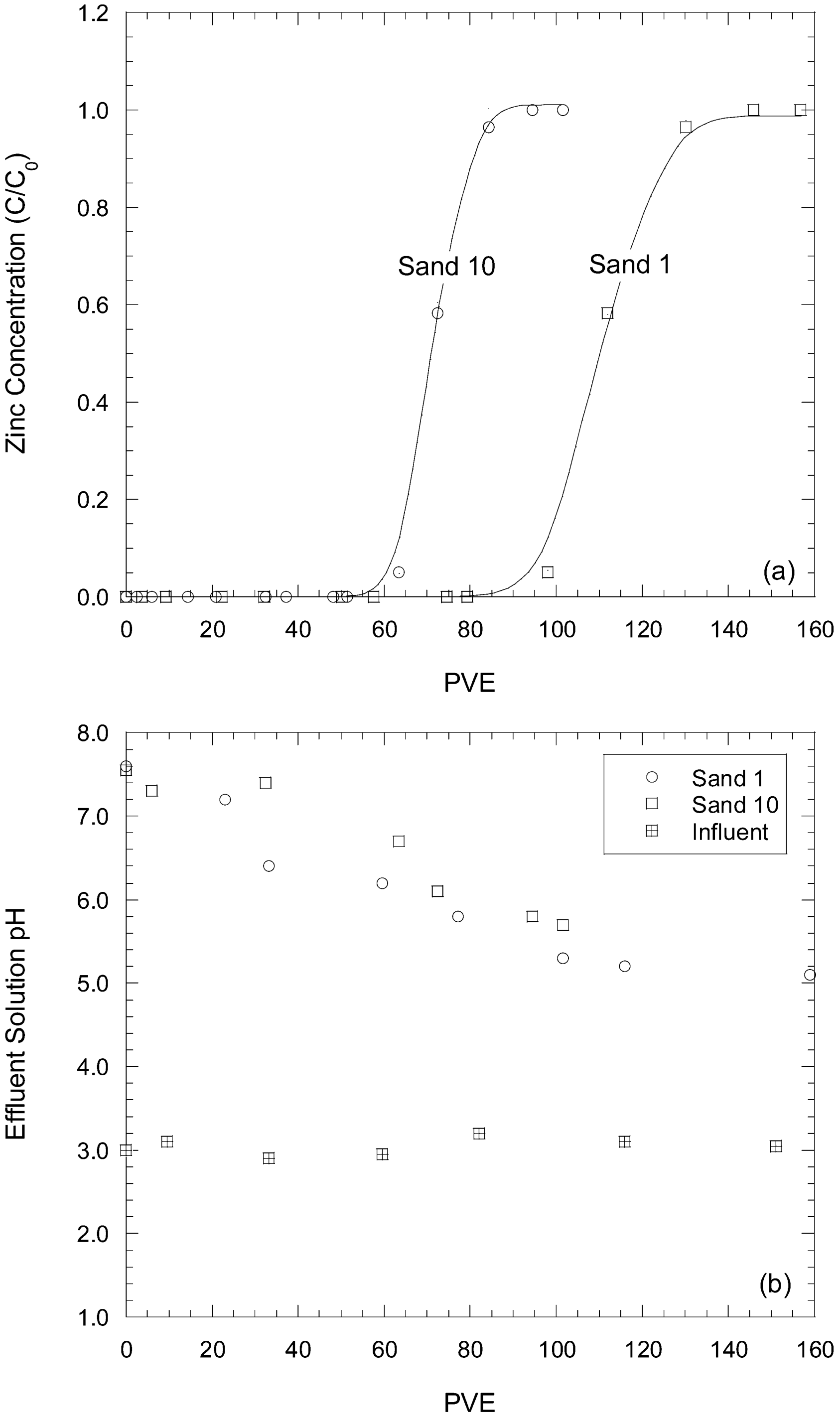

Fig. 7.11. Results of Column Tests for Sand 1 and 10 When Initial pH was 3.0: (a) Concentrations and (b) Influent and Effluent Solution pH.

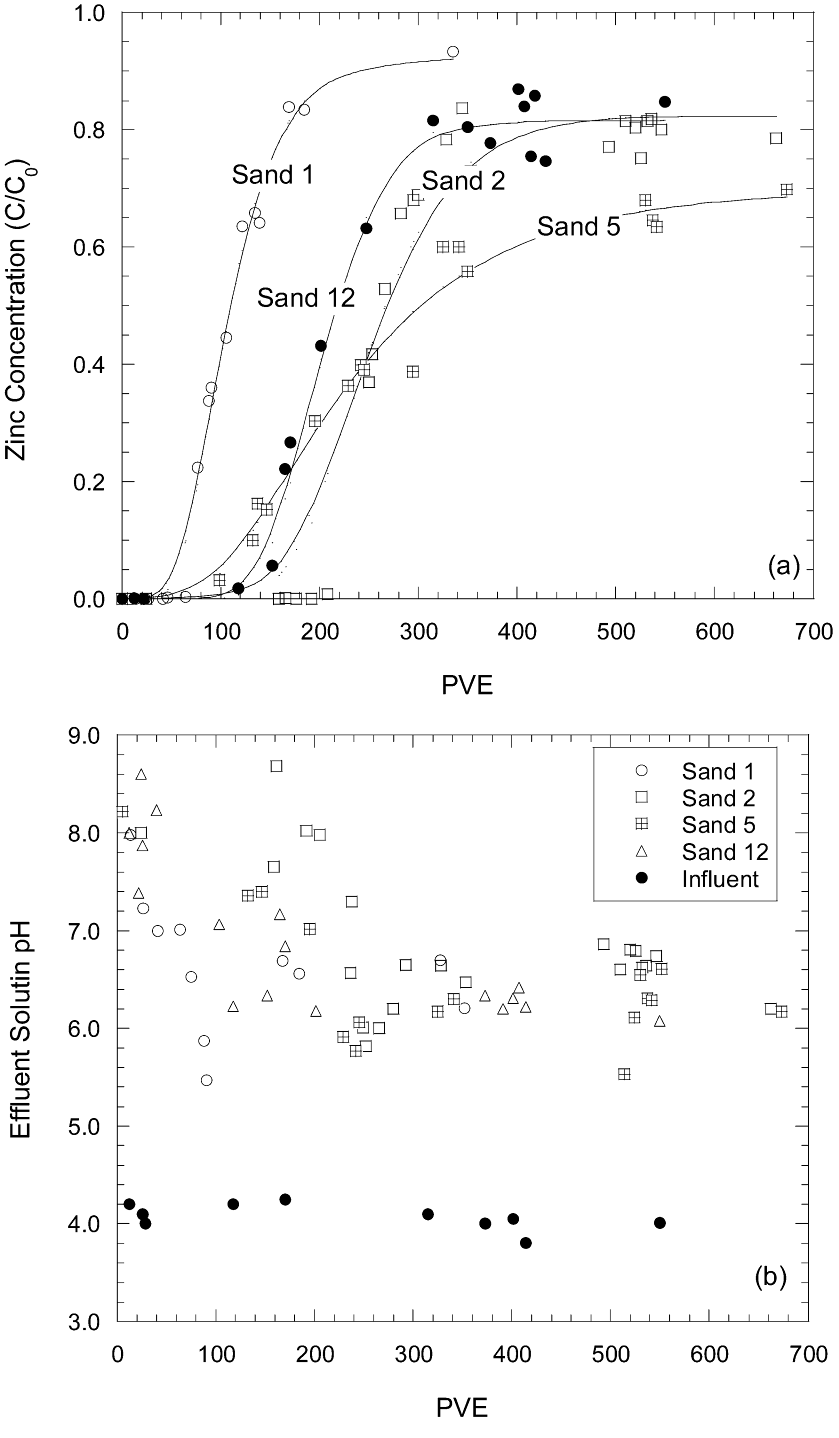

Fig. 7.12. Results of Column Tests for Sand 1, 2, 5, and 12 When Initial pH was 4.0: (a) Concentrations, and (b) Influent and Effluent Solution pH.

Table 7.6. Results of Column Tests Using 50 mg/L Zinc Solution.

Foundry Sand	V_s[a] (cm/s)	D (cm^2/sec)	α_L[b] (cm)	α_L[b] (cm) (estimated)	Influent pH	Equilibrium pH	K_p[c] (L/kg)	K_{obs}[d] (1/hr)
Sand 1	8.69×10^{-3}	6.67×10^{-4}	0.08	2.9	3.0±0.3	5.1	7.4	0.013
Sand 1	1.77×10^{-3}	9.84×10^{-3}	2.40	2.8	4.0±0.3	6.2	31.7	0.069
Sand 2	2.60×10^{-3}	1.79×10^{-3}	0.69	2.8	4.0±0.3	6.6	75.8	0.102
Sand 5	2.73×10^{-3}	8.82×10^{-3}	3.23	1.8	4.0±0.3	6.2	77.7	0.209
Sand 10	8.15×10^{-3}	8.16×10^{-4}	0.10	4.2	3.0±0.3	5.9	19.7	N.A.
Sand 12	2.52×10^{-3}	1.37×10^{-3}	0.54	1.8	4.0±0.3	6.3	53.7	0.103

[a] Seepage Velocity, [b] Longitudinal Dispersivity, [c] Partition coefficient, [d] First-Order Rate Constant.

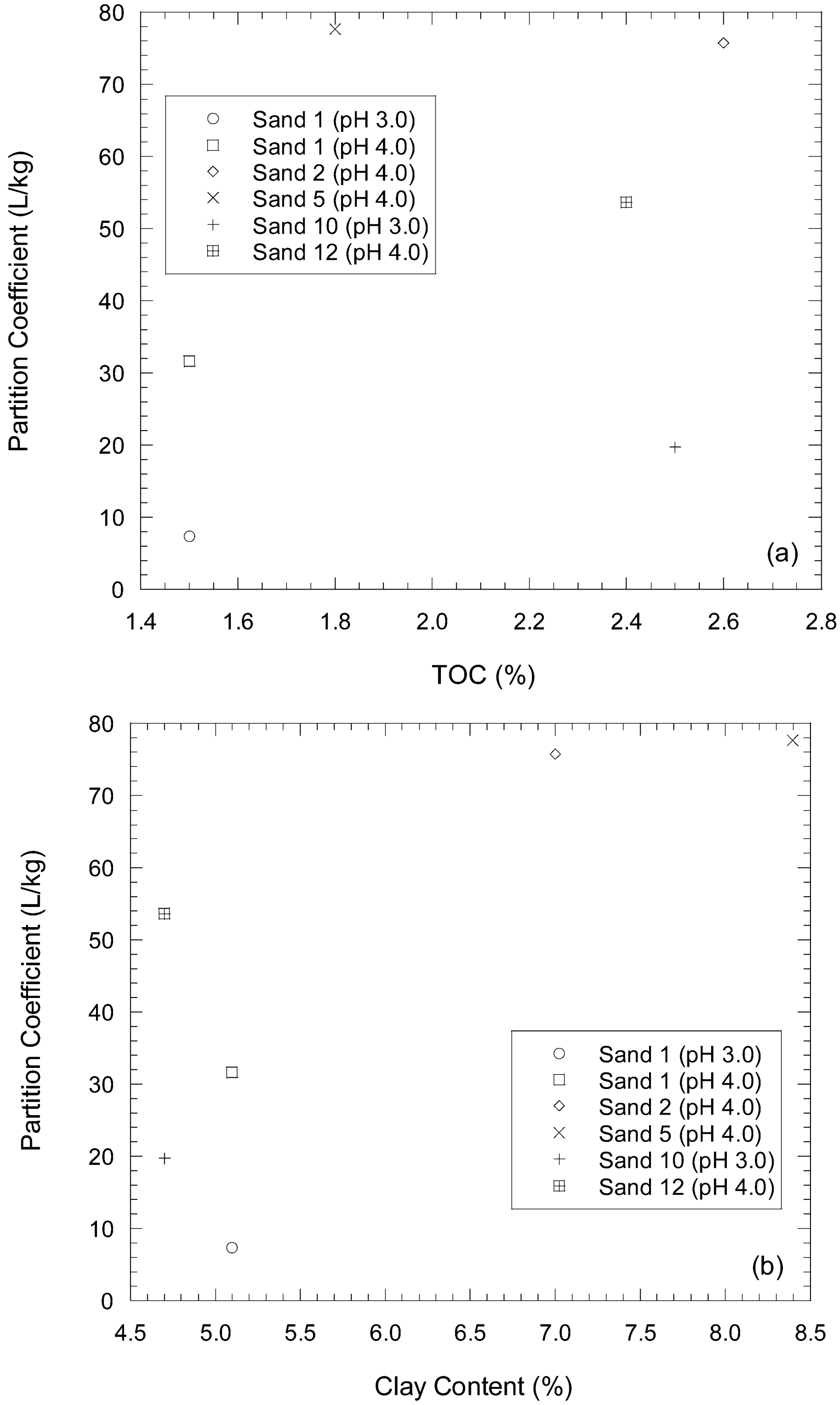

Fig. 7.13. Effect of (a) TOC, (b) Clay Content, (c) Total Iron Content, and (d) Effluent pH on Partition Coefficient.

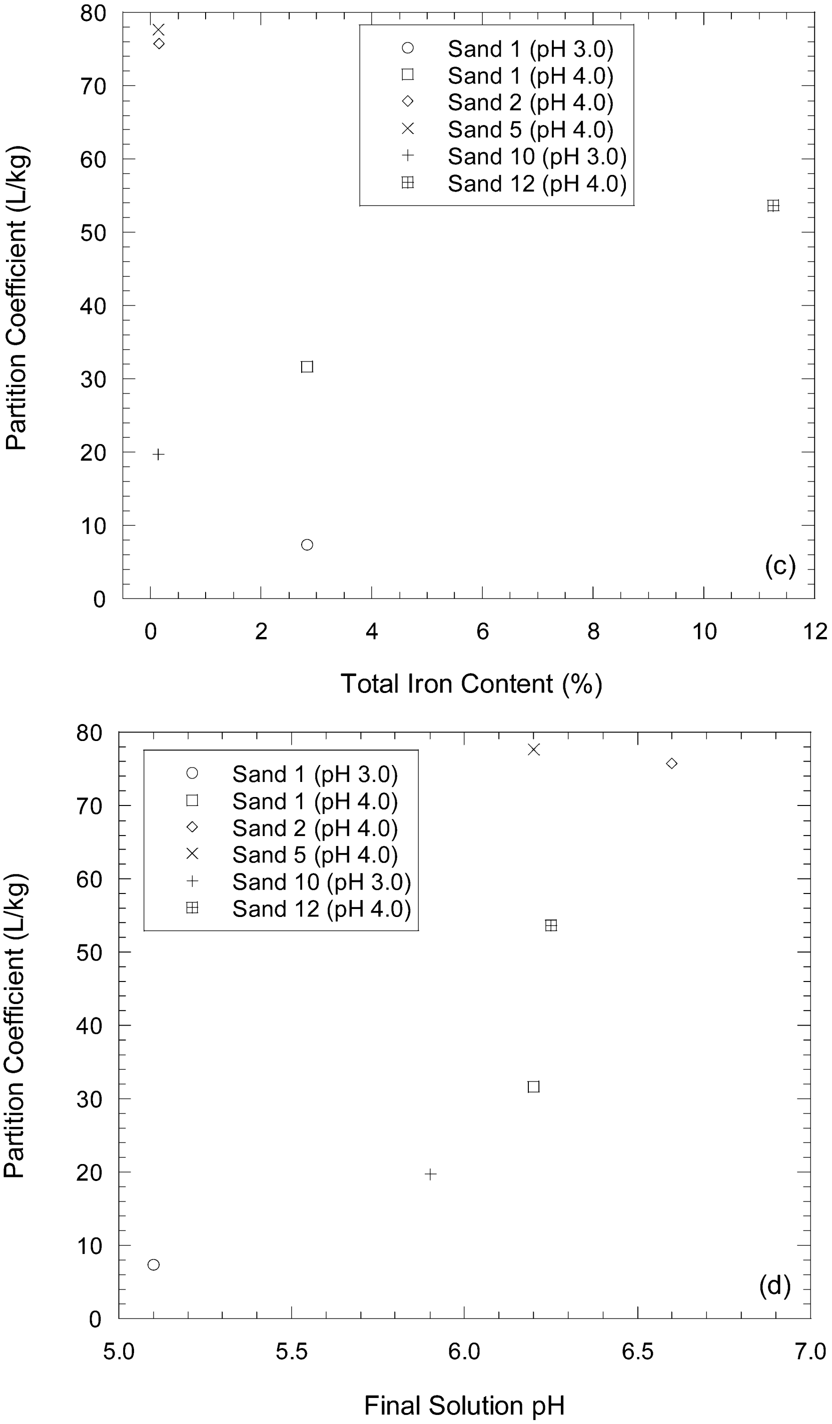

Fig. 7.13. Effect of (a) TOC, (b) Clay Content, (c) Total Iron Content, and (d) Effluent pH on Partition Coefficient (Continued).

and clay content appear to have a modest effect on the partition coefficient, but final solution pH appears to be the most important factor. Total iron content appears to have almost no effect on the partition coefficient. A multivariate regression analysis was conducted at the 0.05 significant level to define relationship between the partition coefficient and TOC, total iron content, clay content and final pH. The equation is ($R^2 = 0.85$):

$$K_p = -223 + 10.6\ C + 33.9\ pH \tag{7.4}$$

where K_p is a partition coefficient (L/kg) for zinc, C is clay content (%), and pH is the final solution pH. TOC is not included in Eq. 7.4 because it was not significant at the 0.05 level.

7.3.2 Rate Constant

The rate constant obtained from the column tests ranged from 0.013 (Sand 1) to 0.209 hr^{-1} (Sand 5). No rate constant was obtained from Sand 10 tested with low solution pH 3.0 because the effluent concentration was essentially the same as influent concentration.

The effects of TOC, clay content, total iron content, and final effluent solution pH on the rate constant for the foundry sands are shown in Fig. 7.14. A multivariate regression analysis was conducted at the 0.05 significant level to define a relationship between the rate constant and sand properties. The regression equation is ($R^2 =0.69$):

$$K_{obs} = -0.158 + 0.0413\ C \tag{7.5}$$

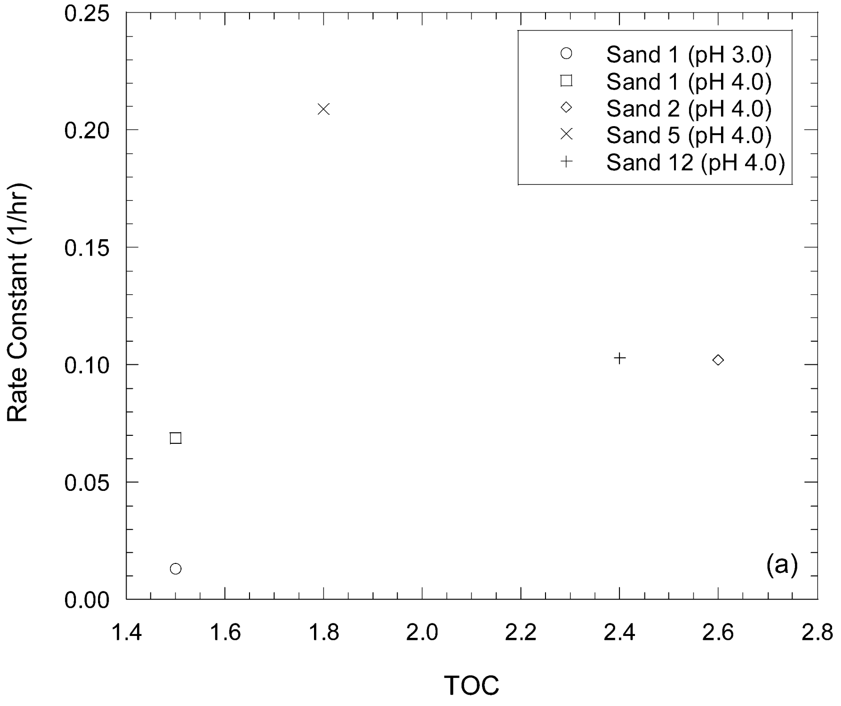

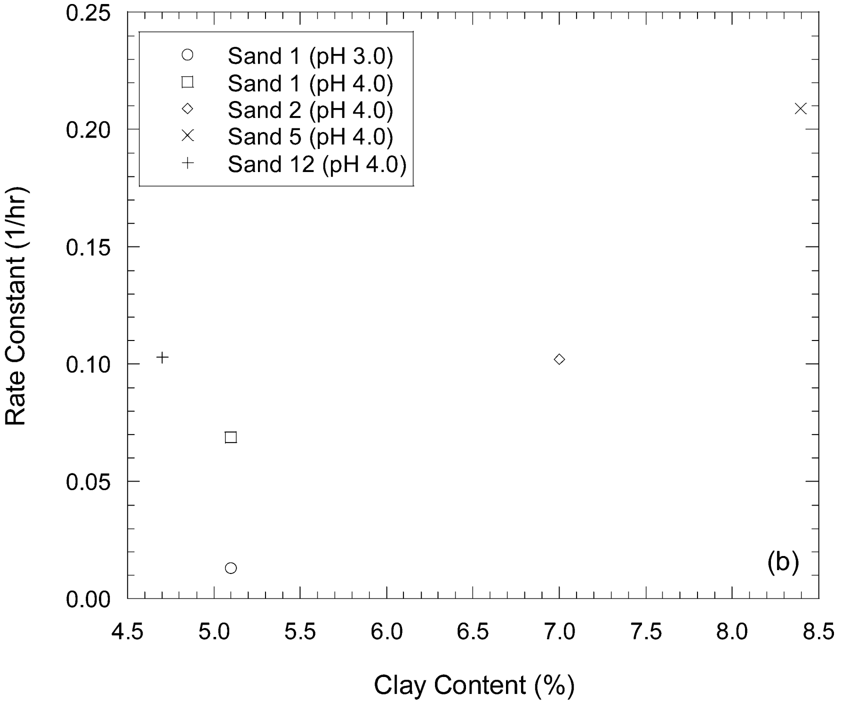

Fig. 7.14. Effect of (a) TOC, (b) Clay Content, (c) Total Iron Content, and (d) Final Effluent Solution pH on Rate Constant.

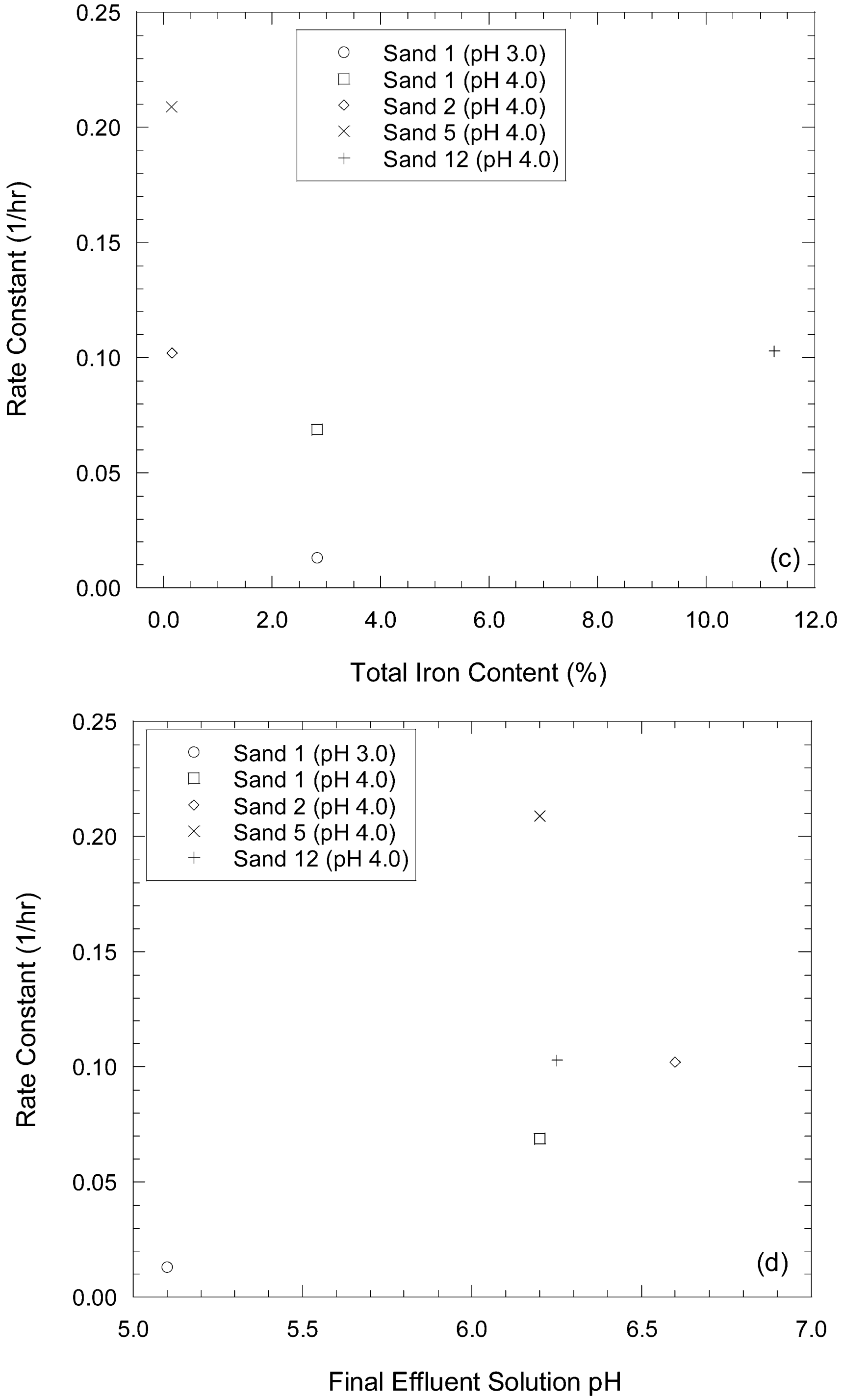

Fig. 7.14. Effect of (a) TOC, (b) Clay Content, (c) Total Iron Content, and (d) Final Effluent Solution pH on Rate Constant (Continued).

where K_{obs} is a first-order rate constant (1/hr), and C is clay content (%). TOC, total iron content, and final solution pH are not included in regression equation because these parameters were not statistically significant.

7.3.3 Comparison Between Batch and Column Tests.

Given the importance of pH in zinc removal, comparisons between the batch tests and column tests must be made at comparable pH. The pH reported for the batch sorption test is the pH measured at the end of the test (10 hr). In contrast, the effluent solution pH for the column tests was measured at various times as the effluent was collected. Thus, the average effluent pH was used to compare results from the column tests to those from the batch tests.

Partition coefficients and solution pH obtained from batch sorption tests and column tests are shown in Fig. 7.15. For Sands 1 and 10 tested at pH 3.0, the partition coefficients obtained from batch and column tests are comparable. In contrast, for Sands 1, 2, 5, and 12 tested at influent pH 4.0, the partition coefficients from the column tests are 4 or 5 times higher than those obtained from the batch sorption tests. The column tests yield higher partition coefficients because the solution pHs for the column tests are higher than those for the batch sorption tests (Fig. 7.15b).

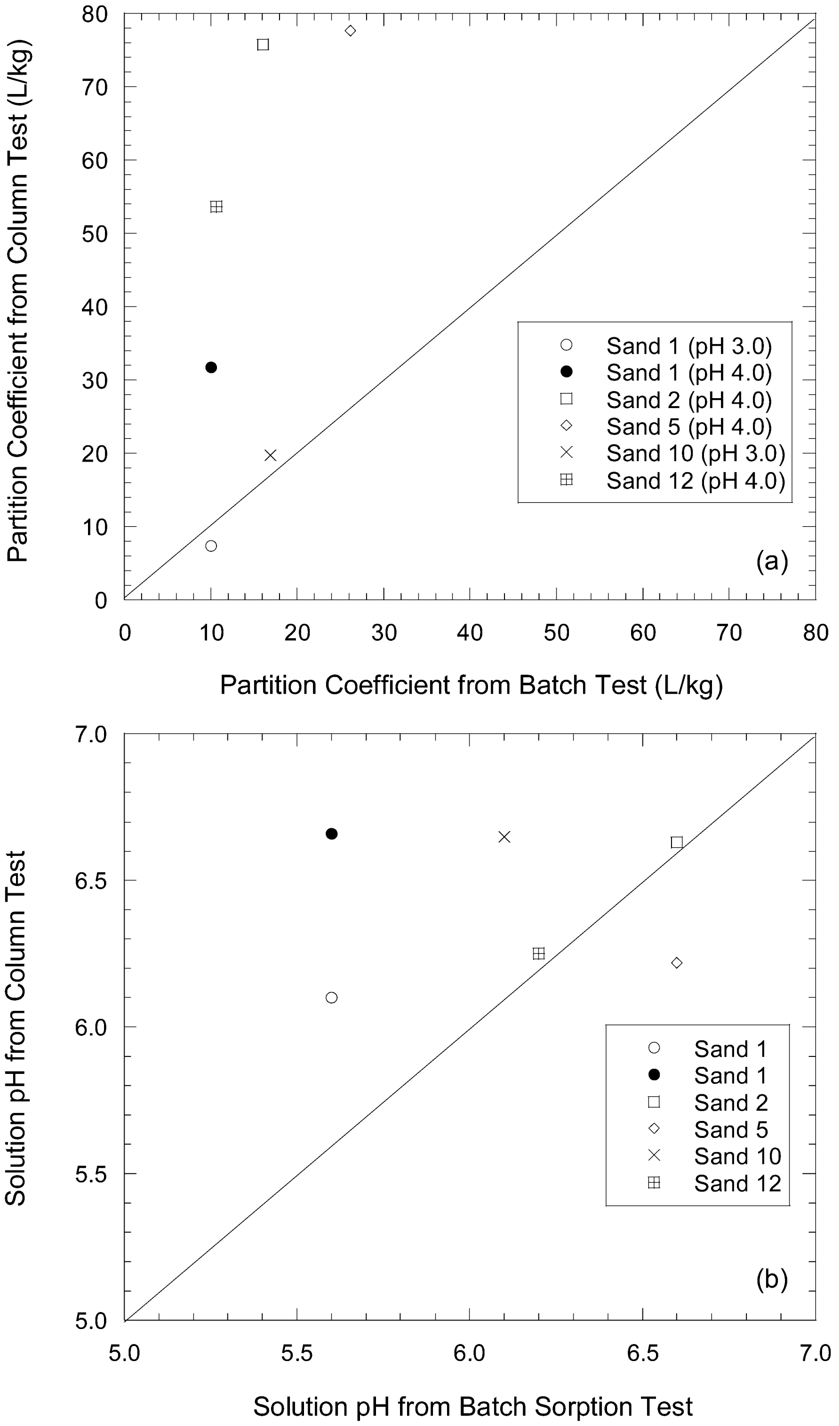

Fig. 7.15. Comparisons of (a) Partition Coefficients and (b) Solution pHs for Batch and Column Tests. pH Values Noted in Parentheses Correspond to Influent Condition. Final pH was Used as Solution pH for Column Test.

The accuracy of the empirical equations (Eqs. 7.2 and 7.3) obtained from the batch kinetic tests was evaluated using the column test data. Eq. 7.2 was used to predict partition coefficients using data obtained from the column tests. A comparison of the measured and estimated partition coefficients is shown in Fig. 7.16. Good agreement is shown when initial solution pHs are considered (Fig. 7.16a). However, there is little agreement between the estimated partition coefficient and the partition coefficients from the column tests when solution pHs obtained at breakthrough of zinc are used for the estimation.

Rate constants obtained from the column tests and the batch kinetic tests are shown in Fig. 7.17. The rate constants obtained using both methods are comparable, and appear to be modestly affected by solution pH.

7.4 PRB DESIGN

PRB thicknesses were computed using Eq. 3.21 to illustrate how PRBs can be used for treating groundwater contaminated with zinc. The mechanical dispersion coefficient was calculated by multiplying one-tenth of the barrier thickness by the seepage velocity. The molecular diffusion coefficient for zinc was calculated by multiplying the aqueous diffusion coefficient of zinc by the tortuosity. The aqueous diffusion coefficient of zinc (7.37×10^{-6} cm^2/s) was obtained using an average aqueous diffusion coefficient (Li and Gregory 1974), and a tortuosity of 0.4, which was obtained from typical values of tortuosity ranging from 0.31 to 0.64 (Bear 1972). The molecular diffusion coefficient

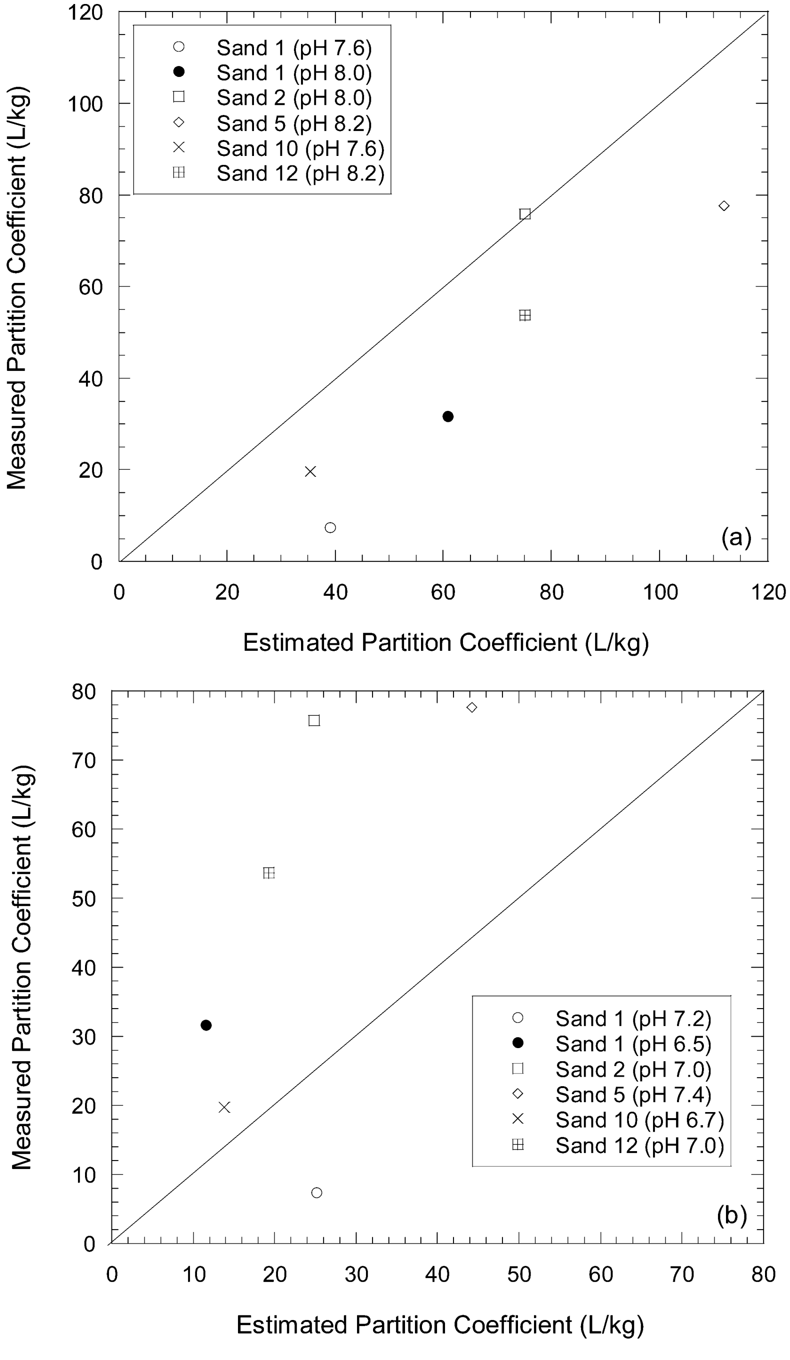

Fig. 7.16. Comparison of Partition Coefficients Obtained from Column Tests and Estimated Using Eq. 7.2 with (a) Initial Solution pH and (b) Solution pH at Breakthrough. pHs Noted in Legend Correspond to Initial Solution pH (a) and Solution pH at Breakthrough (b).

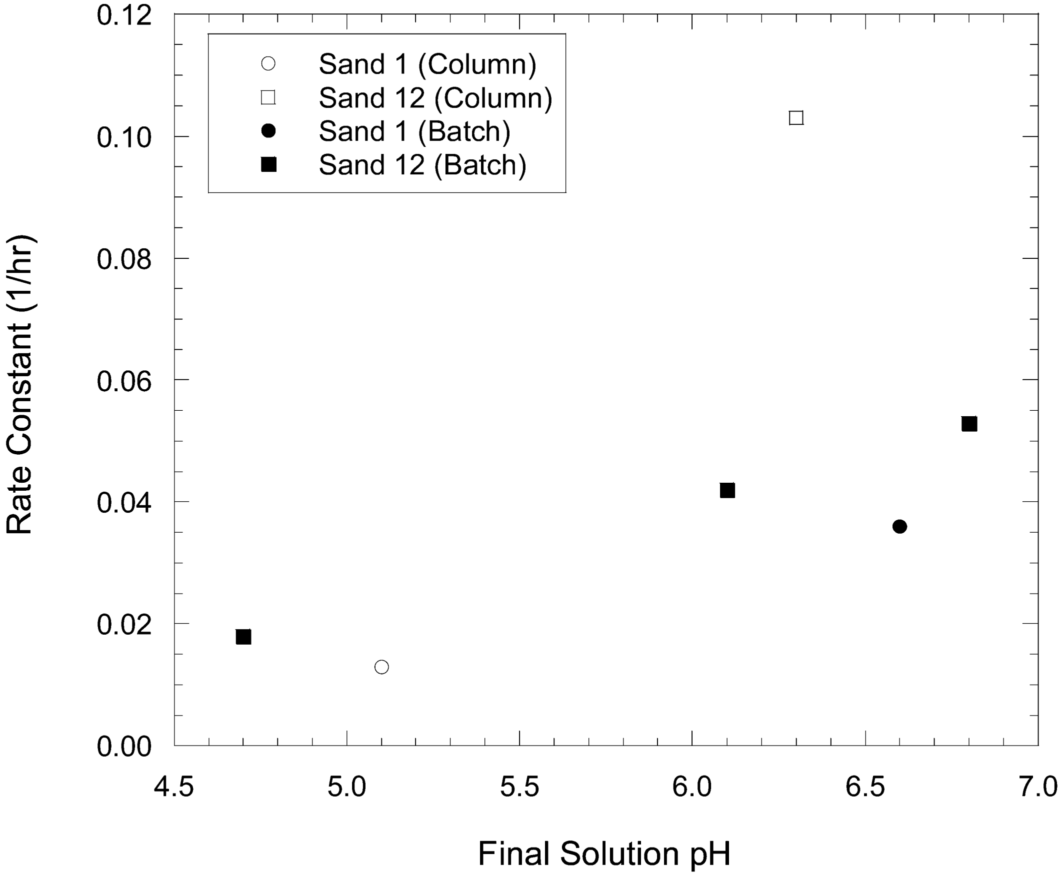

Fig. 7.17. Comparison of Rate Constants Obtained from Column Tests and Batch Kinetic Tests.

contributed less than 3% to the hydrodynamic dispersion coefficient for the seepage velocities that were used. Thus, the value assumed for the tortuosity factor is not significant.

The seepage velocity used in the calculations ranged between 0.01 m/d and 0.1 m/d (Rust Environment & Infrastructure 1995, Benner et al. 1997, Mueller et al. 1997). A typical zinc concentration for acid rock drainage is approximately 400 mg/L (Shokes and Moller 1999) and MCL for zinc is 2.5 mg/L. Thus, the normalized zinc concentration to meet the MCL (C/C_0) was set at 0.00625.

Eq. 7.5 was used to estimate the bulk first-order rate constant as a function of sand properties. Calculations were made for clay contents ranging from 4 to 10%, and seepage velocities of 0.01 and 0.1 m/d. Partition coefficients were estimated using Eq. 7.4, which is a function of clay content and effluent solution pH at equilibrium. Clay contents and seepage velocity were varied as was described for the rate constant. Final pHs of 5 and 7 were used. The final pH was assumed to be 2 pH units higher than the influent pH, based on the results shown in Figs. 7.11 – 7.12. In a field setting, the effluent pH will most likely be more than 2 pH units higher than the influent pH. Thus, this assumption is conservative.

Relative concentrations are shown in Fig. 7.18 for various barrier thicknesses. A thinner barrier is required as the clay content increases. In

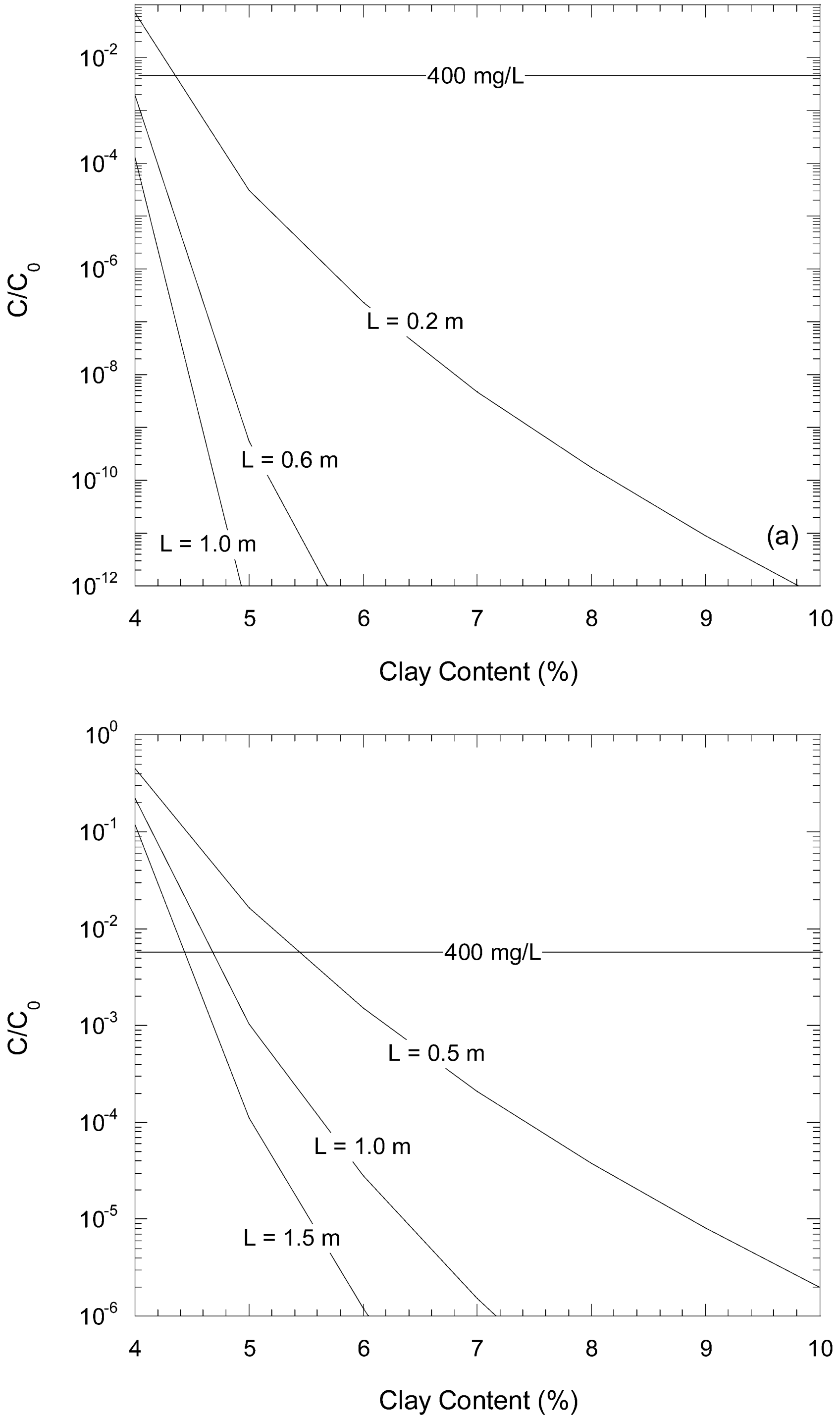

Fig. 7.18. Normalized Zinc Concentrations as a Function of Clay Content and Barrier Thickness: (a) V_s = 0.01 m/d (b) V_s = 0.1 m/d.

general, barriers less than 1-m thick are can be used if the clay content is higher than 5%.

The time to equilibrium is shown in Fig. 7.19 as a function of clay content and equilibrium solution pH. The barrier thickness and seepage velocity were fixed at 1.0 m and 0.1 m/d, respectively. The time to reach equilibrium increases as equilibrium pH and clay content increase. For equilibrium pH 7, the time to reach equilibrium is more than 80 yrs when the clay content is a modest 5.5%

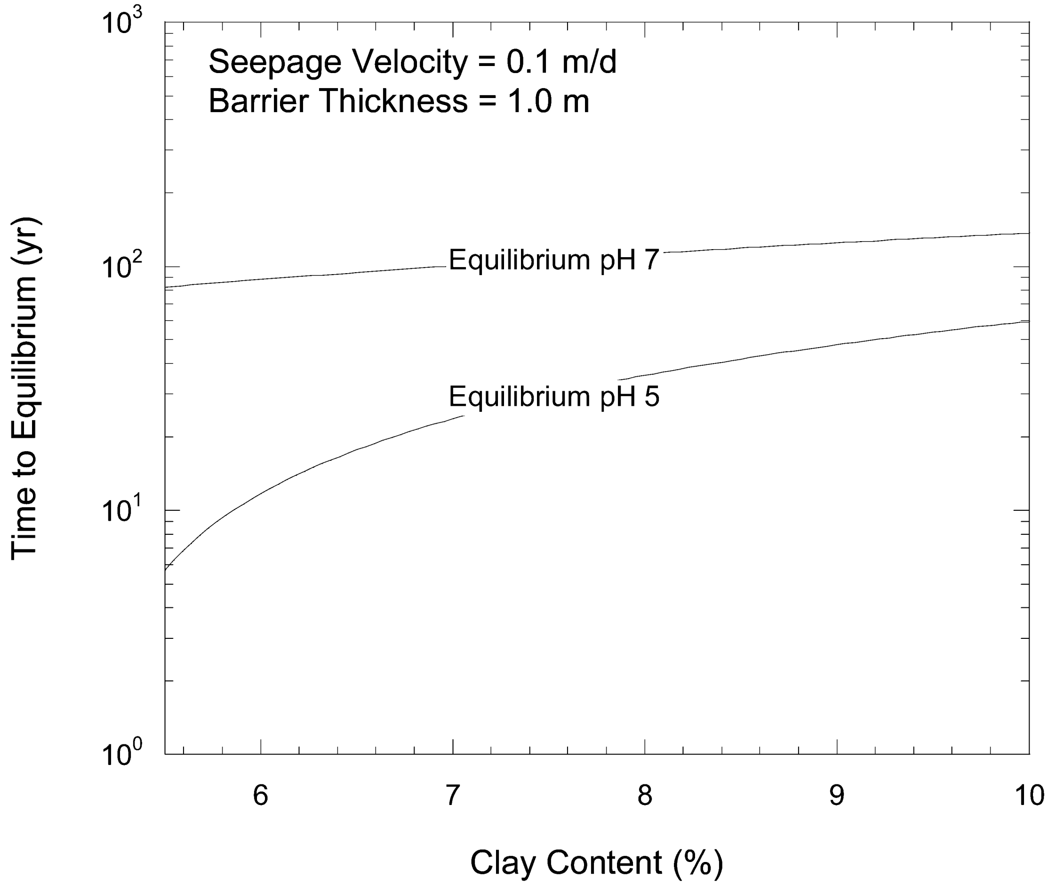

Fig. 7.19. Time to Equilibrium as a Function of Clay Content and Effluent Solution pH.

SECTION EIGHT

RESULTS OF COLUMN LEACHING TESTS

Column leaching tests were conducted to assess the leaching behavior of foundry sands under more realistic conditions. The experimental conditions are summarized in Table 8.1. Five foundry sands (Sands 1, 2, 4, 10, and 12) were selected to provide a broad range of TOC (0.5% to 2.6%) and clay content (4.7% to 10.5%). Two reference materials (i.e., Peerless iron and torpedo sand) were also tested for comparison.

Seepage velocities for the foundry sands and the torpedo sand were calculated assuming the effective porosity was equal to the total porosity. Total porosity was used because the dry density was less than 1.60 Mg/m^3 for all of the foundry sands as well as the torpedo sands. In Section 5.3.2, the total porosity and effective porosity were found to be essentially same when the dry density was less than 1.60 Mg/m^3 (Table 5.8). For Peerless iron, the effective porosity was calculated using the ratio of effective porosity to total porosity reported in Table 5.8.

Madison tap water was used as influent solution. Prior to use, the tap water was sparged with N_2 gas to remove the dissolved oxygen. Sparging with N_2 gas resulted in DO concentrations less than 0.6 mg/L. Other procedures used for the column leaching tests are discussed in Section 3.6.

Table 8.1. Experimental Conditions for Column Leaching Tests.

Medium	Clay (%)	Total Iron (%)	TOC (%)	Method	V_s [a] (cm/s)	ρ_d [b] (Mg/m^3)	n[c]	n_e[d]
Sand 1	5.1	2.83	1.5	LMR[f]	5.97×10^{-4}	1.43	0.45	0.45
				CB[g]	6.87×10^{-4}	1.49	0.43	0.43
Sand 2	7.0	0.15	2.6	CB	1.89×10^{-3}	1.49	0.40	0.40
Sand 4	10.5	0.29	0.5	CB	1.89×10^{-3}	1.49	0.40	0.40
Sand 10	4.7	0.14	2.5	CB	4.85×10^{-4}	1.32	0.49	0.49
				CB	7.44×10^{-4}	1.31	0.51	0.51
Sand 12	4.7	11.26	2.4	CB	6.94×10^{-4}	1.41	0.48	0.48
				CB	8.71×10^{-4}	1.39	0.49	0.49
Iron	N.A.[e]	100	N.A.	CB	6.74×10^{-4}	2.12	0.72	0.45
				LMR	1.10×10^{-3}	1.94	0.75	0.47
				CB	1.99×10^{-3}	2.09	0.73	0.46
Torpedo Sand	N.A.	N.A.	0.4	LMR	6.95×10^{-4}	1.56	0.41	0.41
				LMR	9.33×10^{-4}	1.48	0.44	0.44
				CB	1.71×10^{-3}	1.47	0.44	0.44

[a] Seepage velocity, [b] Dry density, [c] Total porosity, [d] Effective porosity, [e] N.A. = Not applicable. [f] LMR = Mass leaching ratio approach, [g] Concentration-basis approach.

Effluent from the foundry sands and two reference materials (i.e., Peerless iron and torpedo sand) was analyzed for Cr, Fe, and Pb. Fe and Pb were selected because concentrations of Fe and Pb obtained from the water leaching tests exceeded Category 1 standards for many of the foundry sands. Cr typically did not exceed the Category 1 standards in the water leach tests, but relatively large amounts of hexavalent Cr (although not exceeding the Category 1 standard) were found in the total elemental analyses of the foundry sands. Therefore, Cr was also measured to confirm that Cr is inactive in more realistic environments (i.e., a flow-through condition). Typical elution curves for Cr, Fe, and Pb obtained from the foundry sands and Torpedo sand are shown in Figs. 8.1 and 8.2.

Two analyses were conducted using the effluent data to determine the metal leaching characteristics. One analysis was performed based on instantaneous concentrations of metals in the effluent (Fig. 8.1). The other employed the cumulative mass leaching ratio (LMR) method (Fig. 8.2). Both analysis methods are explained in Sec. 3.7.2. The concentration-basis method was used for tests that were initially conducted. The LMR method was used for subsequent tests to alleviate uncertainty regarding the initial concentration used in the concentration-basis method.

For the instantaneous concentration approach, the first effluent concentration (measured after approximately 1 pore volume has passed through

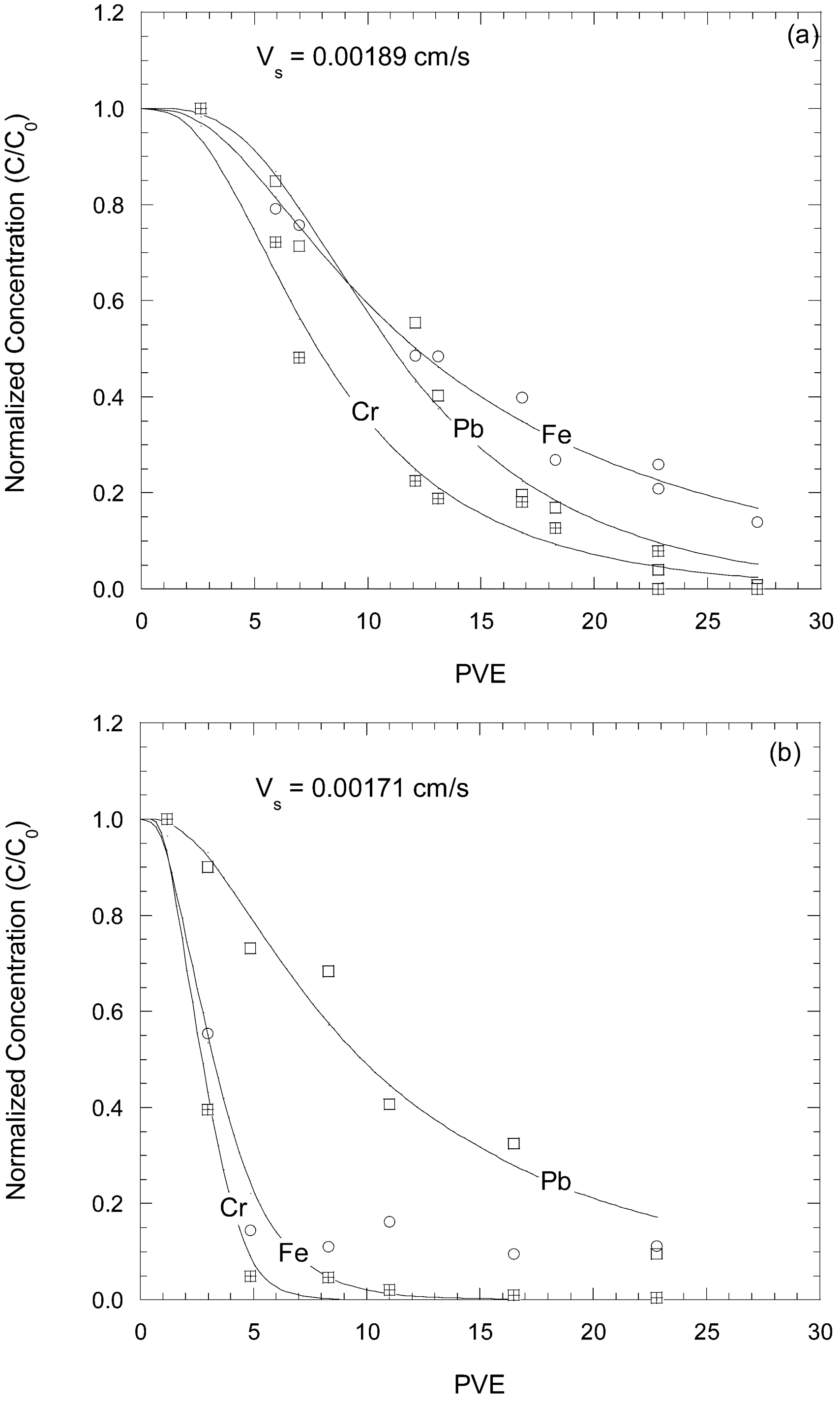

Fig. 8.1. Elution Curves for Cr, Fe, and Pb for (a) Sand 2 and (b) Torpedo Sand. Curves Corresponds to Eq. 3.27 Fit Using Instantaneous Concentrations.

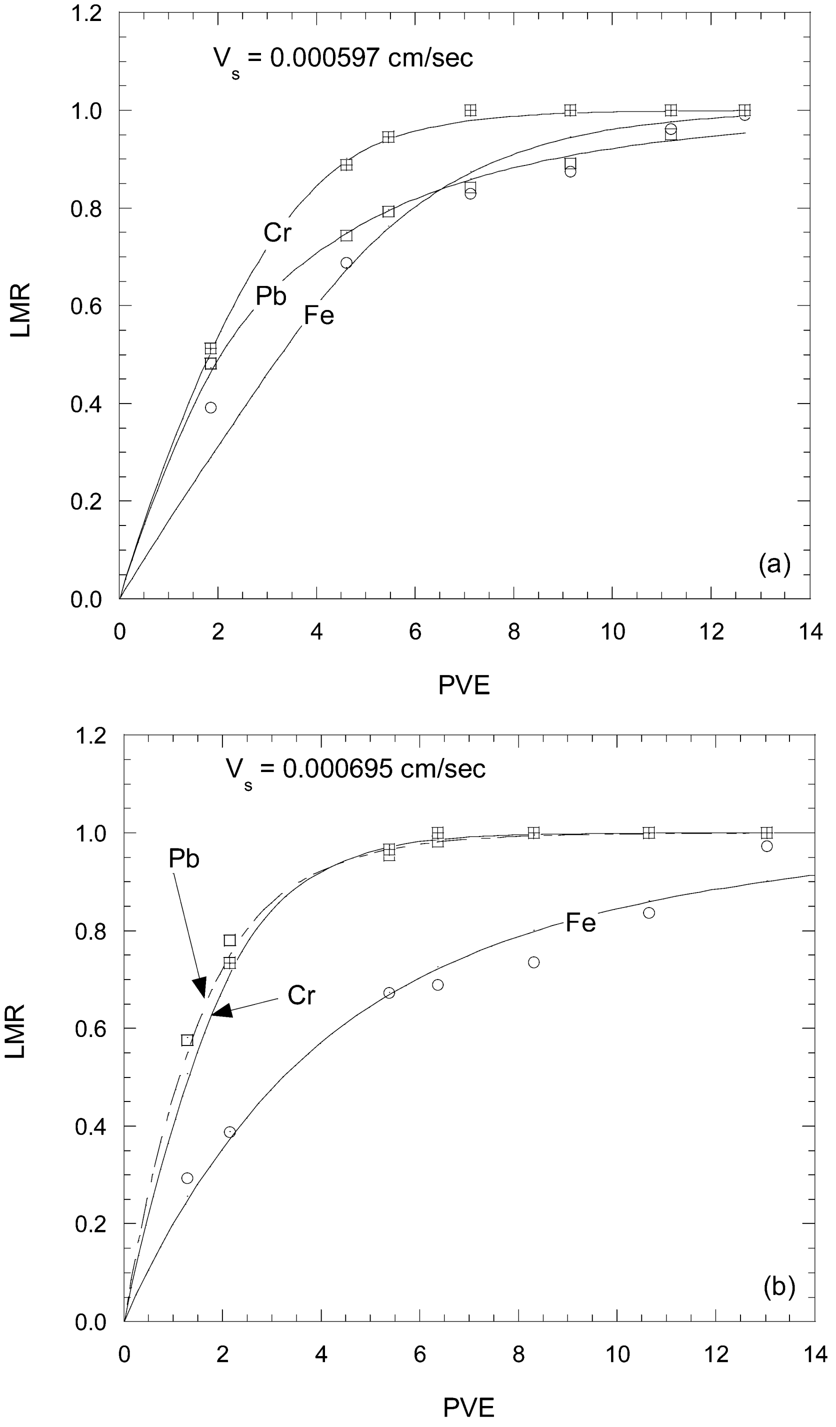

Fig. 8.2. Elution Curves for Cr, Fe, and Pb for (a) Sand 1 and (b) Torpedo Sand. Model Fit was Conducted Using Cumulative Mass Leaching Ratio.

the column) was assumed to be the initial concentration. All subsequent concentrations were normalized relative to the initial concentration. In contrast, for the LMR approach, the amount of mass leached at each step was normalized to the total leached mass, which was calculated by summing the amount of mass leached during the entire testing period. For example, the total leached mass of Cr (M_0 = 1.31 μg) for Sand 1 (Fig. 8.2) was obtained when M_0 became constant after 7 pore volumes. Thus, the leaching mass ratio (LMR_M) at 1.85 pore volumes was calculated by dividing the mass leached between 0 and 1.85 pore volumes (0.67 μg) by M_0, resulting in an LMR of 0.51 at 1.85 pore volumes.

The dispersion coefficients and retardation factors obtained from the analyses are summarized in Table 8.2. The minimum and maximum concentrations from the column tests for the concentration method are also shown in Table 8.2. For those materials tested using both the concentration-basis and LMR methods (Sand 1, Peerless iron, and Torpedo sand), similar partition coefficients and dispersion coefficients were obtained using both methods.

8.1. PARTITION COEFFICIENT

For the foundry sands, the partition coefficients ranged from 1.0 L/kg (Sand 10) to 10 L/kg (Sand 12) for Fe, 0.8 L/kg (Sand 1) to 3.6 L/kg (Sand 4) for Cr, and 0.45 L/kg (Sand 1) to 3.2 L/kg (Sand 4) for Pb. In general, the partition coefficients for Cr and Pb were similar, and were slightly lower than those for Fe.

Table 8.2. Results of Column Leach Tests: Dispersion Coefficient, Partition Coefficient, Maximum and Minimum Concentrations for Fe, Cr, and Pb.

Medium	Method	V_S (cm/s)	Fe				Cr				Pb			
			D^a (cm^2/s)	$K_p{}^b$ (L/kg)	$C_{max}{}^c$ (μg/L)	$C_{min}{}^d$ (μg/L)	D (cm^2/s)	K_p (L/kg)	C_{max} (μg/L)	C_{min} (μg/L)	D (cm^2/s)	K_p (L/kg)	C_{max} (μg/L)	C_{min} (μg/L)
Sand 1	LMR[f]	5.97×10^{-4}	1.12×10^{-3}	1.7	-[e]	-	1.45×10^{-3}	0.8	-	-	8.11×10^{-3}	0.6	-	-
	CB[g]	6.87×10^{-4}	7.26×10^{-3}	1.1	720	48	-	-	-	-	3.73×10^{-4}	0.3	22	0
Sand 2	CB	1.89×10^{-3}	1.20×10^{-2}	4.3	2,309	321	6.75×10^{-3}	2.3	15.8	0	4.91×10^{-3}	3.2	35.8	0.29
Sand 4	CB	1.89×10^{-3}	2.34×10^{-3}	3.9	2,322	139	1.70×10^{-2}	3.6	28.6	1	6.00×10^{-3}	1.3	42.1	0
Sand 10	CB	4.85×10^{-4}	4.61×10^{-4}	0.7	823	11	-	-	-	-	4.45×10^{-4}	0.7	12.1	0.9
	CB	7.44×10^{-4}	3.17×10^{-3}	1.3	1,123	106	-	-	-	-	-	-	-	-
Sand 12	CB	6.94×10^{-4}	3.52×10^{-2}	10.7	415	123	-	-	-	-	3.76×10^{-4}	0.6	11.8	0.1
	CB	8.71×10^{-4}	4.19×10^{-2}	9.1	873	323	-	-	-	-	-	-	-	-
Peerless Iron	CB	6.74×10^{-4}	6.17×10^{-4}	0.5	1,200	56	-	-	-	-	-	-	-	-
	LMR	1.10×10^{-3}	7.76×10^{-4}	0.4	-	-	-	-	-	-	-	-	-	--
	CB	1.99×10^{-3}	1.93×10^{-2}	2.1	635	38	1.08×10^{-3}	0.5	38.9	0	7.88×10^{-3}	1.3	8.2	0.66
Torpedo Sand	LMR	6.95×10^{-4}	8.23×10^{-3}	1.0	-	-	2.31×10^{-3}	0.4	22.4	0	4.19×10^{-3}	0.2	6.2	1.4
	LMR	9.33×10^{-4}	4.78×10^{-3}	0.9	-	-	-	-	-	-	9.21×10^{-4}	0.3	7.7	0
	CB	1.71×10^{-3}	6.03×10^{-3}	1.8	278	27	2.19×10^{-3}	0.7	20.5	0	1.68×10^{-2}	1.1	11.0	1.1

[a] Dispersion coefficient, [b] Partition coefficient, [c] Maximum concentration (μg/L), [d] Minimum concentration (μg/L), [e] Hyphens indicate that measurements were not made, [f] Mass leaching ratio approach, [g] Concentration-basis approach.

Higher partition coefficients for Fe may have been obtained due to persistent Fe dissolution from the foundry sands. The analytical model being used does not include a component for dissolution, and thus dissolution of Fe is reflected as a higher retardation factor and larger partition coefficient.

The partition coefficients for Cr, Fe, and Pb for Peerless iron and torpedo sand are comparable to or lower than those for foundry sands. No significant difference exists between the partition coefficients for Cr, Fe, and Pb obtained for Peerless iron and those for torpedo sand.

A multivariate regression analysis was conducted on the data obtained from the column leaching tests using a significance level of 0.05. The objective was to determine how properties of the sand (i.e., clay content, iron content, and TOC) affect sorption and to develop equations that can be used to predict the partition coefficients for Fe, Cr, and Pb. The equation for Fe is ($R^2 = 0.97$)

$$K_{p,\,Fe} = -\,11.5 + 1.32\ C + 0.87\ I + 0.05\ TOC \tag{8.1}$$

where $K_{p,Fe}$ is the partition coefficient (L/kg) for Fe, C is clay content (%), I is total iron content (%), and TOC is a total organic carbon content (%).

Eq. 8.1 indicates that the partition coefficient increases as the clay content, total iron content, and TOC increase. The partition coefficient should increase with clay content and TOC because more sorption sites are available when either of these variables is larger. The positive dependency on total iron content may reflect how dissolution influences the retardation factor and partition coefficient, as described in Section 8.2.

A statistically significant regression could not be obtained for Pb. For Cr, only a univariate analysis could be conducted due to lack of data. The equation for Cr is:

$$K_{p,\,Cr} = -1.5 + 0.5\ C \tag{8.2}$$

where $K_{p,Cr}$ is the partition coefficient for Cr and C is clay content (%). As with Fe, $K_{p,Cr}$ increases with clay content because of the greater availability of sorption sites.

8.2 DISPERSION COEFFICIENT

Dispersion coefficients from the column leaching tests are summarized in Table 8.2. Dispersivities were calculated from the dispersion coefficients using Eq. 3.24. A comparison was then made between the measured dispersivities and dispersivities estimated as 10% of the column length (e.g., $\alpha_L = 0.1$ L). The comparison is shown in Table 8.3.

The measured dispersivities for Fe are comparable to the estimated dispersivities, except for Sand 12. Higher dispersivities were obtained for Sand 12 because the analytical model (Eqs. 3.26 and 3.27) only considers desorption, whereas leaching from Sand 12 was probably due to desorption and dissolution. The slow dissolution process results in tailing of the Fe concentrations, which can only be simulated with Eq. 3.27 by using high values for the dispersion coefficient and the partition coefficient. This effect is illustrated in Fig. 8.3.

Table 8.3. Comparisons of Longitudinal Dispersivity Obtained from Estimation and Model Fit.

Medium	V_s (cm/sec)	α_L[a] (Estimated) (cm)	Method	α_L (Eqs. 3.26 – 3.27) (cm)		
				Fe	Cr	Pb
Sand 1	5.97×10^{-4}	1.9	LMR[c]	1.9	2.4	13.6
Sand 1	6.87×10^{-4}	1.9	CB[d]	10.5	N.A.[b]	0.6
Sand 2	1.89×10^{-3}	1.5	CB	6.3	3.6	2.6
Sand 4	1.89×10^{-3}	1.5	CB	1.2	9.0	3.2
Sand 10	4.85×10^{-4}	2.9	CB	1.0	N.A.	0.9
Sand 10	7.44×10^{-4}	2.9	CB	4.3	N.A.	N.A.
Sand 12	6.94×10^{-4}	2.0	CB	50.7	N.A.	N.A.
Sand 12	7.26×10^{-4}	1.9	CB	20.9	N.A.	0.5
Sand 12	8.71×10^{-4}	1.9	CB	48.1	N.A.	0.5
Iron	4.19×10^{-4}	1.8	LMR	0.9	N.A.	N.A.
Iron	6.90×10^{-4}	2.0	CB	0.7	N.A.	N.A.
Iron	1.26×10^{-3}	1.9	LMR	9.8	0.5	4.0
Torpedo Sand	6.95×10^{-4}	1.9	LMR	11.8	3.3	6.0
Torpedo Sand	9.33×10^{-4}	2.0	CB	5.1	N.A.	1.0
Torpedo Sand	1.71×10^{-3}	2.0	LMR[f]	3.5	1.3	9.8

[a] Longitudinal dispersivity, [b] N.A. = Not applicable, [c] Mass leaching ratio approach, [d] Concentration-basis approach.

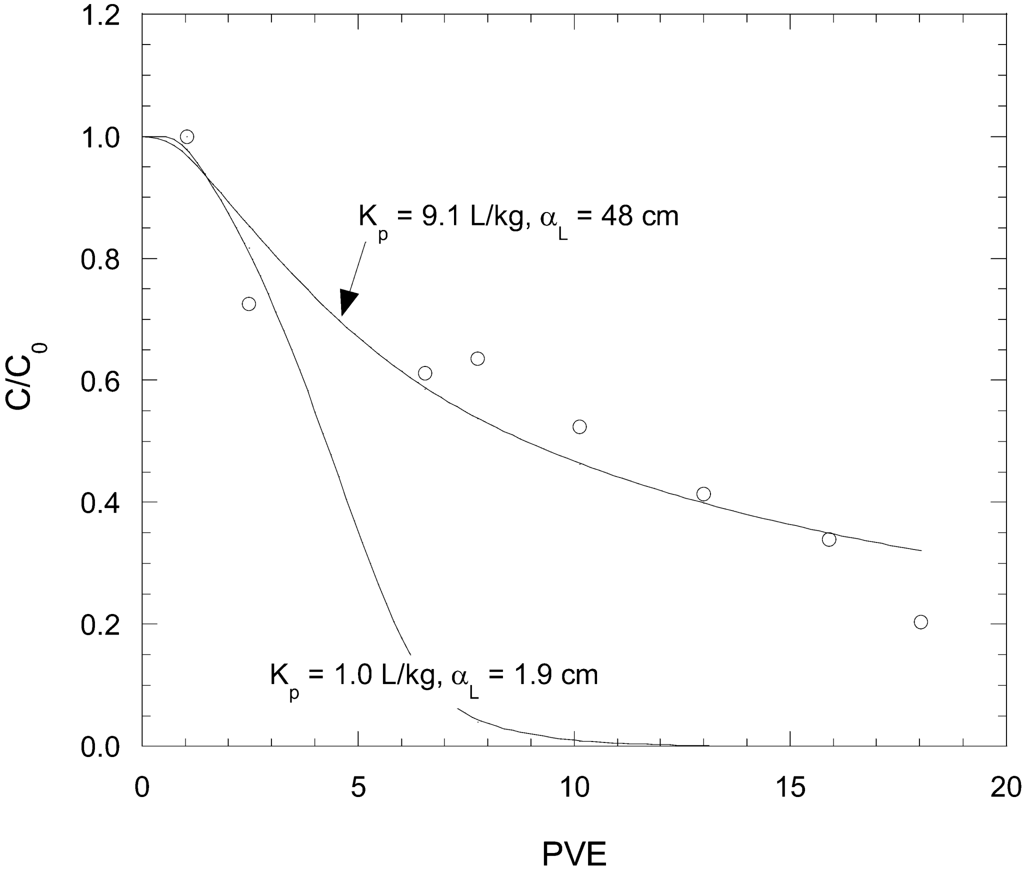

Fig. 8.3. Elution Data for Fe for Sand 12 and Curves for Eq. 3.27 Using Fitted K_p and α_L (9.1 L/kg, α_L = 48 cm) and Typical K_p and α_L (1.0 L/kg, α_L = 1.9 cm)

When a typical dispersivity and partition coefficient are used (K_p = 1.0 L/kg and α_L = 1.9 cm). Eq. 3.27 captures the leaching behavior at the beginning of the test, but does not capture the tailing at the end of the test (Fig. 8.3).

8.3 REQUIRED PORE VOLUMES TO MEET MCLS

The effluent data were compared to MCLs for Cr, Fe, and Pb to determine how many pore volumes of flow would be required before effluent from a PRB would meet groundwater quality standards. A summary of the pore volumes of flow required (PVER) to meet MCLs is in Table 8.4.

For Cr and Pb, effluent concentrations were always below MCLs for the foundry sands, Peerless iron, and torpedo sand (Table 8.4) and thus PVER is zero. In contrast, Fe concentrations were higher than the MCL (300 μg/L) at the onset of the column leaching tests. The exception was for torpedo sand, which had an initial Fe effluent concentration (C_{max}) of 278 μg/L.

PVER for Fe varies between 2.5 and 28, and depends on the initial Fe concentration and partition coefficient, as shown in Fig. 8.4. A regression equation was developed using a significance level of 0.05 to predict PVER as a function of the partition coefficient and initial Fe concentration. This equation is:

$$\mathrm{PVER} = -6.53 + 3.81\, K_p + 0.00711\, C_{IN} \qquad (8.3)$$

where K_p is the partition coefficient for Fe (L/kg) and C_{IN} is the initial effluent concentration of Fe (μg/L).

Table 8.4. Partition Coefficients, Maximum Concentrations, and Required Pore Volumes of Effluent Required (PVER) to Meet MCLs for Fe, Cr, and Pb for Foundry Sands, Peerless Iron, and Torpedo Sand.

Medium	V_S (cm/sec)	Fe (300 μg/L)[a]			Cr (100 μg/L)			Pb (50 μg/L)		
		K_P[b]	C_{max}[c]	PVER[d]	K_P	C_{max}	PVER	K_P	C_{max}	PVER
Sand 1	6.87×10^{-4}	1.1	720	4	0.8	N.A.[e]	0	0.3	22	0
Sand 2	1.89×10^{-3}	4.3	2,309	28	2.3	15.8	0	3.2	35.8	0
Sand 4	1.89×10^{-3}	3.9	2,322	23	3.6	28.6	0	1.3	24.7	0
Sand 10	4.85×10^{-4}	0.7	823	3.3	N.A.	N.A.	N.A.	0.7	12.1	0
	7.44×10^{-4}	1.3	1,123	4.9	N.A.	N.A.	N.A.	N.A.	N.A.	N.A.
Sand 12	7.26×10^{-4}	10.7	415	2.6	N.A.	N.A.	N.A.	0.6	11.8	0
	8.71×10^{-4}	9.1	324	2.5	N.A.	N.A.	N.A.	N.A.	0.93	0
Peerless Iron	4.19×10^{-4}	0.5	1,200	3.5	0.5	N.A.	N.A.	N.A.	N.A.	N.A.
	1.26×10^{-3}	2.1	635	7.8	0.4	38.9	0	1.3	8.2	0
Torpedo Sand	1.71×10^{-3}	1.8	278	0	0.7	20.5	0	1.1	11.0	0

[a] MCL, [b] Partition coefficient, [c] Maximum effluent concentration (μg/L), [d] Required pore volume of effluent to meet MCL, [e] N.A. = Not applicable.

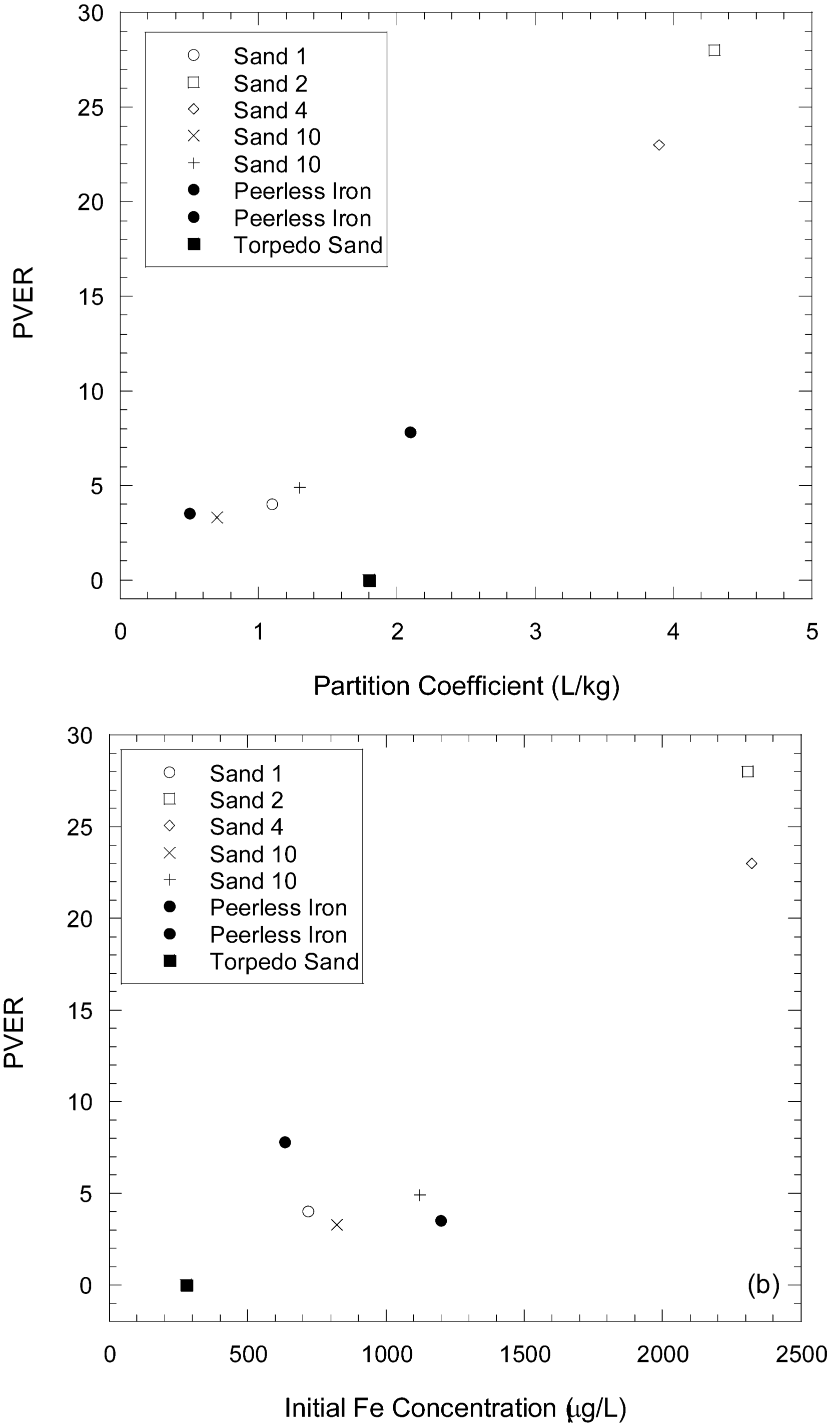

Fig. 8.4. Relationship Between PVER and (a) Partition Coefficient and (b) Initial Fe Concentration.

8.4 COMPARISON: WATER LEACH TESTS AND COLUMN LEACH TESTS

Initial effluent concentrations obtained from the column leach tests are compared with those from the water leach tests (described in Sec. 4) in Table 8.5. The initial concentrations from the column leach tests are appreciably higher than those from the water leach tests. The initial Fe concentrations from the column leach tests using foundry sands are 3.7 times higher, on average, than the concentrations from the water leach tests. For Cr, the initial concentrations are 11 times higher than those from the water leach tests, on average, and for Pb, the initial concentrations are 37 times higher than those from the water leach tests.

The elevated initial concentrations from the column leach tests cannot be attributed solely to dilution in the water leach tests. Adjustments to concentrations from the water leach tests to reflect the solid-solution ratio in the column tests resulted in initial concentrations for the column tests that were much higher than the measured initial concentrations. For example, adjusting the concentration from the water leach tests using Sand 1 to reflect the solid-solution ratio in the column test yielded an initial concentration of 6202 μg/L, whereas the measured initial concentration in the column test was 720 μg/L.

The concentration from the water leach tests can be empirically related to the initial concentration from the column tests as shown in Fig. 8.5. Regression on the data in Fig. 8.5 yielded the following equations:

Table 8.5. Concentrations of Fe, Cr, and Pb from Column Tests and Water Leach Tests. Concentrations from Column Tests are the Maximum Concentration at the Onset of the Test.

Medium	Fe (μg/L)		Cr (μg/L)		Pb (μg/L)	
	Column Test	Batch Test	Column Test	Batch Test	Column Test	Batch Test
Sand 1	720	96	N.A.[a]	1.1	22	0.4
Sand 2	2,309	659	15.8	1.6	36	0.9
Sand 4	2,322	1,483	28.6	2.5	42	1.7
Sand 10	823	256	N.A.	1.9	12	0.3
	1,123	256	N.A.	1.9	N.A.	0.3
Sand 12	415	128	N.A.	0.8	12	0.2
	324	128	N.A.	0.8	0.9	0.2
Peerless Iron	1,200	231	N.A.	13.1	N.A.	15
	635	231	38.9	13.1	8	15
Torpedo Sand	278	8	20.5	1.4	11	0.08

[a] Not applicable.

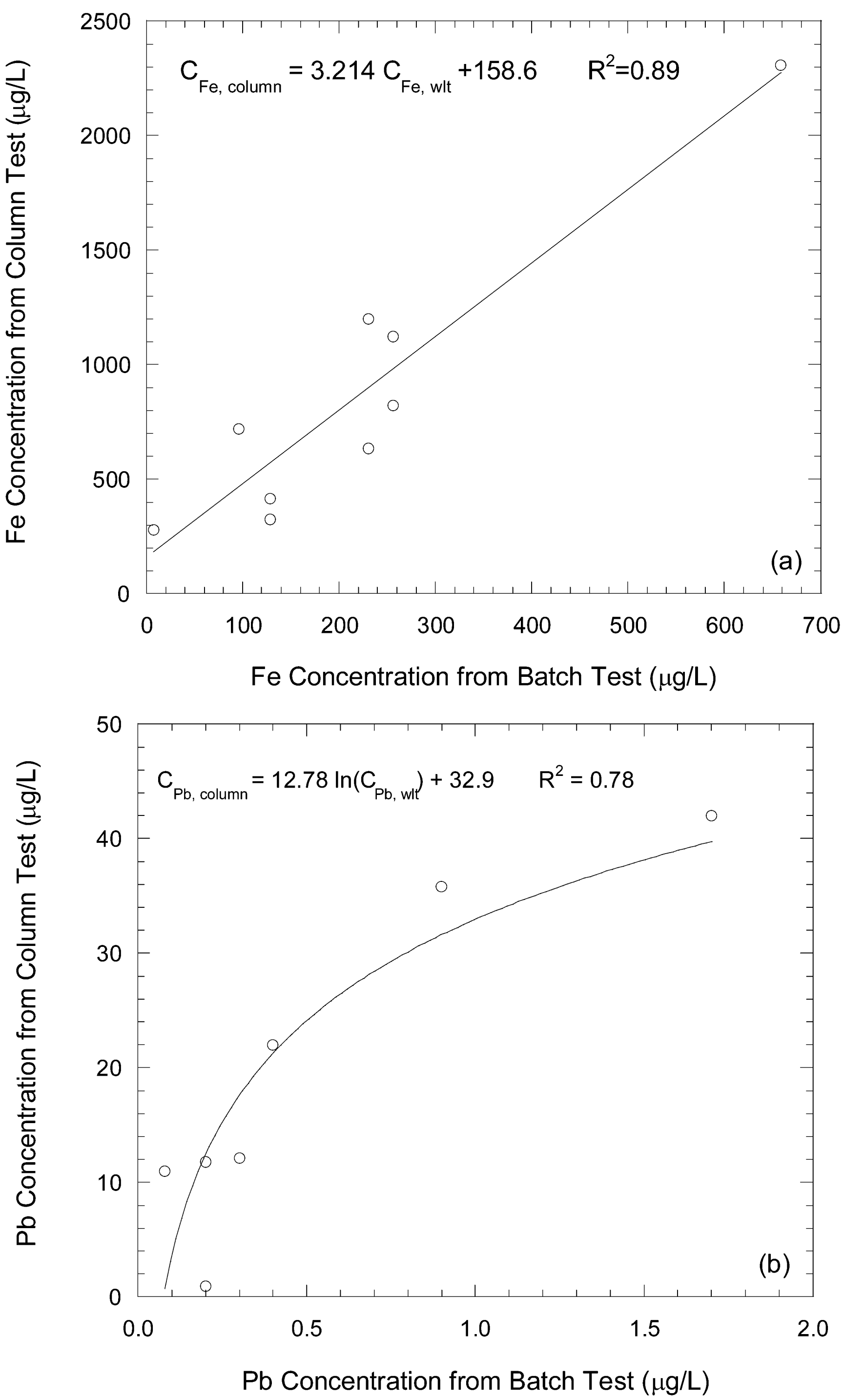

Fig. 8.5. Relationship Between Column Test and Batch Test: (a) Concentration of Fe, (b) Concentration of Pb, and (c) Concentration of Cr.

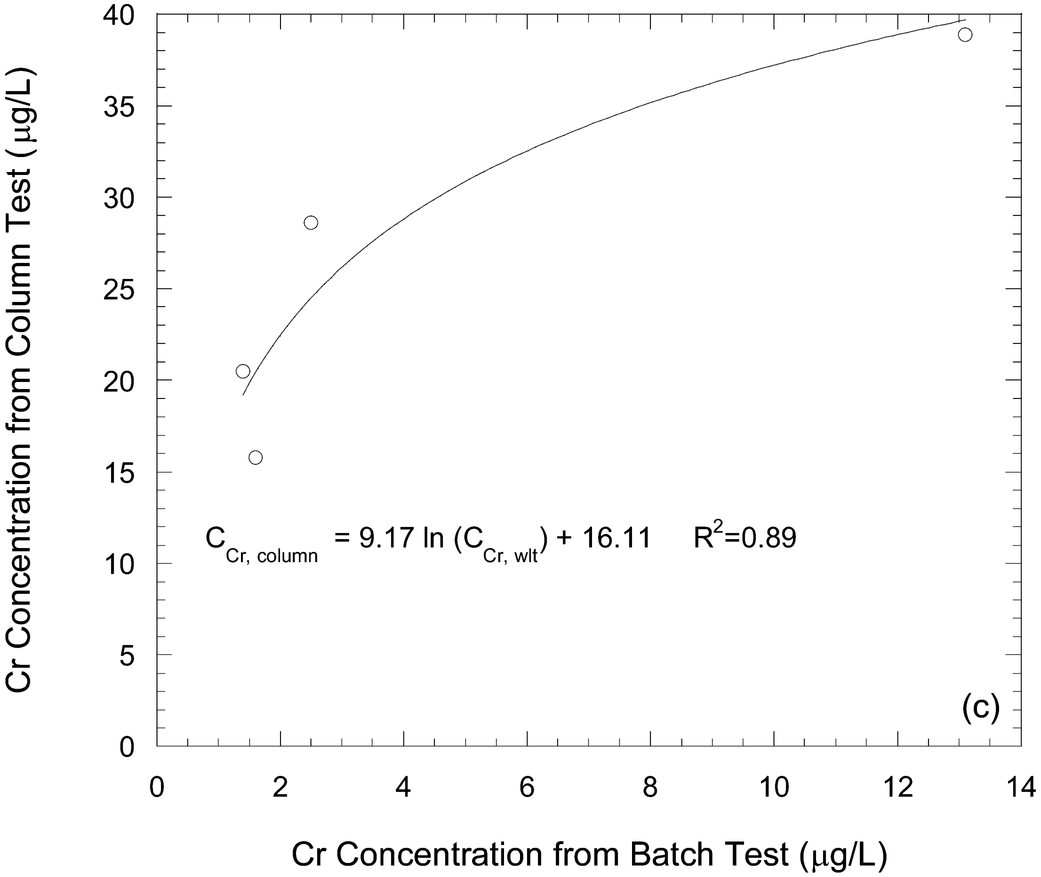

Fig. 8.5. Relationship Between Column Test and Batch Test: (a) Concentration of Fe and (b) Concentration of Pb, and (c) Concentration of Cr (Continued).

$$C_{Fe,\ column} = 3.214\ C_{Fe,\ wlt} + 158.6 \quad (8.4)$$

$$C_{Pb,\ column} = 12.78\ \ln(C_{Pb,\ wlt}) + 32.9 \quad (8.5)$$

$$C_{Cr,\ column} = 9.17\ \ln(C_{Cr,\ wlt}) + 16.11 \quad (8.6)$$

where $C_{Fe,\ column}$ is the initial Fe concentration from the column test and $C_{Fe,\ wlt}$ is the Fe concentration from the water leach test. Similar definitions apply to $C_{Pb,\ column}$, $C_{Pb,\ wlt}$, $C_{Cr,\ column}$, $C_{cr,\ wlt}$. The Fe concentration for Sand 4 was not used in the regression analysis because the data for Sand 4 were inconsistent with the other data. Eqs. 8.4 – 8.6 have $R^2 = 0.89$, 0.78, and 0.89, respectively.

A multivariate regression analysis was also conducted on the data obtained from the water leach tests to determine if concentrations from the water leach tests could be predicted using basic properties of the foundry sands (i.e., clay, total iron, and TOC). The significance level was 0.05. As for the partition coefficient from the column tests, a statistically significant regression could not be obtained for Cr. The equation for Fe is ($R^2 = 0.63$):

$$C_{Fe,\ wlt} = -1115 + 120\ C + 316\ TOC \quad (8.7)$$

where $C_{Fe,\ wlt}$ is the concentration of Fe from the water leach test (μg/L), C is clay content (%), and TOC is total organic carbon content (%). For Pb, the equation is ($R^2 = 0.84$):

$$C_{Pb,\ wlt} = -0.85 + 0.24\ C - 0.01\ I \quad (8.8)$$

where $C_{Pb,\ wlt}$ is the concentration of Pb from the water leach test (μg/L), I is total iron content (%). Eqs. 8.7 and 8.8 indicate that the concentrations of Fe and Pb increase with clay content, which reflects the tendency of sands with higher clay content to sorb more metals. Thus, more metals are available for release during the water leach test. TOC only appears to affect concentrations of Cr and Fe. The concentration of Pb tends to decreases with total iron constant, possibly due to precipitation promoted by iron corrosion.

8.5 PREDICTION OF PVER

A procedure for predicting PVER is shown in Fig. 8.6. Clay content (%), total iron content (%), and TOC of the candidate material are determined, and then the partition coefficients for Fe and Cr are estimated using Eqs. 8.1 and 8.2. Concentrations for Fe and Pb for the water leach test are estimated using Eqs. 8.7 – 8.8. Then the initial concentrations (i.e., C_0 in Eq. 3.27) for field conditions are estimated using Eqs. 8.4 – 8.6. Eq. 3.27 is then used to predict the effluent concentration as a function of pore volumes of effluent. The PVER is obtained when the effluent concentration predicted with Eq. 3.27 is less than the MCL.

PVERs computed using this procedure are compared to the measured PVERs for Fe in Fig. 8.7. The actual PVERs are from the column leach tests, and are summarized in Table 8.5. The predicted and actual PVER are comparable.

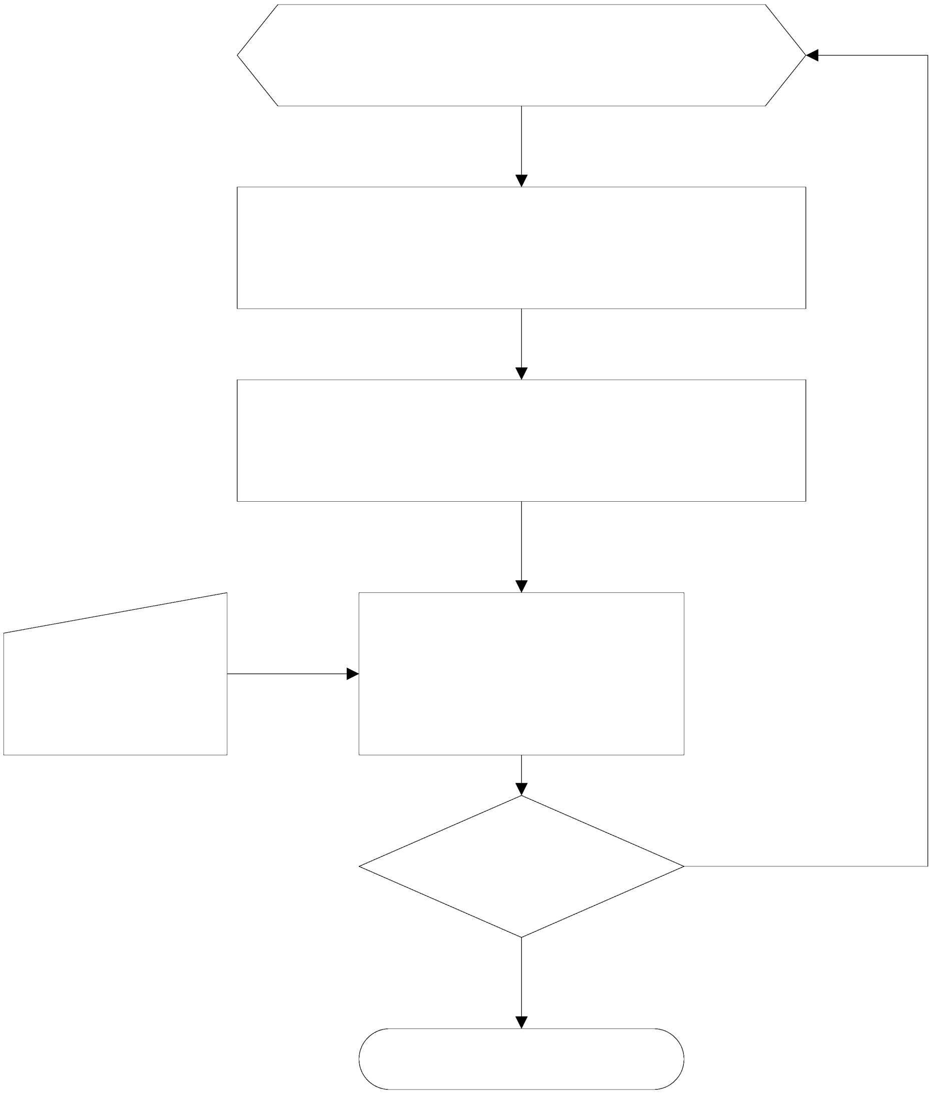

Fig. 8.6. Flow Chart to Estimate PVER Using Data from Water Leach Test.

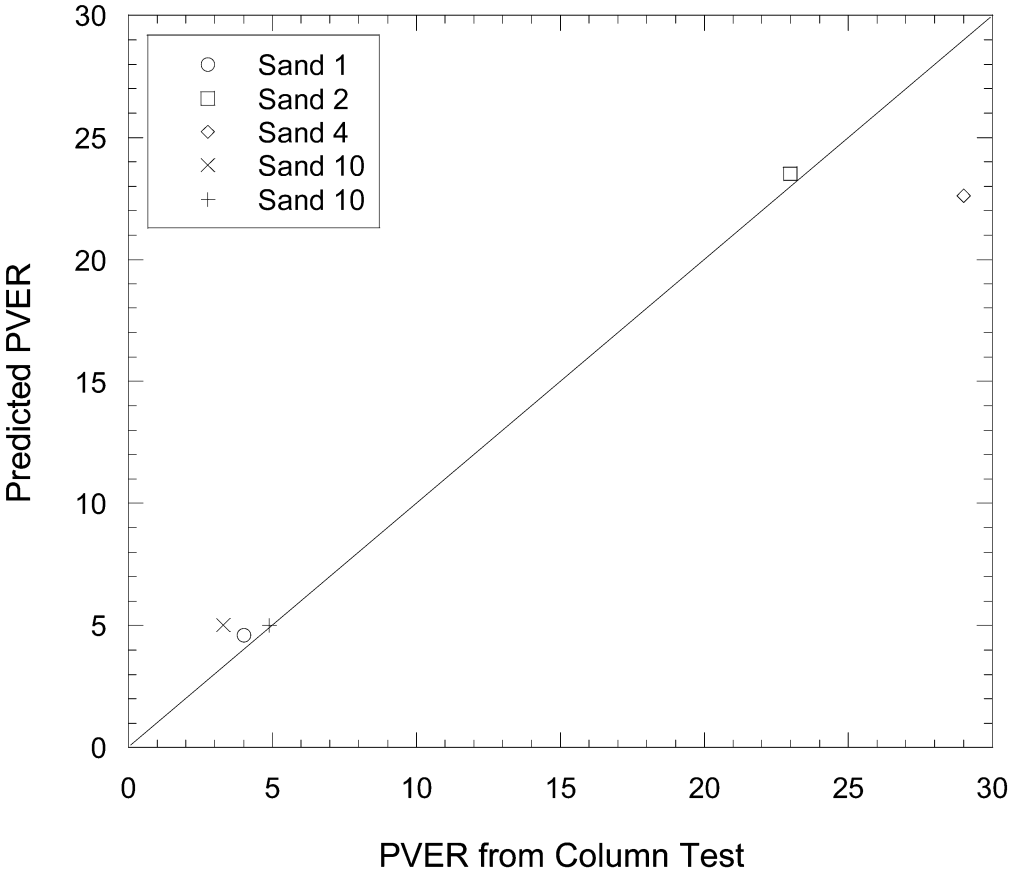

Fig. 8.7. Comparison of PVER for Fe Predicted Using Method in Sec. 8.5 and PVER from Column Tests (Table 8.5).

SECTION NINE

SUMMARY AND CONCLUSIONS

The objective of this study was to evaluate the potential use of waste foundry sand as an inexpensive medium for permeable reactive barriers (PRBs). Batch and column tests were conducted to evaluate the reactivity and sorptive capacity of twelve foundry sands for common groundwater contaminants. The batch tests are conventional expedient tests conducted for design purposes. The column tests more accurately simulate field conditions. Contaminants used in the tests included TCE, the herbicides alachlor and metolachlor, and zinc. Parameters obtained from these tests were then used to size PRBs for typical field conditions.

Tests were also conducted to evaluate the leaching characteristics of foundry sands. Batch water leach tests, column leach tests, and total elemental analyses were conducted. The water leach tests and total elemental analyses were conducted to categorize the foundry sands in accordance with Section NR 538 of the Wisconsin Administration Code. The column leach tests were conducted to evaluate leaching that might occur under field conditions where foundry sands are used as a PRB medium.

The following sections summarize the findings of the tests conducted for each contaminant that was considered, and the results of the leaching tests.

9.1 CHLORINATED SOLVENTS (TCE)

Foundry sands have a high sorption capacity for TCE, with partition coefficients ranging from 4.0 L/kg to 41.6 L/kg. A linear sorption model can be used to describe the sorption isotherms when the TCE concentrations are modest (i.e., 1 mg/L or higher). When the concentration is lower than 1 mg/L, the partition coefficient is likely to be larger than that indicated by the linear model. Partition coefficients obtained from column tests also tend to be higher than those obtained from batch tests. Therefore, using linear isotherms derived from batch tests should result in conservative designs.

Normalized rate constants for reduction of TCE obtained from the batch tests are similar for foundry sand iron and Peerless iron, which suggests that the iron in the foundry sands is comparable to Peerless iron. However, for the column tests, different rate constants were obtained for the foundry sands and Peerless iron. The rate constants obtained from the column tests were also different from those obtained from the batch tests. The rate constants for the foundry sands were slightly higher than those from the batch tests, whereas the rate constant for Peerless iron from the column tests were lower than those obtained from the batch tests. These findings indicate that rate constants for foundry sands obtained from the batch tests should conservative.

Calculations showed that the required PRB thickness depends on the source TCE concentration and the iron content in foundry sands. For source TCE concentrations less than 400 mg/L and seepage velocities less than 0.1 m/d, PRBs containing foundry sand will meet MCLs if they are 1 m thick and the iron content is higher than 3%. For the seepage velocities less than 0.01 m/d, the iron content only need to be 0.3% for a 1-m-thick PRB to meet the MCL for TCE.

9.2 CHLORINATED HERBICIDES ALACHLOR AND METOLACHLOR

Partition coefficients for alachlor and metolachlor obtained from the batch sorption tests were found to be similar even though K_{OW} for alachlor is lower than that for metolachlor. Because the solubilities of these compounds are proportional to K_{OW}, which is not usual, solubility and K_{OW} compensate, resulting in similar partition coefficients.

Partition coefficients obtained from column tests were lower than those obtained from the batch tests. Reduction of alachlor and metolachlor by residual iron during the batch tests as well as differences in the soil-solution ratios may be responsible for the higher partition coefficients obtained from the batch tests. Partition coefficients from column tests with alachlor were 0.58 to 0.80 times those from the batch tests. For metolachlor, the ratios were 0.57 through 0.81. For conservative design, partition coefficients for herbicides obtained from batch tests can be reduced by a factor of two to represent conditions that are likely to occur under more realistic conditions.

Normalized rate constants (K_{SA}) for alachlor and metolachlor obtained from the column tests were 1.5 and 1.6 times lower, on average, than those from batch tests. The average K_{SA} obtained from the column tests were 5.08×10^{-4}

L/m^2-hr (alachlor) and 3.44×10^{-4} L/m^2-hr (metolachlor), whereas the K_{SA} from the batch tests were 7.7×10^{-4} L/m^2-hr (alachlor) and 5.5×10^{-4} L/m^2-hr (metolachlor). Thus, rate constants obtained from batch tests using foundry iron and herbicides should be reduced by a factor of 1.6 for design.

Designing PRBs containing foundry sands to remediate alachlor and metolachlor in groundwater using a 10-fold reduction in concentration is usually conservative. In this case, a 1 m thick barrier can be constructed for seepage velocities less than 0.1 m/d provided the foundry sand contains at least 1% iron.

9.3 METALS (ZINC)

The partition coefficients for zinc vary on a broad range depending on properties of the foundry sands (TOC, clay content, total iron content) and solution pH. Among these properties, solution pH was found to be the most important factor. Empirical equations were developed from the batch tests to predict partition coefficients as a function of foundry sand properties and solution pH.

Rate constants obtained from the batch kinetic tests and the column tests were found to be comparable when the solution pHs were comparable. An empirical equation was developed from the column test data to predict the rate constant as a function of clay content of the foundry sand.

Calculations made with this equation and an analytical solution of the ADRE showed that the required PRB thickness depends on the source zinc concentration and clay content in foundry sands. For source zinc concentrations less than 400 mg/L and seepage velocities less than 0.1 m/d, PRBs with less than 1 m thickness can be constructed with foundry sands provided the clay content is higher than 5%.

9.4 LEACHING

Results of the water leach tests and the total elemental analyses showed that all of the foundry sands are Category 2 materials per Section NR 538 of the Wisconsin Administrator Code. However, tests on Peerless iron, torpedo sand, and a typical fill material indicate that these materials, which are commonly placed below the groundwater table, also are Category 2 materials. Thus, using foundry sand as a PRB medium should pose no greater risk than that imposed using conventional construction materials.

Additional column leaching tests were conducted to determine characteristics of the leachate under flow conditions more representative of the field. Effluent from these tests was analyzed for three metals (Fe, Cr, and Pb). Cr and Pb in the effluent were always below MCLs. For Fe, however, several pore volumes of flow were often required to meet the MCL.

The number of pore volumes required to meet the MCL (PVER) was found to depend on the initial concentration of Fe in the effluent and the partition coefficient. A method was developed to predict the PVER using properties of the foundry sands and the results of water leach tests and column leach tests.

Predictions of PVER made with this method were found to be comparable to PVER determined from the column tests.

9.5 SUGGESTIONS FOR PARAMETERIZATION

Proper determination of the transport parameters (partition coefficient, rate constant, and dispersion coefficient) is the first step in design of PRBs. These parameters can be estimated using the equations presented in this study using basic properties of foundry sands (i.e., TOC, clay content, total or zero-valent iron content). These estimated parameters can be used for feasibility analysis and preliminary design. Relatively simple batch tests can then be used to confirm the partition coefficient and rate constant, and to refine the design. If parameters from the batch tests are significantly different from the estimates, then column tests should be conducted to obtain parameters for conditions that better simulate the field.

SECTION TEN

REFERENCES

Abichou, T., Benson, C., and Edil, T. (2000), “Foundry Green Sands as Hydraulic Barriers: Laboratory Study,” *Journal of Geotechnical and Geoenvironmental Engineering,* 126(12), 1174-1183.

Arnold, W. and Roberts, A. (1998), “Pathways of Chlorinated Ethene and Chlorinated Acetylene Reaction with Zn(0),” *Environmental Science and Technology*, 32(19), 3017-3025.

Bailey, S., Olin, T., Bricka, M., and Adrian, D. (1999), “A Review of Potentially Low-Cost Sorbents for Heavy Metals,” *Water Research*, 33(11), 2469-2479.

Bear, J. (1972), *Dynamics of Fluids in Porous Media*, American Elsevier Publishing Co., New York, N.Y.

Benner, S., Blowes, D., and Ptacek, C. (1997), “A Full-Scale Porous Reactive Wall for Prevention of Acid Mine Drainage,” *Ground Water Monitoring and Remediation*, 17(3), 99-107.

Blowes, D., Ptacek, C., Cherry, J., Gillham, R., and Robertson, W. (1995), “Passive Remediation of Groundwater Using In Situ Treatment Curtains,’ *Geoenvironment 2000: Characterization, Containment, Remediation, and Performance in Environmental Geotechnics (2)*, Daniel, D. and Acar, Y. (Eds.), ASCE, GSP 46, 1588-1607.

Blowes, D., Ptacek, C., and Jambor, J. (1997), “In-Situ Remediation of Cr(VI)-Contaminated Groundwater Using Permeable Reactive Walls: Laboratory Studies,” *Environmental Science and Technology*, 31(12), 3348-3357.

Burkhard, L. (2000), “Estimating Dissolved Organic Carbon Partition Coefficients for Nonionic Organic Chemicals,” *Environmental Science and Technology*, 34(22), 4663-4668.

Carmo, A., Hundal, L., and Thomson, M. (2000), “Sorption of Hydrophobic Organic Compounds by Soil Materials: Application of Unit Equivalent Freundlich Coefficients,” *Environmental Science and Technology*, 34(20), 4363-4369.

Chesters, G., Sisiman, G., Levy, B., Alhajjar, B, Fathulla, R., Harkin, J. (1989), "Environmental Fate of Alachlor and Metolachlor", *Reviews of Environmental Contamination and Toxicology,* 110:1-74.

Chiou, C., McGroddy, S., and Kile, D. (1998), "Partition Characteristics of Polycyclic Aromatic Hydrocarbons on Soils and Sediments," *Environmental Science and Technology*, 32(2), 264-269.

Chiou, C., Kile, D., and Rutherford, D. (2000), "Sorption of Selected Organic Compounds from Water to a Peat Soil and Its Humic Acid and Humic Fractions: Potential Sources of the Sorption Nonlinearity," *Environmental Science and Technology*, 34(7), 1254-1258.

Doust, H., and Huang, J. (1992), "The Fate and Transport of Hazardous Chemicals in the Subsurface Environment," *Water Science and Technology*, 25(1), 169-176.

Elder, C. (2000), "Evaluation and Design of Permeable Reactive Barriers Amidst Heterogeneity," PhD Dissertation, Department of Civil and Environmental Engineering, University of Wisconsin-Madison.

Estes, T., Shah, R., and Vilker, V. (1988), "Adsorption of Low Molecular Weight Halocarbons by Montmorillonite," *Environmental Science and Technology*, 22(4), 377-381.

Eykholt, G. and Sivavec, T. (1995), "Contaminant Transport Issues for Reactive-Permeable Barriers," *Geoenvironment 2000: Characterization, Containment, Remediation, and Performance in Environmental Geotechnics* (2), Daniel, D. and Acar, Y. (Eds.), ASCE, GSP 46, 1608-1621.

Eykholt, G. and Davenport, D. (1998), "Dechlorination of the Chloroacetanilide Herbicides Alachlor and Metolachlor by Iron Metal," *Environmental Science and Technology*, 32(10), 1482-1487.

Eykholt, G. (1999), "Analytical Solution for Networks of Irreversible First-Order Reactions," *Water Research*, 33(3), 814-826.

Fort, J. (2000), "Physical Performance of Granular Iron Reactive Barriers Under Aerobic and Anoxic Conditions, MS Thesis, Dept. of Civil and Environmental Engineering, University of Wisconsin-Madison.

Francis, A. and Dodge, C. (1998), "Remediation of Soils and Wastes Contaminated with Uranium and Toxic Metals," *Environmental Science and Technology*, 32(24), 3923-3998.

Gibbons, R., Dolan, D., Keough, H., O'Leary, K., and O'Hara, R. (1992), "A Comparison of Chemical Constituents in Leachate from Industrial Hazardous Waste & Municipal Solid Waste Landfills," *Proc. 15th Annual Madison Waste Conf.*, Madison, WI, 251-276.

Gillham, R. and O'Hannesin, S. (1994), "Enhanced Degradation of Halogenated Aliphatics by Zero-Valent Iron," *Ground Water*, 32(6), 958-967.

Gu, B., Liang, L., Cameron, P., West, O., and Korte, N. (1997), "Degradation of Trichloroethylene (TCE) and Polychlorinated Biphenyl (PCB) by Fe and Fe-Pd Bimetals in the Presence of a Surfactant and a Cosolvent," *Proc., Intl. Containment Technol. Conf.*, U.S. DOE, U.S. EPA, and Dupont Co., 760-766.

Jarre, P. and Kociolek, P. (1999), "Examples of the Use of Reactive Treatment Barriers," *Proc. XVII Conference of Geotechnics of Torino, Nov. 23-25, 1999*, Italian Geotechnical Society, Torino, Italy, Vol. 17.07, 1-27.

Javed, S. and Lovell, C. (1994), "Use of Waste Foundry Sand in Highway Construction," Report JHRP/INDOT/FHWA-94/2J Final Report, Purdue School of Engineering.

Johnson, T., Scherer, M., and Tratnyek, P. (1996), "Kinetics of Halogenated Organic Compound Degradation by Iron Metal," *Environmental Science and Technology*, 30(8), 2634-2640.

Joshi, A. and Chaudhuri, M. (1996), "Removal of Arsenic from Ground Water by Iron Oxide-Coated Sand," *Journal of Environmental Engineering*, 122(8), 769-771.

Kalkhoff, S., Kolpin, D., Thurman, E., Ferrer, I., and Barcelo, D. (1998), "Degradation of Chloroacetanilide Herbicides: The Prevalence of Sulfonic and Oxanilic Acid Metabolites in Iowa Groundwaters and Surface Waters," *Environmental Science and Technology*, 32(11), 1738-1740.

Karanfil, T. (1999), "Role of Granular Activated Carbon Surface Chemistry on the Adsorption of Organic Compounds," *Environmental Science and Technology*, 33(18), 3217-3224.

Kershaw, D. and Pamucku, S. (1997), “Ground Rubber: Reactive Permeable Barrier Sorption Media,” *In Situ Remediation of the Geoenvironment*, Evans, J. (Ed.), ASCE, GSP 71, 26-40.

Kim, J. (1996), “Retardation of Volatile Organic Compound Movement in Landfills Using Scrap Tires,” PhD Dissertation, Department of Civil and Environment Engineering, University of Wisconsin-Madison.

Kim, J., Park, J., and Edil, T. (1997), “Sorption of Organic Compounds in the Aqueous Phase onto Tire Rubber,” *Journal of Environmental Engineering*, 123(9), 827-834.

Kolpin, D., Barbash, J., and Gilliom, R. (1998), “Occurrence of Pesticides in Shallow Groundwater of the United States: Initial Results from the National Water-Quality Assessment Program,” *Environmental Science and Technology,* 32(5), 558-566.

Koppensteiner, B. (1998), ”The Degradation of the Herbicides Alachlor and Metolachlor by Iron Metal in Water and Soil Systems,” *M.S. Thesis*, Dept. of Civil and Environmental Engineering, University of Wisconsin-Madison.

Knocke, W. and Hemphill, L. (1981), “Mercury(II) Sorption by Waste Rubber,” *Water Research*, 15(2), 275-282.

Kuan, W., Lo, S., Wang, M., and Lin, C. (1998), “Removal of Se(IV) and Se(VI) from Water by Aluminum-Oxide-Coated Sand,” *Water Research,* 32(3), 915-923.

Li, Y. and Gregory, S. (1974), “Diffusion of Ions in Sea Water and in Deep-Sea Sediments,” *Geochim. Cosmochim. Acta*., 38, 703-714.

Lien, H. and Zhang, W. (1999), “Transformation of Chlorinated Methanes by Nanoscale Iron Particles,” *Journal of Environmental Engineering*, 125(11), 1042-1047.

Lowry, G. (1995), “Kinetics of the Enhanced Dechlorination of Trichloroethylene Using Zero-Valent Iron,” M.S. Thesis, Department of Civil and Environmental Engineering, University of Wisconsin-Madison.

Mathews, A. and Zayas, I. (1989), “Particle Size and Shape Effects on Adsorption Rate Parameters,” *Journal of Environmental Engineering*, 115(1), 41-55.

McBride, M. (1994), *Environmental Chemistry of Soils*, Oxford University Press, New York, NY.

McMahon, P., Dennehy, K., and Sandstrom, M. (1999), "Hydraulic and Geochemical Performance of a Permeable Reactive Barrier Containing Zero-Valent Iron, Denver Federal Center," *Ground Water*, 37(3), 396-404.

Moo-Young, H. and Zimmie, T. (1996), "Geotechnical Properties of Paper Mill Sludges for Use in Landfill Covers," *Journal of Geotechnical and Geoenvironmental Engineering*, 122(9), 768-775.

Mueller, J., Borchert, S., Klingel, E, Smyth, D., Shikaze, S., Tischuk, M., and Brourman, M. (1997), "Integrated Funnel-and-Gate/GZB Product Recovery Technologies for In Situ Management of Creosote NAPL-Impacted Aquifers," *Proc., Intl. Containment Technol. Conf.*, U.S. DOE, U.S. EPA, and Dupont Co., 865-871.

Namasivayam, C. and Ranganathan, K. (1995), "Removal of Cd(II) from Wastewater by Adsorption on "Waste" Fe(III)/Cr(III) Hydroxide," *Water Research*, 29(7), 1737-1744.

Nelson, D. and Sommers, L. (1982), "Total Carbon, Organic Carbon, and Organic Matter," *Methods of Soil Analysis*, Part 2. Chemical and Microbiological Properties-Agronomy Monograph No. 9 (2nd Edition), Page, A., Miller, R., and Keeney, D. (Eds.), 539-579.

O'Connor, D. and Connolly, J. (1980), "The Effect of Concentration of Absorbing Solids on the Partition Coefficient," *Water Research*, 14, 1517.

Orth, W. and Gillham, R. (1996), "Dechlorination of Trichloroethene in Aqueous Solution using Fe^0," *Environmental Science and Technology*, 30(1), 66-71.

Paulson, A. (1999), "Modeling Removal of Cd, Cu, Pb, and Zn in Acidic Groundwater during Neutralization by Ambient Surface Waters and Groundwaters," *Environmental Science and Technology*, 33(21), 3850-3856.

Phillips, D., Gu, B., Watson, D., Roh, Y., Liang, L., and Lee, S. (2000), "Performance Evaluation of a Zerovalent Iron Reactive Barrier: Mineralogical Characteristics," *Environmental Science and Technology*, 34(19), 4169-4176.

Phillips, P., Wall, G., Thurman, E., Eckhardt, D., and Vanhoesen, J. (1999), "Metolachlor and Its Metabolites in Tile Drain and Stream Runoff in the

Canajoharie Creek Watershed," *Environmental Science and Technology*, 33(20), 3531-3537.

Ponder, S., Darab, J., and Mallouk, T. (2000), "Remediation of Cr(VI) and Pb(II) Aqueous Solutions Using Supported, Nanoscale Zero-valent Iron," *Environmental Science and Technology*, 34(12), 2564-2569.

Powell, R., Blowes, D., Gillham, R., Schultz, D., Sivavec, T., Puls, R., Vogan, J., Powell, P., and Landis, R. (1998), "Permeable Reactive Barrier Technologies for Contaminant Remediation," *EPA/600/R-98/125*, Washington DC.

Rael, J., Shelton, S., and Dayaye, R. (1995), "Permeable Barriers to Remove Benzene: Candidate Media Evaluation," *Journal of Environmental Engineering*, 121(5), 411-415.

Ricou, P., and Lėcuyer, I., and Cloirec, L. (1999), "Removal of Cu^{2+}, Zn^{2+} and Pb^{2+} by Adsorption onto Fly Ash and Fly Ash/Lime Mixing," *Water Science and Technology*, 39(10-11), 239-247.

Roberts, A., Totten, L., Arnold, W., Burris, D., and Campbell, T. (1996), "Reductive Elimination of Chlorinated Ethylenes by Zero-Valent Metals," *Environmental Science and Technology*, 30(8), 2654-2659.

Rowley, A. and Husband, F., and Cunningham, A. (1984), "Mechanisms of Metal Adsorption from Aqueous Solution by Waste Tire Rubber," *Water Research*, 18(8), 981-984.

RUST Environment & Infrastructure (1995), Phase I – Detailed Site Investigation of a Dissolved-Phase Plume, Denver Federal Center, *Report to the Federal Highway Administration*, Denver, Colorado.

Schwarzenbach, R., Gschwend, P., and Imboden, D. (1993), *Environmental Organic Chemistry,* John Wiley, New York.

Schlimm, C. and Heitz, E. (1996), "Development of a Wastewater Treatment Process: Reductive Dehalogenation of Chlorinated Hydrocarbons by Metals*," Environmental Progress*, 15(1), 38-47.

Shokes, T. and Möller, G. (1999), "Removal of Dissolved Heavy Metals from Acid Rock Drainage Using Iron Metal," *Environmental Science and Technology*, 33(2), 282-287.

Shackelford, C., and Glade, M. (1997), "Analytical Mass Leaching Model for Contaminated Soil and Soil Stabilized Waste," *Ground Water*, 35(2), 233-242.

Shimizu, Y., Takei, N., and Terashima, Y. (1992), "Sorption of Organic Pollutants from Vapor Phase: the Effects of Natural Solid Characteristics and Moisture Content," *Water Science and Technology*, 26(12), 79-87.

Shoemaker, S., Greiner, J., and Gillham, R. (1995), "Permeable Reactive Barriers," *Assessment of Barrier Containment Technologies: A Comprehensive Treatment for Environmental Remediation Application*, Rumer, R. and Mitchell, J. Eds., International Containment Technology Workshop, Baltimore, Maryland, August 29-31, 301-353.

Sivavec, T., Mackenzie, P., Horney, D., and Baghel, S. (1997), "Redox-Active Media for Permeable Reactive Barriers," *Proc., Intl. Containment Technol. Conf.*, U.S. DOE, U.S. EPA, and Dupont Co., 753-759.

Sosnowski, C. (1996), "Flow Performance and Chemical Profiles through Granular Iron under Anaerobic and Anoxic Conditions," *MS Thesis*, Department of Civil and Environmental Engineering, University of Wisconsin-Madison.

Sparks, D. (1995), Redox Chemistry of Soils, Chapter 8, *Environmental Soil Chemistry*, Academic Press, San Diego, CA.

Starr, R. and Cherry, J. (1994), "In Situ Remediation of Contaminated Groundwater: The Funnel and Gate System," *Ground Water*, 32(3), 465-476.

Stevenson, F. (1994), *Humus Chemistry: Genesis, Composition, Reactions*. 2nd Ed. John Wiley and Sons, New York, NY.

Stumm, W. and Morgan, J. (1970), *Aquatic Chemistry*, Wiley-Interscience, New York, 1970.

Su, C. and Puls, R. (2001), "Arsenate and Arsenite Removal by Zerovalent Iron: Kinetics, Redox Transformation, and Implications for in Situ Groundwater Remediation," *Environmental Science and Technology*, 35(7), 1487-1492.

Tharin, D. (1974), "Tire Rubber Removes Mercury from Process Stream," *Proc. 4th Annual Environmental Engineering and Science Conf.*, Louisville, KY, 369-386.

Tratnyek, P., Johnson, T., Scherer, M., and Eykholt, G. (1997), “Remediating Groundwater with Zero-Valent Metals: Chemical Considerations in Barrier Design,” *Ground Water Monitoring and Remediation*, 17(4), 108-114.

U.S. EPA (1990), *WERL Treatability Data Base*, Risk Reduction Engineering Laboratory, U.S. EPA, Cincinnati, OH.

U.S. EPA (1997), “Permeable Reactive Subsurface Barriers for the Interception and Remediation of Chlorinated Hydrocarbons and Chromium(VI) Plumes in Ground Water,” National Risk Management Research Laboratory, EPA/600/F-97/008, Ada, OK.

van Genuchten, M. (1981), “Analytical Solutions for Chemical Transport with Simultaneous Adsorption, Zero-Order Production and First-Order Decay,” *Journal of Hydrology*, 49, 213-233.

Warren, K., Arnold, R., Bishop, T., Lindholm, L., and Betterton, E. (1995), “Kinetics and Mechanisms of Reductive Dehalogenation of Carbon Tetrachloride Using Zero Valent Metals,” *Journal of Hazardous Materials*, 41, 217-227.

Wasay, S., Haron, M., Uchiumi, A., and Tokunaga, S. (1996), “Removal of Arsenite and Arsenate Ions from Aqueous Solution by Basic Yttrium Carbonate,” *Water Research*, 30(5), 1143-1148.

Weber, E. (1996), “Iron-Mediated Reductive Transformations: Investigation of Reaction Mechanism,” *Environmental Science and Technology*, 30(2), 716-719.

Wüst, W., Köber, R., Schlicker, O., and Dahmke, A. (1999), “Combined Zero- and First-Order Kinetic Model of the Degradation of TCE and cis-DCE with Commercial Iron,” *Environmental Science and Technology*, 33(23), 4304-4309.

Zytner, R. (1992), “Adsorption-Desorption of Trichloroethylene in Granular Media,” *Water, Air, and Soil Pollution*, 65, 245-255.

APPENDIX A

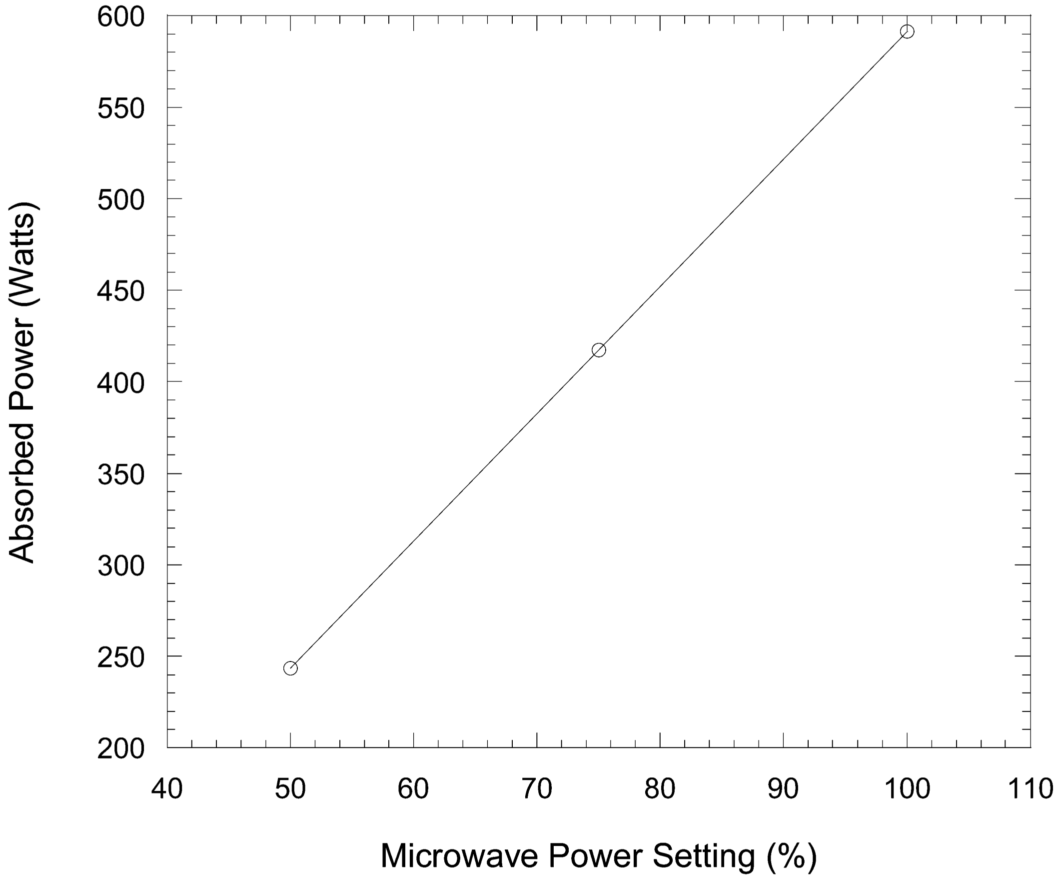

Fig. A1. Calibration of Microwave Equipment for Acid Digestion Following USEPA Method 3051. Absorbed Power on 1 L DI Water in Glass Beaker was Calculated by Using Difference of Temperature Before and After Heating Using Microwave at Different Power Settings. 574 W Corresponds to 97.5% Power Setting. Thus, Digestion was Conducted in Fluorocarbon Vessels for 10 min with 97.5% Power Setting.

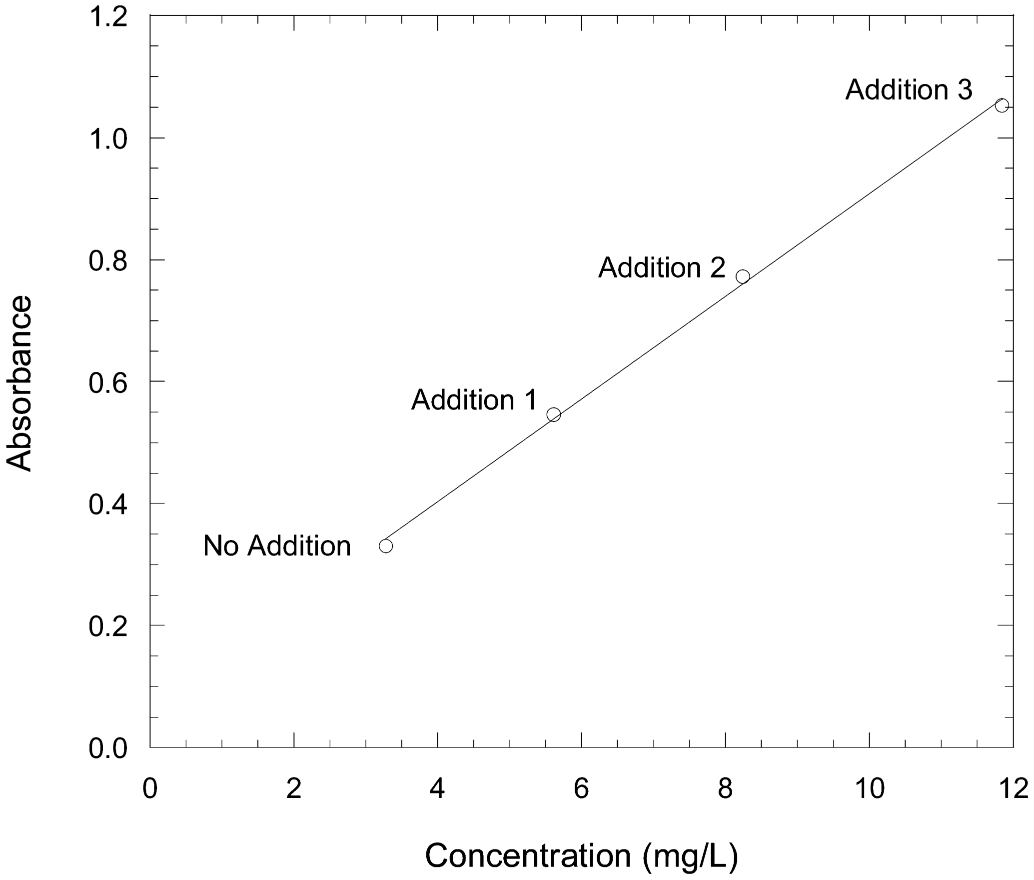

Fig. A2. Results of Standard Additions for Sample Solution Extracted from Sand 10. Three Additions were Conducted to Obtain approximately 50 (Addition 1), 100 (Addition 2), and 150% (Addition 3) of the Expected Absorbance from Endogenous Analyte in the Sample.

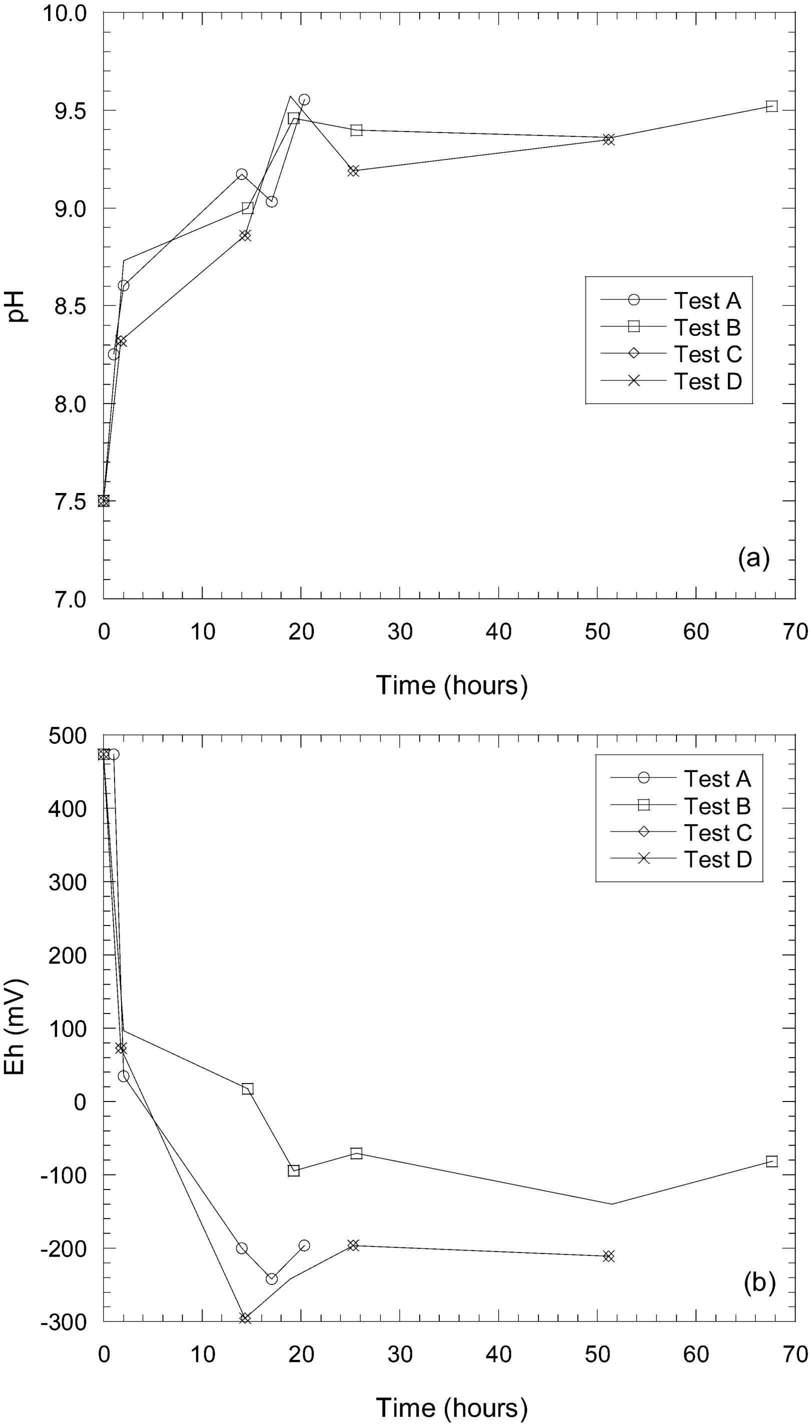

Fig. A.3. pH and Eh from the Batch Degradation Tests for Test A through Test D (Table 5.1).

APPENDIX B

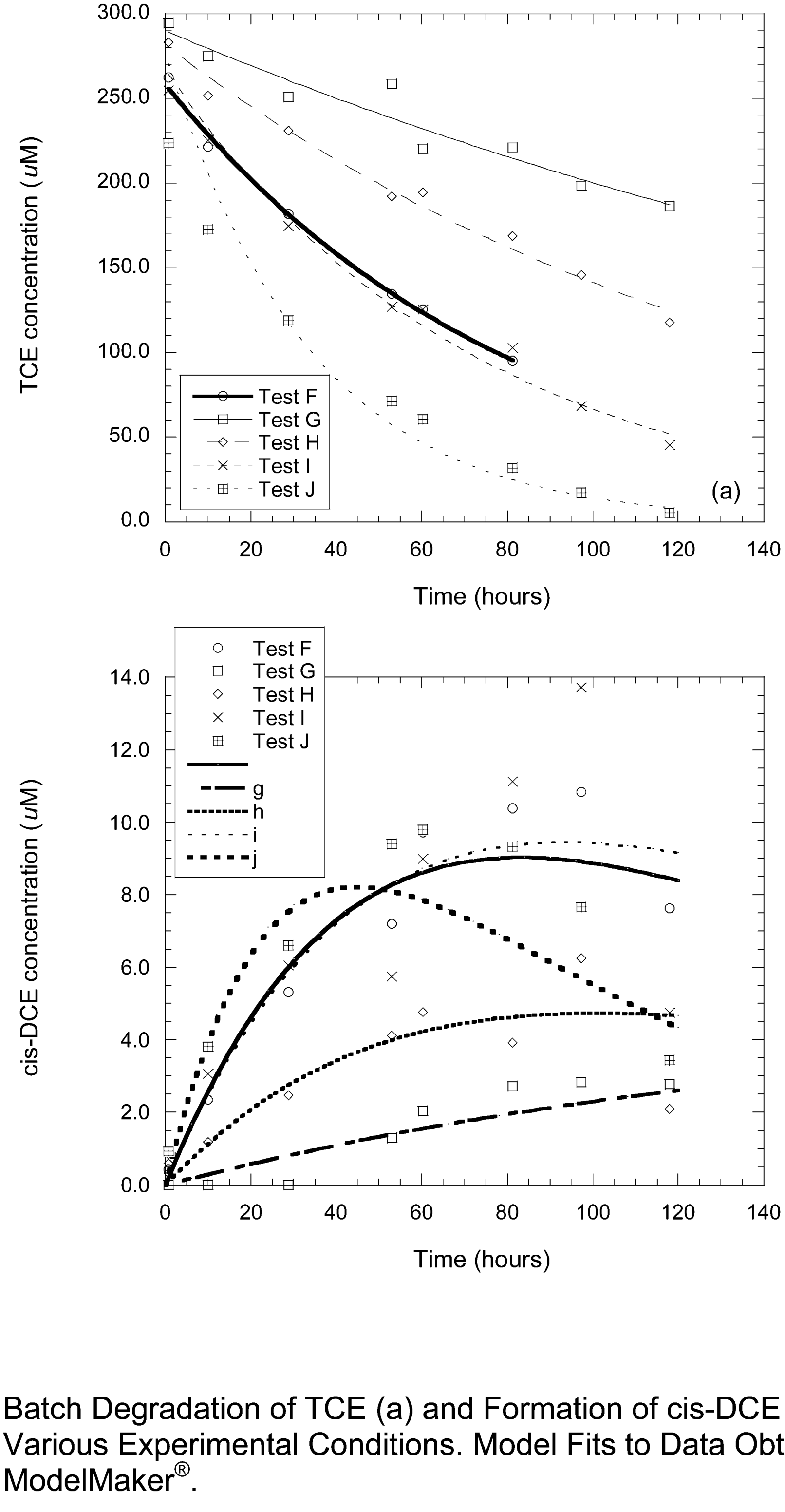

Fig. B.1. Batch Degradation of TCE (a) and Formation of cis-DCE (b) under Various Experimental Conditions. Model Fits to Data Obtained Using ModelMaker®.